ARGONNE NATIONAL LABORATORY

ANL-SMFR-1

Small Modular Fast Reactor Design Description

prepared as a joint effort by
Argonne National Laboratory
Commissariat à l'Energie Atomique
Japan Nuclear Cycle Development Institute

Argonne Is Operated by The University of Chicago for the U. S. Department of Energy Office of Science

THE UNIVERSITY OF CHICAGO

cea

JNC

About Argonne National Laboratory

Argonne is managed by The University of Chicago for the U.S. Department of Energy's Office of Science, under contract W-31-109-Eng-38. The Laboratory's main facility is outside Chicago, at 9700 South Cass Avenue, Argonne, Illinois 60439. For information about Argonne and its pioneering science and technology programs, see www.anl.gov.

Small Modular Fast Reactor
Design Description

Joint Effort
by
Argonne National Laboratory (ANL)
Commissariat a l'Energie Atomique (CEA)
and
Japan Nuclear Cycle Development Institute (JNC)

Project Leaders

Y. I. Chang and C. Grandy, ANL
P. Lo Pinto, CEA
M. Konomura, JNC

Technical Contributors

ANL: J. Cahalan, F. Dunn, M. Farmer, S. Kamal, L. Krajtl, A. Moisseytsev, Y. Momozaki, J. Sienicki, Y. Park, Y. Tang, C. Reed, C. Tzanos, S. Wiedmeyer, and W. Yang
CEA: P. Allegre, J. Astegiano, F. Baque, L. Cachon, M. S. Chenaud, J-L Courouau, Ph. Dufour, J. C. Klein, C. Latge, C. Thevenot, and F. Varaine
JNC: M. Ando, Y. Chikazawa, M. Nagamura, Y. Okano, Y. Sakamoto, K. Sugino, and H. Yamano

TABLE OF CONTENTS

TABLE OF CONTENTS (Contd.)

TABLE OF CONTENTS (Contd.)

Small Modular Fast Reactor
Design Description

Joint Effort
by
Argonne National Laboratory (ANL)
Commissariat a l'Energie Atomique (CEA)
and
Japan Nuclear Cycle Development Institute (JNC)

ABSTRACT

This report describes the design of Small Modular Fast Reactor that has been developed jointly by Argonne National Laboratory (ANL), Commissariat a l'Energie Atomique (CEA), and Japan Nuclear Cycle Development Institute (JNC) as an international collaborative effort.

A reactor size of 50 MWe was selected for a specific niche application to small grid systems, where industrial infrastructure is not sufficient and the unit cost of electricity generation is very high with conventional technologies. Examples of this are remote areas in Alaska, small grid systems in developing countries, Pacific-basin islands, remote military locations, and similar unique situations.

Numerous innovative design features have been incorporated into the SMFR design including a metallic fueled core with high internal conversion ratio so that refueling for reactivity reasons is not required for 30 years, inherent passive safety characteristics achievable by sodium cooling, simplified reactor system for modular construction and transportability, and supercritical CO_2 Brayton cycle power conversion system.

I. INTRODUCTION

In the near term, the current generation commercial reactors and evolutionary advanced light water reactors are expected to be the choice for nuclear power expansion. However, in the long term, advanced reactor concepts are needed to meet the waste management, further enhanced safety, nonproliferation, and resource challenges that must accompany the deployment of increasing numbers of nuclear power plants.

Since the potential timing of such advanced reactor needs is at least 2020 and beyond, there appears to be little incentive to commit investments at this time. However, there is a strong case for a small modular fast reactor, which can satisfy some special near-term market niche, while at the same time making a truly advanced scaleable reactor technology available for longer-term applications. Such a unique market niche does exist for small grid systems in the 10 to 50 MWe range, where industrial infrastructure is not sufficient and the unit cost of electricity generation is very high with conventional technologies. Examples of this are remote areas in Alaska, small grid systems in developing countries, Pacific-basin islands, remote military locations, and similar unique situations.

It is also obvious, however, that such a reactor can provide a relatively inexpensive test bed for demonstrating advanced technology, if the technology is suitably chosen, and in particular, technologies for hydrogen co-generation and desalination capabilities can be explored and developed.

The Small Modular Fast Reactor (SMFR) described in this report has been developed jointly by Argonne National Laboratory (ANL), Commissariat a l'Energie Atomique (CEA) of France, and Japan Nuclear Cycle Development Institute (JNC) as an international collaborative effort to achieve technical consensus. However, a U.S. siting was assumed for specific design options that depend on country-specific regulatory requirements.

The SMFR is aimed at exploiting characteristics inherent to fast reactors for application to small grid applications. The basic goal is to make the operation, the safety, and the refueling as simple and effective as possible. In the latter instance, no refueling at all during the reactor core lifetime is a particular goal.

The characteristics that make this a real possibility are the following:

1. Because of the non-corrosive characteristic of sodium coolant, the reactor core and primary system components need not degrade even over very long residence times in the reactor. In fact, the entire in-reactor system can be designed to so minimize the maintenance requirements that the reactor system can be sealed in a "cartridge."

2. The excellent neutron economy available from metallic fuel can be exploited to design a core with internal conversion ratio of greater than unity so that refueling for reactivity reasons is not required for an entire cartridge lifetime of 30 years.

This ultra long lifetime also eliminates vulnerabilities to terrorism, because new fuel, routine spent fuel handling and out of reactor fuel storage – the areas most susceptible to fissile material diversion - are non-existent at a plant site of this kind. This feature enhances physical security sufficiently that siting of such a reactor can reasonably be considered almost anywhere.

Further enhancing non-proliferation attributes, the initial fuel envisioned would contain all the actinide elements from high burnup LWR spent fuel. Such fuel is unsuitable as weapons material, in the first place, and furthermore as it is securely sealed in the reactor for its 30-year lifetime, the arrangement provides about the most assured proliferation resistance possible, from either national level proliferators or sub-national terrorist groups.

The SMFR incorporates all the passive safety features developed over the past two decades for this type of reactor which emphasize design features that protect the plant from damage in the event of failures, both human and safety system. Such passive safety design relies on the laws of nature to ensure the continuation of the essential functions of reactor safety even under accident conditions, that is, the maintenance of proper balance of heat generation and heat removal, the removal of decay heat, and in the last instance the containment of any and all radioactive material.

The efficacy of such passive safety was demonstrated through two landmark tests conducted on the Experimental Breeder Reactor-II (EBR-II), namely loss-of-flow without scram and loss-of-heat-sink without scram tests. With the automated safety systems disabled, the two most demanding accident initiating events were deliberately induced with the reactor at full power, first one then the other. Each time the reactor simply coasted to a safe low power state without any damage at all to the fuel or any reactor component. These tests proved conclusively that passive safety design is achievable for metallic fueled fast reactors with sodium cooling.

The SMFR also helps with the problem of long-lived nuclear waste generation. The radiological toxicity of LWR spent nuclear fuel in the very long term (hundred thousands years and beyond) is dominated by Np-237 and its precursors Am-241 and Pu-241, which ultimately decay to Np-237, with 14-yr and 432-yr half-lives, respectively. But in the SMFR, these isotopes do not continue to build up, instead the initial amounts of these actinides are actually reduced by about 40% as they burn up in the reactor over its 30 year life time. To illustrate the significance of this, if the remaining amount is compared to the cumulative amounts that would be generated in an LWR for the same energy production, we find a reduction by a factor of thirty. The remaining spent fuel from the SMFR will be processed through very simple and compact pyroprocessing at an off-site location and recycled back into another SMFR thus achieving even further reductions in the long term toxicity.

There will be an important reduction in the long term heat of the residue as well, as this cycle returns all minor actinides, important radioisotope contributors to shorter term decay heat production, back to reactor fuel for burnup and thus complete destruction. This is to be compared to the situation in thermal spectrum reactors, where some amount of plutonium is burned, but a

significant fraction is merely transmuted to higher actinides, which therefore continue to increase. The important point is that it is only in a fast neutron spectrum that all actinides can be burned up, leading to very large differences between the waste products of this SMFR reactor and that of thermal spectrum reactors over long times.

In the short term there is little difference between various reactor types as short lived fission products generation is unchanged regardless of spectrum or reactor type, but the radioactive toxicity of fission products declines much more quickly than that of the actinides. The differences become more and more significant as time passes.

II. OVERALL PLANT DESCRIPTION

In order to develop and incorporate innovations, the following specific design goals have been established for the SMFR:

- Long-life core (30 years) with no refueling
- Proliferation resistance for export market
- Modular construction and transportability
- Inherent safety and passive systems
- Easy operation and maintenance
- Simple design to reduce cost
- Actinide transmutation
- Hydrogen co-generation and desalination capabilities.

These high-level design goals are achieved in the reference design, which has been jointly developed by ANL, CEA and JNC. The key plant design parameters for the SMFR are summarized in Table II-1.

Table II-1. SMFR Plant Design Parameters

Reactor Power	~50 MWe/ 125 MWth
Core Fuel	Metal Fuel
Core Life	30 years without refueling
Plant Life	60 years
Reactor Vessel Size	5.8 m diameter, 16 m height
Coolant	Sodium
Coolant Temperature, Inlet/Outlet	355ºC/510ºC
Power Conversion Cycle	Supercritical CO2 Brayton Cycle
Thermal Efficiency	38 %

The overall plant site is depicted in Figure II-1, and the primary system, the intermediate system and the Brayton cycle power conversion system are depicted in Figure II-2. As shown In Figure II-3, the primary and intermediate systems are embedded below the grade level.

The primary system is configured as a typical pool-type arrangement, with the reactor core, primary pumps, intermediate heat exchangers, and direct reactor auxiliary cooling system (DRACS) heat exchangers all contained within the reactor vessel. Within the reactor vessel, the primary electromagnetic pumps (2) take a suction from the lower regions of the cold pool and discharge the sodium into a header that distributes the sodium into 3 feeder pipes. The feed pipes distribute sodium evenly into the inlet plenum. The inlet plenum distributes the primary sodium to the inlet of the core assemblies located in the assembly lower adaptor. The core assemblies are individually orificed for proper flow distribution. The sodium is heated as it flows through the core and exits the core assemblies at the outlet plenum. The hot sodium then rises into the redan and then enters the inlet of the intermediate heat exchanger (IHX). The primary sodium flow

Figure II-1. SMFR Plant View

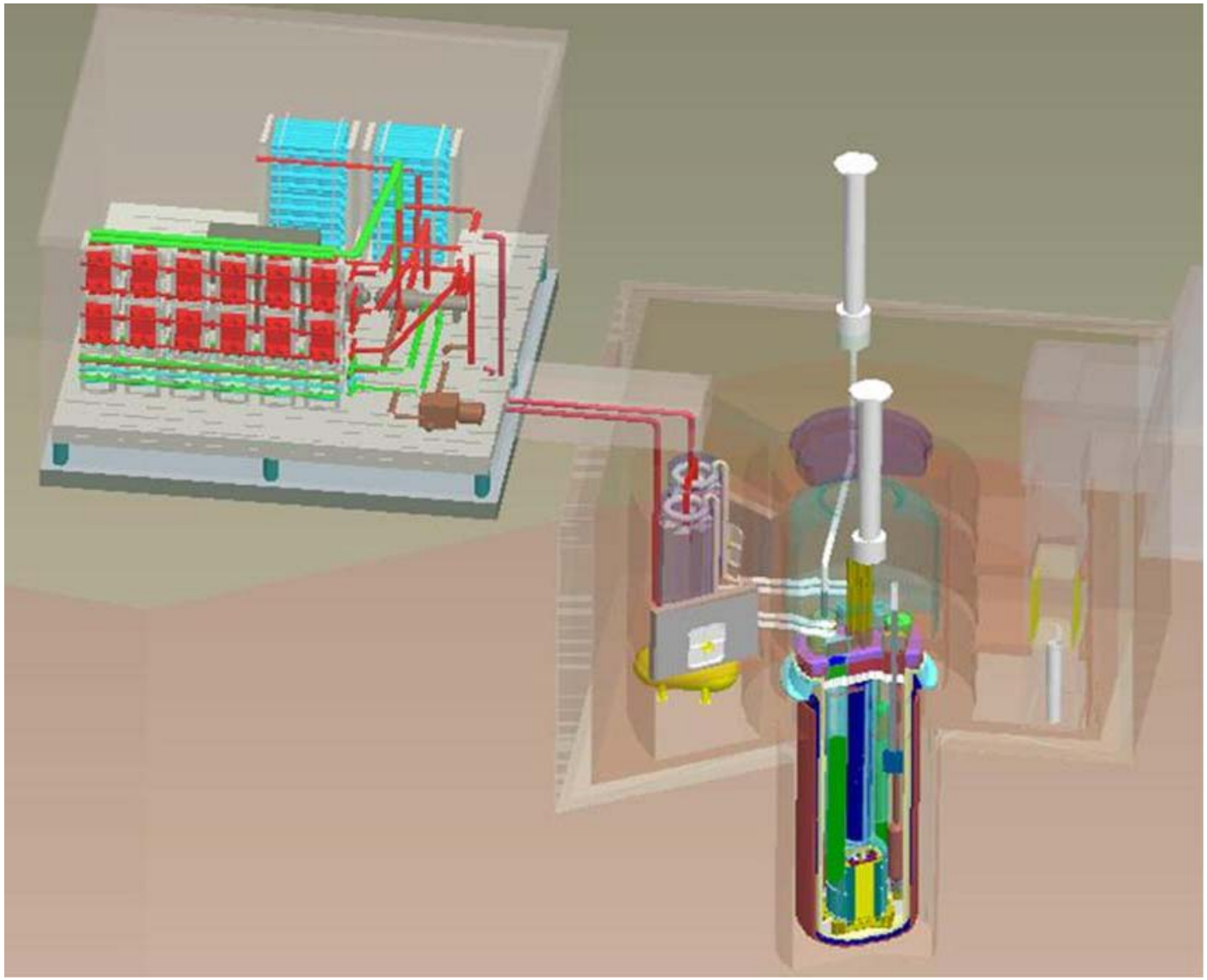

Figure II-2. Primary System, Intermediate System, and Brayton Cycle Power Conversion System

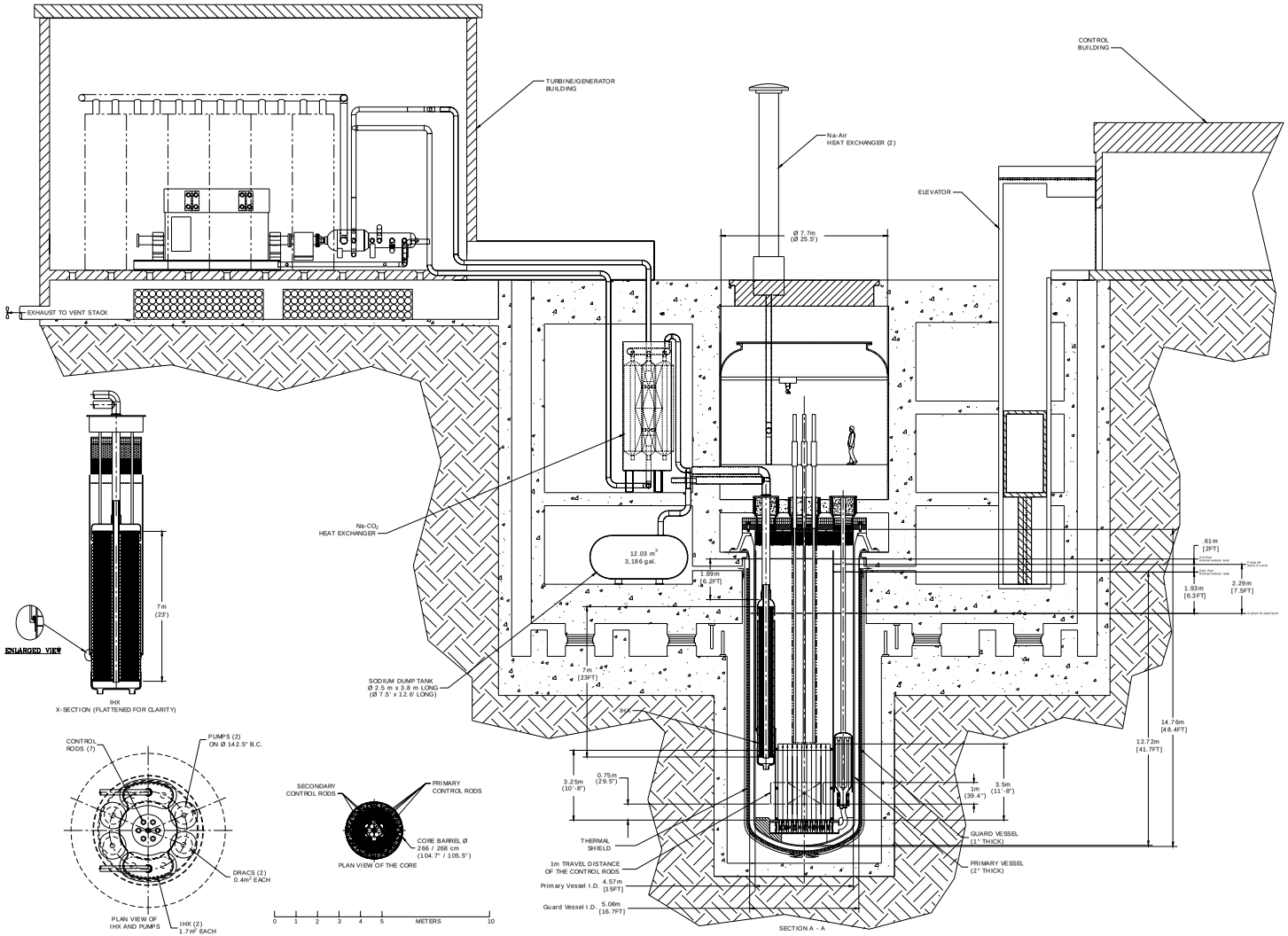

Figure II-3. Elevation View of Primary, Intermediate, and Brayton Cycle Power Conversion Systems

enters the IHX shell about 30 cm below the upper tubesheet to minimize thermal shock of the tubesheet during transient conditions. The sodium flows down through the shell side of the IHX around baffle plates that evenly distributes the sodium in the IHX. After the primary sodium transfers its heat to the intermediate sodium, it exits the IHX about 30 cm above the lower tubesheet and into the lower regions of the cold pool. The IHX is contoured to the shape of the annular gap between the redan and the reactor vessel to minimize the overall diameter of the reactor vessel. A guard vessel surrounds the reactor vessel to capture and contain any reactor vessel leakage and to prevent the IHX inlet, DRACS heat exchangers, and core assemblies from being uncovered.

The intermediate sodium exits the IHX and flows to the Na-to-CO_2 heat exchanger located on the nuclear island. The Na-to-CO_2 heat exchanger is part of the Brayton Cycle power conversion unit. The intermediate sodium heats up the supercritical CO_2 which then flows into the turbine generator performing work and generating electricity. The CO_2 then goes through a series of recuperator heat exchangers, cooler, and compressors before it re-enters the Na-to-CO_2 heat exchanger.

The CO_2 rejects about 60% of its heat to the forced draft cooling tower which provides the ultimate heat sink for the Brayton cycle power conversion unit. The overall thermodynamic cycle is shown in Figure II-4.

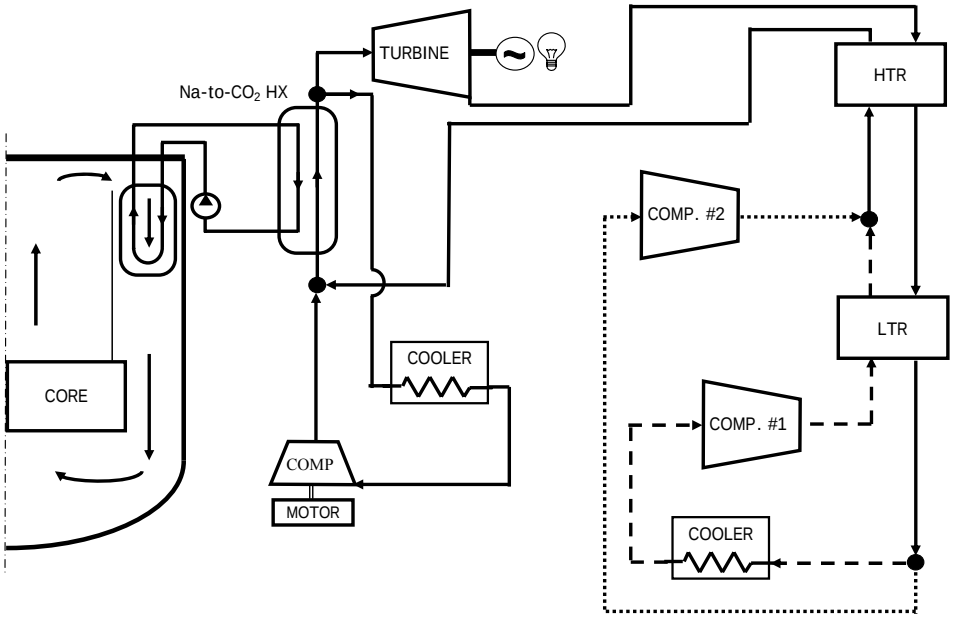

Figure II-4. Overall Thermodynamic Cycle

III. REACTOR MODULE AND SUPPORT STRUCTURES

A. Reactor Module Arrangement

The reactor module, shown in Figure III-1, is a small transportable module that consists of the reactor vessel, core, core support structure, inlet plenum and grid plate structure, reactor vessel enclosure, and various plugs. The intermediate heat exchangers and sodium pumps are located in the reactor vessel. The reactor module is located below grade in a silo structure that is hardened and provides a low profile. The structure has base isolation to reduce its susceptibility to earthquakes. The reactor module is supported from the top with a conical ring. The reactor module is located in the center (plan view) of the reactor building and is surrounded by rooms containing the intermediated piping loops, sodium-to-CO_2 heat exchangers, intermediate pumps, and support equipment. The reactor module is cooled using a guard vessel/concrete cavity cooling system.

The reactor vessel and its support structures are connected with a bolting system which could facilitate disassembly and the ultimate decommissioning process.

The reactor vessel assembly consists of:

- Reactor vessel
- Guard vessel
- Reactor vessel enclosure
- Core support structure
- Core barrel and redan assembly
- Removable plugs
- Top (cold) support structure
- Internals structures

B. Reactor Vessel

The reactor vessel contains the reactor core, entire primary coolant, intermediate heat exchangers, primary electromagnetic pumps, direct reactor auxiliary cooling system (DRACS) heat exchangers, and internal structures. The diameter and overall height of the reactor vessel are 4.6m and 14.8m, respectively. The reactor vessel is made of Type 316 stainless steel, while the guard vessel is made of Type 304. The complete reactor vessel assembly is located below grade in a steel-lined concrete cavity of the reactor containment building. The reactor vessel and its cover constitute the primary structural boundary that envelopes and supports the reactor core, primary sodium coolant, reactor cover gas, auxiliary core components, primary sodium pumps, IHXs, and other associated reactor equipment. In addition to providing the primary structural boundary, support and containment, the reactor vessel and reactor vessel enclosure provide internal and interfacing equipment alignment features. All penetrations into the reactor vessel are through the top cover. There is an inert gas (argon) blanket between the reactor vessel cover and the bulk sodium free surface. The primary plant systems are shown in Figure III-2.

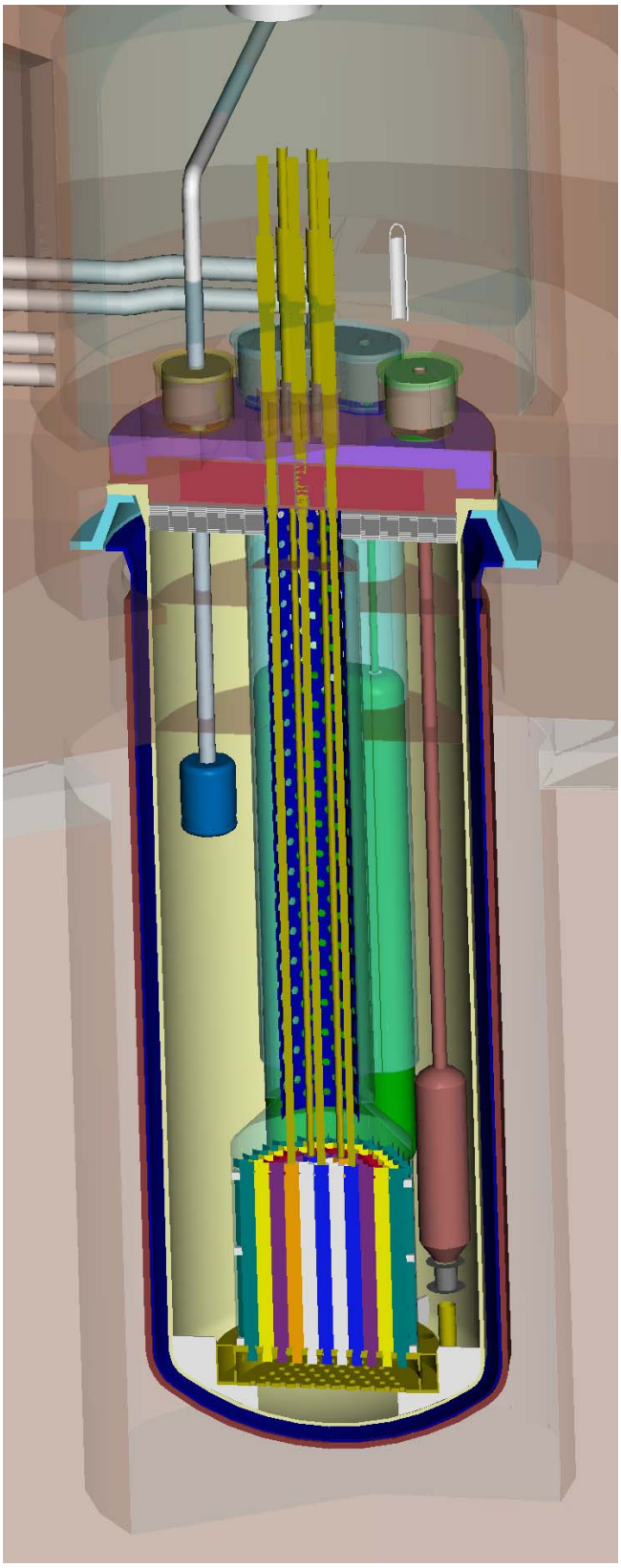

Figure III-1. Reactor Module

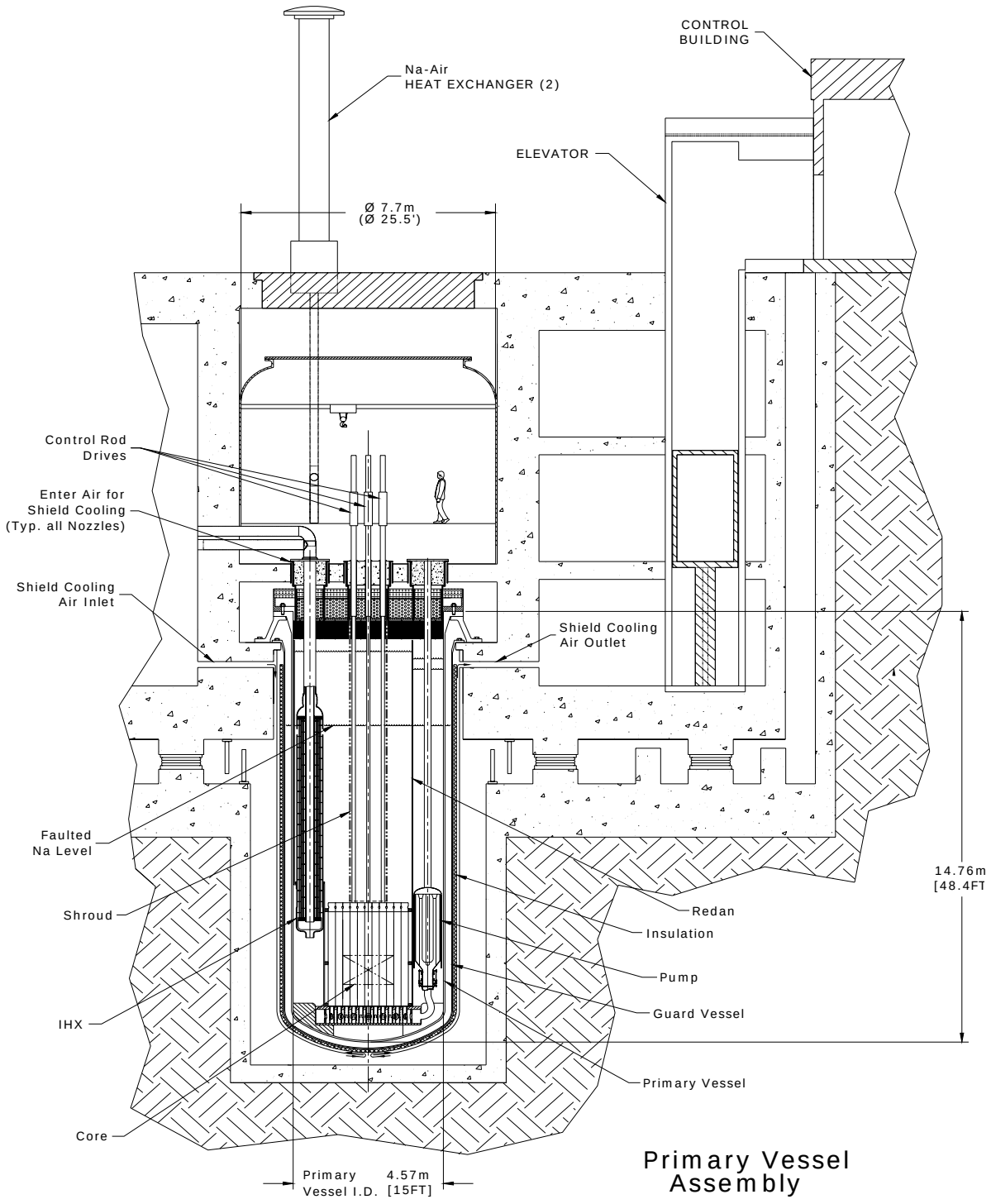

Figure III-2. Primary Plant Systems

The plan view of the reactor vessel assembly is shown in Figure III-3. Figure III-4 shows the design concept for the support of the reactor vessel. The height of the reactor vessel is established from the fuel assembly length, the intermediate heat exchanger length, and the need to keep the intermediate heat exchanger inlet covered by sodium during a leak of the reactor vessel where sodium would drain into the guard vessel. The "faulted" primary sodium level is indicated in Figure III-2. The diameter of the reactor vessel is established from the core diameter and IHX characteristics with respect to sodium hydraulic and heat transfer requirements and the requirement to be able to remove the primary components, such as the IHX, primary sodium pumps, and DRACS heat exchangers. The reactor vessel and its cover are designed to the requirements of the ASME B&PV Code, Section III, Division 1, Subsection NH for the combined loads of the entire volume of primary sodium, the primary system equipment, and the core support structure. In addition, the design will meet ASME B&PV Code requirements for normal and transient thermal loads as well as loads and displacement resulting from design basis earthquakes. The top-supported reactor vessel is suspended from a continuous conical-shaped skirt as shown in Figure III-4. The skirt provides separation between the reactor vessel and the guard vessel, and contains several access ports to permit periodic inspection of the area, and to provide access to the annulus between the reactor vessel and the guard vessel. The reactor vessel is fastened to the support skirt.

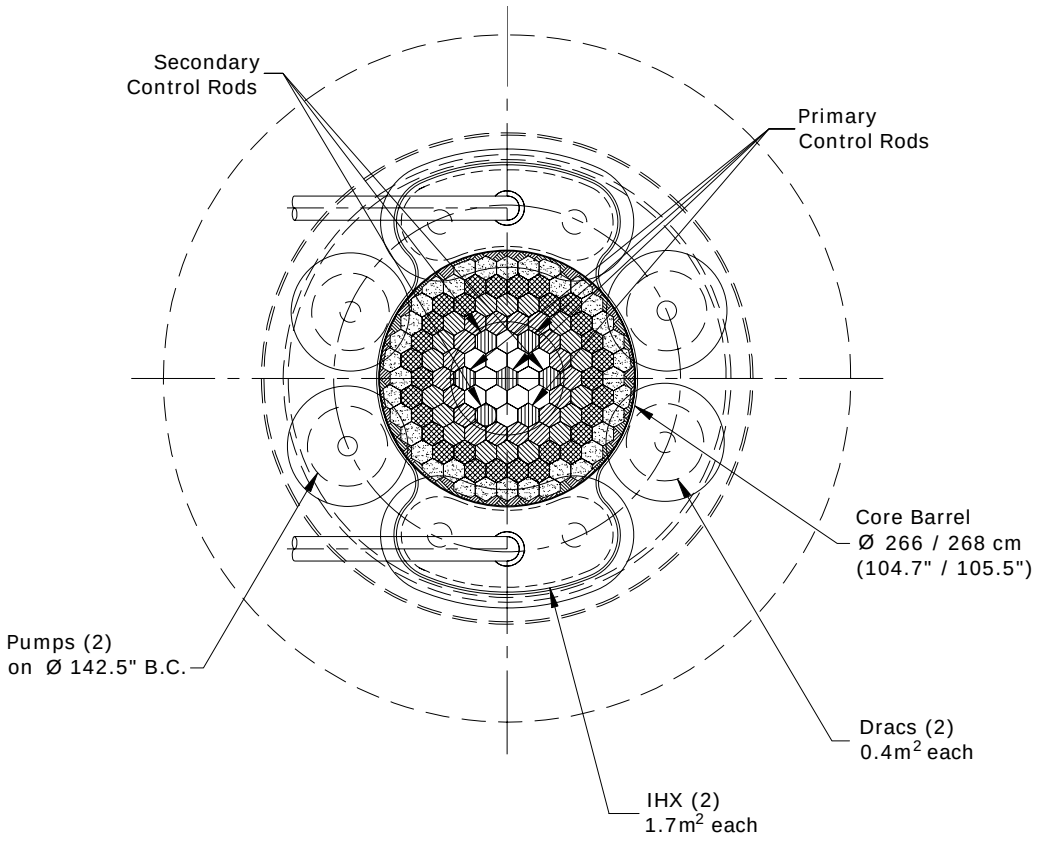

Figure III-3. Plan View of Reactor Vessel Assembly

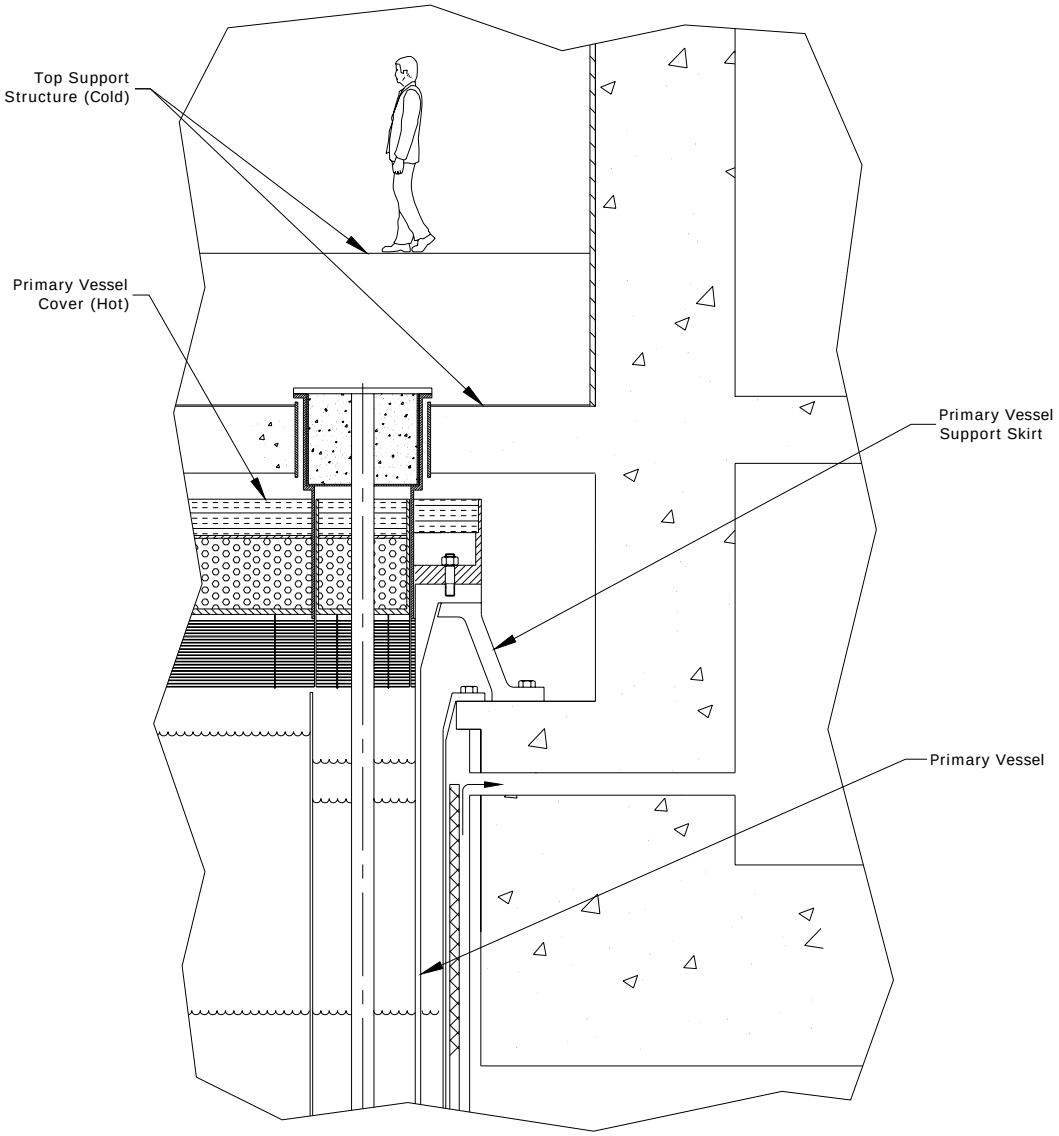

Figure III-4. Reactor Vessel Support

The reactor vessel assembly is designed to:

1. Accommodate high static loads at design temperatures.
2. Minimize the dead load deflections and thermal bowing of the reactor vessel and its cover to facilitate equipment alignment.
3. Provide a type of structure which can be erected on site to stringent tolerance requirements.
4. Ensure symmetrical radial thermal expansion of the primary tank about the vertical center of the entire primary tank assembly.

C. Guard Vessel

The guard vessel provides the secondary containment for the primary sodium in the very unlikely event that the reactor vessel develops a leak. The guard vessel is sized such that the gap (~22 cm) between it and the reactor vessel is:

a. Wide enough to accommodate in-service inspection devices
b. Narrow enough to prevent the primary sodium from dropping to an unacceptable level within the reactor vessel if the reactor vessel should develop a leak. The sodium level must remain high enough to keep the IHX inlet covered to provide a path for natural convection cooling of the core during a leak in the reactor vessel.

The guard vessel is constructed of Type 304 stainless steel. If carbon steel were acceptable, it would facilitate the use of magnetically-operated remote devices needed to carry out the periodic in-service inspection (ISI) required for the reactor vessel and associated structures and components. With the Type 304 stainless steel, the equipment used for ISI would require use of friction or scissors-like devices to scan the entire outer surface of the reactor vessel.

Insulation is provided on the exterior of the guard vessel to reduce the heat lost to the guard vessel cooling system.

D. Reactor Vessel Enclosure

The reactor vessel enclosure is similar to that used on EBR-II. There are major differences, however, which result in a more feasible design for this size plant. The main features that are different from EBR-II are:

1. The guard vessel does not connect to the reactor vessel enclosure.
2. The reactor vessel and reactor vessel cover are supported by a continuous conical ring skirt (not by the upper-cold structure with hangers such as used on EBR-II).

The approach of two separate structures, the reactor vessel cover and the upper (cold) support structure is the same as that used in EBR-II. There are numerous benefits which arise from this approach, namely simplification of the upper (cold) structure since all primary heat transport system components are supported by the reactor vessel cover, provision of reliable and accurate location of all of the primary heat transport and fuel handling components, and trouble-free alignment between the components and structures located within the bulk primary sodium and those supported on the reactor vessel cover.

E. Core Support Structure

The core support structure, shown in Figure III-5, provides support for the lower internals structure, the core assemblies, the core barrel assembly, the primary sodium inlet pipes, brackets, and baffles. It is designed to the requirements of the ASME B&PV Code, Section III, Division 1, Subsection NG, Core Support Structures. The core support structure consists of a steel web structure that is formed to the contours of the reactor vessel bottom head and becomes an integral

part of the reactor vessel. All core support structure components are under compression, therefore there is no need for performing ISI on these components.

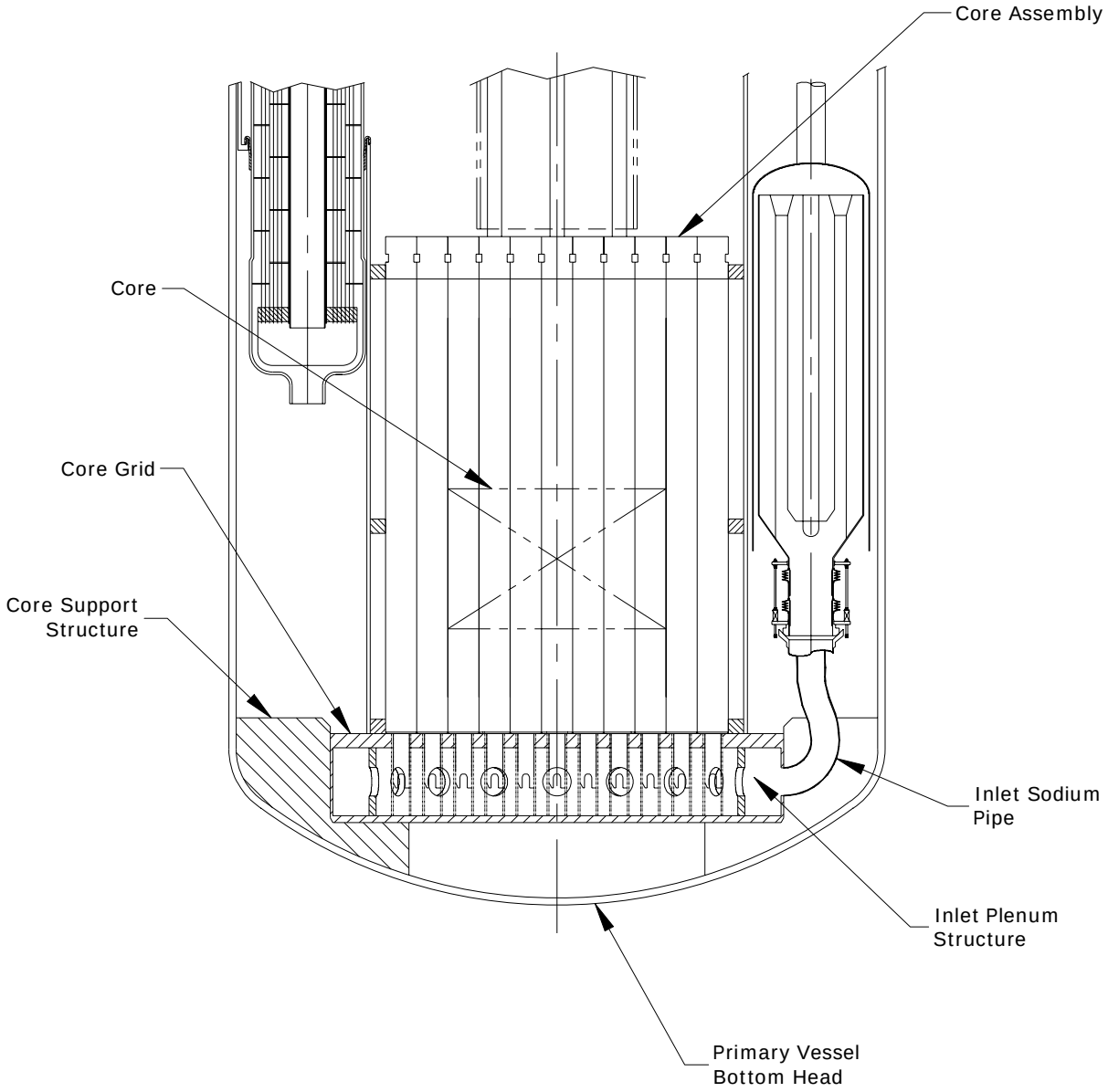

Figure III-5. Core Support Structure

F. Core Barrel Assembly

The reactor core barrel assembly consists of the core barrel, core grid, and the inlet plenum structure. The entire assembly is supported on the core support structure as shown in Figure III-5. The core barrel and cover assembly is not leak tight, and permits a certain amount of the inlet

sodium to leak into the bulk primary coolant. This feature promotes the establishment of natural circulation cooling of the core in the event of loss of the primary pumps.

G. Top Support Structure

The top support structure above the reactor vessel cover shown in Figure III-4 provides support for the fuel handling system during core change-out, the upper concrete biological shielding over the reactor vessel cover, and operating floor loads, including heavy, shielded casks used to remove large components from the reactor vessel. The top support structure is completely independent from the reactor vessel assembly.

The fact that the top support structure is decoupled from the reactor vessel assembly can be exploited to achieve design simplification. There is, however, one design aspect that will require attention since numerous vertical nozzles supporting all equipment within the reactor vessel must pass through and support flanges must be provided above the top support structure. This structure needs to be constructed with relatively close tolerances around each nozzle in order to avoid radiation shine passing up around each nozzle.

H. Reactor Containment Boundary

The SMFR Primary containment boundary is comprised of the reactor vessel, reactor vessel enclosure, the tubes in the intermediate heat exchanger and in the direct reactor auxiliary heat exchanger, and the sodium purification piping and components. These components maintain the containment for the primary radioactive sodium and form the first containment boundary. This initial boundary also includes the instrument thimbles and the cover gas piping system.

If this first boundary is breached, then the next secondary confinement is composed of the reactor guard vessel, the reactor containment, the intermediate sodium piping and sodium-to-CO_2 heat exchangers, the direct reactor auxiliary cooling system intermediate piping and systems, the stainless steel-lined compartments around the reactor vessel support, the purification system cell confinement, and the reactor building (which is maintained at a negative pressure with HEPA-filtered ventilation).

If there is a breach in a thimble or cover gas system, the gas operates at a slightly higher pressure than the sodium and therefore, there will be no release of sodium to the environment. The reactor building always operates at a negative pressure compared to the outside environment. All effluents are filtered via high-efficiency particulate air filters before they are released into the environment.

I. Integrity of Primary Coolant Boundary

It has been postulated that a structural failure or leak which would develop in the reactor vessel could prove to be a major economic setback. The purpose of this discussion is to show that current, proven technology can be applied to ensure a leak-tight primary coolant boundary over the plant lifetime, reducing the probability of such a leak occurring to a very low level.

In the pool-type design, the reactor and the entire radioactive primary coolant are contained in a single reactor vessel. This arrangement results in a direct and simple containment for the primary sodium, with no penetrations in the reactor vessel wall below the primary sodium surface. The SMFR design avoids, wherever possible, the use of dissimilar materials and the oftentimes difficult welding techniques associated with these dissimilar materials.

The surrounding environment of sodium is common to all of the primary system components, which mitigates pipe (duct) expansion stresses and minimizes effects of pipe leaks. A very high level of structural and leak-tight integrity of the reactor vessel and its surrounding guard vessel is achieved with the use of both proven design features and intrinsic characteristics of the sodium system. This basic foundation is supported by established fabrication, field construction, and quality control procedures, comprehensive testing plus inspections and finally, regular in-service monitoring and surveillance.

Inherent characteristics of the sodium system that mitigate potential challenges to the reactor vessel include non-corrosiveness of sodium to structural materials. The operating pressure of the bulk sodium is very low, generally limited to the hydrostatic head of sodium. This leads to low stresses in the reactor vessel structure and permits large design margins and the use of thin-walled plates for fabrication which, in turn, enhances the reliability of nondestructive examination methods which may be used for in-service inspection.

To ensure system safety, design features are included, such as the backup guard vessel, that give unimpaired capability for removal of reactor decay heat in the event of reactor vessel leakage.

Design features that promote the integrity of both the reactor vessel and the guard vessel are viable due to the following basic characteristics of the pool-type arrangement:

1. There are no attachments or penetrations in the shells and bottom head of either the reactor vessel or the guard vessel, except for the core support structure.
2. The vessels have simple geometries, e.g., right circular cylinders and smooth, curved bottom heads.
3. The core support structure is attached to the bottom head of the reactor vessel with a set of formed steel webs contoured to the shape of the reactor vessel bottom head. This eliminates welds at points of high stress.

In addition, the Type 316 stainless steel material, used throughout the reactor vessel assembly (with the possible exception of the guard vessel), has several favorable characteristics:

1. Excellent compatibility with the sodium coolant.
2. Excellent ductility/toughness properties, even at total neutron fluences higher than expected at the reactor vessel boundaries.
3. No appreciable high temperature aging degradation with a primary sodium coolant temperature of about 510ºC.
4. Excellent weldability.

5. High fracture toughness prevents rapid crack propagation and makes a leak-before-break strategy feasible.

Another unique feature is that the reactor vessel is interfaced with the cold pool, which results in a low and approximately constant temperature for the reactor vessel wall, and for the guard vessel as well. This approach has two very important benefits:

1. The reactor vessel temperature is almost always at the low sodium-inlet temperature (about 355 to 410°C) except for the upper sections of the reactor vessel which sees the increased temperature of the hot sodium pool.
2. Deleterious effects of large and frequent temperature transients are avoided by maintaining this temperature relatively constant.

With regard to radiation damage, adequate shielding in the core barrel as well as the distance to the reactor vessel wall results in total neutron fluences well below any level which would be of concern during the 60 year design life for the plant.

J. In-Service Inspection

The in-service inspection (ISI) is planned based on the requirements of ASME B&PV Code Section XI Division 3, which specifies the rules and requirements for inspection and testing of nuclear safety grade components used in liquid metal cooled nuclear reactor plants. The objective of the code is to confirm integrity of function of parts necessary to safety, and satisfy the needs to protect plant investment and high plant availability. To meet the objectives, the ISI plan is developed with emphasis on classification of system components and delineating appropriate ISI technologies, and provision of adequate access within the intent of compact reactor system design, so that inspection of all components are possible. The ISI plan shall provide for both routine and non-routine inspections without causing significant detrimental effect in plant availability and reliability. Non-routine inspections may be follow-up examinations in the event normal ISI activities indicate deviations from normal operating or structural conditions, or conducted as a part of maintenance activities. Table III-1 summarizes the ISI and maintenance requirements in the plan.

ASME B&PV Code Section XI specifies four types of examinations used during ISI: visual, surface, continuous monitoring, and volumetric. For normal ISI of the reactor components, the Code only requires the use of visual inspection and continuous monitoring. To this end, ASME Code Article IMA-2200 specifies the following definitions of visual examination:

- VTM1: close range examination to detect discontinuities and imperfections on the surface of components, including such conditions as cracks, wear, corrosion, or erosion.
- VTM2: examination of exterior surfaces in such a way that accumulations of liquids, liquid drops, and smoke are discernable.
- VTM3: examination to determine the general mechanical and structural conditions of components and their supports by verifying parameters such as clearance, settings, and physical displacements; and to detect discontinuities and imperfections, such as loss of integrity as bolted or welded connections, loose or missing parts, debris, corrosion, wear, or

erosion. VTM3 visual examination may be conducted using scanners, and dimensional gauges that function under liquid metal.

Table III-1. Summary of ISI&M Requirements

Major Components	ISI		Maintenance		
	Scheduled Inspection	Access	Preventive	Corrective	Access
Control Rod System					
- Control Rod Drive Mechanism	Not Required	N/A	TBD	Replace part	Port (6)
- Control Rod Drive Line	Not Required	N/A	TBD	Replace	Port (6)
Reactor Internals					
Integrally Welded Structures	Visual (VTM3) (1)	Ports(3)	Not planned	Not planned	N/A
-Core Support Structure					
-Core Barrel					
-Passive Core Restraint					
-Coolant Flow Ducts & Plenum					
-Thermal Barrier (Redan)					
Internals attached by other than welding	Visual (VTM3) (1)				
Reactor Support		Ports			
- Support Skirt Welds & Bolts	Visual (VTM3) (2)	& Pit (4)	NA	NA	
Reactor & Containment Vessel	Visual (VTM2) (2) CM	7" gap, Ports(5)	NA	NA	NA
Primary EM Pump	CM	N/A	TBD yrs	Replace	Port (6)
IHX	CM	N/A	Not planned	Replace	Port (6)
DRACS	CM	N/A	Not planned	Replace	Port (6)
Reactor Closure					
- Stationary Deck	CM,Visual(VTM3)		NA	NA	

(1) Primarily dimensional gauging and under-sodium scanning. Maybe supplemented with readily available information from continuous monitoring.
(2) Conducted using a remote operated vehicle with camera and light
(3) Access port in the reactor enclosure head for in-vessel inspection machine access.
(4) Inspection pit around the reactor support skirt
(5) Access port in the upper outer skirt of reactor containment vessel
(6) Plant design shall include provision to permit access for removal of large components. Provisions include ports in the reactor enclosure shield deck hatch and containment, and an extension to the roof to accommodate the handling and removal of large components.

Remote controlled vehicle (RCV) equipped with cameras and light source is used for visual inspection of reactor vessel and guard vessel welds. The RCV may also be equipped with electromagnetic acoustic transducer (EMAT) to perform volumetric inspection of the weld joints in the event structural defects or indications are revealed that may require such additional or alternative examinations. The EMAT does not require a fluid couplant and has the required high temperature rating suitable for the anticipated service conditions. A clearance of 22 cm is provided in the annulus between the reactor vessel and the guard vessel, and entry provision is provided in the reactor vessel support skirt. Figure III-6 provides conceptual depiction of the deployment of RCV for ISI. The RCV with camera can also be used for inspection of the reactor support structure. Access provision from the head access area and the inspection pit around the reactor support skirt provides unobstructed access for the RCV.

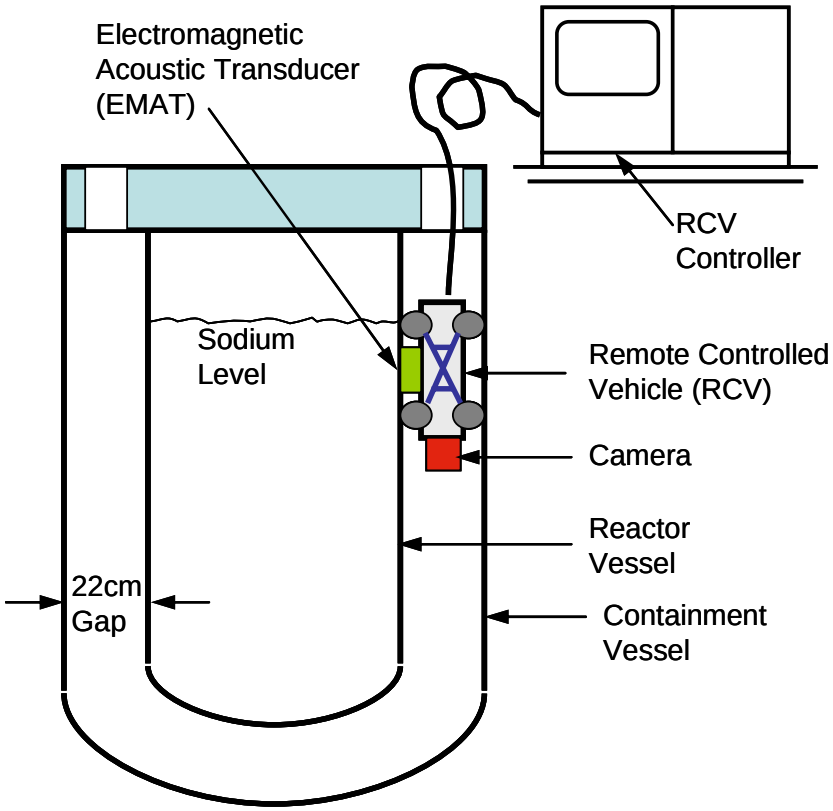

Figure III-6. Remote Inspection of Reactor Vessel Weld

Periscopes with optional camera and light protruding through the reactor deck can be used for visual examination of in-reactor vessel components above the sodium level. It is intended to observe the locations and general conditions of the structural components. Multiple access ports are provided through the reactor deck and closure.

Dimensional gauging is a simple and effective method for checking the integrity of reactor internal structures below the sodium level. In this approach, gauging probe is used for indexing core barrel and other specially provided gauging points on in-vessel components, thus verifying structural integrity of components. However, due to the absence of a rotatable plug and compact in-vessel layout, accessing various locations inside the reactor vessel is not possible with conventional dimensional gauging tools. To resolve such difficulty, a specially designed indexing mechanism, namely in-vessel inspection machine (IVIM), shall be adopted. The mechanism shall be developed in such a way that has 1) multiple degrees-of-freedom mobility to provide dexterous accessibility to a large area, 2) slim structure to fit in the tight in-vessel spaces, and 3) high structural rigidity to render adequate indexing accuracy. Figure III-7 shows a graphical depiction of a conceptual IVIM design based on pantograph mechanism. Entry provisions are provided in the reactor enclosure head for IVIM access to both cold and hot pool areas.

The under-sodium viewing (USV) system consists of one or more ultrasonic scanning transducers, which can be used in imaging mode for mapping under-sodium components, or

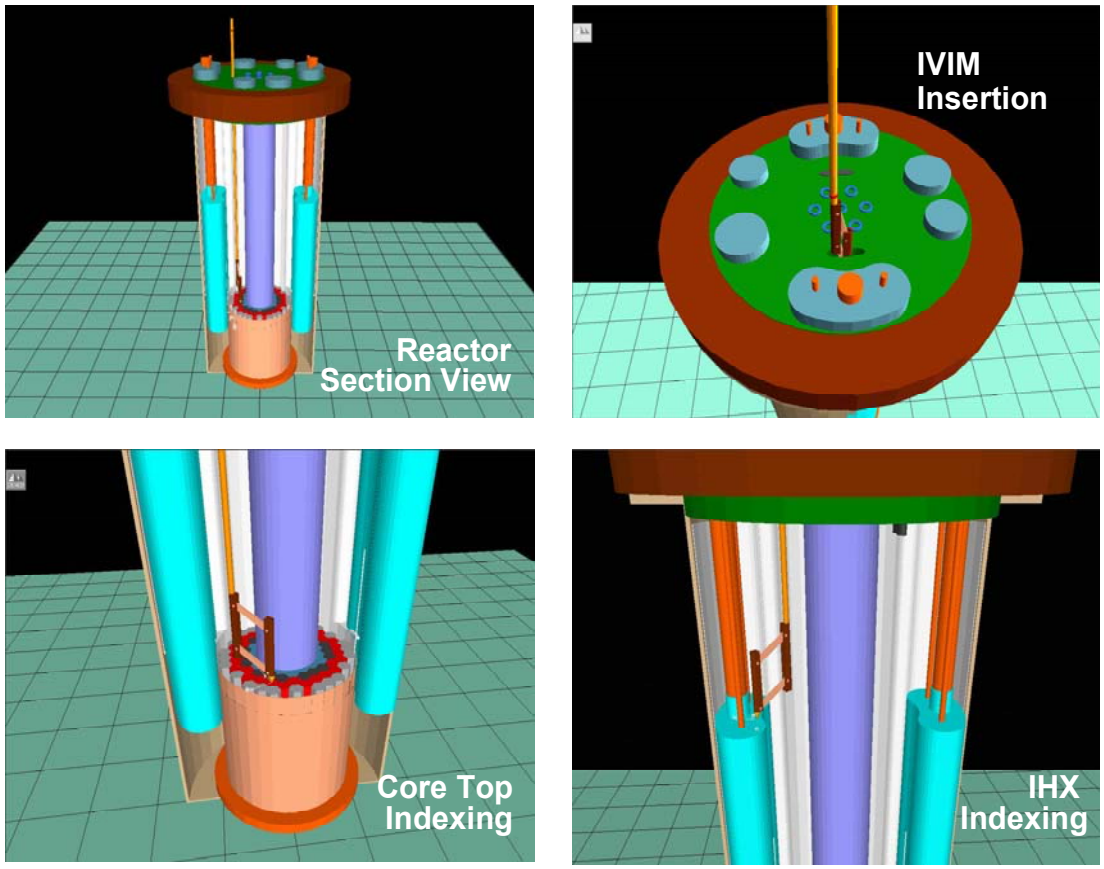

Figure III-7. Dimensional Gausing with In-Service Inspection Machine

in sweeping (ranging) mode to identify the presence of obstacles. The USV system in the hot pool may be used for visual inspection of the upper core former ring, upper end of the core barrel, and portions of the inner redan wall. It can also be used as a core sweep or mapping before and after fuel handling. The USV system in the cold pool may be used to perform scanning and dimensional gauging of the core support structure, the redan structure, and reactor internal piping system. The USV system will be mounted at the distal link of the IVIM and inserted through ISI port in the reactor enclosure head for access to both cold and hot pool areas. The IVIM shall provide interface for the USV. Also, design provisions need to be made for the transducer head to be able to scan the difficult-to-reach areas on the top of the core directly under the upper core structure.

Inspection Plan and Schedule

ISI plan and schedule is established in compliance with ASME B&PV Code Section XI, Division 3. The inspection will normally be conducted during a temporary shutdown of the reactor, and scheduled in accordance with ASME Code.

For inspection of the reactor internals, the ASME Code Table IMB-2500-1 specifies visual examination (VTM-3) or alternative use of continuous monitoring. In accordance with the

schedule in Table IMB-2412-1, 100% of the internal structure will be inspected over a 10 year period.

The sodium surface and in-reactor vessel components above the sodium level will be examined using a periscope with an optional camera and light. For normal ISI, it is not intended that most components will be observed at close range and, thus, a small crack will probably not be detected. Hence, the ISI will look for the effect of such a crack on the integrity of the structure, so that small shifts in position and separation at attachment can be observable. The upper vessel component inspection will be performed three times in ten years, when the reactor is temporarily shutdown. The location of the inspection will switch each inspection interval in order to attain most complete coverage.

For components below the sodium level, the normal ISI approach is based on dimensional gauging and under-sodium viewing. However, direct examinations can be supplemented or replaced by additional, readily available information from continuous monitoring. For instance, continuous monitoring of sodium levels, outlet temperature of a limited number of core assemblies and the pressure in the pump discharge manifold will provide indication of the integrity of the pressurized components (e.g., core barrel, inlet plenum, and primary piping discharge manifold) in hard-to-access areas of the reactor pool as will statistical analysis of EM pump power.

Continuous monitoring will be the primary source of information on the operation of the EM pumps and IHX. Dimensional gauging will be performed by indexing the IVIM on several specified locations on the top of the former ring and other structural components in the hot pool. The technique determines possible shifts in elevation of components. The verification of the proper location of a component, such as the top of the core barrel, can also imply a proper location for the core support structure. If a significant change is indicated by continuous monitoring or dimensional gauging, under-sodium viewing will be used to further investigate the condition. Gauge blocks and gauge marks are set at key locations to serve as reference marks for under-sodium scanning. Inspection will generally be conducted during temporary shutdown of the reactor, and scheduled in such a way that mapping of the entire area will be completed over a 10 year period.

Problems observed through the normal ISI will be further investigated by follow-up examinations. These follow-up examinations are more extensive and may involve removal of components and lowering of the sodium level. The results of the follow-up examination will be used to verify structural failure and to plan detailed maintenance procedures. Maintenance approaches are identified for most of the components in the reactor vessel. However, some major structures do not have outlined maintenance plans because it is considered improbable that a relevant structural failure can be repaired.

The ASME Code Table IMB-2500-1 specifies visual examination (VTM-2) and continuous monitoring of the reactor vessel. Continuous monitoring of the reactor vessel for sodium and gas

leakage will be provided. Sensors and measurement techniques are readily available for this purpose. Periodic visual inspection will be performed so that 33% of the exterior surface welds are inspected in 10 years and, thus, 100% of the reactor vessel will be inspected in 30 years, in accordance with the schedule in Table IMB-2412-1. The visual inspection is performed using a camera and light source, which are mounted on a remotely controlled vehicle (RCV) installed in the annulus between the reactor vessel and the guard vessel, as shown in Figure III-6. It may be necessary to provide cooling of the camera. The RCV will use linked wheels which extend to wedge between the reactor vessel and the guard vessel.

.

The ASME Code Table IMC-2500-1 specifies visual inspection (VTM-3) of 100% of the containment vessel welds during an inspection interval of 10-year period. The inspection will be conducted using a TV camera carried by a ROV. The containment vessel is also required to be continuously monitored for leakage by ASME Code Article IMC-5210, and undergo a leakage rate test by Article IMC-5220. Continuous monitoring of pressure in the reactor vessel/guard vessel annulus provides initial detection of leak. Follow up examinations will consist of remote visual examination of the annulus, and analysis of gas samples taken from the annulus.

The reactor closure will be continuously monitored for leaks, using radiation detectors in the head access area. Analysis of reactor cover gas and the primary sodium purity will provide follow-up indications.

The reactor support in the head access area will be inspected according to ASME B&PV Code Section XI, Division 3. Table IMF-2500-1 specifies the support welds and bolts are to be visually inspected (VTM-3) during each inspection interval. 100% of the reactor support skirt welds and bolts are inspected over every 10-year period, in accordance with the schedule in Table IMB-2412-1. The skirt and welds inspection is performed with remote visual examination using a camera on RCV. The bolt inspection consists of visually inspecting the nut and checking the torque against specified value. If personnel entry is required, proper radiation shielding shall be provided.

K. Seismic Isolation System

When an earthquake occurs, the seismic waves travel through the ground where the reactor is supported causing the reactor structures to shake back and forth along with the ground. Reactor structures must be designed to sustain the inertia force generated by the vibration. The earthquake motion obviously depends on the characteristics of the site where the reactor is located. This makes the seismic design of the reactor site-dependent. One of the design requirements is to modularize the reactor construction to reduce capital cost. The reactor structure design has to be standardized regardless of seismic conditions. To make this standardization feasible the site specific seismic design has to be decoupled from the structural design. This can be achieved by incorporating the base isolation into the reactor structure.

The fundamental principle of base isolation is to provide a layer with low horizontal stiffness between the structure and the foundation so that the structure is decoupled from the horizontal

components of the earthquake motion. This layer gives the reactor structure a fundamental frequency that is much lower than that of the same reactor structure without this soft layer. Also, this fundamental frequency is much lower than the predominant frequencies of the ground motion. As a result; the ground motion transmitted into the structure is modified (the isolator functions as a low pass filter). The high frequency contents in the ground motion will be filtered out along with the high energy associated with these frequencies. Since the base isolator has low horizontal stiffness, a large horizontal displacement will take place during the earthquake. This large displacement needs to be accommodated in the structural design. A moat wall with a seismic gap of 90 cm is built around the reactor structure.

The base isolation system used in the SMFR is the high-damping rubber bearing (HDRB) concept shown in Figure III-8. It is steel laminated elastomeric seismic bearing made from natural rubber. Each bearing is designed to be capable of carrying a vertical load of 320 metric tons. Table III-2 provides a list of the design parameters for the bearing.

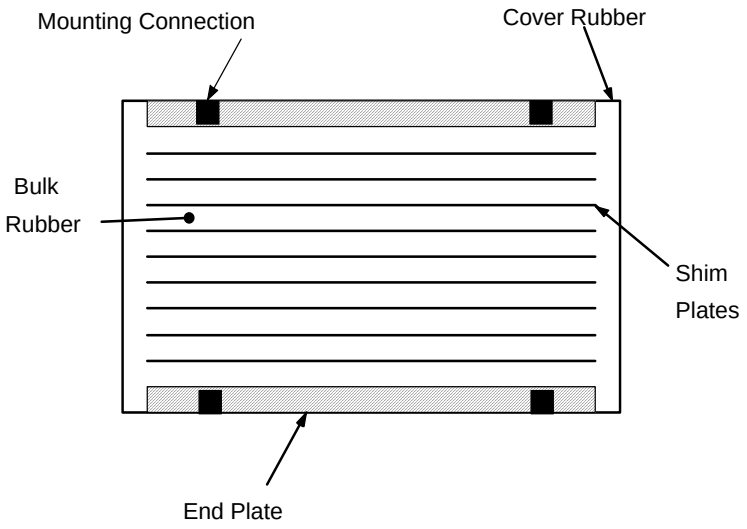

Figure III-8. Laminated Elastomeric Seismic Isolation Bearing

Table III-2. Design Parameters for HDRB Seismic Isolation

Horizontal Frequency	0.5 Hz
Design Shear Strain	100%
Shear Displacement	27.8 cm
Damping Coefficient	>12%
Maximum Shear Strain	300%
Outside Diameter	120 cm
Height	50 cm
Total Rubber Height	27.8 cm
Rubber Layers	29
Steel Shims	28

The weight of reactor structure is estimated to be 11,000 metric tons. A total of thirty-six (36) bearings are used to support the reactor structure. These isolators are housed in between the basement concrete slab and the foundation concrete slab shown in Figure III-9. The arrangement of these isolators is shown in Figure III-10. Each seismic isolator is inserted at the mid-height of a 140 cm by 140 cm reinforced concrete column that transfers the weight of the super-structure through the isolator to the foundation. These columns provide a 150 cm high space for inspection and maintenance. Each isolator unit has a steel fabricated ring surrounding the isolator and attached to the basement concrete slab. These rings function as a physical stop, in case of a higher than expected structural response. This is to avoid collision of the reactor structure and the moat wall.

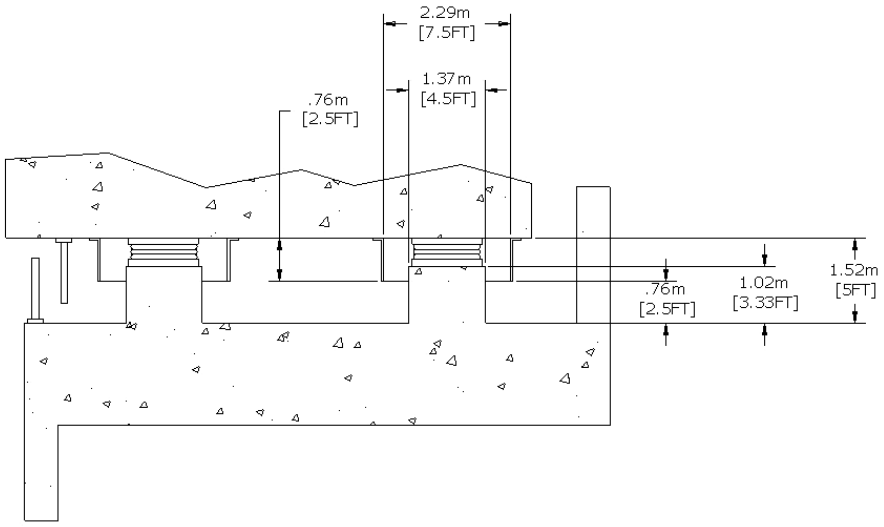

Figure III-9. Seismic Isolation System Layout

The mechanical properties of the rubber bearing are temperature dependent. Its stiffness and damping properties decrease as the temperature increases. The rubber will stiffen in low temperature with the danger of crystallization. To avoid the degradation of the bearing due to ambient temperature, the space housing the isolators is heated to maintain the temperature in the range of 0 °C to 60 °C. Even though the stiffness of the rubber bearing changes significantly when the temperature is below -20 °C, the lower operating temperature is set to be 0 °C for SMFR. This is based on the actual performance of rubber bearings in real earthquakes. During 1995 Kobe earthquake in Japan, the rubber bearings installed in the Matsumura Gumi Laboratory building did not attenuate the ground motion due to the fact that the ambient temperature was 0 °C and the isolator area was not heated. [1]

A preliminary structural/seismic analysis indicates that the maximum stress at the top of the reactor vessel can be reduced by a factor of 8 in a base isolated reactor structure compared with the corresponding fixed-base structure.

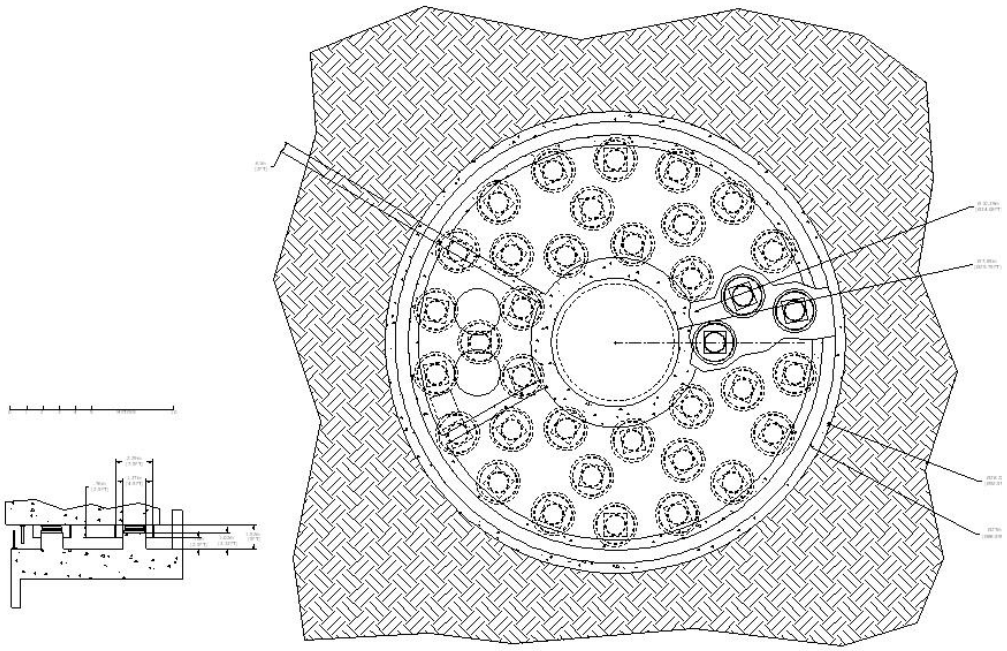

Figure III-10. Seismic Bearing Layout

Elastomeric bearing manufactured from natural rubber can easily exceed a 60-years design life. These types of bearings have been in use for about 40 years for bridges and have proved satisfactory over this period. Shear testing on these old bearings showed an average increase in stiffness of only 7% and also showed that oxidation was restricted to a distance from 10 mm to 20 mm from the surface. [1]

An alternative choice for the base isolation system is the multiple friction pendulum system (MFPS) shown in Figure III-11. [2] It consists of a doubled concave slider and an articulated slider on a spherical surface with a hinge mechanism. The system mimics the kinematics of a pendulum, forcing the structure to rise slightly as it moves horizontally. This movement generates a restoring force to return the super structure back to its original position. The energy is dissipated by friction. The advantage of this system is that the isolated period is independent of the weight of the structure. In additional, since the movement of the structure always starts from the mass center of the structure, the torsional response is minimized. Twenty (20) bearing are needed since each bearing is designed to carry a vertical load of 600 metric tons. The radius of curvature is calculated to be 112 cm for a natural period of 3 seconds. The overall size of the bearing is 100 cm by 100 cm with the height of 35 cm. The concrete column size is 120cm by 120 cm. The isolator is made of stainless steel and its operating temperature is from -125 °C to 250 °C.

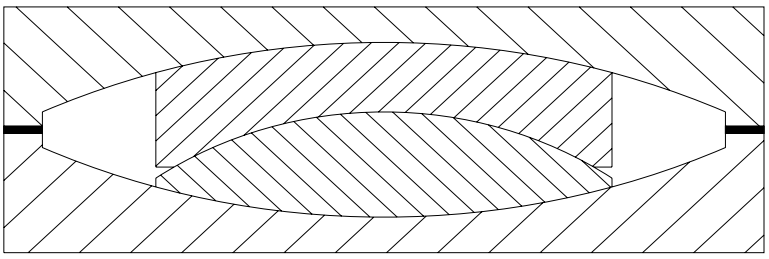

Figure III-11. Multiple Friction Pendulum System

References

1. Trevor E. Kelly, "Base Isolation Structures – Design Guidelines," Holmes Consulting Group Ltd., July 2001.

2. C. S. Tsai, T. C. Chiang and B. J. Chen, "Seismic Behavior of MPFS Isolated Structure under Near-Fault Sources and Strong Ground Motions with Long Predominant Periods," Seismic Engineering-2003, PVP Vol. 466, ASME, Cleveland, Ohio, 2003.

IV. REACTOR CORE

A. Core Configuration

The main goal in core design was to achieve a 30 year lifetime with no refueling. A near zero reactivity swing is required to achieve this design goal without excessive reactivity control requirements or a significant decrease in power density. This necessitates an internal conversion ratio slightly larger than 1.0, which in turn requires a sufficiently high fertile isotope fraction (i.e., low fissile enrichment). For a dense fuel loading design, metal fuel with high volume fraction is selected. To attain a high fuel volume fraction without increasing the core pressure drop, it is necessary to employ a large pin diameter design. The enrichment zoning strategy is adopted to achieve power flattening. To achieve the design goals of proliferation resistance and actinide transmutation, the fuel was based on transuranic elements recovered from high burnup light water reactor (LWR) spent fuel. Low-swelling stainless steel (HT9) cladding was selected because of the high fluence expected during the long life core.

The reference core design has been developed through trade-off and optimization studies, focused on minimizing reactivity swing and flattening radial power distribution over the 30 year core lifetime. The principal design variables investigated include the fuel pin diameter, assembly size, active core height, core configuration, material volume fractions, enrichment zoning and ratios, and lower reflector and fission gas plenum lengths. Key thermal-hydraulic and materials-related design constraints include the fuel smeared density of 75%, peak 2σ cladding inner wall temperature less than 650°C, peak 2σ fuel center line temperature less than the melting temperature of ternary metal fuel, and maximum irradiation damage of in-vessel structures less than 5 dpa.

The reference core is a homogeneous, metal alloy fuel design with 114 assemblies – 48 fuel assemblies, 30 reflector assemblies, 36 shield assemblies, and 7 control rod assemblies. The reference core configuration is shown in Figure IV-1. This core configuration is designed to produce 125 MWt with an average coolant temperature rise of 155°C. The inlet temperature is 355°C, and the bulk outlet temperature is 510°C. The active core height is 100 cm and there are no axial blankets. The coolant pressure drop across pin bundle is 0.058 MPa.

The core life is 30 years with a 90% capacity factor. Three-zone fuel enrichment (i.e., TRU fractions) is used to reduce the radial power peaking and to enhance internal conversion over the 30 year lifetime. The fuel assemblies are grouped into inner, middle, and outer core zones with different enrichments; a relatively low enrichment is used for the inner core to increase the internal conversion. The enrichment zoning is summarized in Table IV-1. The fuel alloy is U-TRU-10%Zr, and the TRU composition is presented in Table IV-2. The fuel alloys are assumed to expand axially 5% due to fission gas induced swelling at the early burnup stage. This expansion is accommodated in the core reactivity design and its impact on neutronics performance parameters is explicitly included.

Flow orificing is provided within the assembly inlet modules that are located within the coolant inlet plenum and core support structure. In this way, flow orificing is not associated with an assembly, but rather with a location within the core layout. Individual assembly orifices are

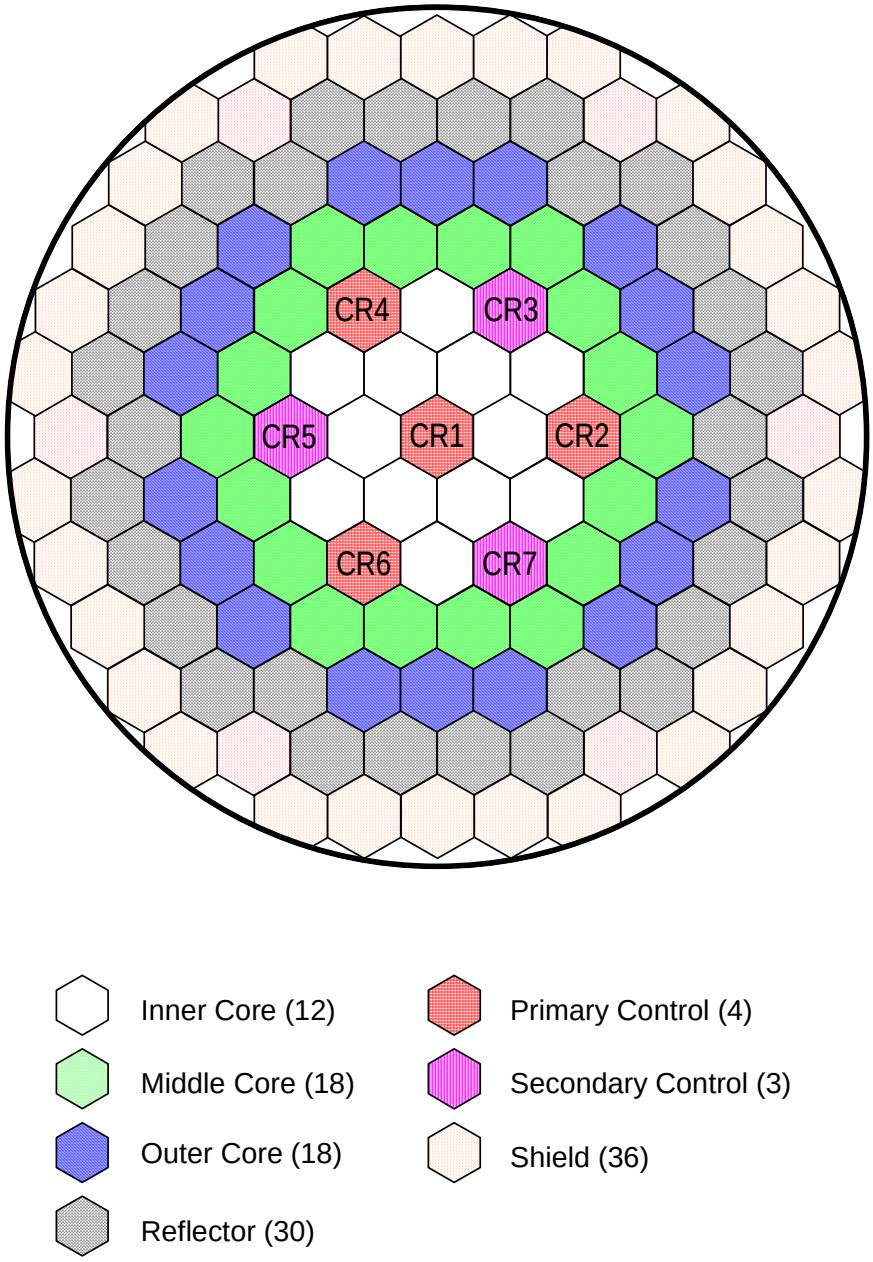

Figure IV-1. Core Configuration of SMFR Reference Design

Table IV-1. Enrichment Zoning

	Inner Core	Middle Core	Outer Core
Relative Enrichment	1.0	1.45	1.55
TRU Content	10.30%	14.93%	15.96%

Table IV-2. TRU Isotopic Composition (%)

Np-237	6.73
Pu-238	2.78
Pu-239	48.92
Pu-240	23.01
Pu-241	6.91
Pu-242	5.00
Am-241	4.64
Am-242m	0.02
Am-243	1.46
Cm-243	0.01
Cm-244	0.49
Cm-245	0.04
Cm-246	0.01

designed such that the peak 2σ cladding mid-wall temperatures at the beginning of life (BOL) and end of life (EOL) are equal.

Two independent sets of control rod assemblies are employed for reactivity control and reactor shutdown. The primary system is composed of one central assembly (CR1) and three assemblies in the third row (CR2, CR4, and CR6), and the secondary system consists of three assemblies in the third row (CR3, CR5, and CR7). Reactivity control for normal operation, load following and shutdown is accomplished by bank (uniform) movement of four primary control rod assemblies in the fuel region of the core.

B. Assembly Design Description

The design of core assemblies maximizes the use of common structural components, with the exception of the assembly internals. All core assemblies use the same hexagonal duct and handling socket. Fuel, shield and control rod assemblies use sealed-type pins to contain the fuel and absorber materials and fission products. Reflector assemblies contain pin bundles of solid HT9 rods. The bottom of fuel pins similarly consist of solid HT9 rods for lower axial shielding. Tables IV-3 thru IV-6 present key assembly design parameters for fuel, reflector, shield, and control rod assemblies, respectively, and Figure IV-2 shows the schematic view of fuel assembly.

Table IV-3. Fuel Assembly Design Data

ASSEMBLY DATA	
Number of Pins per Assembly	127
Assembly Pitch (cm)	22.165
Interassembly Gap (cm)	0.250
Duct Outside Flat-to-Flat Distance (cm)	21.915
Duct Wall Thickness (cm)	0.300
Duct Material	HT9
Assembly Overall Length (cm)	393
PIN DATA	
Fuel Material	U-TRU-10%Zr
Bond Material	Sodium
Cladding Material	HT9
Cladding Thickness (cm)	0.050
Pin Diameter (cm)	1.750
Pin Pitch-to-Diameter Ratio	1.064
Fuel Slug Diameter (cm)	1.429
Fuel Smeared Density (%)	75
Wire-wrap Pitch (cm)	30.48
Wire Diameter (cm)	0.107
Pin Overall Length (cm)	325
Active Core Length (cm)	100
Fission Gas Plenum Length (cm)	150
Lower Shield Height (cm)	75
VOLUME FRACTIONS (%)	
Fuel Slug	0.479
Sodium Bond	0.160
Sodium Coolant	0.227
Structural Material	0.135

Table IV-4. Reflector Assembly Design Data

ASSEMBLY DATA	
Number of Pins per Assembly	91
Assembly Pitch (cm)	22.165
Interassembly Gap (cm)	0.250
Duct Outside Flat-to-Flat Distance (cm)	21.915
Duct Wall Thickness (cm)	0.300
Duct Material	HT9
Assembly Overall Length (cm)	393
PIN DATA	
Pin Material	HT9
Pin Diameter (cm)	2.140
Pin Pitch-to-Diameter Ratio	1.030
Wire-wrap Pitch (cm)	30.48
Wire Diameter (cm)	0.040
Pin Overall Length (cm)	325
VOLUME FRACTIONS (%)	
Structural Material	0.822
Sodium Coolant	0.178

The fuel assembly has an overall length of 393 cm and contains 127 fuel pins arranged in a triangular pitch array. Fuel pins are made of sealed cladding containing a metallic fuel column of 100 cm length. Sodium is filled as the initial thermal bond between the fuel column and the cladding. The fuel pin is helically wrapped with wire. The wire-wrap maintains the pin spacing so that the coolant can flow freely through the pin bundle. A 150 cm long fission gas plenum is located above the fuel slug and sodium bond. The fuel assemblies are 21.92 cm across the outer hex flats and are positioned within the assembly at a 22.17 cm triangular pitch spacing with a 0.25 cm inter-assembly gap. The 100 cm high active core starts at 113 cm from the bottom of the assembly. Immediately below the core is a 75 cm reflector region, with the reflector being an integral part of the fuel pin in the form of an extended fuel pin bottom end cap.

The control rod assembly consists of an absorber bundle contained within a duct. The absorber bundle is a closely packed array of tubes containing compacted boron carbide pellets. The natural boron whose B-10 enrichment is 19.9 atom % is used. The pins are each helically wrapped with wire and bundled into a triangular pitch, hexagonal pattern. The bundle of pins is contained in a thin duct that channels flow through the bundle and protects the pins from damage as they slide within the outer fixed duct. The outer duct of the control rod assembly has the same

Table IV-5. Shield Assembly Design Data

ASSEMBLY DATA	
Number of Pins per Assembly	19
Assembly Pitch (cm)	22.165
Interassembly Gap (cm)	0.250
Duct Outside Flat-to-Flat Distance (cm)	21.915
Duct Wall Thickness (cm)	0.300
Duct Material	HT9
Assembly Overall Length (cm)	393
PIN DATA	
Pin Material	B_4C
B-10 Enrichment in Boron (at. %)	19.9
Bond Material	Helium
Cladding Material	HT9
Cladding Thickness (cm)	0.260
Pin Diameter (cm)	4.664
Pellet Diameter (cm)	3.589
Pellet Fabrication Density (% T.D.)	90
Pellet Smeared Density (%)	75
Pin Overall Length (cm)	325
VOLUME FRACTIONS (%)	
B_4C	0.452
He Bond	0.151
Sodium Coolant	0.184
Structural Material	0.213

external dimensions as the fuel assembly duct except for the nosepiece which has unique discrimination features to preclude inadvertent installation into an unassigned core position. The duct directs coolant flow to the absorber bundle. The control system is designed to be operated with the absorber bundle partially inserted at all times.

C. Core Performance Characteristics

The parameters of interest with respect to core neutronics include the fuel enrichment requirements, fuel burnup, conversion ratio, fuel inventory and mass flow, power and flux distributions, reactivity control requirements and worth, and reactivity feedback coefficients.

Table IV-6. Control Rod Assembly Design Data

ASSEMBLY DATA	
Number of Pins per Assembly	91
Assembly Pitch (cm)	22.165
Interassembly Gap (cm)	0.250
Duct Outside Flat-to-Flat Distance (cm)	21.915
Duct Wall Thickness (cm)	0.300
Duct Material	HT9
Bypass Gap (cm)	0.400
Interior Duct Outside Flat-to-Flat Distance (cm)	20.516
Interior Duct Wall Thickness (cm)	0.300
Assembly Overall Length (cm)	393
PIN DATA	
Pin Material	B_4C
B-10 Enrichment in Boron (at. %)	19.9
Bond Material	Helium
Cladding Material	HT9
Pin Diameter (cm)	1.725
Pin Pitch-to-Diameter Ratio	1.034
Pellet Diameter (cm)	1.406
Pellet Fabrication Density (% T.D.)	90
Pellet Smeared Density (%)	85
Wire-wrap Pitch (cm)	30.48
Wire Diameter (cm)	0.054
Pin Overall Length (cm)	TBD
Pellet Length (cm)	105
Gas Plenum Length (cm)	TBD
VOLUME FRACTIONS (%)	
B_4C	0.332
He Bond	0.059
Sodium Coolant	0.398
Structural Material	0.212

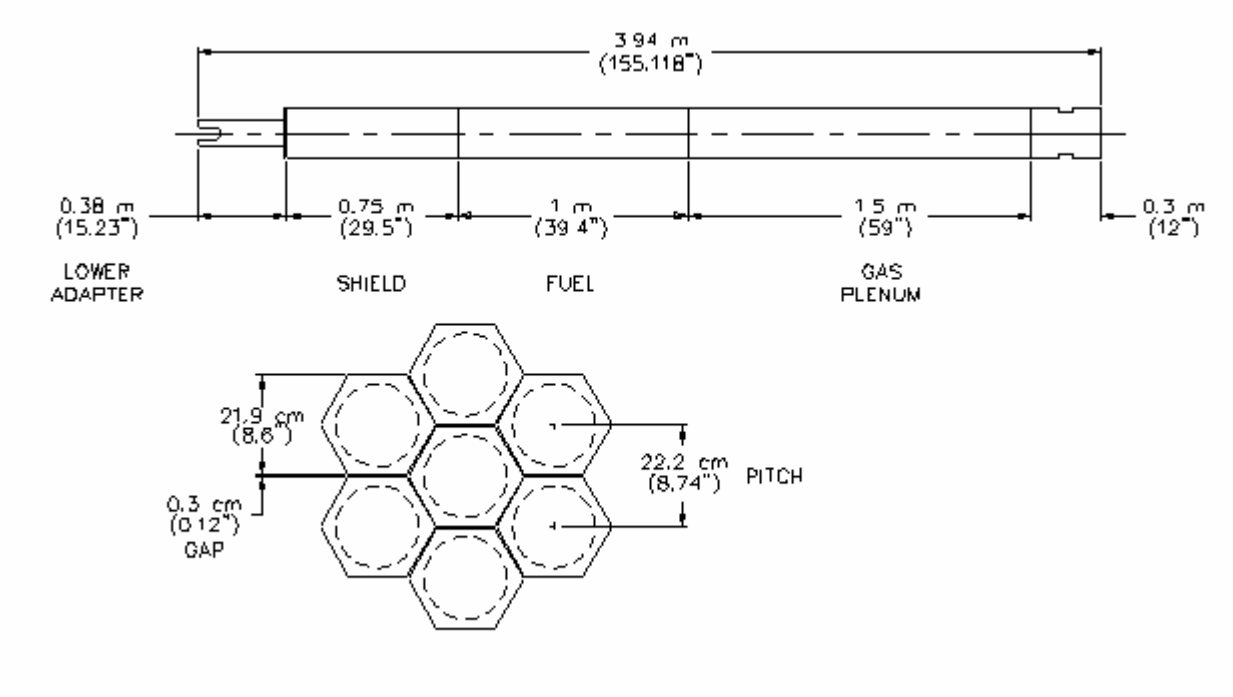

Figure IV-2. Fuel Assembly

Fuel cycle analyses to determine these parameters were performed with the DIF3D/REBUS-3 code system [1-2]. The region-dependent 21-group cross section set generated for the metal fuel core with the ETOE-2/MC^2-2/SDX code system [3-5] based on ENDF/B-V.2 was used.

Equilibrium and non-equilibrium cycle analyses were performed using 3-dimensional hexagonal-z geometry models with individual assemblies. Irradiation swelling of metal fuel and material thermal expansion at operating conditions were modeled by adjusting the hexagonal pitch, axial meshes, and the fuel and structure volume fractions appropriately and by displacing bond sodium into lower part of the plenum. Block nuclide depletion was performed by dividing each fuel assembly into five axial depletion zones. For flux calculations, the hexagonal-z nodal diffusion theory option of DIF3D [6] was mainly employed, and VARIANT transport theory option [7] was used for comparison. The TRU fraction in fuel was first determined from the equilibrium cycle analysis such that k-effective at the beginning of life (BOL) is 1.0, and detailed non-equilibrium cycle analyses with refined burn time intervals were performed using this TRU fraction.

The key core performance characteristics are summarized in Table IV-7. The feed TRU fractions are 10.30, 14.93, and 15.96 wt. % for the inner, middle, and outer core zones, respectively. The total heavy metal inventory is 13,849 kg and the TRU inventory 1,960 kg. The burnup reactivity swing defined here as the difference between the maximum and minimum excess reactivity is only 1.6$ over the 30 year core lifetime. As shown in Figure IV-3, the excess reactivity initially decreases slightly mainly due to axial expansion of the metal fuel, and then increases gradually due to fissile material buildup in the inner core. After reaching its maximum at around 17 effective full power years (EFPY), it decreases monotonically because of the insufficient conversion resulting from reduced fertile material. The average conversion ratio is

Table IV-7. Core Performance Characteristics

Core Lifetime (year)	30
Capacity Factor (%)	90
TRU Fraction in Inner/Middle/Outer Core (wt. %)	10.30/14.93/15.96
Initial Heavy Metal Loading (kg)	13,840
Initial TRU Loading (kg)	1,960
Specific Power (kW/kg)	9.03
Reactivity Swing ($)	1.6
Conversion Ratio	1.005
Peak Fast Fluence (>0.1 Mev, 10^{23} n/cm^2)	5.10
Core Average Power Density (W/cc)	56.5
Power Peaking Factor at BOL/EOL	1.588/1.609
Average/Peak Discharge Burnup (MWd/kg)	86.7/133.2

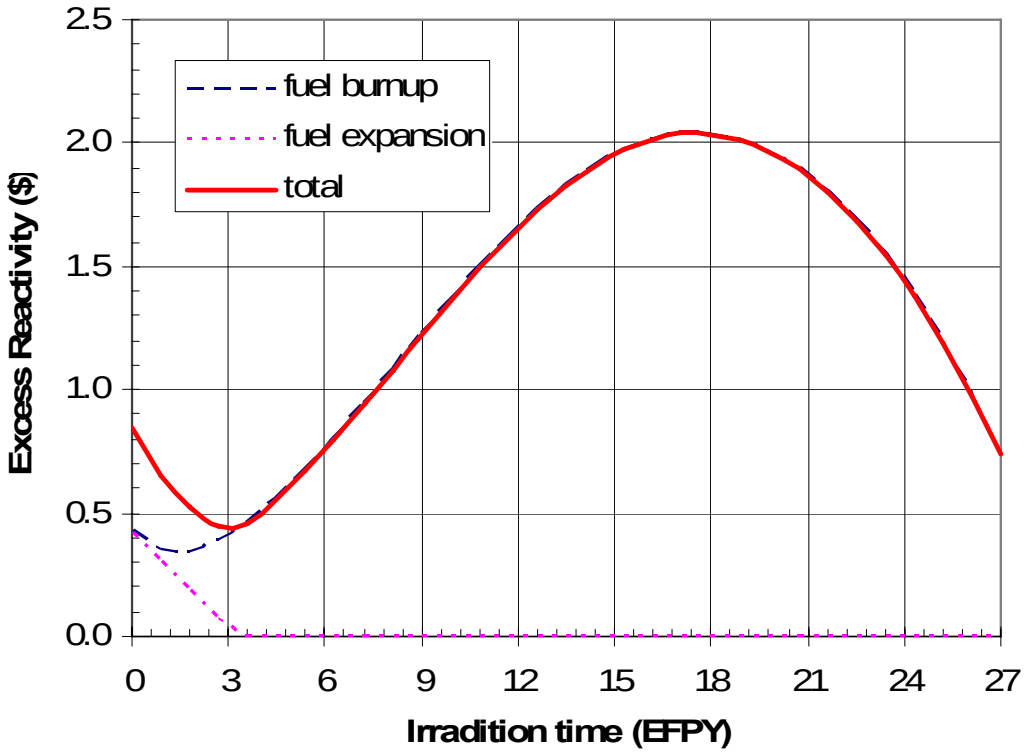

Figure IV-3. Excess Reactivity versus Irradiation Time

1.005. The average discharge burnup is 87 MWd/kg, and the local peak discharge burnup is 133 MWd/kg, lower than the limit of 150 MWd/kg.

Reactivity coefficients and kinetics parameters were calculated for the BOL, MOL (mid of life), and EOL core configurations. The MOL configuration corresponds to 17 EFPY where the excess reactivity attains its maximum value over the core lifetime. A 5% axial growth of metallic fuel was assumed in the MOL and EOL configurations, since virtually all length increase with burnup takes place during the burnup interval before the swelling fuel contacts the cladding, which occurs at ~1% burnup. The coolant, fuel, and structure density coefficients and the coolant void coefficient were determined using the VARI3D perturbation code [8]; the linear perturbation theory option was used for density coefficients, while the exact perturbation theory option was employed for the coolant void coefficient. The effective delayed neutron fraction and prompt neutron lifetime were also calculated using the VARI3D code. The radial and axial expansion coefficients and the control rod worth were determined by direct eigenvalue differences of the base and perturbed conditions using the DIF3D code.

Table IV-8 provides neutron kinetics parameters and reactivity feedback coefficients except for control rod driveline expansion coefficients, which is discussed in Section IV.D. The delayed neutron fractions (β_{eff}) are 0.0039, 0.0036, and 0.0035 at BOL, MOL, and EOL, respectively. The prompt neutron lifetime is about 220 ns throughout the core lifetime. The Doppler coefficients are calculated to be about -0.07 cents/°C and -0.05 cents/°C for flooded and voided sodium cases, respectively. The voided Doppler coefficient is slightly less negative due to the hardened neutron spectrum.

Table IV-8. Neutron Kinetics Parameters and Reactivity Feedback Coefficients

	BOL	MOL	EOL
Delayed Neutron Fraction	0.0039	0.0036	0.0035
Prompt Neutron Lifetime (μs)	0.219	0.216	0.216
Sodium Void Worth ($)	3.83	4.46	4.65
Sodium Density Coefficient (cents/°C)	0.09	0.11	0.11
Fuel Density Coefficient (cents/°C)	-0.51	-0.53	-0.55
Structure Density Coefficient (cents/°C)	0.03	0.04	0.04
Radial Expansion Coefficient (cents/°C)	-0.19	-0.20	-0.20
Axial Expansion Coefficient (cents/°C)	-0.07	-0.07	-0.07
Doppler Coefficient (cents/°C)	-0.07	-0.07	-0.06
Voided Doppler Coefficient (cents/°C)	-0.05	-0.05	-0.05

The reactivity effect of sodium voiding (or density reduction) consists of two principal effects of opposite sign: 1) a negative reactivity due to increased neutron leakage, and 2) a positive reactivity due to hardening of neutron energy spectrum. For a sodium-cooled, Pu-U fueled core, the positive spectral effect over-weighs the negative leakage effect, resulting in a positive sodium void worth. At EOL, the total sodium void worth is 4.65$ when the flowing sodium inside the assembly duct in all axial sections of all the fuel assemblies is voided.

The reactivity effect of expanding core size, either radially or axially, consists of two effects of opposite sign: 1) a negative density effect due to reduced fuel density, and 2) a positive geometry effect from the enlargement of the core that leads to reduction of neutron leakage. For uniform expansion, the net effects are negative, resulting in radial expansion coefficient of about -0.20 cents/°C and axial expansion coefficient of -0.07 cents/°C. The uniform axial expansion coefficient mainly contributes to the axial fuel expansion feedback during transient events. As the fuel temperature rises, axial fuel expansion increases the core height and thus provides a rapid negative reactivity. The uniform radial expansion coefficient accounts for two important inherent reactivity feedback mechanisms: the radial thermal expansion of the grid plate which is governed by the coolant inlet temperature, and the radial thermal expansion of core load pads. Both mechanisms are expected to provide negative reactivity feedback with the rising core temperature.

Calculations for in-vessel structure fast fluence and displacement per atom (dpa) were performed using the TWODANT transport code [9]. Neutron fluxes for BOL and EOL configurations were determined in RZ geometry with S_{16} angular discretization. The fast fluence and dpa were estimated using the average values of BOL and EOL fluxes and 28-group dpa cross sections generated using the NJOY code [10] based on ENDF-VI. In-vessel structure shielding appears to be adequate: peak irradiation damage for the 30-year core lifetime is about 1.5 dpa for the grid plate and less than 0.5 dpa for core barrel.

For core thermal-hydraulic analyses, coupled neutron and gamma heating calculations were performed using the triangular-z finite difference option of the DIF3D code; the gamma source distribution was determined using the GAMSOR code [11]. The sub-channel analysis code SE2-ANL [12] was employed for whole core temperature calculations. Sodium flow is distributed to the assemblies with the overall goal of equalizing pin cladding damage accrual and thus pin reliability. Using 14 orifice groups with six groups for fuel assemblies, assembly flow rates were determined such that the peak 2σ cladding mid-wall temperatures of individual fuel assemblies are equalized over the core lifetime. Hot channel factors are included in temperature predictions to account for core design, analysis, fabrication and operational uncertainties and variations. Hot channel factors for PRISM MOD B design were used for 2σ cladding and fuel temperature calculations.

Figure IV-4 shows the assembly power distributions at BOL and EOL. A significant power shift over the 30 year lifetime is observed; high power region is moved from the outer core at BOL to the inner core at EOL due to the relatively high conversion ratio of the inner core, and the peak EOL-to-BOL assembly power ratio is about 1.56. However, by appropriate coolant flow allocation, all the design constraints are met with enough margins. Figure IV-5 shows the assembly flow rates determined to equalize the peak 2σ cladding mid-wall temperatures over the

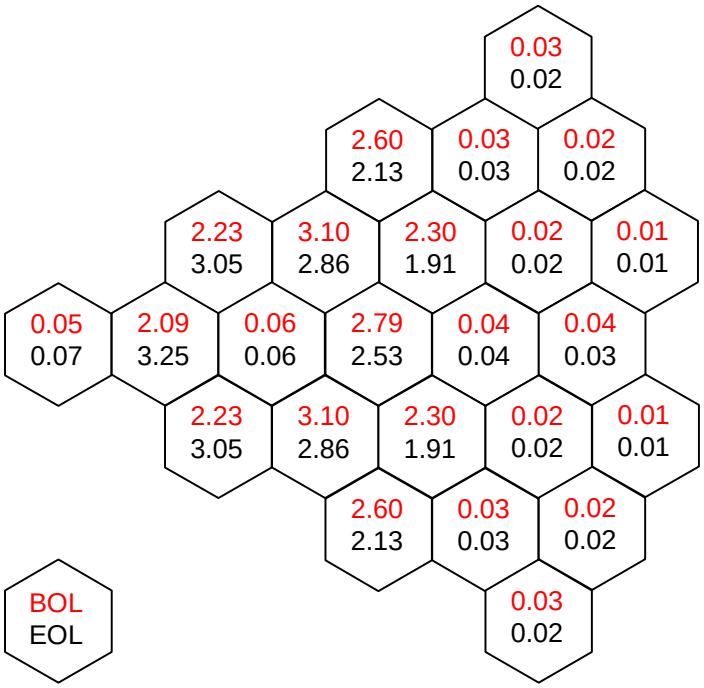

Figure IV-4. Assembly Power Distribution (MW)

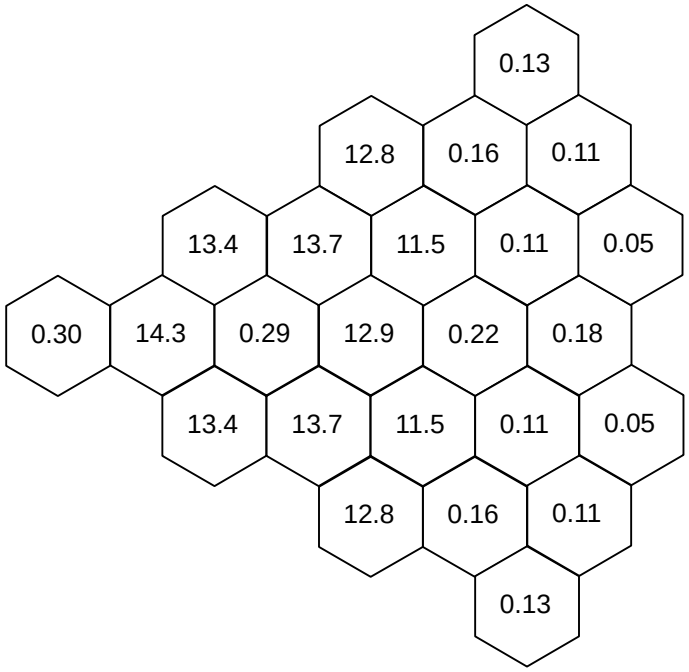

Figure IV-5. Assembly Flow Rates (kg/s)

core lifetime. Figures IV-6 to IV-8 respectively provide the peak 2σ cladding inner wall temperatures, minimum 2σ margins to fuel melt, and mixed mean coolant outlet temperatures of individual assemblies. The peak 2σ cladding inner wall temperature is 632 °C, which is lower than the fuel-clad eutectic temperature (650 °C) by ~18 °C. The peak 2σ fuel center line temperature is lower than fuel melting temperature by ~300 °C. Figure IV-8 also shows that the coolant outlet temperature from an assembly does not differ more than 20°C from average temperature of six surrounding assemblies both at BOL and EOL.

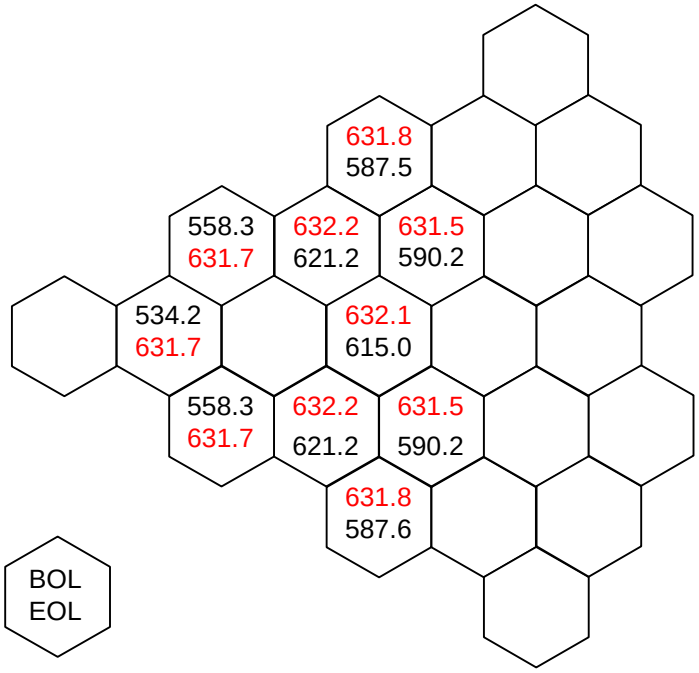

Figure IV-6. Peak 2σ Temperatures at Clad Inner Diameter (°C)

D. Reactivity Control Requirements

As mentioned in Section IV.A, two independent safety-grade reactivity control systems were employed: a primary and a secondary system. The primary system is composed of one central assembly and three assemblies in the third row, and the secondary system consists of three assemblies in the third row. The primary system is required to have sufficient reactivity worth to bring the reactor from any operating condition to cold sub-critical at the refueling temperature with the most reactive control assembly stuck at the full power operating position. Any operating condition means an overpower condition together with a reactivity fault. The maximum worth of a control assembly is used as the base of this reactivity fault. The primary system also serves to compensate for the reactivity effects of the fuel burnup and axial growth of metal fuel. The reactivity associated with uncertainties in criticality and fissile loading is accommodated by the primary control system.

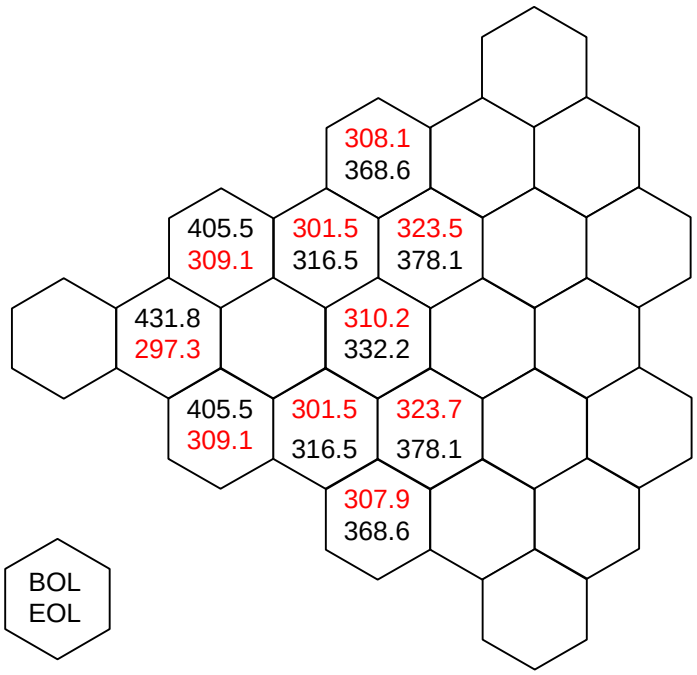

Figure IV-7. Minimum 2σ Margin to Fuel Melt (°C)

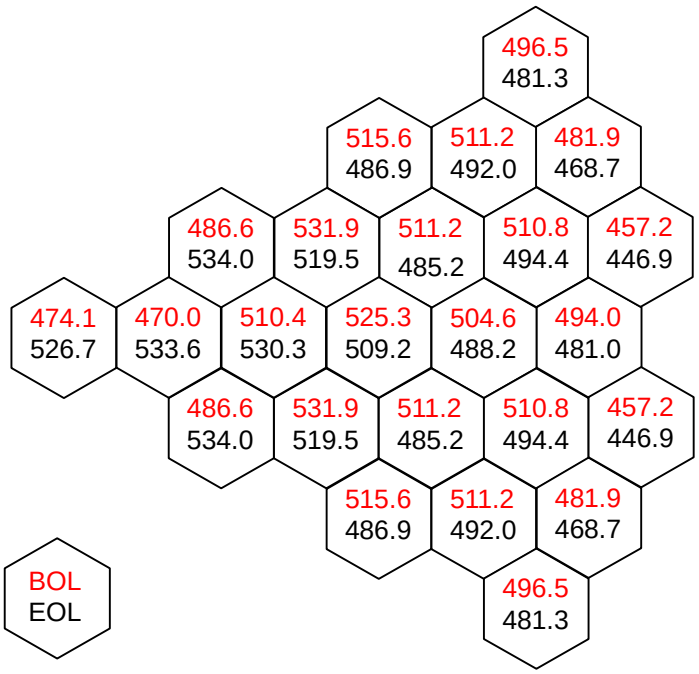

Figure IV-8. Mixed Mean Coolant Outlet Temperature (°C)

The secondary system is required to shut down the reactor from any operating condition to the hot standby condition, also with the most reactive assembly inoperative. It does not have to duplicate the primary system capability to hold down the excess reactivity for the fuel cycle since this excess reactivity is not additional reactivity to be overridden at an accident. Although the secondary system must shut down the reactor without insertion of the primary control assemblies, it is not necessary to assume that the primary assemblies are removed from the core during an accident situation. Since reactivity uncertainties are accommodated by the primary system, they are not a part of the secondary system requirements. However, the reactivity fault is included in the secondary requirements since the secondary system should override the uncontrollable withdrawal of one primary control assembly which is being used for burnup control.

The control requirements include the axial fuel expansion effect and temperature defect. The fuel axial growth is expansion with fuel burnup from the accumulation of fission products. For this assessment, a 5% axial growth is assumed as in the equilibrium fuel cycle analysis. The reactivity effect of this axial growth of fuel is estimated to be 0.42$ at the beginning of core life. Temperature defect is the reactivity change from hot full-power critical to zero power refueling temperature. The calculated temperature defects are summarized in Table IV-9. The refueling and coolant inlet temperatures are assumed to be 205^{o}C and 355°C, respectively. The estimated temperature defects from hot full power to cold shutdown at BOL, MOL, and EOL are 1.01$, 0.88$, and 0.83$, respectively.

Table IV-9. Temperature Defects

Contribution	Hot full power to hot standby			Hot standby to cold shutdown		
	BOL	MOL	EOL	BOL	MOL	EOL
Doppler ($)	0.16	0.17	0.13	0.10	0.11	0.09
Axial expansion ($)	0.23	0.15	0.16	0.15	0.10	0.10
Radial expansion ($)	0.43	0.45	0.47	0.28	0.30	0.31
Sodium density ($)	-0.21	-0.25	-0.26	-0.14	-0.16	-0.17
Total ($)	0.61	0.53	0.50	0.40	0.35	0.33

The calculated control rod assembly worth is presented in Table IV-10 for various combinations of control rod assemblies. As discussed in Section IV.C, the high power region is moved from the outer core at BOL to the inner core at EOL due to the relatively high conversion ratio of the inner core. As a result, the control assembly worth increases with burnup. Note that at BOL, the worth of a control assembly in row 3 is larger than the central assembly.

Table IV-10. Control Rod Assembly Worth ($)

	Number of inserted CRs	BOL	MOL	EOL
Primary System				
CR 1 (central assembly)	1	2.61	4.98	5.64
1 assembly in row 3	1	2.63	3.59	3.78
2 assemblies in row 3	2	5.74	7.87	8.30
CR 1 & 1 assembly in row 3	2	4.85	8.25	9.14
All 3 assemblies in row 3	3	10.08	13.68	14.41
CR 1 & 2 assemblies in row 3	3	7.70	12.27	13.42
All 4 assemblies	4	11.89	18.04	19.55
Secondary System				
1 assembly in row 3	1	2.63	3.59	3.78
2 assemblies in row 3	2	5.74	7.87	8.30
All 3 assemblies	3	10.08	13.68	14.41

The transient over-power initiators were estimated from the reactivity worth curves of primary system control assemblies. To account for the control assembly interaction effects, the maximum worth of a control assembly was determined by withdrawing the most reactive control assembly from the configuration where all the primary control assemblies in rows 1 and 3 are inserted. Figures IV-9 to IV-11 show the primary system reactivity worth curves at BOL, MOL, and EOL, respectively. The solid curve shows the core reactivity as a function of control rod tip position from the bottom of active core for the case where all the primary control assemblies are moving together. The dash-dotted curve corresponds to the case where the most reactive assembly is located at the top of active core and the other assemblies are moving together. The dotted curve is the reactivity worth curve of the most reactive control assembly, which is one of the control assemblies in row 3.

The total worth of this maximum worth control assembly is 4.2$, 5.8$, and 6.1$ at BOL, MOL, and EOL, respectively. At the full power operating condition, only the fuel cycle excess reactivity is held down by the primary control system. As a result, the reactivity held down by inserted control assemblies at full power operating condition is 0.7$, 2.3$, and 1.1$ at BOL, MOL, and EOL, respectively. The reactivity addition by the accidental withdrawal of the most reactive control assembly is 0.18$, 0.51$, and 0.16$ at BOL, MOL, and EOL, respectively.

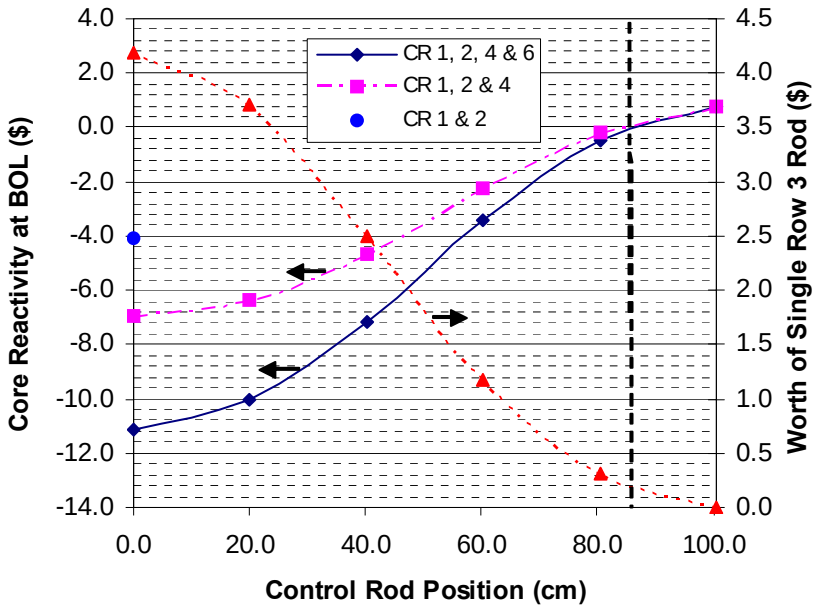

Figure IV-9. Reactivity Worth of Primary Control System at BOL

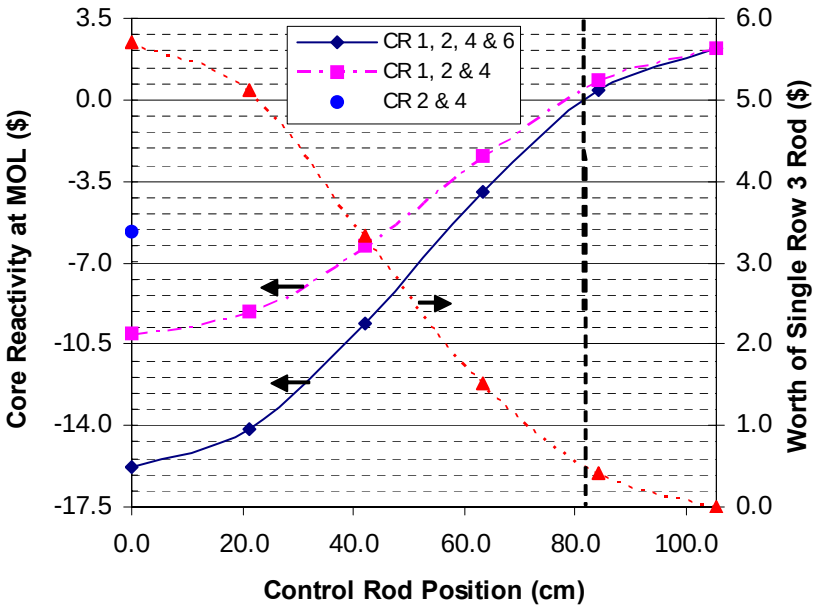

Figure IV-10. Reactivity Worth of Primary Control System at MOL

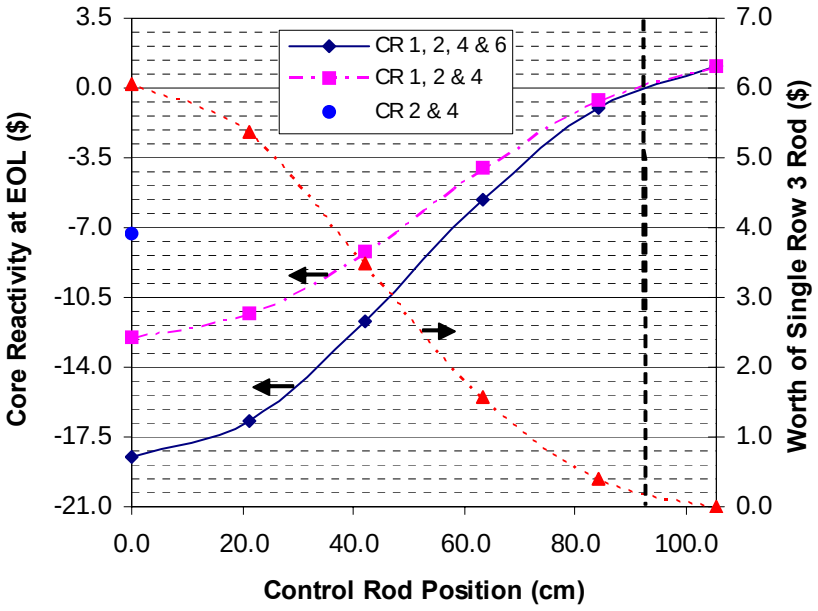

Figure IV-11. Reactivity Worth of Primary Control System at EOL

Table IV-11 summarizes the reactivity worth requirements for both primary and secondary control systems. The overpower margin is allocated to permit the reactor to operate at 115% of the rated power and is equivalent to 15% of the temperature defect from hot full power to hot standby (i.e. power defect). The fuel cycle excess reactivity attains its maximum at MOL and is 2.04$. Since the fuel cycle analysis was performed with expanded core geometry, the reactivity associated with the axial fuel growth is added at BOL. The uncertainties consist of 50% of total burnup reactivity, 20% of total temperature defect, 20% of fuel axial growth, and assumed 1.00$ each for criticality prediction and fissile loading (tolerance for manufacture uncertainty). These uncertainties were adopted from the PRISM design except for the burnup reactivity uncertainty, which was increased from 15% to 50%. The total uncertainty is obtained by statistically combining all uncertainties.

In Table IV-12, the control requirements are compared with the reactivity available in the control system. The shutdown margins of primary and secondary systems were determined with the assumption that the most reactive assembly is stuck. The shutdown margins of primary and system are 4.12$, 7.02$, and 10.15$ at BOL, MOL, and EOL, respectively. The shutdown margins of the secondary system are somewhat smaller, resulting in 3.97$, 6.75$, and 7.57$ at BOL, MOL, and EOL, respectively.

The control rod worth curves presented in Figures IV-9 to IV-11 also provide control rod driveline expansion coefficients for reactivity feedback. Control rod expansion coefficients are governed principally by the total rod worth and the insertion depth of the rods. As discussed above, the control assembly worth increases with burnup, since the high power region is moved from the outer core at BOL to the inner core at EOL due to the relatively high conversion ratio of

the inner core. As a result, the control rod expansion coefficient also increases with burnup. The calculated control rod expansion coefficients are 6.0, 8.8, and 9.6 cents/cm at BOL, MOL, and EOL, respectively.

Table IV-11. Reactivity Worth Requirements ($) of Primary and Secondary Control Systems

	Primary system			Secondary system		
	BOL	MOL	EOL	BOL	MOL	EOL
Temperature defect	1.01	0.88	0.82	0.61	0.53	0.50
Full power to hot standby	0.61	0.53	0.50	0.61	0.53	0.50
Hot standby to refueling	0.40	0.35	0.33			
Overpower margin	0.10	0.09	0.08	0.10	0.09	0.08
Fuel cycle excess reactivity	0.85	2.04	0.74			
Burnup reactivity	0.42	2.04	0.74			
Fuel axial growth	0.42					
Uncertainties (RMS)	1.44	1.75	1.47			
Temperature defect (20%)	0.20	0.18	0.16			
Burnup reactivity (50%)	0.21	1.02	0.37			
Fuel axial growth (20%)	0.08					
Criticality prediction	1.00	1.00	1.00			
Fissile loading	1.00	1.00	1.00			
Reactivity fault	0.18	0.51	0.16	0.18	0.51	0.16
Total	3.58	5.26	3.26	0.88	1.12	0.73

Table IV-12. Comparison of Control Requirements and Available Reactivity Worth

	Primary system			Secondary system		
	BOL	MOL	EOL	BOL	MOL	EOL
Number of control assemblies	4	4	4	3	3	3
Reactivity worth of system ($)	11.89	18.04	19.55	10.08	13.68	14.41
Worth of 1 stuck assembly ($)	4.20	5.57	6.13	5.23	5.81	6.11
Reactivity worth available ($)	7.70	12.27	13.42	4.85	7.87	8.30
Maximum requirement ($)	3.58	5.26	3.26	0.88	1.12	0.73
Shutdown margin ($)	4.12	7.02	10.15	3.97	6.75	7.57

References

1. K. L. Derstine, "DIF3D: A Code to Solve One-, Two-, and Three-Dimensional Finite-Difference Diffusion Theory Problems," ANL-82-64, Argonne National Laboratory (1984).

2. B. J. Toppel, "A User's Guide to the REBUS-3 Fuel Cycle Analysis Capability," ANL-83-2, Argonne National Laboratory (1983).

3. "NESC No. 350 ETOE-2 Documentation," National Energy Software Center Note 83-84, August 25, 1983.

4. H. Henryson II, B. J. Toppel, and C. G. Stenberg, "MC^2-2: A Code to Calculate Fast Neutron Spectra and Multigroup Cross Sections," ANL-8144, Argonne National Laboratory (1976).

5. W. M. Stacey, Jr., et al, "A New Space-Dependent Fast-Neutron Multigroup Cross Section Preparation Capability," *Trans. Am. Nucl. Soc*., **15**, 292 (1972).

6. R. D. Lawrence, "The DIF3D Nodal Neutronics Option for Two- and Three-Dimensional Diffusion Theory Calculations in Hexagonal Geometry," ANL-83-1, Argonne National Laboratory (1983).

7. G. Palmiotti, E. E. Lewis, and C. B. Carrico, "VARIANT: VARIational Anisotropic Nodal Transport for Multidimensional Cartesian and Hexagonal Geometry Calculation," ANL-95/40, Argonne National Laboratory (1995).

8. C. H. Adams, "Specifications for VARI3D – A Multidimensional Reactor Design Sensitivity Code," FRA-TM-74, Argonne National Laboratory (1975).

9. R. E. Alcouffe, F. W. Brinkley, D. R. Marr, R. D. O'Dell, "User's Guide for TWODANT: A Code Package for Two-Dimensional, Diffusion-Accelerated, Neutral-Particle Transport," LA-10049-M, Los Alamos National Laboratory (1990).

10. R. E. MacFarlane, "NJOY 99/2001: New Capabilities in Data Processing," presentation at the Workshop on Reactor Physics and Analysis Capabilities for Generation IV Nuclear Energy Systems, Argonne National Laboratory, Argonne, February 18-19, 2003.

11. R. N. Hill, "Coupled Neutron-Gamma Heating Calculations," Intra-laboratory Memo, Argonne National Laboratory, February 2, 1988.

12. W. S. Yang, "Fortran 77 Version of SE2-ANL," Intra-laboratory Memo, Argonne National Laboratory, March 3, 1993.

V. PRIMARY HEAT TRANSPORT SYSTEM

The primary heat transport system consists of the primary sodium pumps, the primary piping, the core barrel and redan assembly, and the intermediate heat exchanger. The components are configured in a manner to provide forced primary coolant flow through the reactor core and through the intermediate heat exchanger, thereby transferring the nuclear heat from the reactor core to the intermediate heat transport system and ultimately to the power conversion system. The following sections describe these components.

A. Primary Sodium Pumps

The primary sodium pump, shown in Figure V-1, is a standard single stator, single pass, annular linear induction pump that provides the primary coolant flow to the inlet plenum. There are two primary pumps located and submerged in the cold pool section of the reactor vessel. The inlet of the primary pump is located at a higher elevation in the reactor vessel than the pump discharge. A shroud located outside of the stator provides a duct that allows for taking suction from the bottom portions of the cold pool. Once the pump is turned on, it takes suction towards the bottom of the primary tank and the sodium flows up and around the stator windings.

The sodium then enters the inlet to the primary pump at the top of the pump. The sodium flows down through the annular gap between the stator and the inner iron core. The primary sodium is then discharged from the pump into the discharge header where the flow is split into three downcomer pipes that supply primary sodium to the inlet plenum. There are no moving parts in the sodium pump and therefore maintenance is minimal. The pump is designed to withstand the high temperatures encountered in the reactor vessel during normal and off-normal transient conditions. The primary pump assembly can be removed from the reactor vessel. A bus bar feeds power through the reactor vessel enclosure to the pump stator windings. Table V-1 gives design information for the primary sodium pumps.

Table V-1. Electromagnetic Pump Design Parameters

Power (kW)	360
Mass (kg)	1,980
Pole Count	10
Coil Count	60
Temperature (C)	355
Volumetric flow rate (m3/s)	0.383
Discharge Pressure	200
Length (m)	2.75
Shroud outer diameter (m)	0.84

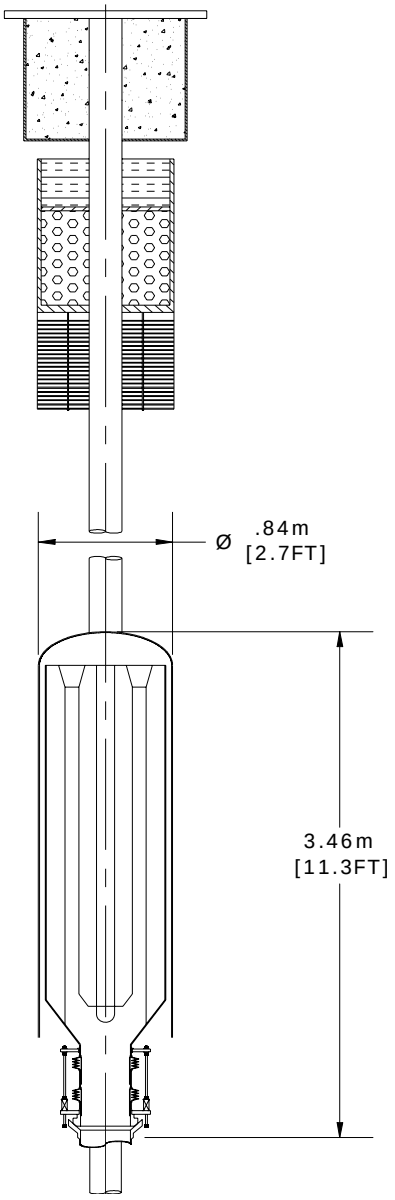

Figure V-1. Electromagnetic Primary Sodium Pump

B. Primary Piping

The primary piping consists of a main header with three permanent pipes, each leading from one of the two primary electromagnetic pumps. The main header is connected to a flexible coupling. The other pipe end is welded to the core inlet plenum. Each primary piping assembly is supported to take the appropriate mechanical, thermal and hydraulic loads. The pump hangs from the reactor vessel enclosure and is connected to the inlet pipe header by a special, nonrigid, easily disconnected, low leakage articulated coupling. This articulated core inlet pipe coupling is shown in Figure V-2.

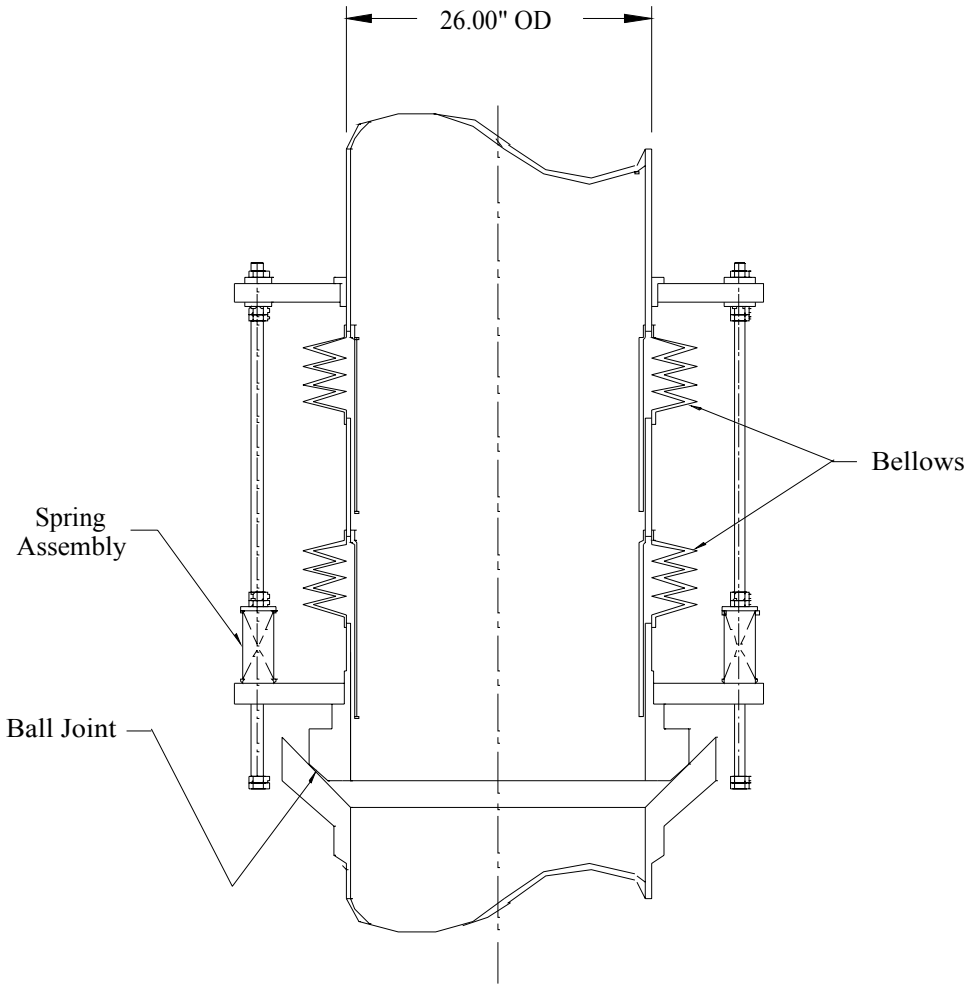

Figure V-2. Articulated Core Inlet Pipe Coupling

The coupling allows lateral and vertical movement without losing metal-to-metal contact, and accommodates relative displacements between the pipe and the pump. The coupling has a slip joint to extend or retract the coupling length with a ball joint at the bottom end. The ball joint at the bottom end is unattached and connects with the mating seat on the reactor core vessel inlet plenum pipe. During installation, the pump is lowered vertically into the reactor vessel. When the bottom ball joint contacts with the mating seat on the inlet plenum pipe, the coupling is compressed creating spring pressure in the coupling. The spring pressure maintains the coupling in position and seals the ball joint against the mating joint of the inlet plenum pipe.

The coupling allows the pump to be removed or installed without cutting the inlet pipe. The coupling can permit some leakage, but must provide flexibility to accommodate thermal movements, be sufficiently stable to avoid flow induced vibrations, and accommodate seismic loads. No valves or movable flow control devices are part of the internal piping. Pipe insulation is not required.

C. Core Barrel and Redan Assembly

The core barrel and redan assembly (see Figure III-5) is a single integrated unit that provides the internal structure for the reactor core assemblies and provides a barrier between the hot and cold sodium pools. The core barrel is a right circular cylinder fabricated from stainless steel. It is attached to the inlet plenum and lower support structure. It also provides support for the core restraint system.

The redan is a single integrated unit that separates the hot pool from the cold pool, and provides for communication of the hot sodium from the discharge of the reactor core to the inlet of the intermediate heat exchanger. It consists of multiple plates welded together that form a contoured shape around the intermediate heat exchangers and the upper internal structure.

The intermediate heat exchangers and upper internal structure are located within the redan. The primary pumps and DRACS heat exchangers are located outside the redan in the cold pool. The redan contains the hot sodium from the core outlet and helps to minimize leakage from the hot sodium to the cold sodium sides of the redan.

The redan is supported vertically by and seal welded to the core barrel and is a permanent structure within the primary reactor vessel. A mechanical Labyrinth seal between the IHX and redan reduces the leakage of hot primary sodium from the hot pool into the cold pool.

D. Intermediate Heat Exchanger

The IHXs transfer heat from the radioactive sodium coolant in the primary heat transport system to the nonradioactive sodium coolant in the intermediate heat transport system. Two sodium-to-sodium heat exchangers rated at 62.5 MWt each are used to transfer the 125 MWt core power at full-power conditions corresponding to core inlet and outlet temperatures of 355 and 510˚C, respectively.

There are several factors that are important in the evaluation of the overall IHX design. These factors include material of construction, tube configuration (straight vs. bent), shell vs. tube-side primary flow, elevation of the IHX within the primary system, shape of the IHX (in plan view), primary flow-side pressure drop (i.e., low pressure loss is needed to ensure adequate natural convection primary sodium flow during loss-of-flow events), and the possible inclusion of a second internal coil near the upper region of the IHX to serve as a shutdown heat removal system. The various design choices that have been made, along with the underlying rationale for these choices, are described below.

The heat exchanger arrangement selected is a shell-and-tube counter-current flow arrangement with the primary flow on the shell-side, and secondary sodium flow on the tube side. Major features of these heat exchangers are graphically depicted in Figure V-3, while key design information is provided in Table V-2. The tube-side secondary flow was selected to simplify cleaning of the heat exchanger tubes in the event of a leak in the CO_2 Brayton cycle system.

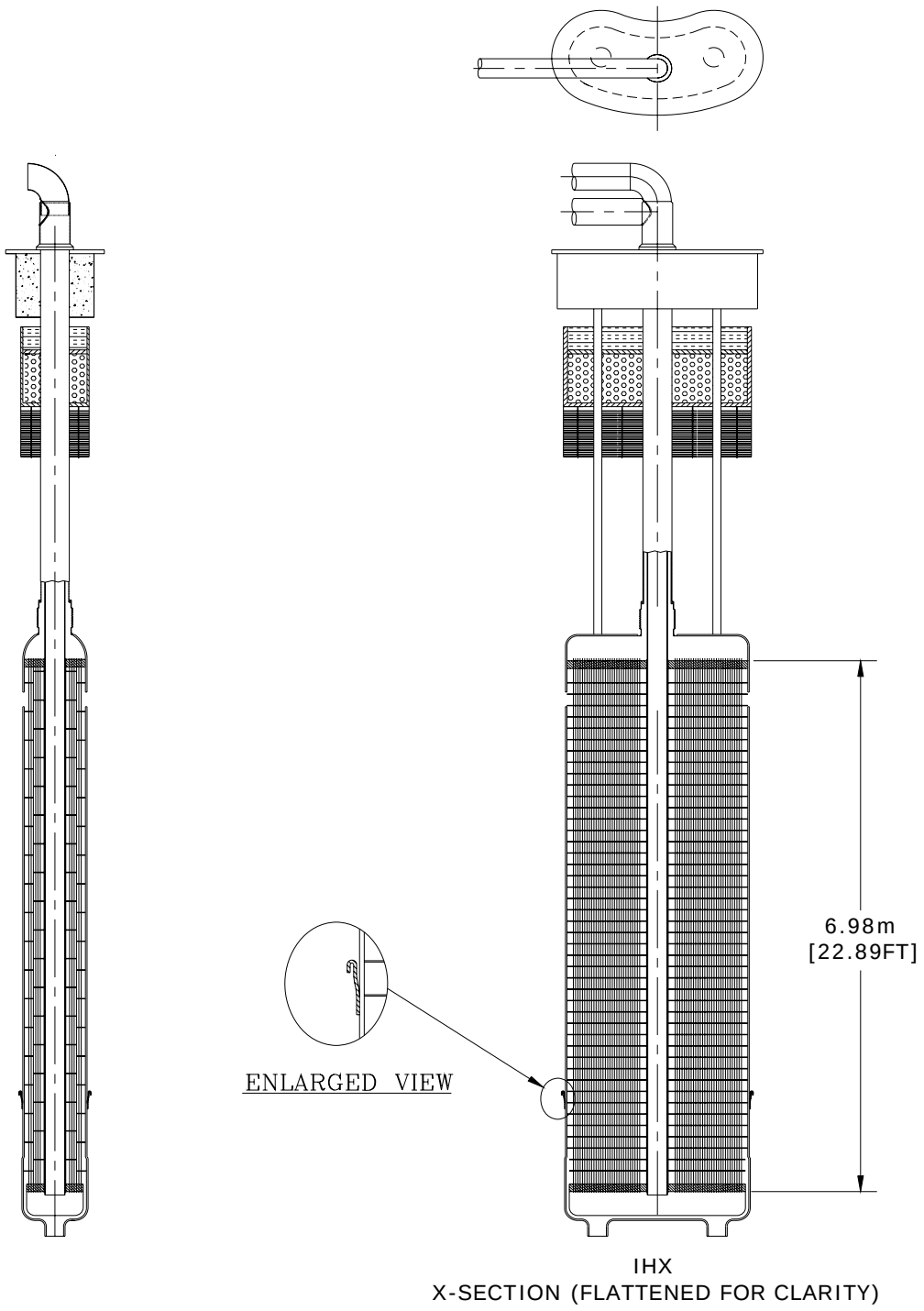

Figure V-3. Intermediate Heat Exchanger

Table V-2. Intermediate Heat Exchanger Design Parameters

Heat transfer capacity	62.5MWt
Heat transfer area	875 m^2
Primary sodium temperature inlet	510 ˚C
Primary sodium temperature outlet	355 ˚C
Primary sodium mass flowrate	314 kg/s
Secondary sodium temperature outlet	342 ˚C
Secondary sodium temperature inlet	497.6 ˚C
Secondary side sodium mass flowrate	314 kg/s
Tube outer diameter	1.59cm
Tube wall thickness	0.889mm
Tube Pitch	2.75 cm
Tube length	7 m
Number of tubes	2500
Upper Tube Sheet – Area	1.64 m^2
Upper Tube Sheet – Thickness	75 mm
Lower Tube Sheet – Area	1.64 m^2
Lower Tube Sheet – Thickness	75 mm
Downcomer piping – OD	25.4 cm
Downcomer piping – thickness	9.1 mm
Downcomer piping – length	12.5 m
Outlet piping – OD	30.48 cm
Outlet piping – thickness	9.5 mm
Outlet piping – length	5.65 m
Shell Baffle plates – thickness	6.4 mm
Shell Baffle plates – quantity	18
IHX shell side pressure drop	3.3 kPa
IHX tube side pressure drop	5.3 kPa
Shell height	7.84 m
Shell outside circumference	5.42 m
Shell thickness	19 mm
Cross-sectional area	1.7 m^2
Material	9Cr-1Mo tubes

As show in Figure V-3, each IHX is vertically suspended from two rigid pipes that are welded to the IHX shroud. These pipes extend upward from the hot pool and are welded to the underside of a removable integral plug in the reactor vessel head. The IHXs are located within the redan, which is contoured (in plan view) to accommodate the kidney-shaped IHX design that has been selected to minimize the reactor vessel diameter.

Primary sodium enters the shell side of each IHX through a series of 20 cm diameter circular openings in the shell approximately 30 cm below the upper tube sheet. These openings allow sodium from the hot plenum to enter the IHX with minimal head loss. Also, having the sodium entering the IHX below the upper tubesheet minimizes the thermal shock to the relatively thick tubesheet during transients. The primary sodium then flows downward through the shell and exits the IHX approximately 30 cm above the lower tubesheet (again to minimize thermal shock) through two 25 cm diameter pipe connections that pass through the redan to the cold plenum.

The piping connections between the IHX shell and redan contain seals to prevent sodium bypass from the hot to cold pools. Minor leakage of these seals is permissible. As shown in Figure V-3, the shell side includes a series of horizontally mounted, disk and donut-type baffle plates uniformly spaced at 37 cm intervals along the length of the tube bank. Aside from providing lateral support for the tubes, these plates promote cross-flow and mixing that enhances thermal performance on the shell side (primary sodium side). The plates are made from 6.4 mm steel plate and occlude ~50 % of the vertical flow path at each plate location.

As shown in Figure V-3, cold intermediate sodium enters the IHX through a central 25.4 cm downcomer. The downcomer delivers the cold sodium through the lower tube sheet into a header manifold, where it then turns 180º and rises through the tube bank in counter current flow to the shell side primary sodium. The hot intermediate sodium exits the tubes into an upper header manifold, and then flows through an annular riser which is concentric to the downcomer. The downcomer is double walled with an annular gap for thermal insulation between the hot and cold streams. As shown in Figure V-3, both the downcomer and the annular riser pipes are equipped with bellows just above the shroud to accommodate any differences in thermal expansion between the piping and the body of the IHX itself (each unit is rigidly attached to the removable plug in the reactor vessel head). The upper tube sheet is welded to the shroud, while the lower tube sheet floats. Thus, the design accommodates differential thermal expansion within the tube bank also.

The inner wall of the shell operates near the bulk temperature of the sodium in the hot plenum. Since primary sodium flow is on the shell side of the IHX, there is no need for an insulating annulus to eliminate heat losses to the bulk sodium or to alleviate high thermal stresses in the shell.

Modified 9Cr-1Mo steel was chosen as the material of construction primarily because the thermal conductivity is higher than that of the austenitic steels such as Type 304 stainless steel. Since the heat transfer in sodium-to-sodium heat exchangers can be dominated by the tube wall thermal resistance, using modified 9Cr-1Mo steel results in considerable reduction in the required heat transfer area. The use of Type 304 stainless steel tubes would result in the need for as much as 20% more heat transfer area as compared to modified 9Cr-1Mo tubes with the same design characteristics. In addition, modified 9Cr-1Mo has a lower thermal expansion coefficient compared to Type 304 stainless steel. The higher thermal conductivity material results in lower temperature differences in component sections and, coupled with the reduced thermal expansion, results in lower thermal stresses in structural members. This is advantageous during thermal transients. Straight tubes are selected to simplify fabrication and reduce flow induced vibration problems.

The design of the IHX has been selected such that the primary flow of sodium on the shell side provides a low pressure drop. Low pressure drop on the primary side is important from two viewpoints: 1) minimizing the pressure-related structural requirements for the IHX shell, and 2) promoting the ability to establish natural circulation of the primary sodium in the case of a loss-of-flow event. Adequate natural convection flow for shutdown heat removal is essential. The DRACS shutdown heat removal system relies on natural circulation of the primary sodium through the core and IHX to the sodium pool surrounding the core barrel. Thus, the IHX has been sized and positioned to locate the primary sodium inlet below the faulted sodium level (primary sodium leak from the primary vessel to the annulus between it and the guard vessel).

To support the ongoing design improvement, the balance of this section is devoted to providing a parametric set of calculations for evaluating the overall size of the IHXs required to transfer the core thermal power to the intermediate sodium. The number of IHX tubes is treated as the independent variable. The required tube length is then calculated as the key model output, and the minimum IHX cross-sectional area is given by tube unit cell cross-sectional area multiplied by the total number of tubes. This approach provides the overall IHX size to be selected on the basis of the available cross sectional area, or the available elevation space, whichever is desired. In addition, the pressure drops on the shell and tube sides are calculated using standard techniques in order to facilitate pump selection and design considerations. The friction coefficient is evaluated as a function of the flow Reynolds number from well known correlations valid for fluid flow in smooth tubes. Tube bank entrance and exit loss coefficients are simply assumed to equal 0.5 and 1.0, respectively. Pressure loss on the shell side is calculated with a simple, empirically based model that includes the effects of the baffle plates. This model was calibrated against the EBR-II IHX pressure loss data, since the EBR-II heat exchangers included baffle plates.

In the analysis, the forced convection heat transfer coefficients on shell and tube sides is calculated using the well-known Lockhart-Martinelli correlation which was developed on the basis of forced convection heat transfer from liquid metals:

$$Nu = \frac{hD}{k} = 5.0 + 0.025\left(\mathrm{Re}\,\mathrm{Pr}\right)^{0.8}$$

where

Nu	=	Nusselt number,
h	=	forced convection heat transfer coefficient,
D	=	equivalent diameter of flow channel,
	=	tube ID for tube-side flow,
	=	4xflow area/wetted perimeter for shell side,
Re	=	Reynolds No. = $\rho uD/\mu$,
Pr	=	Prandlt Number = $\mu c/k$,
u	=	flow velocity,
k	=	thermal conductivity,
ρ	=	density ~ 832 kg/m^3,
c	=	specific heat ~ 1283 J/kg-ºC, and
μ	=	viscosity ~ 2.76x10^{-4} kg/m-s.

For pitch-to-diameter ratios of > 1.1, the above correlation results in errors of no more than 10 % on the shell side of the IHX.

The tube diameter and pitch were selected to be identical to the PRISM IHX design. For completeness, the calculations were carried out assuming two different temperature differences between the primary and secondary sides: $\Delta T = 10^{\circ}C$, and $\Delta T = 5^{\circ}C$. In both cases, the temperature rise across the secondary side of the IHX was held constant at $\Delta T = 170\ ^{\circ}C$. The thermal conductivity of the 9Cr-1Mo tubes was set equal to 28 W/m-˚C.

The results of the calculations are shown in Figures V-4 thru V-7, which provide the planar area, tube length, and pressure drop across shell and tube sides vs. number of HX tubes. The current vessel design provides ~1.64 m^2 of cross sectional area to accommodate each IHX. Thus, from Figure V-4, an IHX with a total of ~ 2500 tubes is selected to fit into the available planar area. From Figure V-3, for the case of $\Delta T = 10^{\circ}C$ between the primary and secondary sides, the active tube length must be ~ 7 m to achieve the target thermal rating of 62.5 MW per IHX. This fixes the minimum required elevation space that needs to be available to accommodate the IHXs. From Figures V-5 and V-6, the pressure drop across the primary and secondary sides of the tube bank are found to be 3.3 and 5.3 kPa, respectively, for the assumed 10˚C temperature differential.

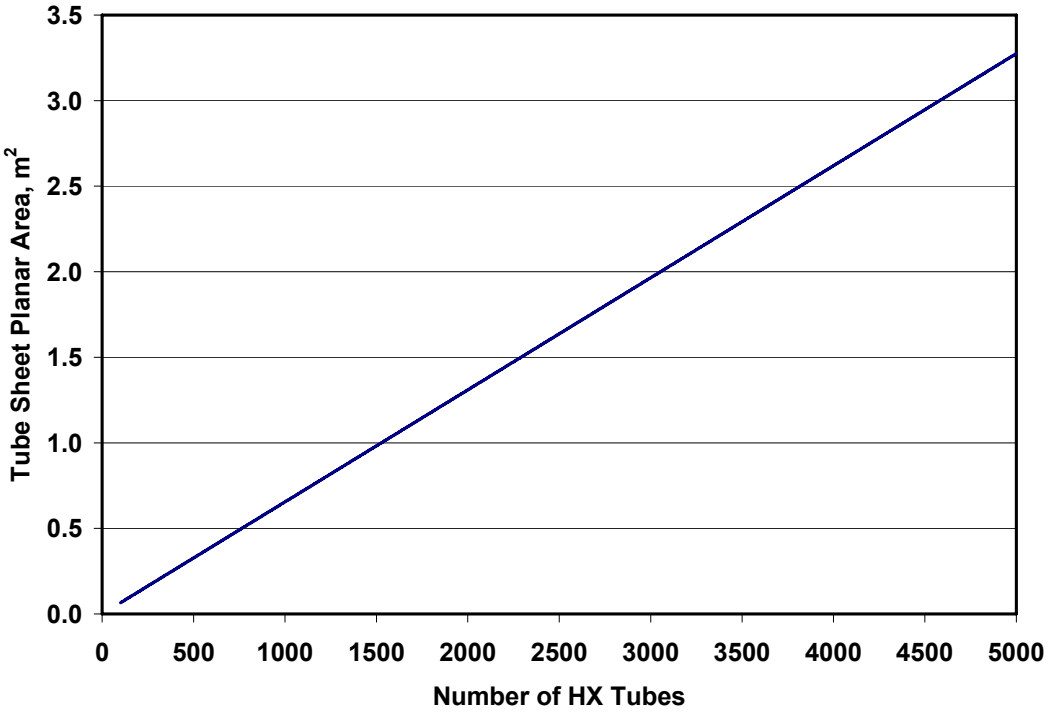

Figure V-4. Tube Sheet Planar Area vs. No. of Tubes for 5 and 10 ˚C ΔT's Between Primary and Secondary Na Outlet Temperatures

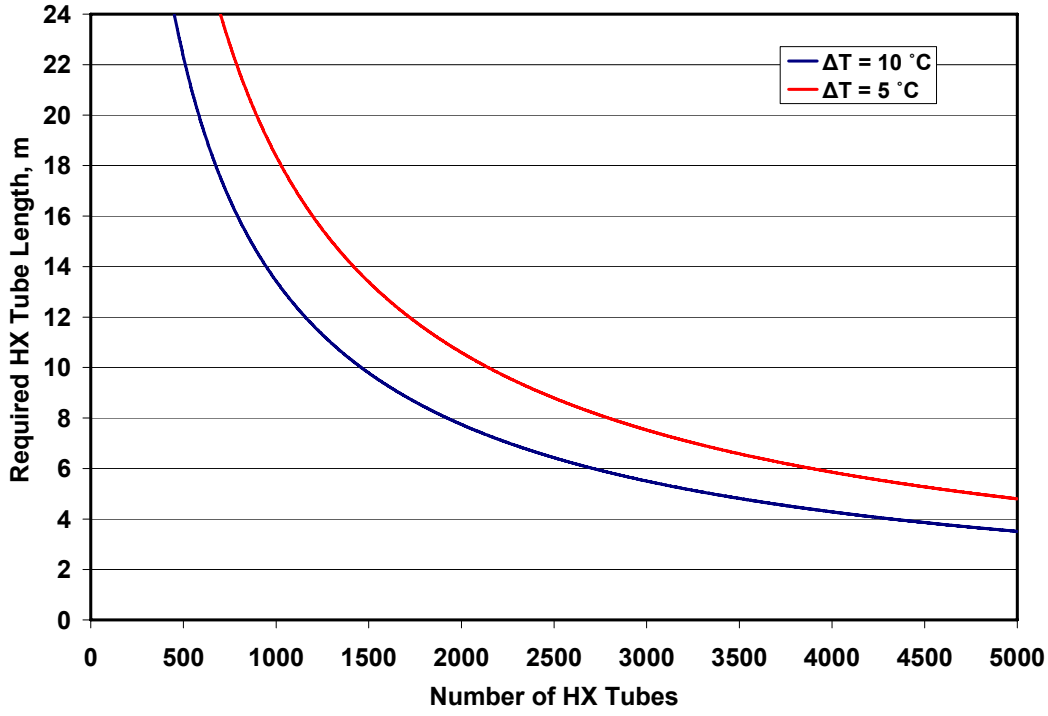

Figure V-5. IHX Tube Length vs. No. of Tubes for 5 and 10 ˚C ΔT's Between Primary and Secondary Na Outlet Temperatures

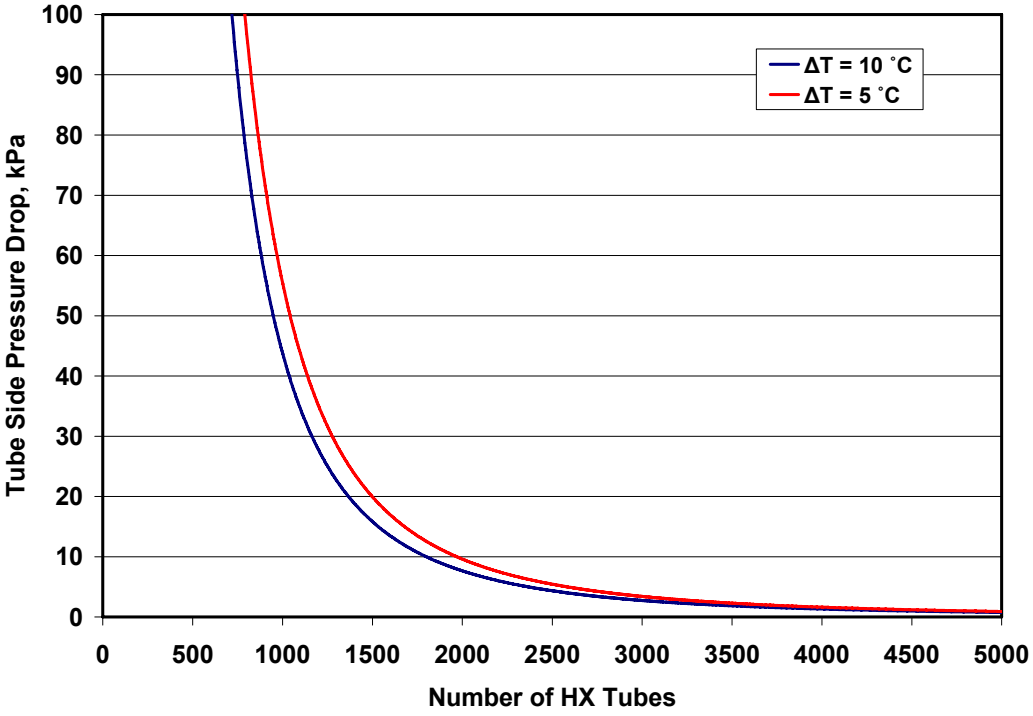

Figure V-6. Secondary (Tube) Side ΔP vs. No. of Tubes for 5 and 10 ˚C ΔT's Between Primary and Secondary Na Outlet Temperatures

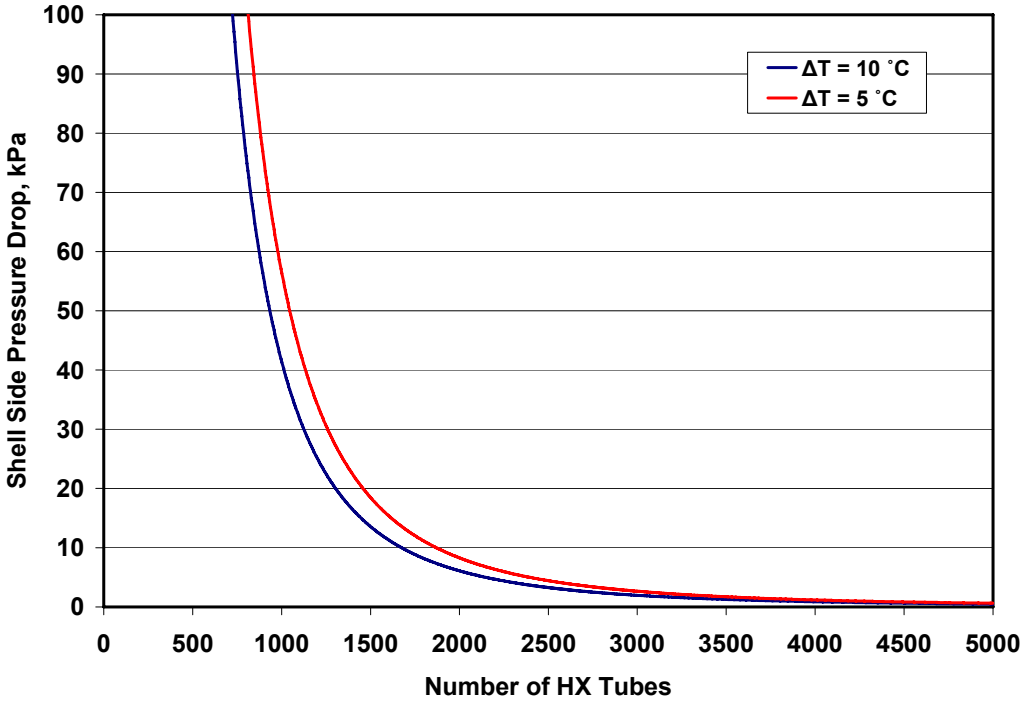

Figure V-7. Primary (Shell) Side ΔP vs. No. of Tubes for 5 and 10 ˚C ΔT's Between Primary and Secondary Na Outlet Temperatures

VI. INTERMEDIATE HEAT TRANSPORT SYSTEM

The intermediate heat transport system provides an isolation coolant circuit between the primary reactor coolant and the supercritical carbon dioxide Brayton cycle power conversion system. This intermediate circuit prevents leaks in the sodium-to-CO_2 heat exchanger from directly impacting the reactor. The intermediate heat transport system consists of the intermediate sodium pump, the intermediate piping, the sodium-to-CO_2 heat exchanger, and the auxiliary sodium systems.

A. Intermediate Sodium Pump

The intermediate pump is similar to the primary sodium electromagnetic pump in design. The intermediate pump does not contain the shroud around the pump as in the primary pump.

B. Intermediate Piping

The intermediate piping extends from the outlet of the IHX and includes the hot and cold leg piping in the intermediate circuit. The piping has heat tracing to prevent the sodium from freezing. The piping has a 25.4cm outer diameter and is made from Type 316 stainless steel. The intermediate piping is located on the nuclear island.

C. Sodium-CO_2 Heat Exchanger

There are two sodium-to-CO_2 heat exchangers, in which heat is transferred from the sodium in the intermediate circuit to the CO_2 in the supercritical CO_2 Brayton cycle. The sodium-to-CO_2 heat exchangers incorporate compact printed circuit heat exchangers (PCHEs). Printed circuit heat exchangers have been selected for the following reasons:

- Potential for reducing the volume occupied by the sodium-to-CO_2 heat exchangers as well as the heat exchanger mass relative to traditional shell-and-tube heat exchangers,
- Potential for enhanced reliability and reduced requirements for inspection by elimination of the potential for failure of the boundary between the sodium and CO_2 streams. Each PCHE is effectively a monolithic block of stainless steel, containing embedded flow channels. The concerns about tube failures typical of shell-and-tube heat exchangers are not present.

Each PCHE is assumed to be manufactured by hot isostatic pressuring of plates of austenitic stainless steel into which semicircular channels have been chemically etched. Austenitic stainless steel is selected for its resistance to corrosion by both CO_2 and sodium. The individual etched plates are diffusion bonded together by heating to a sufficiently high temperature in the presence of a sufficiently high pressure. The plate stacking arrangement for a general PCHE is illustrated in Figure VI-1, developed by the PCHE manufacturer, Heatric Division of Meggitt (UK) Ltd. The sodium and CO_2 streams are assumed to flow through alternating rows of semicircular channels as shown in Figure VI-2, also from Heatric. The sodium and CO_2 flow through the alternating rows of channels in opposite directions providing for countercurrent heat exchange.

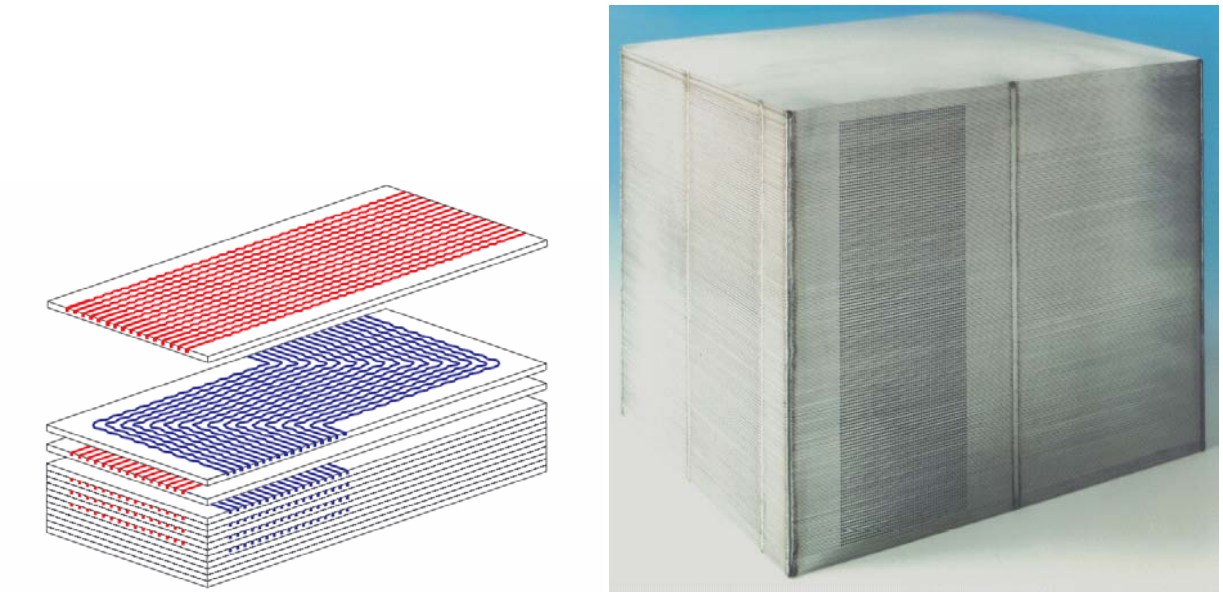

Figure VI-1. Illustration of Stacking of Chemically Etched Plates for Diffusion Bonding to Form Core of Printed Circuit Heat Exchanger (Heatric Division of Meggitt (UK) Ltd.)

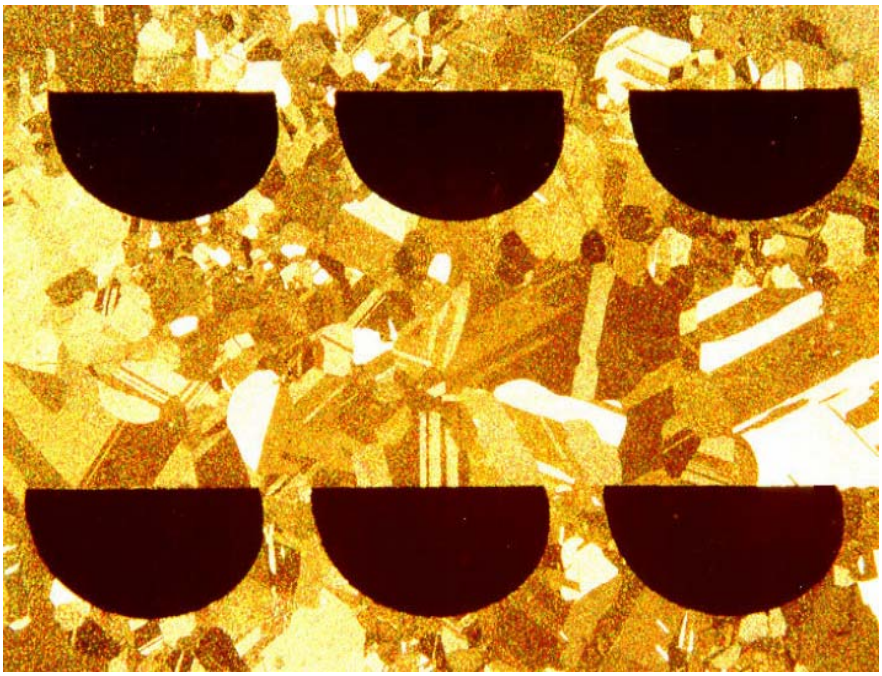

Figure VI-2. Example of Printed Circuit Heat Exchanger Core with Rows of Semicircular Channels (Heatric Division of Meggitt (UK) Ltd.)

Currently, the PCHE manufacturing process limits the width of each plate incorporated into a PCHE to 0.6 m. On the other hand, the length dimension is flexible as individual PCHE core blocks can be welded together. Headers are then welded onto the completed full-length core. Each semicircular channel is selected to have a diameter of 2.0 mm, a lateral pitch of 2.4 mm, and a plate thickness of 1.6 mm. A semicircular channel diameter of 2.0 mm is determined on the basis that for this minimal size, the effects of oxide layer growth upon austenitic stainless steel due to oxidation will not significantly degrade either the heat transfer performance or the strength of the stainless steel ligaments between the sodium and CO_2.

Based upon deterministic heat transfer calculations, it is determined that the PCHEs belonging to the HXs provide sufficiently high cycle efficiency when the channel length is selected to be 4.0 m. From the calculational results, it is also found that for the combined two HXs, 12 PCHEs arranged in a parallel flow configuration provide sufficiently high cycle efficiency. Thus, each HX consists of 6 PCHEs where each PCHE is 4.0 m long and 0.6 m wide in directions normal to the flows.

Table VI-1 shows the detailed parameters of the sodium-to-CO_2 HXs. Figure VI-3 shows the schematic view of the two sodium-to-CO_2 heat exchangers.

Table VI-1. Sodium-to-CO_2 Heat Exchanger Design Parameters (per PCHE)

Heat transfer capacity	10.42	MWt	
Unit side 1	0.6	m	
Unit side 2	0.6	m	
Unit length	4	m	Effective for heat transfer
Sodium channel diameter	2	mm	Semi-circular channel
Sodium plate thickness	1.6	mm	
Sodium channel pitch	2.4	mm	
CO_2 channel diameter	2	mm	Semi-circular channel
CO_2 plate thickness	1.6	mm	
CO_2 channel pitch	2.4	mm	
Material	SS316		
Number of sodium channels	46750		
Number of CO_2 channels	46750		
Void fraction	40.9	%	From channels
Sodium temperature inlet	497.6	^oC	
Sodium temperature outlet	342	^oC	
Sodium flow rate	52.4	kg/s	
CO_2 temperature inlet	337.9	^oC	
CO_2 temperature outlet	479.3	^oC	
CO_2 pressure inlet	19.93	MPa	
CO_2 pressure outlet	19.67	MPa	
CO_2 flow rate	60	kg/s	
Efficiency	88.6	%	(Tc,out-Tc,in)/(Th,in-Tc,in)
Metal mass	6.75	tonnes	
CO_2 mass	46.5	kg	

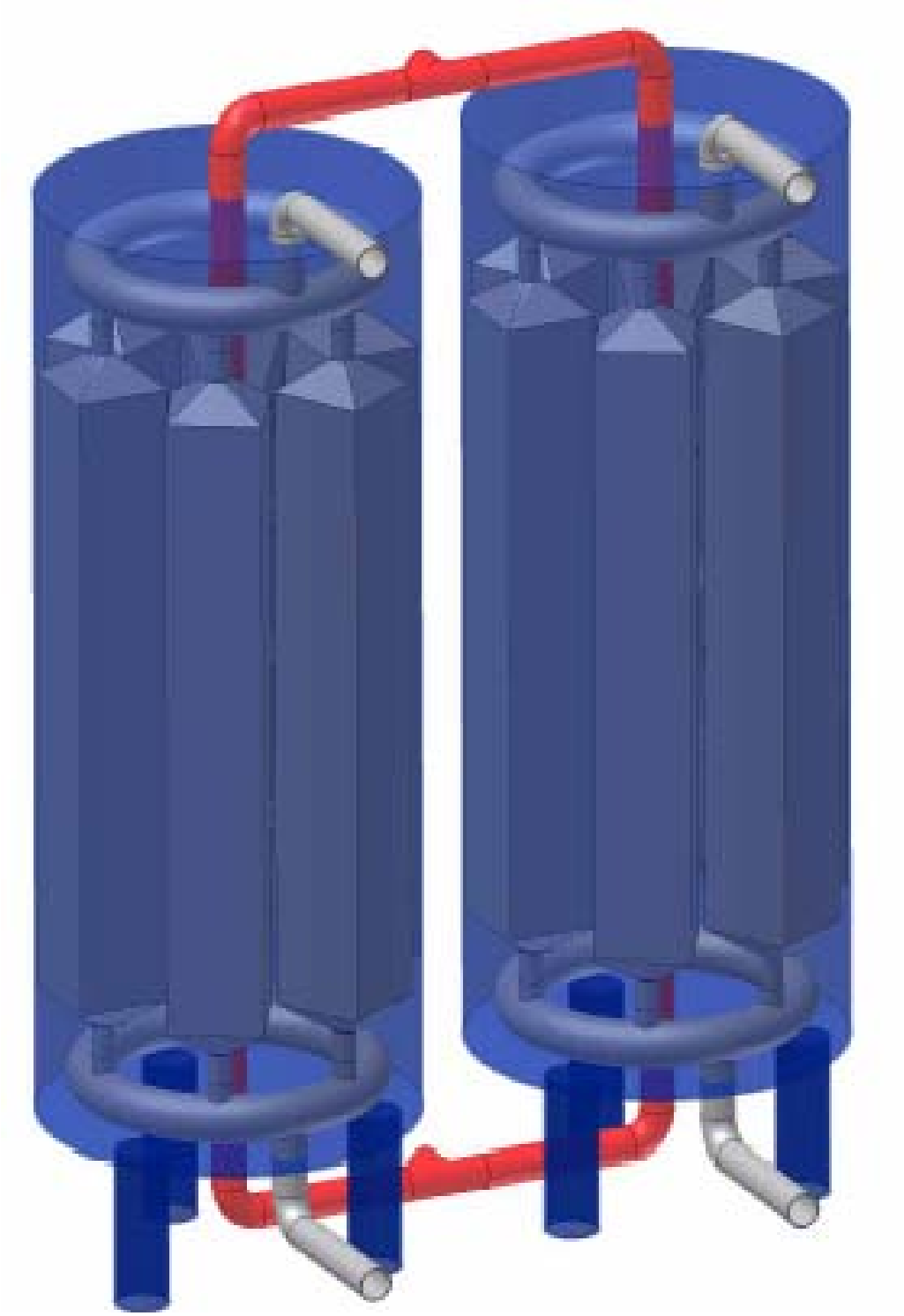

Figure VI-3. Sodium-to-CO_2 Heat Exchangers Incorporating Printed Circuit Heat Exchangers (Cutaway View)

D. Auxiliary Sodium Systems

In order to ensure long term, safe operations of the sodium systems, the chemistry of the system must be controlled and monitored by a set of auxiliary systems that are common to all liquid metal reactors. Although the chemistry does not affect the nuclear operation directly, it is important for the hydrodynamics of the system as well as for the corrosion and contamination control. One goal is to ensure stable hydrodynamics on the long term to promote an efficient and constant heat transfer, which can be affected by oxide formation or mass transfer within the non-isothermal circuit. Another goal is to ensure the maintenance and component handling easiness by reducing the activated corrosion products.

The following auxiliary sodium systems are included:

- Sodium purification system for purification and monitoring of sodium circuits, such as crystallization and plugging indicators
- Cover gas purification system for purification and monitoring of the argon cover gas
- Sodium sampling and analysis system for contamination monitoring
- Primary and secondary sodium storage system
- Sodium reaction system for component handling, cleaning, and decontamination (located in the Maintenance Building)

The sodium purification deals not only with the hydrogen and oxygen impurities introduced during the initial startup or maintenance operations, but also with other potential source of impurities such as the sodium/CO_2 interaction products.

VII. SUPERCRITICAL CO_2 BRAYTON CYCLE POWER CONVERSION SYSTEM

A. Supercritical CO_2 Brayton Cycle Arrangement

The SMFR power conversion system consists of a gas turbine Brayton cycle utilizing supercritical carbon dioxide (S-CO_2) as the working fluid. The S-CO_2 gas turbine Brayton cycle is selected over other cycles for several reasons including the following:

- Relative to a Rankine saturated steam cycle, the use of S-CO_2 eliminates the potential for energetic sodium-water interactions or combustible gas formation;
- Relative to a helium ideal gas (or other ideal gas) Brayton cycle, the S-CO_2 Brayton cycle offers higher thermal efficiency at the 510 °C sodium core outlet temperature;
- The Brayton cycle incorporates a turbine and two compressors that are remarkably small compared with those of either a Rankine saturated steam cycle or an ideal gas Brayton cycle. These small turbine and compressor sizes are expected to significantly reduce the costs of the turbomachinery components;
- Relative to a Rankine saturated steam cycle, the need for steam reheaters, a condenser, feedwater heaters, and a deaerator is eliminated thereby simplifying the power conversion system.

Figure VII-1 shows a comparison of cycle efficiency versus temperature for S-CO_2 Brayton cycle and helium ideal gas Brayton cycle [1]. Over the temperature range of interest to the SMFR, the S-CO_2 cycle clearly provides a significantly greater efficiency.

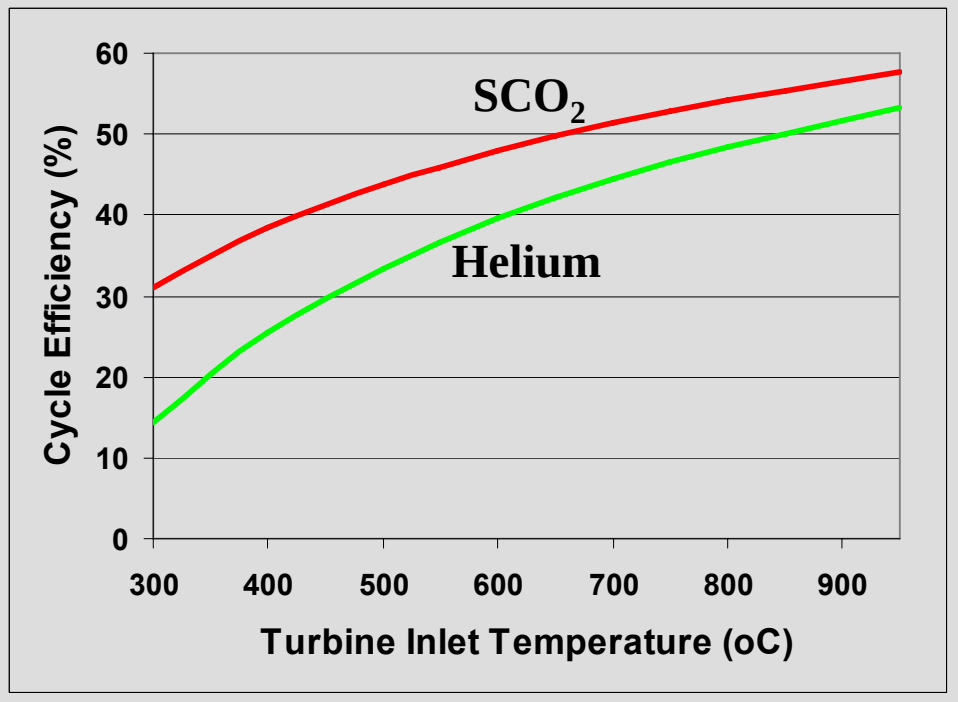

Figure VII-1. Comparison of Efficiencies versus Temperature for S-CO_2 Brayton Cycle and Traditional Helium Ideal Gas Brayton Cycle [1]

Figures VII-2 and VII-3 provide schematic illustrations of the S-CO_2 Brayton cycle coupled to the reactor through an intermediate sodium circuit. During normal operation, the supercritical CO_2 at about 20 MPa pressure is heated by the intermediate sodium loop in the two sodium-to-CO_2 heat exchangers. It then expands to a lower pressure of about 7.4 MPa in the turbine where thermal energy is converted to mechanical rotational energy that drives the generator as well as the two main compressors that are all located on a common shaft (Figure VII.2). The CO_2 then passes through two recuperators, designated the high temperature recuperator (HTR) and low temperature recuperator (LTR), where energy is transferred from the hot CO_2 to preheat CO_2 that has been compressed before it returns to the sodium-to-CO_2 heat exchangers. Preheating the CO_2 increases the cycle efficiency. A portion of the expanded low pressure CO_2 stream equal to 70 % of the total CO_2 flow passes through the cooler where heat is rejected from the cycle. Actual pressure, temperature, and flow rate conditions calculated for the cycle as well as the primary and intermediate sodium coolant systems are shown in Figure VII-3.

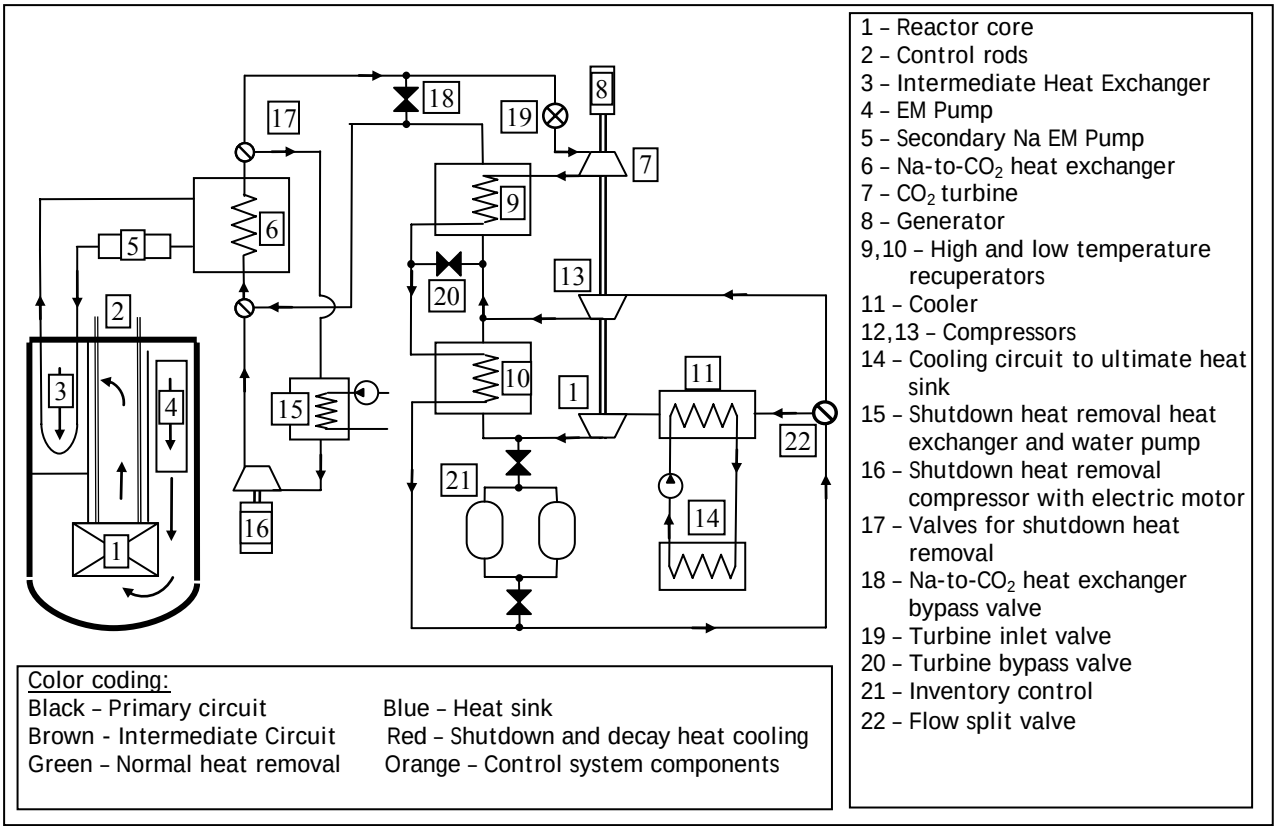

Figure VII-2. Schematic Illustration of S-CO_2 Brayton Cycle Showing Heat Transfer Paths and Control Mechanisms

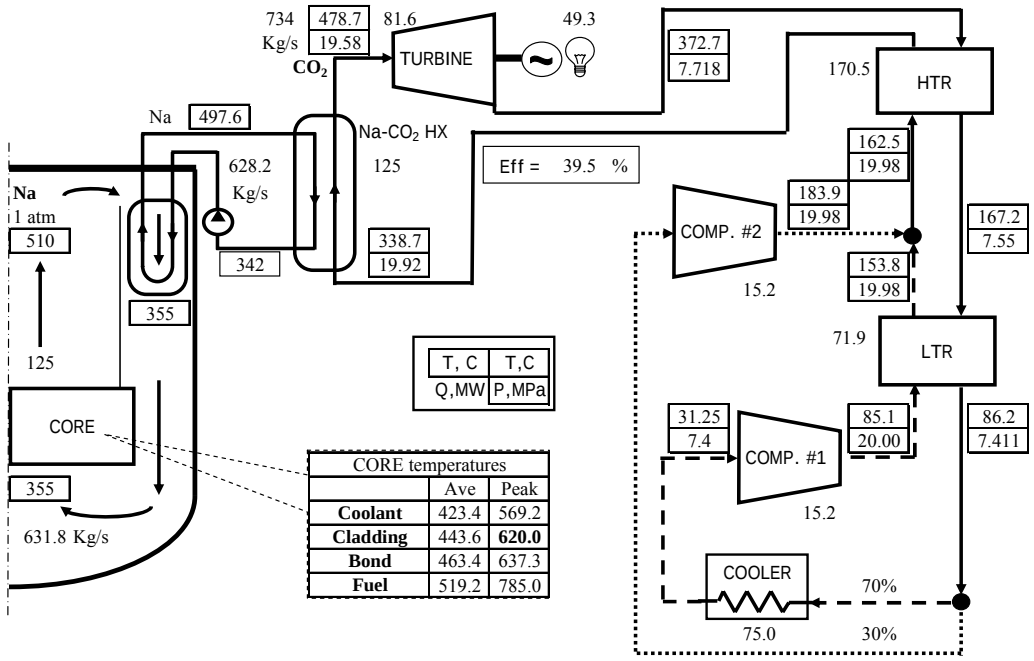

Figure VII-3. Brayton Cycle Temperatures, Pressures, Flow Rates, and Heat Exchange Rates

The CO_2 is expanded in the turbine to a pressure of 7.4 MPa which is immediately above the critical pressure (7.378 MPa). This is done to take advantage of the low compressional work for CO_2 immediately above the critical point. The low work of compression is the salient feature of the cycle that contributes most to its improved efficiency over traditional ideal gas Brayton cycles. In part, this is due to the high density of CO_2 immediately above the critical point (Table VII-1) which is closer to that of an ordinary liquid than an ideal gas in a traditional ideal gas Brayton cycle. Thus, there is an incentive to cool the CO_2 to as near the critical temperature as feasible. The general dependency of cycle efficiency upon the temperature of CO_2 exiting the cooler is shown in Figure VII-4.

Table VII-1. Comparison of Densities and Specific Heats

Fluid	Location	Pressure MPa	Temperature ^{o}C	Density kg/m^3	Specific Heat KJ/kg-K
S-CO_2	Critical point	7.37	30.98	468	Infinite
	Cooler outlet	7.40	31.25	369	56.9
	Compressor outlet	20.00	85.1	562	2.57
	Turbine inlet	19.67	479	135	1.23
	Turbine outlet	7.69	372	63.5	1.15
Helium	Cooler outlet	2.6	27	4.17	5.19
	Compressor outlet	7.0	104	8.93	5.19
Water		0.1	20	998	4.18
Sodium		0.1	420	828	1.36

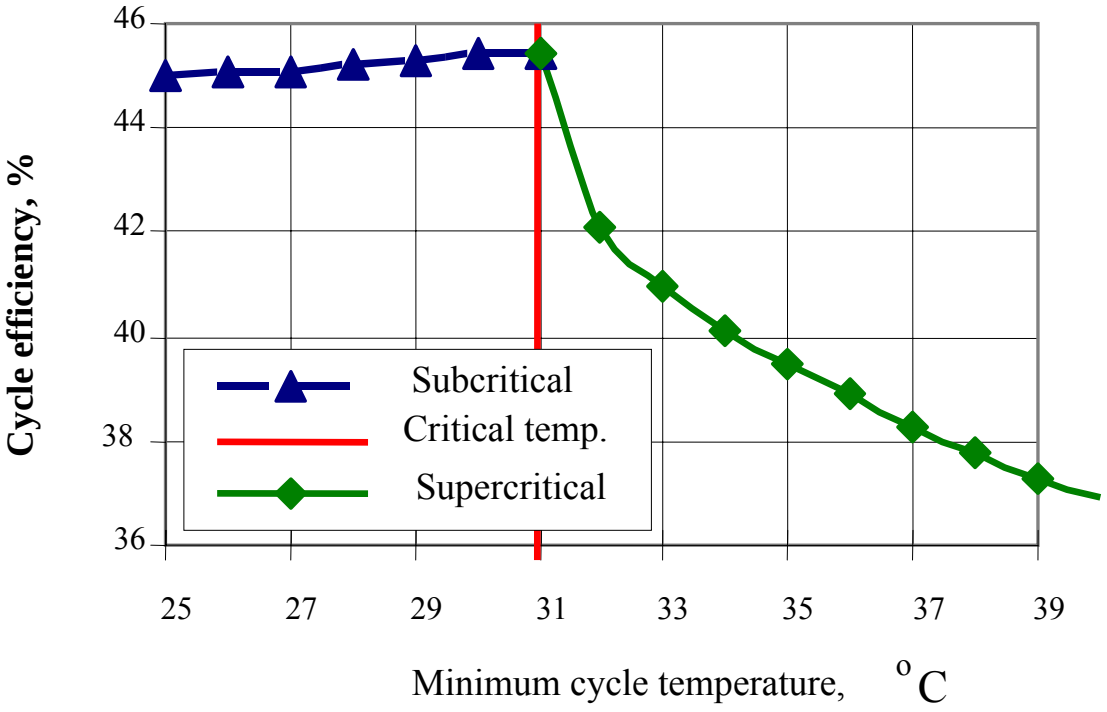

Figure VII-4. Brayton Cycle Efficiency vs. Cooler Outlet Temperature

The cycle splits the CO_2 flow such that only a portion rejects heat in the cooler because of the dependency of the specific heat of CO_2 upon pressure immediately above the critical point. In particular, the specific heat of CO_2 at 20 MPa is significantly greater than that at 7.4 MPa. The high pressure CO_2 from Compressor No.1 entering the low temperature recuperator has a specific heat of 2.57 KJ/kg-K. The low pressure CO_2 exiting the low temperature recuperator has a specific heat of 1.37 KJ/kg-K. Splitting the flow reduces the flow rate through the low temperature recuperator of the cold stream from Compressor No. 1 resulting in a CO_2 cold stream temperature rise in the low temperature recuperator that more closely approaches the temperature drop of the hot stream. This enhances the S-CO_2 cycle efficiency. The flow split fraction, currently equal to 70%, is chosen to optimize the cycle efficiency. The remaining 30% of the CO_2 flow is directly recompressed in Compressor No. 2 and then merged with the remainder of the CO_2 flow before passing through the high temperature recuperator. The difference in specific heats between the cold and hot streams is not as pronounced over the temperature regime of the high temperature recuperator relative to the temperatures of the low temperature recuperator. A cycle efficiency of 39.5% is calculated for the S-CO_2 Brayton cycle with the sodium core outlet temperature of 510°C.

Figure VII-2 also shows the shutdown heat removal path in which the S-CO_2 Brayton cycle components (i.e., turbine, recuperators, compressors, etc.) are isolated enabling the performance of maintenance or repair work on the components. Under nominal shutdown conditions, the CO_2 from the sodium-to-CO_2 heat exchangers passes through a special shutdown cooler where heat is rejected and is returned to the heat exchangers by a shutdown compressor.

Figures VII-5 through VII-7 show the turbine generator building and the arrangement of S-CO_2 Brayton cycle components inside of the building. The turbine generator building has main floor and a basement. The turbine, generator, compressors, recuperator, cooler, shutdown compressor, and shutdown heat removal cooler are located on the main floor. The inventory control tanks and letdown tanks are located in the basement. The small size of the power conversion unit, housing the turbine and two main compressors, is evident. The recuperators and coolers are distributed among six transportable recuperator and cooler modules that are installed side-by-side in a vertical orientation. The recuperator and cooler modules consist of printed circuit heat exchangers (PCHEs) supported by a space frame. In each module, four PCHEs belonging to the high temperature recuperator are located at the top of the space frame, four PCHEs of the low temperature recuperator are located in the middle, and four PCHEs of the cooler are at the bottom of the space frame. The building incorporates a bridge crane for lifting and transporting of components and parts. Ventilation equipment is located adjacent to the building to deliver air for cooling of the generator. The main floor of the turbine generator building incorporates holes that enable dense CO_2 to sink into the lower level of the building, in the event of a CO_2 leak.

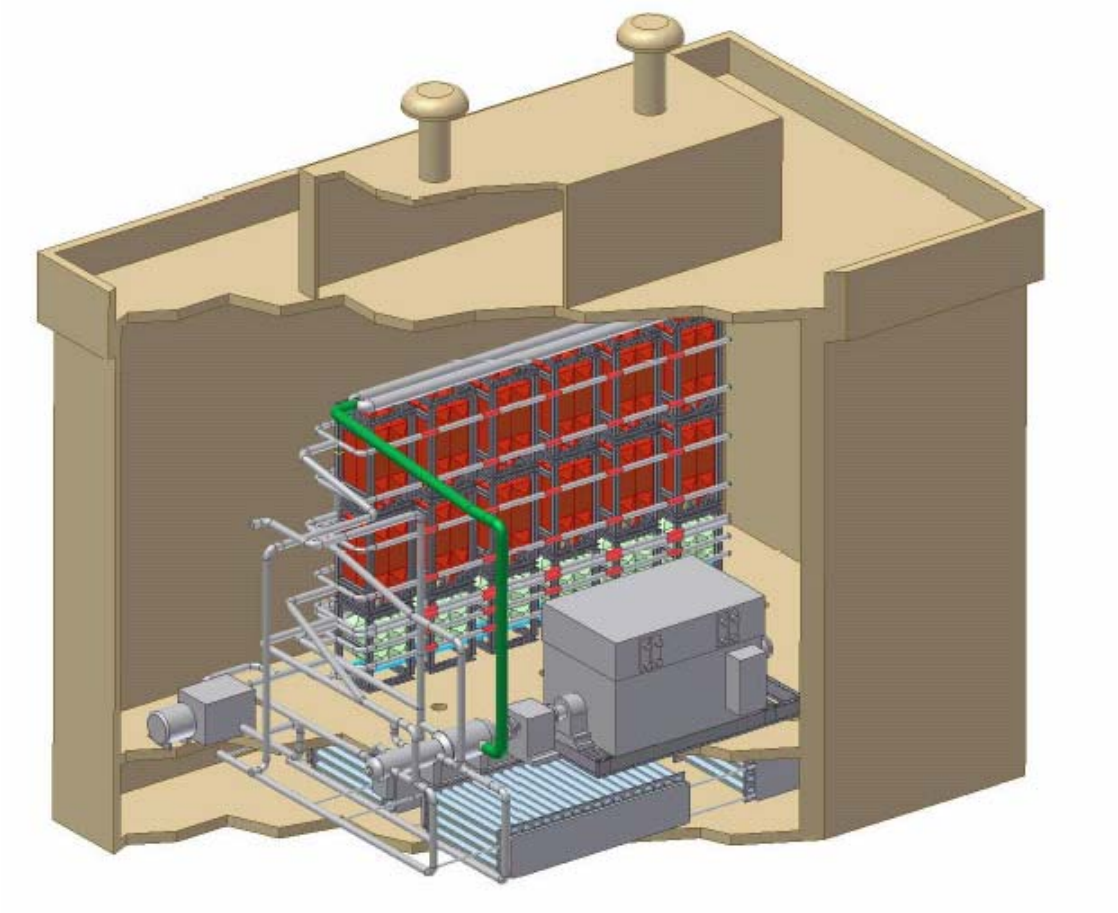

Figure VII-5. Illustration of S-CO_2 Brayton Cycle Inside Turbine Generator Building

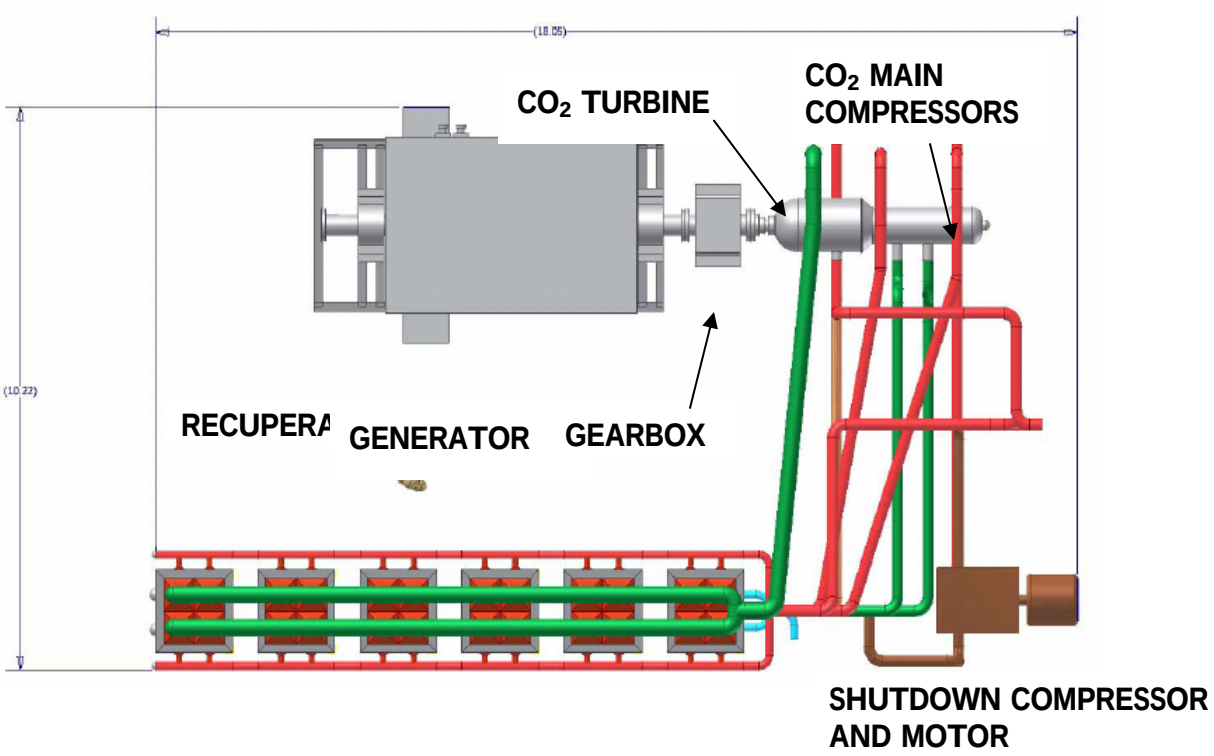

Figure VII-6. Arrangement of S-CO_2 Brayton Cycle Components on Main Floor of Turbine Generator Building

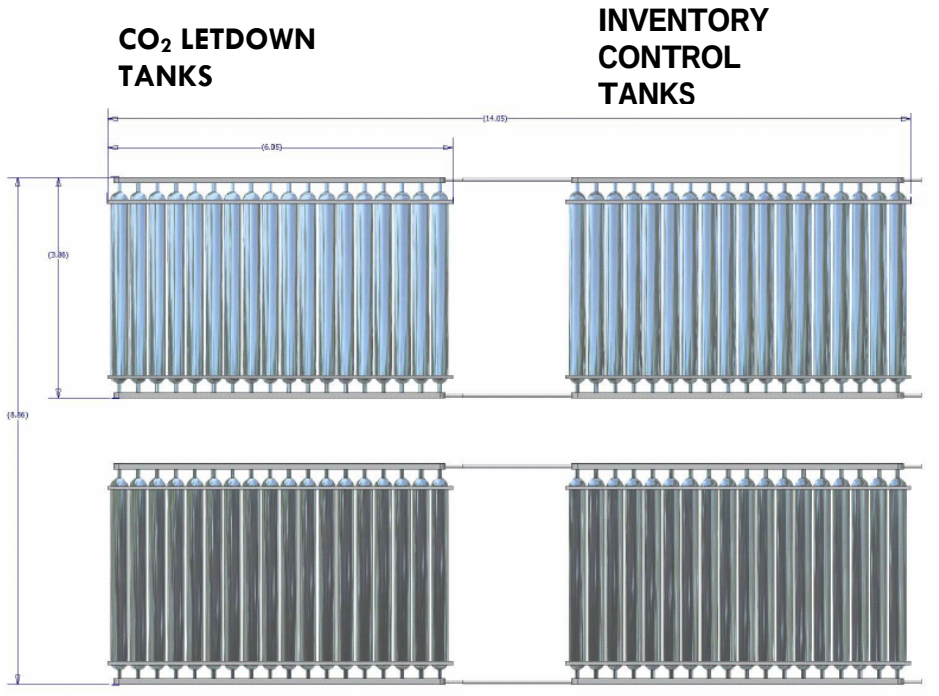

Figure VII-7. Arrangement of S-CO_2 Brayton Cycle Components on Subfloor of Turbine Generator Building.

B. Turbine Generator

The turbine and compressors are located on a common shaft inside of a power conversion unit, inside of a common housing. The turbine is a three-stage axial flow turbine. It has a remarkably small size and weight relative to turbines belonging to ideal gas (e.g., helium) Brayton cycles or an intermediate or low pressure steam turbine of similar power rating. The small turbine size is directly related to the high density of the CO_2 (Table VII-1). In particular, the turbine power reflects the mass flow rate multiplied by the work performed per fluid mass. Because the S-CO_2 density is so high, the mass flow rate with S-CO_2 is much higher than that with an ideal gas such as helium in an ideal gas Brayton cycle or steam in a Rankine saturated steam cycle.

Hence, the size of the turbine required to accommodate the S-CO_2 mass flow rate is small compared with the turbine sizes required for an ideal gas Brayton cycle or a Rankine saturated steam cycle operating at the same reactor power level and core outlet temperature. Dimensions and conditions for the turbine are presented in Table VII-2, which are based upon a turbine design analysis. The turbine is manufactured largely from Inconel-based alloys that are selected for their strength and low coefficients of thermal expansion as well as their resistance to oxidation by CO_2 over the normal operating temperature range.

Table VII-2. Turbine Design Parameters

Power	80.68	MW	
Number of stages	3		
Rotational speed	180	rev/s	
Length	0.72	m	Without casing
Max diameter	0.47	m	Without casing
Hub radius min	12	cm	
Hub radius max	15	cm	
Tip radius min	18.1	cm	
Tip radius max	23.4	cm	
Blade height min	6	cm	
Blade height max	8.4	cm	
Blade chord min	9.3	cm	
Blade chord max	15.7	cm	
Max Mach number	0.63		
CO_2 temperature inlet	479.3	^oC	
CO_2 temperature outlet	372.5	^oC	
CO_2 pressure inlet	19.67	MPa	
CO_2 pressure outlet	7.694	MPa	
CO_2 flow rate	719.9	kg/s	
Efficiency	90.9	%	Total-to-total
CO_2 mass	4.8	kg	

The generator is a commercial "off-the-shelf" component. A generator marketed by Siemens was selected only as representative. The Siemens turbogenerator is a two-pole air-cooled unit designed to the International Standard, IEC 34, and in compliance with the harmonized standards according to European Commission machine guideline, 89/392/EEC.

This generator weighs 86,300 kg. It consists of a base frame, stator core, stator winding, cover, rotor shaft, rotor winding, rotor retaining rings, bearings, and field connections. The rotor shaft consists of forged steel. It is supported on each end by bearings mounted to the base. The base frame and anchoring elements transmit the forces occurring in the machinery to the floor. Other functions of the base include damping of vibration and noise, support of the cooling system enclosure, and support of wiring and cabling.

An oil system for lubrication and an excitation system are also required for operation and are located inside of the turbine generator building. Heat losses arising in the generator interior are dissipated through air. The air cooling system is a self-contained ducted system. Air is drawn by axial-flow fans arranged on the rotor via lateral openings in the stator housing. The rotor is directly air cooled with heat losses transmitted directly from the winding copper to cooling air. The stator is indirectly air cooled. Because the turbine rotates at three times the rotational speed of the generator, the two components are coupled through a reduction gearbox.

C. Compressors

The Brayton cycle requires two main compressors. The two main compressors operate at different conditions and therefore have different numbers of stages, dimensions, and efficiencies. In particular, Compressor No.1 receives CO_2 that has been expanded to a pressure immediately above the CO_2 critical pressure and a temperature immediately above the CO_2 critical temperature. Dimensions and conditions for the two main compressors are shown in Tables VII-3 and -4. Similar to the turbine, the compressors possess remarkably small dimensions due to the high density of supercritical CO_2. The compressors are fabricated from Inconel alloys and austenitic stainless steel for strength, low thermal expansion, and resistance to corrosion by CO_2. A shutdown compressor is also provided to circulate CO2 through the sodium-to-CO2 heat exchanger and remove decay heat when the main cycle components are isolated for maintenance or repair.

A stand-alone shutdown compressor is provided for removal of decay heat during normal shutdown of the reactor. The shutdown heat removal compressor is capable of providing a CO_2 flow rate through the Na-to-CO2 heat exchangers sufficient for heat transport at decay heat levels.

D. Recuperators

The low temperature recuperator (LTR) and high temperature recuperator (HTR) are regenerative heat exchangers that provide for preheating of the compressed CO_2 before it is delivered to the sodium-to-CO_2 heat exchangers using part of the thermal energy of the hotter CO_2 expanded from the turbine. Preheating significantly enhances the efficiency of the cycle.

Table VII-3. Compressor No. 1 Dimensions and Conditions

Power	14.88	MW	
Number of stages	7		
Rotational speed	180	rev/s	
Length	0.5	m	Without casing
Max diameter	0.19	m	Without casing
Hub radius min	5.4	cm	
Hub radius max	6.2	cm	
Tip radius min	9	cm	
Tip radius max	9.6	cm	
Blade height min	2.8	cm	
Blade height max	4.1	cm	
Blade chord min	3.2	cm	
Blade chord max	4	cm	
Max Mach number	0.55		
CO_2 temperature inlet	31.25	^oC	
CO_2 temperature outlet	85.1	^oC	
CO_2 pressure inlet	7.4	MPa	
CO_2 pressure outlet	20	MPa	
CO_2 flow rate	503.9	kg/s	
Efficiency	88.2	%	Total-to-total
CO_2 mass	3.6	kg	

Each recuperator consists of a set of printed circuit heat exchangers (PCHEs). Printed circuit heat exchangers have been selected for the following reasons:

- Potential for reducing the volume occupied by the recuperators as well as the recuperator mass relative to traditional shell-and-tube heat exchangers,
- Potential for enhanced reliability and reduced requirements for inspection by elimination of the potential for failure of the boundary between the hot and cold streams. Each PCHE is effectively a monolithic block of stainless steel containing embedded flow channels. The concerns about tube failures typical of shell-and-tube heat exchangers are not present.

Each PCHE is assumed to be manufactured by hot isostatic pressuring of plates of austenitic stainless steel into which semicircular channels have been chemically etched. Austenitic stainless steel is selected for its resistance to corrosion by CO_2. The individual etched plates are diffusion bonded together by heating to a sufficiently high temperature in the presence of a sufficiently high pressure. This process is illustrated in Figure VI-1 developed by the PCHE manufacturer, Heatric Division of Meggitt (UK) Ltd. The hot and cold streams are assumed to flow through alternating rows of semicircular channels as shown in Figure VI-2 also from Heatric. The CO_2 flows through alternating rows of channels in opposite directions providing for countercurrent heat exchange.

Table VII-4. Compressor No. 2 Dimensions and Conditions

Power	14.97	MW	
Number of stages	10		
Rotational speed	180	rev/s	
Length	0.36	m	Without casing
Max diameter	0.22	m	Without casing
Hub radius min	8.2	cm	
Hub radius max	9	cm	
Tip radius min	10.5	cm	
Tip radius max	11.1	cm	
Blade height min	1.5	cm	
Blade height max	2.9	cm	
Blade chord min	1.5	cm	
Blade chord max	2.2	cm	
Max Mach number	0.46		
CO_2 temperature inlet	87.13	^oC	
CO_2 temperature outlet	184.9	^oC	
CO_2 pressure inlet	7.425	MPa	
CO_2 pressure outlet	19.98	MPa	
CO_2 flow rate	216	kg/s	
Efficiency	87.5	%	Total-to-total
CO_2 mass	0.9	kg	

Each semicircular channel is selected to have a diameter of 1.0 mm, a lateral pitch of 1.2 mm, and a plate thickness of 0.8 mm.

Based upon deterministic heat transfer calculations, it is determined that the PCHEs belonging to both the LTR and HTR provide sufficiently high cycle efficiency when the channel length is selected to be 2.0 m. From the calculational results, it is also found that for each recuperator, 24 PCHEs arranged in a parallel flow configuration provide sufficiently high cycle efficiency. Thus, the LTR and HTR each consist of 24 PCHEs where each PCHE is 2.0 m long and 0.6 m wide in directions normal to the flows. For transportability, the 24 PCHEs for each recuperator are organized into six transportable modules. A single module is shown in Figure VII-8. Each individual module contains four PCHEs belonging to the HTR and located at the top, four PCHEs belonging to the LTR and located in the middle, and four PCHEs belonging to the cooler located at the bottom. The PCHEs comprising each module are supported by a steel space frame. Dimensions and conditions for the HTR and LTR are provided in Tables VII-5 and VII-6, respectively.

E. Inventory Control System

The S-CO_2 Brayton cycle is controlled by means of a combination of control mechanisms illustrated in Figure VII-2. At power levels near 100% nominal, inventory control is used to

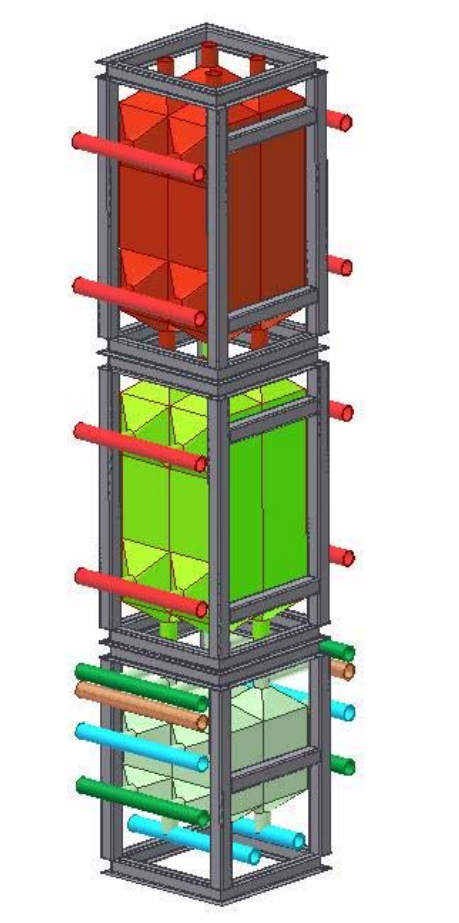

Figure VII-8. Transportable Module (1 0f 6) with Printed Circuit Heat Exchangers for High Temperature Recuperator, Low Temperature Recuperator, and Cooler

control the S-CO_2 Brayton cycle such that the heat removed from the reactor matches the load demand from the electric grid. Inventory control involves the removal or addition of CO_2 from the cycle. The purpose is to decrease or increase the CO_2 flow rate in the circuit without significantly altering the cycle efficiency. By changing the flow rate, the amount of heat transported by the cycle is changed without significantly changing the temperatures. Maintaining the same approximate temperatures maintains the same approximate cycle efficiency.

The inventory control system consists of inventory control tanks and valves that remove CO_2 from the high pressure part of the cycle between Compressor No. 1 and the low temperature recuperator into the inventory control tanks, or that admit CO_2 from the inventory control tanks to the low pressure part of the cycle between the low temperature recuperator and the cooler flow split valve. The valves are activated when either: 1) the pressure in the high pressure part of the cycle rises above a threshold maximum value or the turbine shaft speed increases above a threshold maximum (meaning a reduced load), or 2) the pressure in the low pressure part of the cycle falls below a threshold minimum value or the turbine/compressor shaft speed decreases below a threshold minimum (an increased electrical load).

Table VII-5. High Temperature Recuperator Design Parameters (per PCHE)

Heat transfer capacity	7.03	MWt	
Unit side 1	0.6	m	
Unit side 2	0.6	m	
Unit length	2	m	Effective for heat transfer
Channel diameter	1	mm	Semi-circular channel
Plate thickness	0.8	mm	
Channel pitch	1.2	mm	
Material	SS316		
Number of channels	187,527		Each side
Void fraction	40.9	%	From channels
Hot side temperature inlet	372.5	^{o}C	
Hot side temperature outlet	165	^{o}C	
Hot side pressure inlet	7.694	MPa	
Hot side pressure outlet	7.533	MPa	
Hot side flow rate	30	kg/s	
Cold side temperature inlet	160.5	^{o}C	
Cold side temperature outlet	337.9	^{o}C	
Cold side pressure inlet	19.98	MPa	
Cold side pressure outlet	19.93	MPa	
Cold side flow rate	30	kg/s	
Efficiency	83.7	%	(Tc,out-Tc,in)/(Th,in-Tc,in)
Metal mass	3,375	kg	At 20 ^{o}C
CO_2 mass	49.3	kg	

The inventory control tanks are depicted in Figure VII-9. The tanks consist of a large number of cylindrical tanks fabricated from piping segments onto which are welded hemispherical heads containing nozzles. In particular, each pipe is a 12-inch Schedule 80 (0.69 inch wall thickness) austenitic stainless steel pipe 3.0 m long and internally polished. Austenitic stainless steel is selected for its resistance to corrosion by CO_2. There are a total of 141 such pipes providing a total inventory control volume of approximately 10 m^3. Manifolds connect the pipes together to achieve a single distributed volume. This approach minimizes the cost of the inventory control system volume compared to fabrication of a single tank providing the total volume.

At lower power levels, inventory control is not effective and another control approach is required. An approach for this regime involves turbine inlet/throttle valve control or sodium-to-CO_2 heat exchanger bypass control; a combination of the two might also be employed. The optimal power level below which such an approach may be applied remains to be determined, although it might be expected to be about 50% nominal power.

At all power levels, the flow split of CO_2 to the cooler may be varied from the nominal value of 70 % as a means of maintaining high cycle efficiency.

Table VII-6. Low Temperature Recuperator Design Parameters (per PCHE)

Heat transfer capacity	2.83	MWt	
Unit side 1	0.6	m	
Unit side 2	0.6	m	
Unit length	2	m	Effective for heat transfer
Channel diameter	1	mm	Semi-circular channel
Plate thickness	0.8	mm	
Channel pitch	1.2	mm	
Material	SS316		
Number of channels	187527		Each side
Void fraction	40.9	%	From channels
Hot side temperature inlet	165	^{o}C	
Hot side temperature outlet	87.1	^{o}C	
Hot side pressure inlet	7.533	MPa	
Hot side pressure outlet	7.425	MPa	
Hot side flow rate	30	kg/s	
Cold side temperature inlet	85.1	^{o}C	
Cold side temperature outlet	150.7	^{o}C	
Cold side pressure inlet	20	MPa	
Cold side pressure outlet	19.98	MPa	
Cold side flow rate	21	kg/s	
Efficiency	82.1	%	(Tc,out-Tc,in)/(Th,in-Tc,in)
Metal mass	3,375	kg	At 20 ^{o}C
CO_2 mass	86.6	kg	

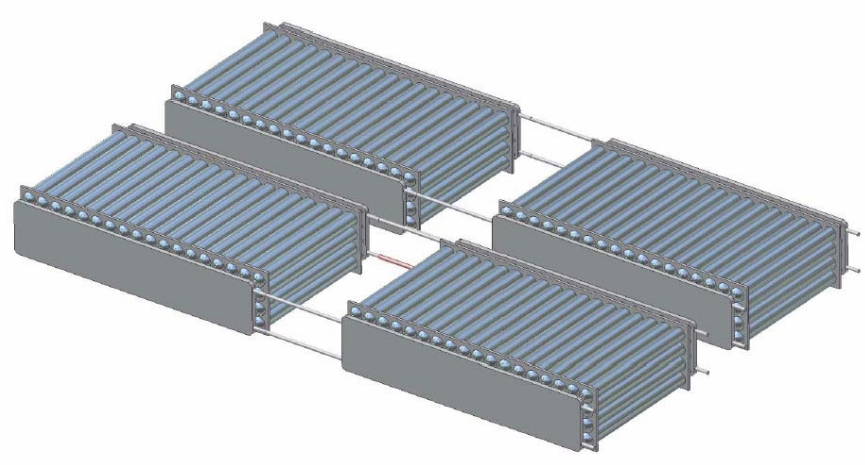

Figure VII-9. Inventory Control (Right Pair) and CO_2 Letdown (Left Pair) Tanks

A separate set of storage tanks identical to those of the inventory control system is provided to enable letdown/removal of CO_2 from the circuit during certain maintenance or repair operations. The inclusion of this feature is tentative and may be deleted in view of the low cost of CO_2.

F. Coolers and Heat Rejection System

The S-CO_2 Brayton cycle heat rejection system consists of a cooler where heat is rejected from CO_2 to water, a water circulating system involving pumps, and cooling towers where heat is rejected from the water to the atmosphere.

The cooler consists of 24 PCHEs. Each PCHE has 1 mm diameter semicircular channels for countercurrent CO_2 and water flow. Based upon deterministic heat transfer calculations, a channel length of 2.0 m is selected to provide high cycle efficiency by cooling the CO_2 to a temperature of approximately 31.25°C. This temperature enhances the cycle efficiency as shown in Figure VII-4. Immediately above the critical pressure and temperature, the specific heat exhibits a spike as shown in Figure VII-10. Within the spike, removal of a given amount of enthalpy results in a relatively smaller reduction in temperature. As the CO_2 is cooled within the spike, the behavior is similar to that of a phase transition in that energy is removed at an approximately unvarying temperature. This behavior is utilized to cool the CO_2 to a temperature (e.g., 31.25°C) very close to but still above the critical temperature (30.98°C) without concern of overcooling the CO_2 to below the critical temperature. Overcooling the CO_2 to below the critical temperature would require heating the CO_2 from subcritical to supercritical conditions as is done in a Rankine cycle. The S-CO_2 cycle operates at temperatures above the critical temperature to avoid the need for the "feedwater heaters" that are part of the Rankine cycle. Dimensions and conditions for the cooler are shown in Table VII-7.

The heat rejection system rejects heat to the atmosphere with two commercially-available, open-evaporative, forced-air counter flow cooling towers. Internally, each cooling tower uses nozzles to evenly distribute water downward over a packing fill. A drift eliminator ensures that the water drops do not leave the cooling tower. The cooling tower uses induced draft, axial fans that have a low air inlet speed which creates a highly efficient distribution of air. The location of the fan on the outlet also causes the hot air to flow far away, which reduces any recirculation. Besides the fans, the cooling towers are also highly efficient due to the use of film fills, which maximize the contact surface between the water and air. The type of packing can be altered depending on the characteristics needed in accordance with the process and surrounding conditions.

The cooling towers have a high efficiency (less than 1 KW electric per 100 KW cooling) due to evaporation. Each unit has a maximum capacity to cool 6300 m^3/h of water to remove 37.1 MW of thermal energy. Power for the units is supplied from the generator and thus factors into the overall plant efficiency. Typically a unit this size is 14.8 square meters in footprint and 10 meters tall.

In order to reduce corrosion in the cooling towers, the manufacturer will use materials such as stainless steel, polyester, and synthetics for all components that are in contact with water.

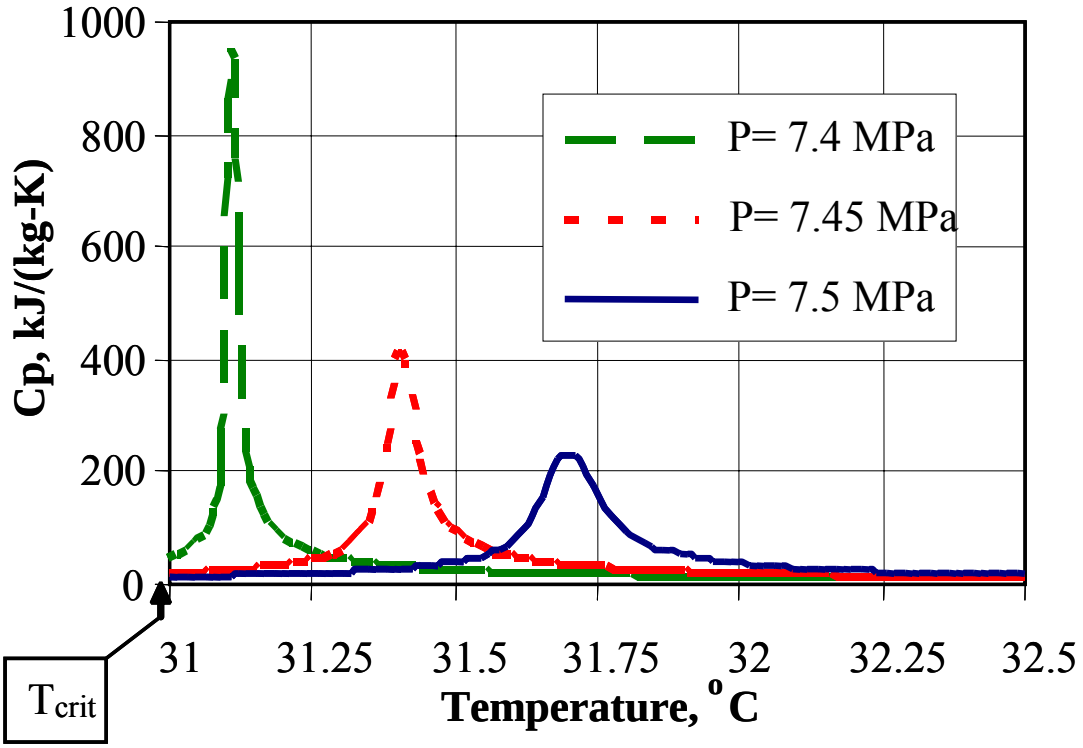

Figure VII-10. Behavior of CO_2 Specific Heat Near the Critical Point

Because of this, a long life-span is expected that does not depend on water treatment or water cleanings.

The cooling towers each employ modular construction and can be transported to the site. Rail or truck (by common carrier) are typical transportation modes for the commercial product. Once on site, the towers can be quickly assembled and installed on an existing concrete foundation. Should a replacement cooling tower be required, another tower could be assembled next to the existing unit and lifted in place fully-assembled, minimizing the shutdown time for replacement of the cooling tower.

The S-CO_2 Brayton cycle heat rejection system also incorporates a special shutdown cooler in which heat is rejected from the CO_2 to the circulating water during normal shutdown of the reactor.

G. Carbon Dioxide Release Mitigation System

Carbon dioxide is a toxic substance at low concentrations in air and causes asphyxiation at higher concentrations. In particular, the OSHA time weighted average permissible exposure limit is 1.0 volume % concentration in air. The time weighted average temporary exposure limit, usually for exposures of 15 minutes duration, is 3 volume %; higher concentrations are fatal. A volume concentration of 30 % produces asphyxiation. Carbon dioxide has a higher density than air at the same temperature. Thus, CO_2 is a heavy gas that will collect in basements and other

Table VII-7. Cooler Design Parameters (per PCHE)

Heat transfer capacity	3.09	MWt	
Unit side 1	0.6	m	
Unit side 2	0.6	m	
Unit length	2.0	m	Effective for heat transfer
Channel diameter	1.0	mm	Semi-circular channel
Plate thickness	0.8	mm	Each side
Channel pitch	1.2	mm	Each side
Material	SS316		
Number of channels	187527		Each side
Void fraction	40.9	%	From channels
CO_2 temperature inlet	87.1	^oC	
CO_2 temperature outlet	31.25	^oC	
CO_2 pressure inlet	7.425	MPa	
CO_2 pressure outlet	7.4	MPa	
CO_2 flow rate	21	kg/s	
Water temperature inlet	30	^oC	
Water temperature outlet	35.8	^oC	
Water pressure inlet	0.334	MPa	
Water pressure outlet	0.101	MPa	
Water flow rate	129.2	kg/s	
Water pump power	0.804	MW	Total all units
Efficiency	10.1	%	(Tc,out-Tc,in)/(Th,in-Tc,in)
Metal mass	3,375	kg	At 20 ^oC
CO_2 mass	41.3	kg	

low areas and spread upon floors or the ground. It is necessary to protect personnel, especially plant personnel, from the effects of accidental CO_2 releases.

The Brayton Cycle Building incorporates a CO_2 release mitigation system for small CO_2 leak rates. In particular, the turbine generator building has a low pressure capability and blowers are provided to remove the gaseous mixture from the building. The CO_2 and air removed from the turbine generator building is mixed with outside air to a concentration below 1 volume % and is released to the atmosphere through a stack.

References

1. V. Dostal, "A Supercritical Carbon Dioxide Cycle for Next Generation Nuclear Reactors," Ph.D. Dissertation, Massachusetts Institute of Technology (2004).

VIII. SHUTDOWN HEAT REMOVAL SYSTEM

The shutdown heat removal system is completely independent from the normal decay heat removal through the intermediate heat transport system, and is activated only when the normal heat removal system is disabled. The system consists of two redundant loops. Each loop consists of a small in-vessel direct reactor auxiliary cooling system (DRACS), a secondary natural draft heat exchanger (NDHX), an expansion tank, and an exterior stack that forms the natural draft pathway for dissipating the decay heat to the atmosphere. A schematic diagram showing key elements of the system is shown in Figure VIII-1.

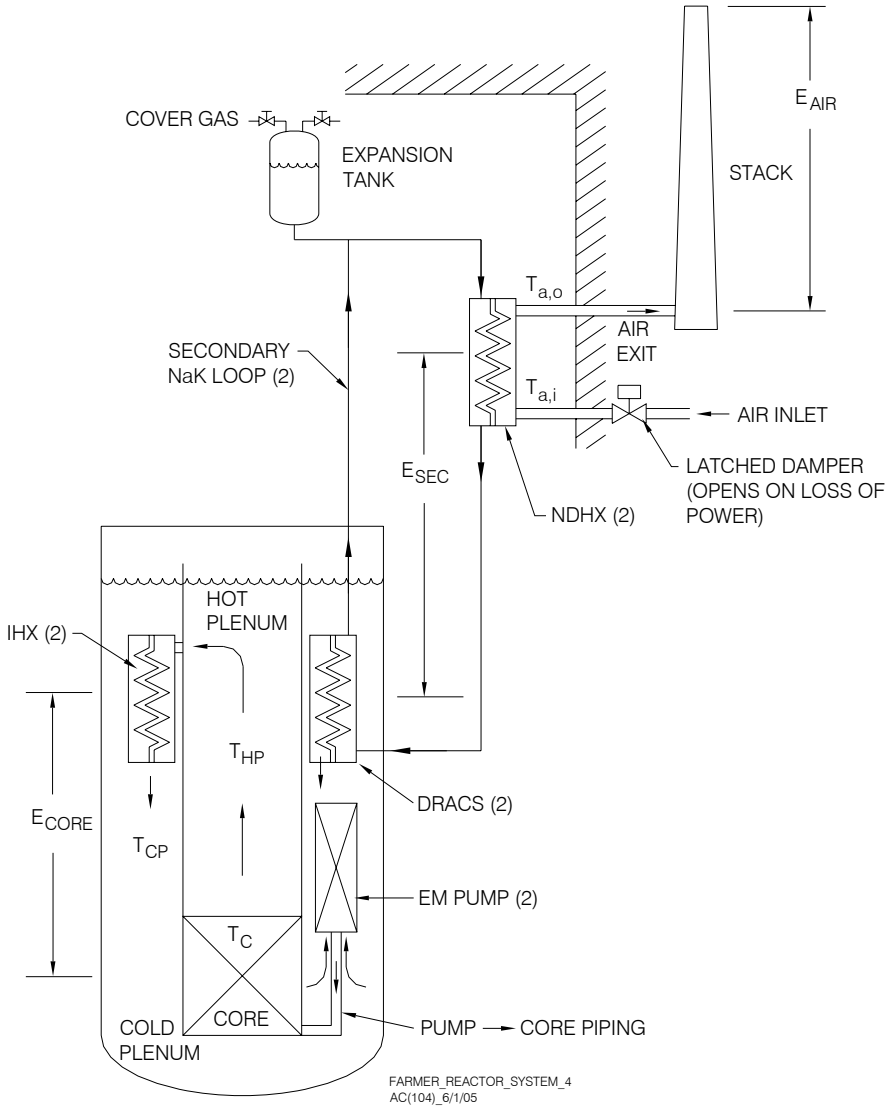

Figure VIII-1. Schematic Diagram of Shutdown Heat Removal System

The DRACS heat exchangers are positioned directly in the sodium cold pool. Moreover, there are no valves or other mechanical devices that isolate the primary sodium from the

DRACSs. Thus, during full power operation, primary cold pool sodium circulates at a modest flow rate through the shell side of the DRACSs. However, when activated, buoyancy-driven natural convection flow of the primary sodium through the DRACS is initiated.

The core decay heat is transferred by natural convection flow of primary sodium from the reactor hot pool through the IHX flow path to the cold pool. Heat from the primary sodium cold pool is then transferred through the DRACS to the secondary sodium-potassium (NaK) eutectic passing through the heat exchanger tubes. In turn, natural convection causes the secondary NaK to circulate through the natural draft heat exchangers where the airflow transfers the heat from the NaK to the atmosphere. The secondary NaK flow circuits (one for each of the two independent systems) are completely passive without any valves or constrictions to limit the flow during normal operation or shutdown conditions.

On the tertiary (air) side of the systems, the natural convection circuits are passive except for magnetically latched dampers that prevent air flow on the air inlet side of the two NDHXs. Upon loss of electrical power to the electro-magnetic latch, the dampers fail by gravity in the open position. The DRACSs are brought into full operation by opening of these dampers. The dampers are designed to provide an air leak rate that corresponds to nominally 1 % of the full design flow rate in the closed position, which results in a parasitic heat loss of ~ 12 kW during full power operation. This minor heat loss is included in the design to maintain the correct natural convection flow patterns in the primary, secondary, and tertiary sides of the system so that proper natural convection flow patterns are established immediately upon system activation. Moreover, continuous heat addition to the system is desirable in regions where the ambient temperature can fall below the NaK freezing temperature of nominally -13 ˚C.

The two DRACSs are designed to remove 625 kW each at normal operating conditions. The thermal rating for each DRACS corresponds to 0.5 % of the core full power rating of 125 MWt. Both DRACSs are capable of removing 1.25 MW of decay heat at design conditions. Since DRACSs are located inside the reactor vessel, any leakage from the DRACSs or ancillary piping will not lead to coolant drain. The DRACS is vertically suspended from two rigid pipes that are welded to the DRACS shroud. These pipes extend upward from the cold pool and are welded to the underside of a removable plug in the reactor vessel head.

Key design parameters for the DRACS are summarized in Table VIII-1. The DRACS is a shell-and-tube, counter-current flow-type heat exchanger with primary flow on the shell-side, and NaK flow on the tube side. Primary sodium from the cold pool enters the shell side of the DRACS though an annular ring opening in the shroud located just below the upper tube sheet. The sodium flows by natural convection down through the tube bundle while dissipating heat. The sodium then returns to the cold pool through a second annular ring opening located just above lower tube sheet. Cold secondary NaK enters the DRACS through a central 5.1 cm diameter downcomer. The downcomer delivers the cold NaK through the lower tube sheet into a header manifold, where it then turns 180º and rises through the tube bank in counter current flow to the shell side primary sodium. The hot secondary NaK exits the tubes into an upper header manifold, and then flows through an annular riser which is concentric to the downcomer. The downcomer is double walled with an annular gap for thermal insulation between the hot and cold streams.

Table VIII-1. DRACS Design Parameters

Heat transfer capacity	625 kWt
Heat transfer area	9.17 m^2
Primary sodium temperature inlet	510 ˚C
Primary sodium temperature outlet	355 ˚C
Primary sodium mass flowrate	3.14 kg/s
Secondary NaK temperature outlet	484 ˚C
Secondary NaK temperature inlet	328 ˚C
Secondary NaK mass flowrate	4.38 kg/s
Tube outer diameter	2.22 cm
Tube wall thickness	0.9 mm
Tube Pitch	3.79 cm
Active Tube length	0.75 m
Number of tubes	179
Upper Tube Sheet - Area	0.23 m^2
Upper Tube Sheet - Thickness	25 mm
Lower Tube Sheet - Area	0.23 m^2
Lower Tube Sheet - Thickness	25 mm
Downcomer piping - OD	5.1 cm
Outlet piping - OD	7.6 cm
Shell OD	22.7 cm
Shell thickness	6.4 mm
Cross-sectional area	0.24 m^2
Material	9Cr-1Mo tubes

As shown in Figure VIII-2, both the downcomer and the annular riser pipes are equipped with bellows just above the shroud to accommodate any differences in thermal expansion between the piping and the body of the DRACS itself (which is rigidly attached to the removable plug in the reactor vessel head). The upper tube sheet is welded to the shroud, while the lower tube sheet floats. Thus, the design accommodates differential thermal expansion within the tube bank also.

Figures VIII-3 through -5 provide the parametric analyses of planar area, tube length, and pressure drop across shell and tube sides vs. number of heat exchanger tubes for a 625 kW DRACS, which formed the basis to set the design parameters presented in Table VIII-1.

Consistent with the thermal rating of the DRACS, each NaK-to-air NDHX is designed to remove 625 kW decay heat. The unit is a horizontal tube, cross-flow design. Key design parameters are summarized in Table VIII-2. The unit will be equipped with fire suppression plate and catch basin to mitigate the effects of a NaK tube bundle leak. The damper to the unit is

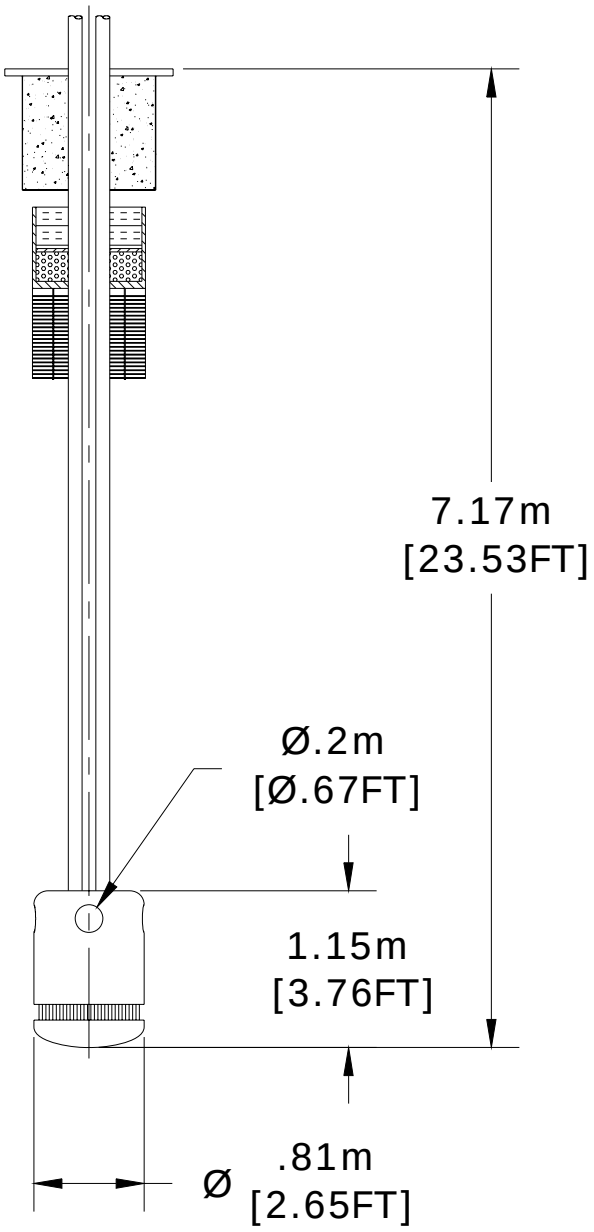

Figure VIII-2. Details of DRACS Design

magnetically latched to fail open under gravity upon loss of electric power. The unit will also have a manual hand-wheel operation capability.

Air flow through each NDHX is induced through a dedicated exhaust stack, one for each unit. Each stack is 5 m high and 8.75 m^2 in cross section. The stacks are of lightweight steel construction and are insulated. Each secondary NaK loop of the SHRS contains an expansion tank to accommodate changes in system volume due to variations in temperature. The tank has one NaK nozzle on the bottom and one gas nozzle on the top, which supplies argon cover gas to the tank and permits pressure control. The tank is located at the high point in the flow loop. The

resultant NaK static head is sufficient to operate the loop with expansion tank cover gas pressures at, or slightly below, atmospheric pressure. In the event of a leak in the DRACS, loss of radioactive primary sodium into the secondary NaK loop will not occur. In the event of a leak in the NDHX, the resultant spill is minimized because of the low expansion tank operating pressure.

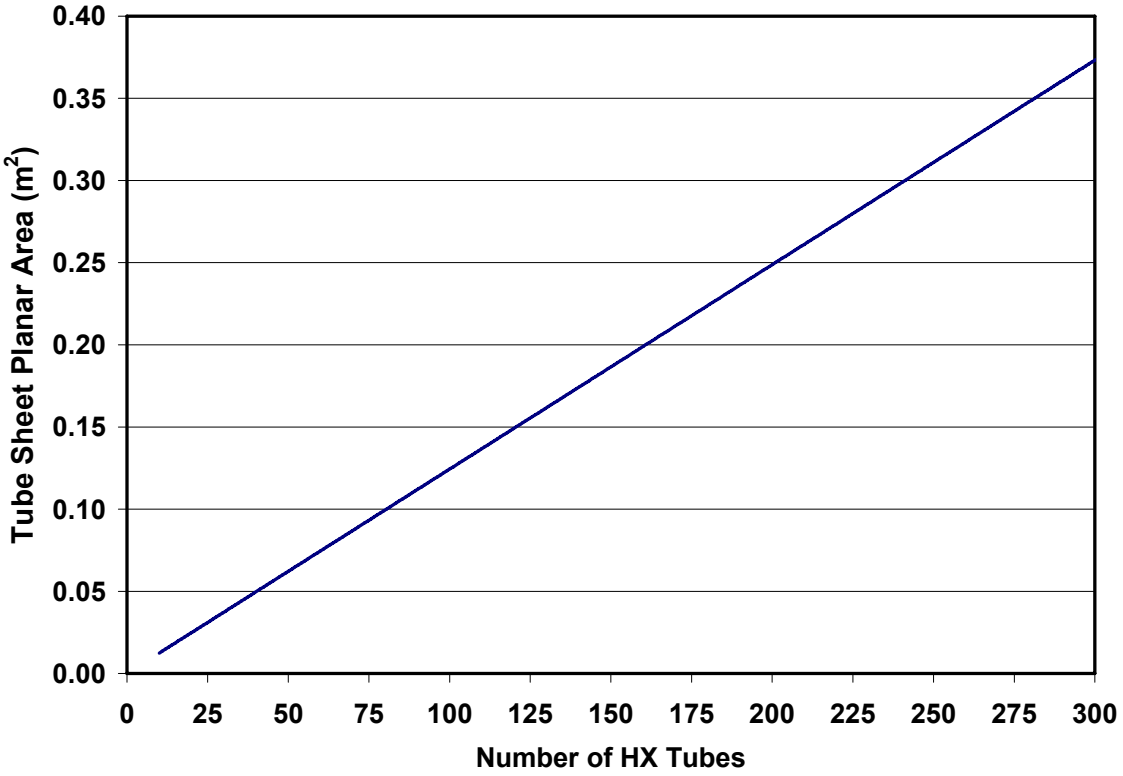

Figure VIII-3. Tube Sheet Planar Area vs. Number of Tubes

Table VIII-2. NDHX Design Parameters

Heat transfer capacity	625 kW
Tube length	2.83 m
HX tube OD	4.22 cm
Tube wall thickness	3.55 mm
Fin height	3.2 mm
Tube horizontal center-to-center spacing	7.62 cm
Tube vertical center-to-center spacing	10.2 cm
Stack riser cross-sectional area	8.25 m^2
Stack height	5.0 m

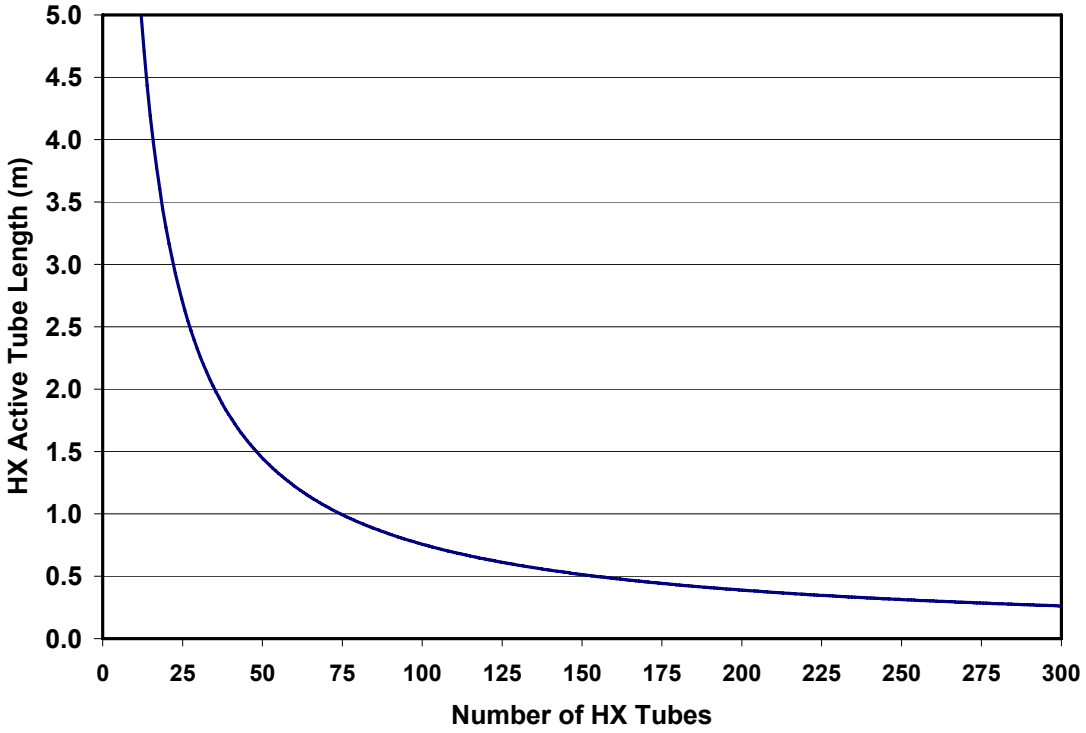

Figure VIII-4. HX Tube Length vs. Number of Tubes

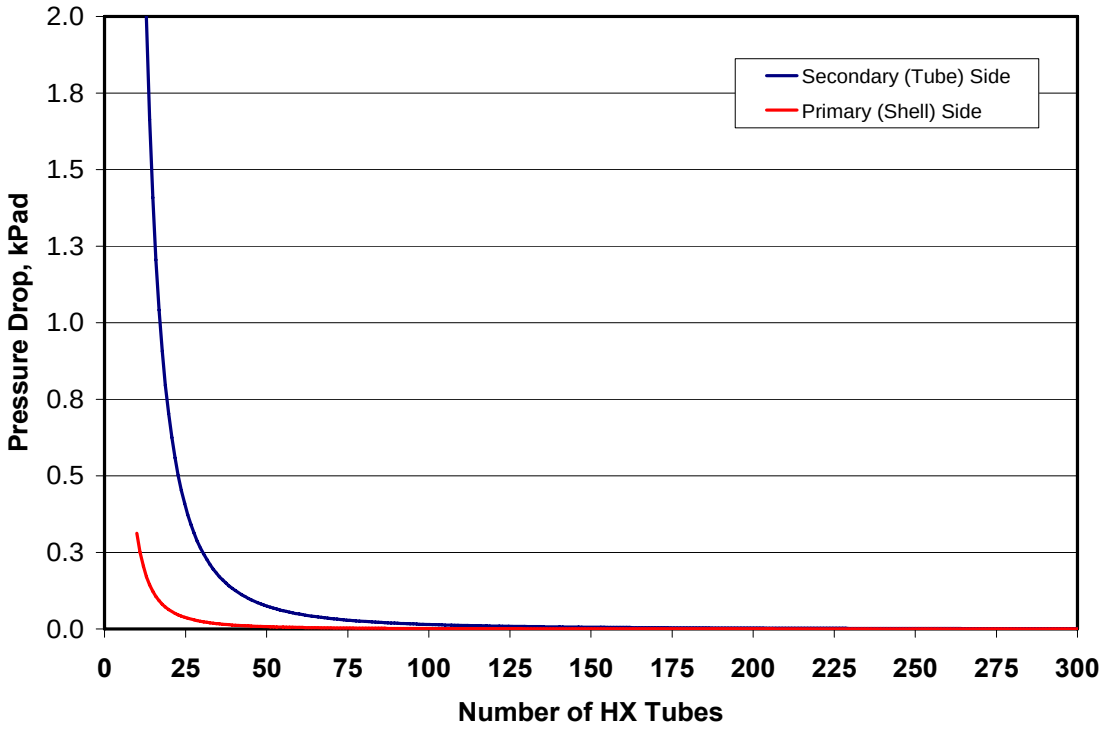

Figure VIII-5. Primary (Shell) and Secondary (Tube) Side ΔP vs. Number of Tubes

IX. FUEL HANDLING STRATEGY

Since there will be no refueling during the 30 year core life, a conventional fuel handing system is not provided. This Section describes the fuel handling strategies for the initial core loading and the end of life core replacement.

For the initial core loading, the fresh fuel assemblies can be handled manually because their low radiation level facilitates manual manipulation. The reactor vessel assembly will contain handling features to prevent movement of the reactor vessel and its internals during transportation. Once the reactor vessel has been installed in the containment structure and is ready to receive fuel, then the fuel assemblies will be loaded manually using the installed crane with workers locating the fuel in the proper grid location. The fuel assemblies will contain fresh fuel and will have a dose rate that allows for manual handling. During initial fuel loading, the new control rods will be inserted in their respective core grid locations.

After the fresh fuel has been loaded in the reactor vessel, the reactor vessel will be filled with argon and sealed. Other components that need installation will be installed in the plant at that time. After the primary components have been installed and dry tested, then the reactor vessel will be filled with nuclear-grade sodium. The sodium will most likely be off-loaded from rail cars or a tanker. The sodium will be purified before being pumped into the primary tank either at the manufacturing plant or at the installation site. After the reactor vessel is filled with sodium, then the primary EM pumps will be turned on and the primary circuits will be checked to determine that the flows and pressures are as expected. After all pre-critical checks are finished, the reactor will be started up until initial criticality has been reached followed by low power testing and then full power operations.

At the end of the 30 year core life, the used core can be replaced with a new core to serve the remainder of the 60 year plant life. For this end of life core changeover, the reactor will be shutdown and all control rods disengaged. The fuel assemblies will be allowed to cool to a decay heat level that the DOT-approved shipping cask can handle. The control rod drive mechanisms and drive lines will be removed from the center reactor plug. The center reactor plug, which contains the upper internal structure, has been designed to be removed.

The removal process will entail installing a caisson over the center reactor plug and mating it with a support flange. The caisson would then be inerted with argon or another appropriate gas. After the caisson is inerted, the center plug (with the upper internal structure) would be pulled into the caisson and then a temporary cover would be installed over the hole to the reactor tank.

The fuel handling machine would then be placed into the location of the center plug and bolted into place. The fuel handling equipment would consist of a single rotating plug and a pantograph design that would then be used to remove the fuel assemblies. The fuel assemblies would be removed one-by-one to an appropriate shielded cask that would be DOT-approved for transporting spent nuclear fuel to a fuel disposition facility.

After the spent core has been removed, a new core will be installed in the core barrel. The new fuel assemblies could be installed after each fuel assembly is removed instead of at the end

of the entire spent fuel removal. The reactor central plug will be re-installed. The control rod drive lines and drives will be re-installed on the reactor central plug. The EM pumps will be turned on and the primary circuits will be checked to determine that all the flows and pressures are as expected. After all pre-critical checks are finished, the reactor will be started up with a new core.

The fuel handling system used for the core changeover does not exist at the reactor site. It will be transported from site to site whenever the end of 30 year core life is reached. It is comprised of the following five main assemblies:

- In-vessel transfer machine
- Rotatable plug
- Fuel unloading machine
- Interbuilding cask
- Spent fuel shipping cask

The in-vessel transfer machine is a separate assembly and is inserted into the rotatable plug for fuel handling. It has a pantograph with a gripper assembly that can extend and rotate to reach all fuel assemblies. The rotatable plug sits on the top support structure and interfaces with a drive motor and indexing device to allow for 360º rotation on the core center axis. By using a combination of the in-vessel transfer machine and the single rotatable plug, all fuel assemblies are accessible.

The fuel unloading machine mates with the rotatable plug during fuel handling operations. The machine has a core gripper that is used to extract fuel assemblies from the reactor vessel. The fuel unloading machine then places the fuel assembly into an inerted interbuilding cask used to transfer the fuel assembly outside the reactor building and to the building where the fuel can be prepared for shipment to the off-site storage/processing facility.

X. OTHER REACTOR PLANT EQUIPMENT

A. Reactor Vessel Heating System

Four electrical reactor vessel immersion heaters provide supplementary heating of the bulk primary sodium to maintain a minimum sodium temperature of 120°C whenever the reactor is not operating at sufficient power to make up for the total heat losses from the primary system. Heaters are also required during the initial sodium fill and startup.

Each heater is installed through a heater nozzle in the reactor vessel cover. Power to the heaters is supplied from 480V 3-phase AC power or, if necessary, by an emergency diesel generator.

B. Shield and Thimble Cooling System

Normally, the heat induced in the biological shield, air baffle tank, and primary support structure, by losses from the reactor vessel bulk sodium, is dissipated by the shield cooling system. The shield cooling system consists of two basic systems operating in parallel: an air recirculating and cooling system and an exhaust air system. Power is normally supplied by the 480V distribution system. If this were to fail, power to the exhaust air system would be supplied by an emergency generator, and to the air recirculating and cooling system by another diesel generator. This shield cooling system also has alternate blowers and air conditioning equipment which is automatically switched on if a failure of the primary units were to occur.

A total heat load generated for the most part by heat losses from the reactor vessel sodium to the surrounding biological shields, is dissipated by the forced circulation of cooling air provided by the shield cooling system. The reactor vessel top support structure, the insulated top surface of the reactor vessel cover, and component nozzles are cooled primarily by the reactor building air which is drawn into the system and flows through ducts to cool these areas.

Recirculated air is made available from the cooling coils and blower and provides cooling for the radial and lower biological shields and the reactor vessel. Since the shield cooling system operates at a slightly lower pressure than the building atmosphere, a certain amount of air in-leakage occurs which simplifies the cooling of certain areas which cannot be connected to a closed system.

A thimble cooling system is provided to maintain the neutron detection instruments, which are positioned in thimbles (not currently shown) next to the core barrel, at a temperature of less than 65°C. Backup cooling includes a standby turbo compressor. If this also fails, thimble cooling can be manually transferred to the shield cooling exhaust system. Operating power for the thimble cooling system is normally supplied from the 480V power distribution system. The thimble cooling loads are automatically transferred to the emergency diesel generator during a loss of electrical power. If neutron detection instruments can be found that withstand ambient core conditions, then the thimble cooling system can be eliminated.

C. Emergency and Backup Systems

There are emergency and backup systems required to ensure that plant monitoring capability is available and for personnel safety under a loss of electrical power situations. Backup power is also provided for investment protection in certain parts of the plant to reduce the possibility of damage due to high temperatures resulting from off-normal conditions.

The emergency and backup systems are integrated with the subsystems that they service, and are usually peculiar to that system. The majority of emergency backup systems are electrical. These include standby gas or diesel generators, battery backup banks, and standby operating components such as pumps, fans, and blowers. The subsystems that incorporate these emergency and backup components include: primary sodium circulation, shutdown cooling, thimble cooling, and shield cooling.

Flywheels are incorporated into the motor generator sets that provide electrical power to the primary and secondary EM pumps. The flywheels provide for an appropriate and specific primary flow coast down that matches the reduction in power during plant shutdown following a scram and assists in the transition from forced flow to convection flow through the reactor.

With failure of the main pumps (loss of flow), the reactor will scram, the motor generator set flywheel will ensure an appropriate pump coastdown to remove the fission product decay heat produced in the reactor. Transition to natural convection will still occur assisted by the motor generator set flywheels. The motor generator set flywheels are located on the pump motor generators sets to maintain power to the pumps during loss of normal and backup power.

The emergency power is supplied by the standby generator. If this power source also fails, a storage battery which is connected in parallel with the rectifier output will operate the pump effectively for approximately 30 minutes. As the batteries discharge, the resulting gradual flow reduction will provide a transition from forced flow to natural convection cooling.

XI. INSTRUMENTATION AND CONTROL SYSTEM

The major elements of the Instrumentation and Control (I&C) system are plant control system, plant protection system, flux monitoring system, cover gas radiation monitoring system, delayed neutron detection system, and process instrumentation system.

The general guiding principles for the instrumentation and control system are:

1. Minimize instrumentation
2. Minimize electrical power requirements
3. Guarantee safety equipment operation
4. Eliminate common mode failures
5. Provide removable and replaceable instrumentation capabilities
6. Provide capability for external instrumentation calibration

A. Plant Control System

Normal reactor operations are conducted using the plant control system. This system takes action to reduce thermal transients and avoids the need for reactor scram. The primary system cold pool heat capacity dampens any thermal transients in the IHTS or the remainder of the plant that could potentially threaten the reactor core. This dampening provides time for the plant control system to take remedial action without the need to scram the reactor. The plant control system functions utilize highly reliable redundant digital equipment and reliable power supplies.

B. Plant Protection System

The plant protection system is independent of the plant control system. The plant protection system, in response to changes in monitored parameters, initiates reactor safety-related trips to shut down the reactor. Each local reactor protection system consists of four identical sensor and electronic logic divisions, each located immediately adjacent to the reactor in equipment vaults. The plant protection system performs independent Class 1E conditioning and monitoring of sensors to determine plant status during and after an accident. All safety-related data handling and information transmission are provided locally by the plant protection system.

The plant protection system is made up of safety-related equipment from the sensor through and including the isolation device that communicates with the plant control system via the fiber-optic data handling transmission system. Each of four division sensors, cabling and electronics is electrically and physically isolated from the other divisions. A list of the instrumentation associated with safety related monitoring is given in Table XI-1.

C. Flux Monitoring System

The flux monitoring system measures reactor power level by monitoring the neutron leakage flux from the reactor. The system is designed to measure neutron flux proportional to reactor power over a span of more than 10 decades from shutdown to 150% of full power. Each of four

Table XI-1. Safety-Related Monitoring Instrumentation

Monitoring Function	Instrumentation
Reactor Flow Paths	Cold Pool Temperature Core Outlet Temperature and Pressure Sodium Level Pump Discharge Pressure
Reactor Power	Neutron Detectors
Fuel Clad Integrity	Fission Gas Monitoring of Cover Gas Delayed Neutron Detection
Reactor Vessel Sodium Leakage	Annulus Gas Pressure Sodium Liquid Leak Detectors Sodium Aerosol Detectors
Shutdown Heat Removal System	NaK Inlet and Outlet Temperature and Flow Rate
Closure Leakage	Upper Containment Radiation Monitors

channels uses a fission chamber for neutron measurement. The fission chambers are placed inside the reactor in stainless-steel thimbles around the core barrel.

D. Cover Gas Radiation Monitoring System

The reactor cover gas radiation monitoring system continuously monitors the reactor cover gas for gaseous fission products via cover gas sampling and failure detection.

E. Delayed Neutron Detection System

This system continuously monitors the reactor primary sodium for delayed neutrons emitted by specific fission products. It operates with the cover gas radiation monitoring system to detect a failed fuel pin. The delayed neutron detectors will be located along the IHX shell monitoring the primary sodium flow through the IHX.

F. Process Instrumentation System

This system measures the parameters of the primary system and other heat transport systems including the intermediate heat transport system and the shutdown heat removal system.

Specifically, the process instrumentation provides sensors for temperature, flow, level, purity, leaks, vibration and acoustic measurements.

XII. BUILDINGS AND STRUCTURES

Figures XII-1 and XII-2 show the overall site plan for the SMFR site. Table XII-1 lists all the site buildings and provides their dimensions and footprint.

Table XII-1. Site Buildings with Dimensions

Building Name	Footprint (ft^2)	Length (ft)	Width (ft)	Height (ft)
Security Gate House	900	30	30	16
Control/Personnel Building	6,319	89	71	30
Reactor Building	7,832	89	89	-
Brayton Cycle Building	3,336	72	46	49
Emergency Generator Building	375	25	15	12
Balance of Plant Service Building	2,250	50	45	20
Cooling Towers (each)	2,352	48	48	33
Radwaste/ Maintenance Facility	6,000	100	60	40/80
Lift Station	1,200	40	30	16
Wastewater Treatment Plant	1,200	40	30	16
Interior Security Perimeter Fence	105,896	435	244	-
Exterior Security Perimeter Fence	242,704	616	394	-

A. Reactor Building

The reactor building, as schematically indicated in Figure XII-3, encloses the entire primary reactor system and is constructed on a seismically-isolated basemat structure. The building is a reinforced-concrete containment structure that contains an inner reactor containment dome, and is designed for a maximum leak rate of 0.1 %/day at an internal pressure of 10 psig. The reactor building is a low profile building structure with the bulk of the building located below grade. All of the primary radioactive systems are located below grade within the reactor building.

The major functions of the reactor building are as follows:

- Contain radioactive material following the unlikely event of an accidental radioactivity release from the primary reactor system.
- House and structurally support the reactor vessel, guard vessel, the shield/air baffle cooling system, support structure of the primary system and temporary fuel handling equipment, biological shielding, and associated equipment and structures.
- Provide adequate space for the operation, maintenance, and removal of equipment housed within the containment structure during periodic maintenance mode and end-of-life core changeover.
- Facilitate sodium and non-sodium fire protection for all safety equipment; this includes separation of redundant systems required for safe shutdown and for maintaining the reactor in safe shutdown condition.
- Provide protection for all safety equipment from the environment and natural phenomena such as floods, winds, tornadoes, and earthquakes.

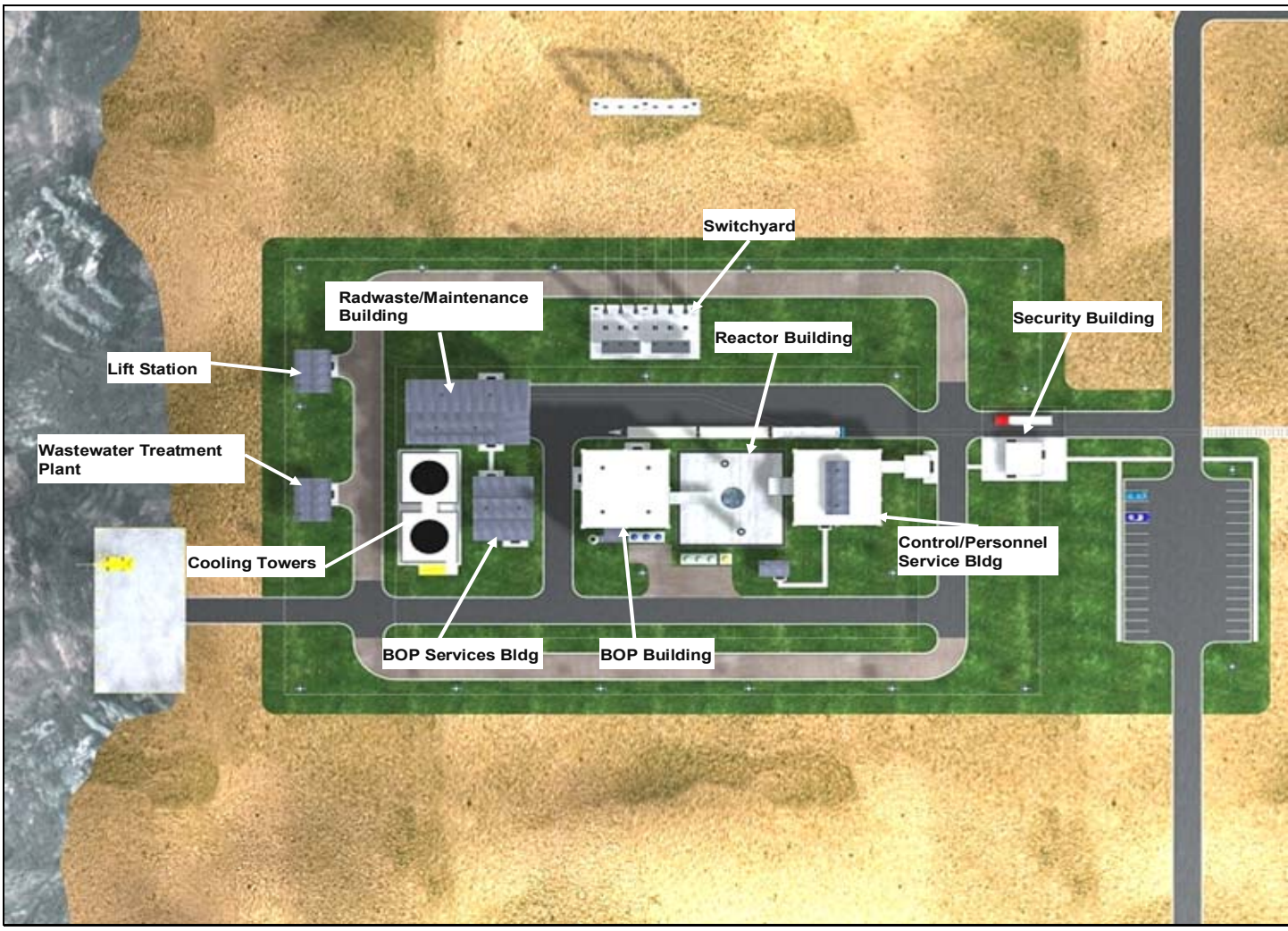

Figure XII-1. Site View from Top

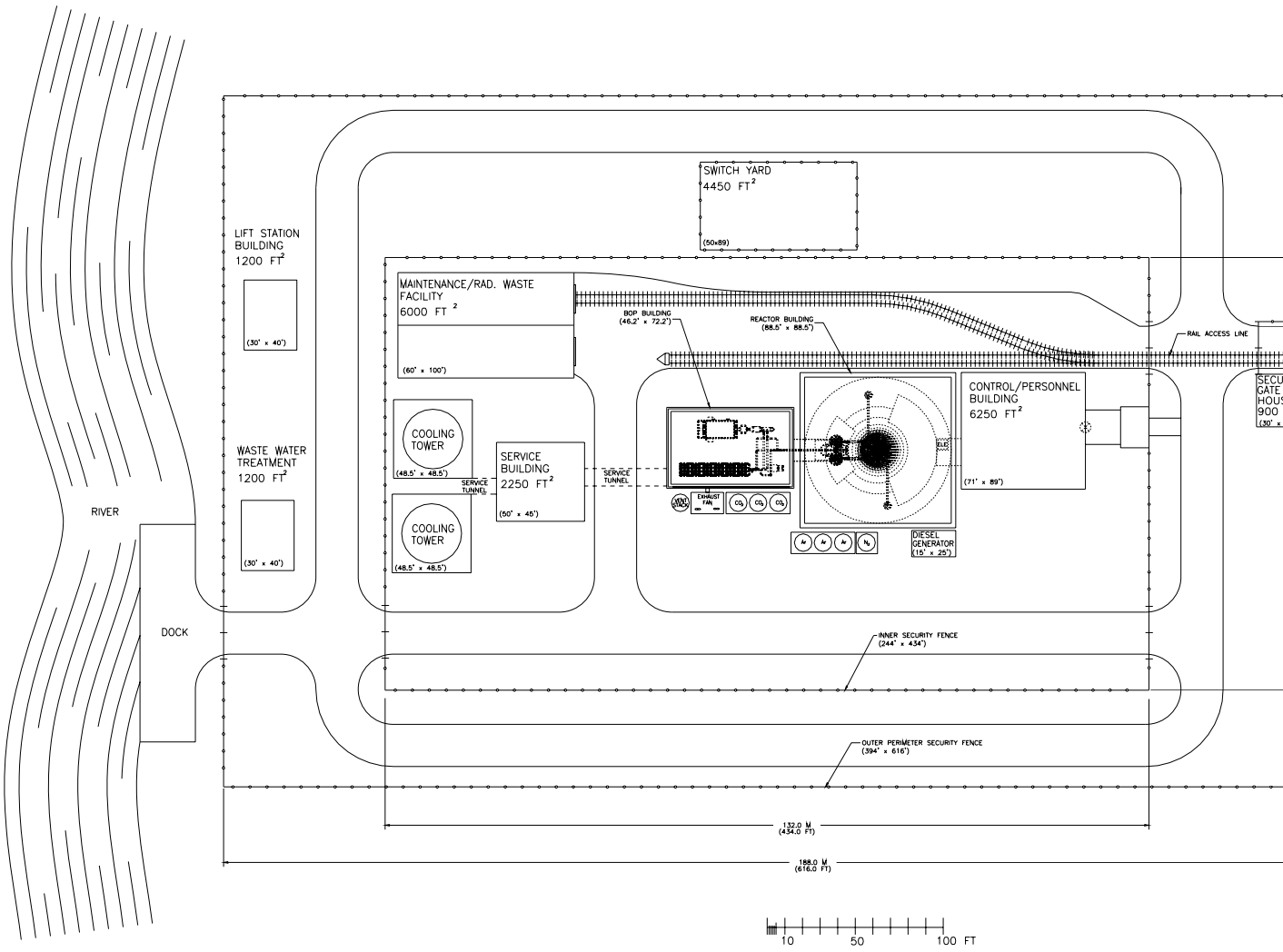

Figure XII-2. Site Plan

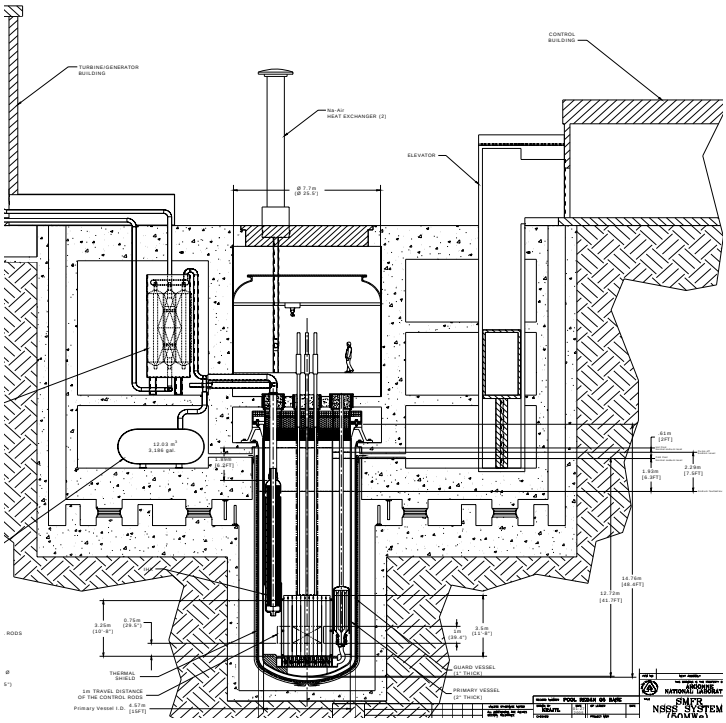

Figure XII-3. Reactor Building with Containment

- Maintain pressure within the containment boundary at less than 0.5 psig negative with respect to the exterior, except during pressurization accidents.
- Limit leakage from the containment boundary to no more than 0.1% of its contained volume per day at an internal pressure of 10 psig.
- Maintain the integrity of the containment boundary during all design loadings, including a maximum long term containment atmosphere temperature of 50°C under normal operating and design basis accident containment atmosphere conditions.

Containment Design Requirements

The reactor building will be designed to the rules of the current ASME Boiler and Pressure Vessel Code, Section III, Division 2, "Code for Concrete Reactor Vessels and Containments," Subsection CC for concrete containment. These rules provide for: material, design, fabrication, construction, examination, testing, marking, stamping, and preparation of reports for prestressed and reinforced concrete containment. The containment components covered by the ASME B&PV Code include: (1) structural concrete pressure resisting shells and shell components; (2) shell metallic liners; (3) and penetration liners extending the containment liner through the surrounding shell concrete.

Additionally, the reactor building must be designed for natural hazards, such as an earthquake, wind and flood. The design must also conform to the NRC regulatory guides (Federal Regulations 10 CFR 50 and 10 CFR 100) for seismic and other natural hazards.

Penetrations and Transfer Openings

A large number of penetrations through the reactor building shell are required for access of personnel, equipment, freight, electrical conductors, and service fluids. These penetrations are grouped into three broad classifications: large mechanical penetrations, small mechanical penetrations, and electrical penetrations. These penetrations use pressure-tight seals consisting of appropriate materials. These seals are protected from the building atmosphere since this atmosphere could become hot enough to destroy the seals should a major sodium/air reaction occur. All seals are designed to withstand the same maximum pressure of 10 psig for the building. To provide adequate assurance that the total leak rate of the reactor containment boundary remains less than the design value of 0.1% of the free volume per day, selected penetrations are leak tested annually.

The large penetrations are comprised of three airlocks (personnel, emergency personnel, and equipment airlocks) and a freight access door. The airlocks allow equipment and personnel access to the reactor plant while maintaining building containment integrity at all times. All airlocks are cylindrical steel-welded shells that have a sealed door at each end. The doors are electrically or mechanically interlocked to allow only one door at a time to be opened. The equipment airlock is the largest of the three; it connects the reactor building to the fuel service facility. The personnel airlock is smaller than the equipment airlock; it connects the operating floor area of the reactor plant to the reactor service building and serves as the normal personnel entrance and exit. The emergency airlock is the smallest of the three. It provides an emergency exit from the reactor building should the personnel airlock become blocked. All airlock doors are periodically pressure tested.

A large freight access penetration in the reactor building is provided for the infrequent use for movement of large items. This penetration is closed during all reactor operations; it is opened only for transferring large items into and out of the reactor building such as the IHX and the core changeover equipment at the end of 30 year life.

Cooling Requirements

The shutdown heat removal system transfers the decay heat from the bulk sodium in the reactor vessel directly to the atmosphere through heat exchangers located on the outside of the reactor building. Therefore, there are no unusual cooling requirements for the reactor building internal atmosphere. A standard heating, ventilation and air conditioning (HVAC) system maintains the internal atmosphere around 22°C at all times.

B. Brayton Cycle Building

The Brayton cycle building is approximately 13m x 22m x 15m high and consists of an upper and lower level. The upper level is fabricated on a slab or grate with sheet metal over frame construction and no windows. The building's heating and air conditioning system maintains an ambient temperature for the enclosed equipment and maintains a slightly negative atmosphere pressure relative to outside. This negative pressure ensures that minor CO_2 leaks in the Brayton

cycle system will be contained within the structure. The building also includes an overhead bridge crane with a capacity sufficient to provide maintenance or removal of equipment.

All ventilation equipment is located adjacent to the building to deliver air for cooling of the generator and ambient temperature control for the building.

The lower level is located below grade. It is sized to contain 2 m^3 of CO_2. There are holes in the upper floor which open to this area. In the event of a leak, this enables dense CO_2 to sink and collect in the lower level. Sensors on the lower level detect the gas and turn on exhaust fans to evacuate the CO_2 through a stack for dispersal. Another option may be ducts to carry the gas away from the site or to a scrubber device. The lower level also contains the inventory control tanks and the letdown tanks which are part of the Brayton cycle system on the upper level. Access to this lower level will be for inspection of the tanks or maintenance purposes only.

C. Reactor Control and Personnel Building

The reactor control building is a multi-story building adjoining the reactor building. This concrete and steel tornado-hardened, Seismic Category 1 structure, houses the control room, technical support center, and the central computer for the overall plant. It also includes space for switchgears, cable routing rooms, motor-generator sets, heating, ventilating and air conditioning equipment, compressed air and other auxiliary systems. Fire protection/suppression systems are also provided.

D. Radwaste/Maintenance Building

The radwaste/maintenance building is a slab-on-grade sheet metal high bay structure that provides two areas, a waste management area and a maintenance area. The waste management area is sized and designed to handle the collection, treatment, staging and shipment for disposal of all regulated wastes generated at the site. Because the plant operates for 30 years without refueling, it will not generate as large a volume of radioactive wastes as a standard reactor with frequent refueling. Waste will be generated from on-going and periodic maintenance work during the life of the plant. Equipment will exist in this building to condition the waste streams that are expected to be generated from this plant.

The maintenance side of the building provides space and equipment for the routine and planned maintenance of the facility and equipment. The maintenance building also has a location in the structure where large components will be assembled prior to installation in the reactor building. A rail spur provides easy access and delivery of components such as the reactor vessel module, primary pumps, intermediate heat exchangers, and Brayton cycle equipment to the maintenance area during installation and checkout of the primary and secondary systems. After the facility has been constructed, then the maintenance building has space and equipment for performing routine and non-routine maintenance of the reactor primary and secondary systems.

E. Security Building

The security building is a single- story reinforced concrete non-seismic category structure

located outside of the administration and service building with a reinforced concrete slab located at grade. The windows are made from bullet-proof glass.

The security building provides a controlled means of access to the plant site to prevent inadvertent access, industrial sabotage or the theft of nuclear materials. This facility will be in a remote area with minimal staff so it is essential that there be adequate site security and only one normal site entrance. All personnel must pass through this building and be checked by the associated security systems for ingress and egress to sensitive plant structures/areas or areas where radioactive materials are stored. The plant security system is monitored and operated from this building. A truck trap is located adjacent to this building that allows for security force control and containment of trucks requiring access to the site for deliveries or pickups.

F. Emergency Generator Building

A gas or diesel generator building is located adjacent to the reactor control building. It houses a modular 1MWe generator that provides emergency power to the primary and secondary systems upon demand. The emergency generator building is shipped as a single integrated unit that can be quickly installed at that site and made operable to support the construction activities during the facility construction, emergency power during reactor operations, and as an alternative source of power during reactor decommissioning.

G. Balance of Plant Service Building

The balance of plant service building provides space for equipment that supports the Brayton cycle building, cooling towers, and other services. This includes recirculation pumps, water conditioning equipment, air compressors, electrical switchgears, motor control centers, plant heating systems, and other support equipment.

H. Lift Station and Wastewater Treatment Plant Building

The lift station building provides pumps and filtration system to pump water from the river to the plant for use in cooling and domestic water services. All wastewaters go through the wastewater treatment plant where the water is conditioned prior to being discharged into the river.

XIII. COMMISSIONING AND DECOMMISSIONING

The reactor systems and facilities will be constructed using basic modules to allow for portability of the reactor components and structures. With the exception of the reactor building and the building foundations, the site building are constructed from steel framing, pre-cast concrete and/or pre-fabricated panels that allow quick assembly and disassembly. The reactor building and site foundations will be poured in place concrete with reinforcing bar. One alternative to shipping pre-cast concrete panels would be to fabricate them on site as needed. Depending upon the site location, some concrete structures that would normally be formed and poured in place could be shipped directly to the site and then assembled.

The reactor will be transported to the site in shippable modules. The reactor module consists of the reactor vessel, enclosure, and fixed internals. Plugs would be used for all the penetrations through the reactor vessel enclosure. Once all the modules and components are shipped to the site, the reactor module will be assembled in the maintenance building in a specially prepared foundation for this work. In the maintenance building, the complete reactor module will be inserted into the silo and then the intermediate heat exchangers, EM pumps, DRACS heat exchangers, and the control rod drive lines will be inserted into their respective locations inside the reactor module. The reactor module assembly will be cleaned and prepared for insertion into the reactor building.

Because the maintenance facility is a very simply constructed building, this building will be one of the first buildings constructed on the site. It will act as the reactor assembly and testing facility until the reactor module has been completely assembled and dry tested. After initial reactor module testing and when the reactor containment facility has been constructed, the reactor module will be removed from the maintenance facility using a large crane and then moved and emplaced into the reactor cavity in the reactor building. The reactor containment will be placed over the reactor module.

Fresh fuel will be installed manually in the reactor through the center refueling access plug. Nuclear-grade sodium will arrive via railcar tankers. The specially designed tankers will be heated and the sodium will be processed through the on-site purification system and its purity confirmed before being drained into the reactor primary system. After sodium is installed in the primary and secondary system, overall system checks will be completed. Then will come the pre-critical testing to confirm that the plant protection system and plant control system are functional and operational. Once all the site systems have been installed and their initial testing completed, the reactor will be started up to the point of initial criticality and all systems will be checked. Then there will be a ramp up to power.

Once the reactor is at its initial power, the reactor with its electrical system will be placed on the local electrical grid supplying electricity both off-site and on-site. After the reactor is stable and supplying electrical power, those electrical components that were using emergency power (or some alternative temporary power source), will be shifted over to site power using their automatic bus transfer devices and then the emergency power will be shutdown and placed into automatic startup mode.

The fuel handling strategy section contains information on how the reactor core will be changed after the initial 30 year core life. However, at the plant end of life, the facility will be decommissioned in much the same manner as the commissioning process. The reactor will be shutdown and the facility auxiliary systems will be placed on an alternative source of power. It would make sense if this alternative source of power were a co-located reactor that will provide the necessary site power to keep the site electrical systems powered during the decommissioning process.

After the reactor has shutdown and the fuel cooled for an adequate time to ensure that active decay heat removal is not necessary (usually about a year), then the reactor will be defueled as described above. The fuel will be shipped to an off-site processing facility. After the fuel has been removed, the sodium will be pumped from the facility into appropriate railcars and shipped to either another SMFR site or to a treatment facility for processing.

The residual sodium in the primary and secondary systems will be treated with moist carbon dioxide gas using the carbon dioxide gas from the Brayton cycle power conversion unit. The moist carbon dioxide gas will readily react with 1-2 inches of sodium depth in the primary and secondary systems. The moist carbon dioxide will react with sodium to form sodium bicarbonate and hydrogen. The reaction is very slow and controlled. After this initial reaction step, the reactor will be dismantled in modules and sections and shipped to an off-site facility for reclamation and component recovery and recycle.

The design of the plant includes appropriate attention to approaches and details that are paramount to, and facilitate the decontamination and decommissioning (D&D) effort required at the end of life for the plant. Some of these features are more or less inherent in the pool-type liquid-metal reactor designs. For example, virtually all primary system components are not only removable but would use a common scheme to effect such removals, i.e., a heavy shielded cask would be placed over the item, sealed to the support flange, and the equipment hoisted up into the cask.

LIST OF ACRONYMS

ANL	Argonne National Laboratory
ANS	American Nuclear Society
ANSI	American National Standards Institute
ASME	American Society of Mechanical Engineers
ATWS	Anticipated Transient Without Scram
BOC	Beginning of Cycle
B&PV	Boiler and Pressure Vessel
CEA	Commissariat a l'Energie Atomique
CFD	Computational Fluid Dynamics
DBE	Design Basis Events
DOE	Department of Energy
DRACS	Direct Reactor Auxiliary Cooling System
EBR-II	Experimental Breeder Reactor II
EM	Electromagnetic
EMAT	Electromagnetic Acoustic Transducer
EOC	End of Cycle
EPA	Environment Protection Agency
FFTF	Fast Flux Test Facility
HEPA	High Efficiency Particulate Air
HTR	High Temperature Recuperator
HVAC	Heating, Ventilation and Air Conditioning
HX	Heat Exchanger
IBC	International Building Code
IEEE	Institute of Electrical and Electronics Engineers
IHTS	Intermediate Heat Transport System
IHX	Intermediate Heat Exchanger
ISI	In-Service Inspection
IVIM	In-Vessel Inspection Machine
JAPC	Japan Atomic Power Company
JNC	Japan Nuclear Cycle Development Institute
LMR	Liquid Metal Reactor
LRB	Laminated Rubber Bearing
LTR	Low Temperature Recuperator
MOC	Middle of Cycle
MOX	Mixed Oxide
MWe	Megawatt Electric
NDE	Non-Destructive Examination
NDHX	Natural Draft Heat Exchanger
NPSH	Net Positive Suction Head
NRC	Nuclear Regulatory Commission
OBE	Operating Basis Earthquake
OSHA	Occupational Safety and Health Administration
PCHE	Printed Circuit Heat Exchanger
PHTS	Primary Heat Transport System

PLOF	Protected Loss of Flow
PLOHS	Protected Loss of Heat Sink
PRISM	Power Reactor Inherently Safe Module
RBCB	Run Beyond Cladding Breach
RCB	Remote Controlled Vehicle
SHRS	Shutdown Heat Removal System
SMFR	Small Modular Fast Reactor
SS	Stainless Steel
SSE	Safe Shutdown Earthquake
TREAT	Transient Reactor Test Facility
TRU	Transuranic
ULOF	Unprotected Loss of Flow
ULOHS	Unprotected Loss of Heat Sink
UTOP	Unprotected Transient Overpower

APPENDIX A. OVERALL SMFR DESIGN REQUIREMENTS

1. Base Requirements

These requirements define functional and performance characteristics of the SMFR plant, and code and regulatory requirements which the plant design must satisfy. They also define features and characteristics of fabrication and construction which are utilized to effect a safe, reliable, and economical design of the SMFR plant.

- The SMFR plant design shall be capable of being licensed and certified by the Nuclear Regulatory Commission (NRC).
- The SMFR plant shall be capable of being located on a remote site with minimal infrastructure support.
- The reference power plant size shall provide 50 MWe.
- The SMFR plant shall utilize modular construction methods such that nuclear plant cost elements which have demonstrated significant instability in the past, specifically field labor and materials and field engineering and services, are minimized and maximum reliance is placed on the cost elements which have demonstrated stability, such as factory-produced equipment and replicated installation.
- The SMFR design shall have passive means of negative reactivity insertion and decay heat removal sufficient to place the reactor system in a safe stable state for specified anticipated transient without scram (ATWS) events without significant damage to the core or reactor system structure.
  (Note: A passive feature is one which relies only on the laws of nature and the integrity of structural members; requires no sensing, switching, motive power, or human interaction; and is not defeated or is difficult to defeat, by human action. Examples of passive features include naturally circulating fluid systems, thermal expansion, mechanical stops, and rupture discs or double-tube steam generator design.)
- The SMFR plant shall have features which minimize the probability of major sodium fires and minimize the damage from such fires.
- The SMFR reactor nuclear island and balance-of-plant design shall minimize operator demands during operation and shall provide ease of plant inspection and maintenance.
- The plant's safety, operational, maintenance and in-service inspection features shall be capable of demonstration and confirmation in an affordable full-scale prototype to provide a credible basis for NRC design certification and user acceptance of the SMFR.
- The SMFR plant shall be designed with emphasis on simplification as a prime consideration to enhance reliability, availability, and maintainability and shall integrate the following functional capabilities into the design:
  - Load following capability over the range of 25 to 100% power, including a 10% step load change.
  - Rapid plant recovery following protection system actuation.
  - Sustain load rejection from rated power without reactor scram.

- The reactor shall be designed to minimize the risk of sabotage or proliferation, either through design features, or by proven safeguards and security techniques, or a combination of the two.
- The design life of the SMFR plant shall be 60 years with a core life of 30 years.
- The design shall comply with all applicable codes and standards issued by the American National Standards Institute (ANSI), the American Nuclear Society (ANS), the American Society of Mechanical Engineers (ASME), and the Institute of Electrical and Electronics Engineers (IEEE).
- The SMFR shall be designed for significant margins of safety under all design basis events (DBE). These margins shall be such that:
  - No clad failure or structural failure shall result from the design basis events, including allowance for uncertainties.
  - The design allowable fatigue life cycles shall be at least twice the expected number of duty cycle transients.
- The SMFR plant design shall meet NRC and DOE release requirements and EPA protective action guidelines and shall incorporate sufficient passive and engineered safety features such that the emergency response is not required.
- As a minimum, the safety grade portions of the SMFR plant shall be designed to withstand a 0.4 to 0.6 g safe shutdown earthquake (SSE) seismic event without loss of function. The minimum operating basis earthquake (OBE) design value shall be ~ 1/3 of the SSE value.
- Nonsafety grade portions of the plant shall be designed to the International Building Code (IBC) requirements such that their intended function is not lost as a result of IBC seismic levels. Seismic Use Group III structures and systems shall ensure that the safety functions of all interfacing safety systems are not compromised at Design Basis Seismic accelerations.
- The SMFR shall transmute minor actinides and minimize the wastes that are generated during the reactor life cycle.
- The SMFR plant shall have the capability to achieve a capacity factor greater than 90%.

2. Technical Requirements

This section contains specific engineering, technical, and/or functional requirements necessary to achieve the desired performance of the SMFR nuclear power plant.

- Plant operating procedures and diagnostics shall be automated to the extent required to minimize operating and maintenance (O&M) cost, public risk, and operator exposure to radiation.
- Diagnostic systems shall be provided to detect incipient accident conditions and to aid identification of operator actions needed to return the plant conditions to normal. No operator action in the control room or remote shutdown locations shall prevent the reactor protection system from performing its safety function nor inhibit the function of the passive safety features.
- The plant design shall include reliable equipment for the balance of plant (or safety-system independence from balance of plant) to reduce the number of challenges to safety systems.

- The design shall minimize required maintenance and facilitate maintenance when needed. The design shall minimize the manpower required for maintenance and minimize the skills required to keep the plant maintained.
- All systems and components shall be designed so that routine maintenance activities may be performed during operations.
- The design shall allow for access, viewing, inspection, and testing of systems and components, working and laydown space for component repair or replacement, and facilitate plant cleanup. Remote maintenance shall be minimized; where remote maintenance/inspection is required, proven robotic methods shall be utilized.
- The maintenance plan shall ensure that all failures with a probability of occurrence greater than 10^{-4} per reactor year shall have a specified plan for corrective action. Failures with a probability of occurrence of less than 10^{-4} events per reactor year shall have a feasible means of corrective action.
- An In-service Inspection (ISI) program shall be developed which meets the intent of Division 3 of Section XI of the ASME B&PV Code. The ISI program shall ensure the nuclear safety-related structures, components, and systems maintain their integrity as necessary to perform their safety functions. The program shall be applied to safety-related components subject to the jurisdiction of Section III of the ASME B&PV Code. For areas not covered by Section III of the ASME B&PV Code, the design shall include inspection provisions consistent with the objective of maintaining safe operable conditions throughout the plant.
- The design of systems and components shall incorporate features to implement required surveillance and ISI with the plant on-line to the greatest degree practical.
- Radiation protection shall be provided to maintain radiation exposure to as low as reasonably achievable (ALARA), in conformance with radiation exposure requirements of this specification and DOE/NRC requirements.
- Provisions shall be made for handling and transporting new and spent cores.
- The normal system for forced convection transfer of reactor heat to the sodium/CO2 heat exchanger shall be the heat transport system (consisting of primary and intermediate heat transport systems). The heat transport system shall provide sufficient capability to prevent exceeding acceptable fuel design limits, and to maintain ASME B&PV Section III Code Levels A and B design limits during conditions of normal operation. The heat transport system shall also be configured to ensure natural circulation coolant flow and to limit sodium coolant inventory loss in the event of a major pipe or vessel rupture.
- The shutdown heat removal system (SHRS) shall be safety grade and shall be designed with sufficient capability to prevent exceeding ASME B&PV Code Section III Level B and fuel design limits in the event that the normal heat sink is unavailable.
- The SHRS shall employ operating principles which assure passive, continuous decay heat removal without human intervention under all postulated accident conditions. It shall incorporate the necessary heat transfer means to prevent exceeding ASME B&PV Code Section III Level C design limits and fuel safety limits when normal decay heat removal means are unavailable.
- The containment system, including all access openings and penetrations, internal compartments, and structures, shall be designed with sufficient margin to accommodate the calculated pressure and temperature conditions under normal operating conditions, DBEs, and specified Anticipated Transients without Scram

(ATWS) events without exceeding the design leakage rate. The design shall provide a barrier against uncontrolled release of radioactivity to the environment, and to ensure that site release limits are not exceeded.

- The containment system margin shall also account for: (1) the effects of potential energy sources, such as decay heat in fission products, potential spray or aerosol formation, and potential exothermic chemical reactions; (2) the limited experimental data available for defining accident phenomena and containment response; and (3) the conservatism and uncertainties of the models that are used.
- The containment system and equipment shall be designed to permit periodic leakage rate testing and surveillance of the containment boundaries.
- The containment system boundary gas leak rate shall not exceed 0.1% volume per day under design basis conditions.
- The containment system shall be capable of maintaining site release limits in the event there is a breach in the primary system boundary.
- A safety grade, Class 1E reactor protection system, which is separate and independent from the plant control system, shall be provided to prevent fuel damage, limit reactor structural challenges to less than ASME B&PV Code Section III Level C limits, and monitor reactor safety functions.
- The reactor protection system equipment for monitoring safe shutdown conditions shall be designed to monitor selected system parameters over their anticipated ranges of normal operation through Design Basis Earthquake (DBE), specified ATWS, and bounding event conditions, including those variables and systems that can affect the fission process, integrity of the reactor core, reactor coolant boundary, and containment and its associated systems.
- Instrumentation for monitoring safe shutdown conditions shall be designed to be highly reliable and fault tolerant.
- Two independent reactivity control systems employing different design principles shall be provided. Sufficient capability shall be provided in each system to ensure that the reactor can be maintained in a safe shutdown state under all operating and postulated accident conditions assuming failure of the other system.
- The IHX and supercritical CO_2 secondary system shall be designed such that any failure of the sodium/supercritical CO_2 boundary in the supercritical CO_2 heat exchanger and resulting sodium/CO_2 reactions will not result in a breach of the IHX to the primary sodium.

APPENDIX B. TECHNICAL RATIONALE FOR METAL FUEL

1. Steady-State Irradiation Performance

Metallic fuel was the original choice in early fast reactors because it is compatible with the liquid metal sodium coolant. The metallic fuel development as fast reactor fuel was abandoned in the late 1960's in favor of ceramic oxide fuel developed for the commercial water cooled reactors. At that time, it was perceived that metallic fuel could not achieve high burnup because the irradiation induced swelling could not be constrained by cladding.

However, EBR-II continued to use metallic fuel as its driver fuel and its burnup capability was drastically improved through discoveries in the late 1960's and irradiation experience in the 1970's. The key discovery was that metallic fuel can achieve high burnup by allowing room for fuel to swell rather than trying to constrain the swelling. The fuel swelling is driven primarily by the internal pressure of fission gas bubbles. Once fuel swells by about 30% in volume, then the fission gas bubbles interconnect and provide passage for fission gas to be released to the plenum located above the fuel rod. By adequately sizing the plenum to contain fission gases released through interconnected porosity, the fuel swelling can be easily constrained by the cladding and a high burnup can be easily achieved. The porosity would also be available to accommodate the inexorable swelling from the accumulation of solid fission products.

A schematic of metallic fuel is shown in Figure B-1. The fuel slug is loaded inside the cladding, and the gap between the slug and cladding is filled with sodium which acts as thermal bond until fuel swells out to the cladding. The fuel slug can be in full length or segmented pieces loaded on top of each other.

Figure B-2 illustrates the effect of fuel swelling on fission gas release for a variety of metal fuel alloys, ranging in burnup from 2.7% to 12.5% and peak operating temperatures of 450 to 840^{o}C.

The original EBR-II Mark-I metal fuel pin was designed with 85% smear density. With the discovery on fuel swelling, the Mark-II fuel design incorporated 75% smear density. The burnup was gradually increased and bulk of Mark-II design achieved 7-8% burnup. The Mark-II cladding also had an indentation above the fuel column to act as a fuel restrainer. The original indentation was a chisel shape, which became a weak point at about 8% burnup. However, with a new cladding design that changed from a chisel to a spherical indent, much higher burnup could be achieved and some fuel pins reached 18.5% burnup. Over 40,000 Mark-II metal fuel pins have been successfully irradiated through early 1980’s. Figure B-3 illustrates the peak burnup distribution of these Mark-II fuel pins.

The EBR-II Mark-I and Mark-II fuels are composed of 95% uranium and 5% fissium alloy. During the first 5 years of EBR-II operation, the fuel was recycled through melt-refining and injection casting refabrication. In this early pyrometallurgical processing, noble metal fission products were recycled back along with the recovered uranium.

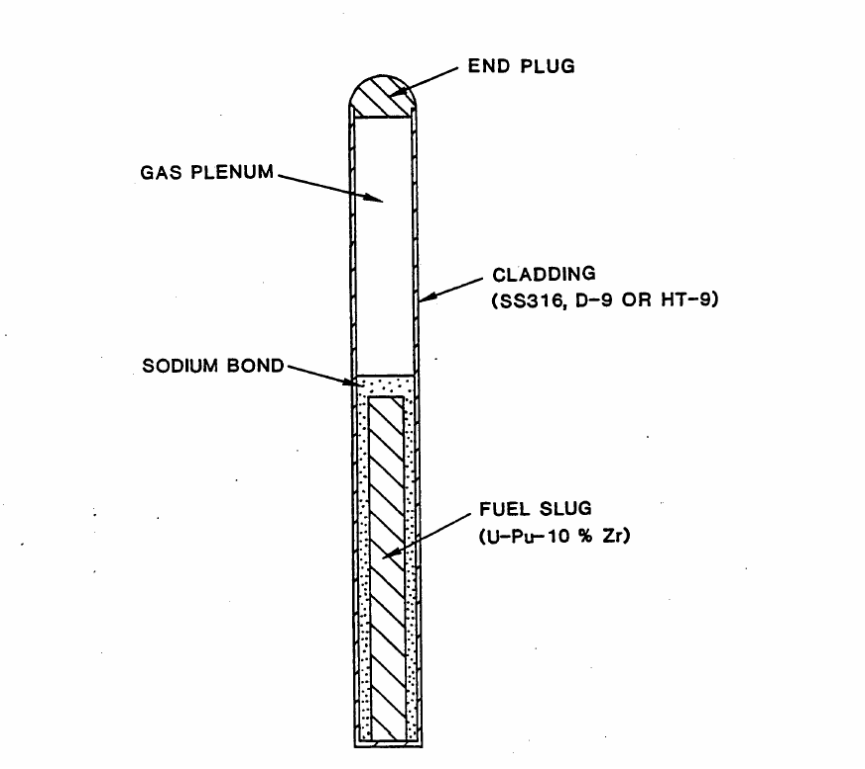

Figure B-1. Schematic of Metallic Fuel Pin

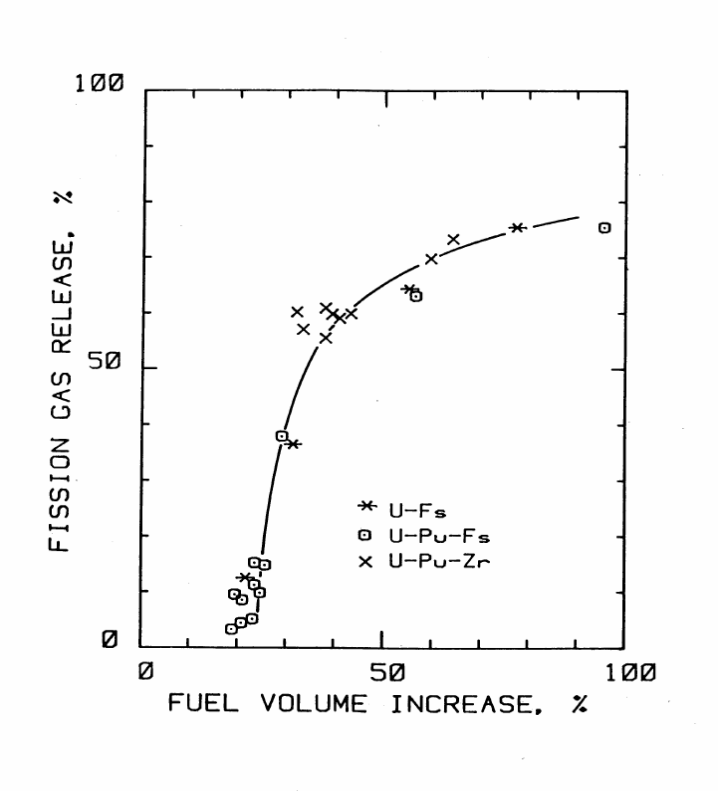

Figure B-2. Effect of Fuel Swelling on Fission Gas Release in Metallic Fuels.

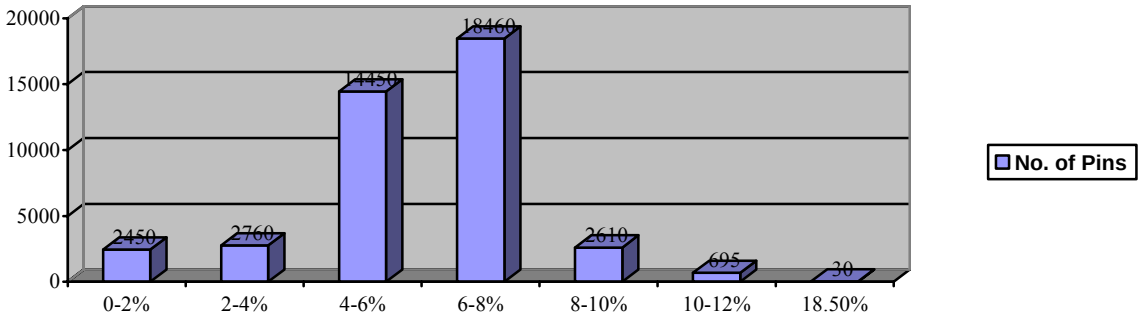

Figure B-3. Burnup Distribution of Mark-II U-Fs Fuel Pins in EBR-II

The equilibrium composition through repeated recycle was approximately as follows:

Molybdenum	2.46%
Ruthenium	1.96%
Rhodium	0.28%
Palladium	0.19%
Zirconium	0.10%
Niobium	0.01%
Total	5.00%

This composite alloy was called "fissium." Because of their beneficial effects on the metal fuel irradiation performance characteristics, the 5% fissium addition was continued for all Mark-I and Mark-II fuels even after the recycle operation ceased in 1969.

When the Integral Fast Reactor (IFR) Program was initiated in 1984, a 10% zirconium addition, replacing 5% fissium, was selected as the reference alloying agent for both uranium and plutonium bearing fuels. Earlier irradiation tests of various alloys indicated that Zr exhibited exceptional compatibility with cladding in addition to significantly increasing the fuel alloy solidus and fuel-cladding eutectic temperatures. Therefore, as the Mark-II driver fuel assemblies reached their irradiation limits, the EBR-II core was gradually converted with new Mark-III fuel based on U-10%Zr with D-9 or SS-316 cladding. Later, Mark-IV fuel with HT-9 cladding was introduced.

At the same time, Experimental Fuels Laboratory was established in 1984 to fabricate plutonium-bearing ternary fuel, U-Pu-10%Zr. A total of 16,811 U-Zr and 660 U-Pu-Zr fuel pins were irradiated in EBR-II in the next 10 years until EBR-II was permanently shut down at the end of September, 1994. Burnup distributions achieved by U-Zr and U-Pu-Zr fuel pins are presented in Figures B-4 and B-5, respectively.

In addition to the 30 years of extensive irradiation experience in EBR-II, seven full assemblies of metallic fuel were irradiated in FFTF. One assembly contained U-Pu-Zr fuel pins, which achieved a peak burnup of 10.2%. The other six assemblies were part of the core conversion qualification tests of U-Zr fuel with HT-9 cladding. All of these assemblies achieved

peak burnup in excess of 10% and the lead test achieved a peak burnup of 16%. The FFTF core conversion with metallic fuel was abandoned when a decision was made to shut down FFTF.

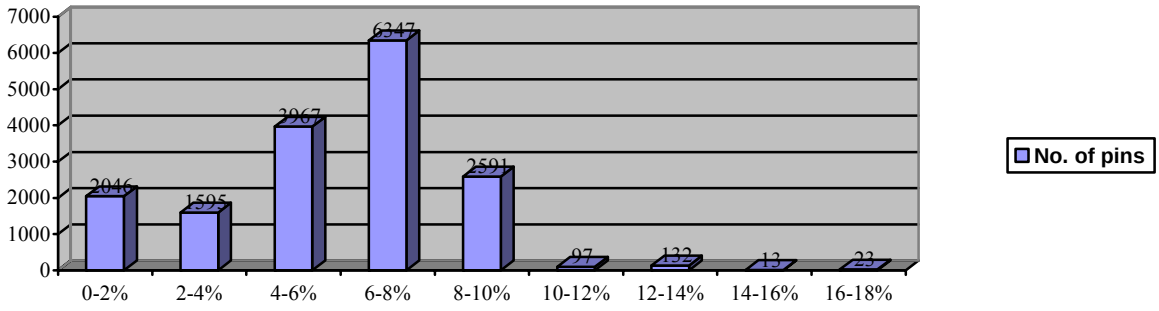

Figure B-4. Burnup Distribution of U-Zr Fuel pins in EBR-II

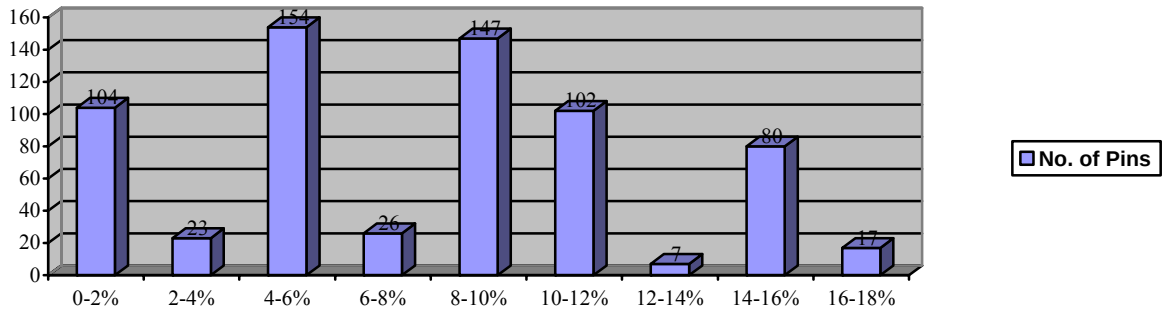

Figure B-5. Burnup Distribution of U-Pu-Zr Fuel Pins in EBR-II

2. Off-Normal Performance Characteristics

Metallic fuel has excellent transient capabilities. The metallic fuel itself does not impose any restrictions on transient operations or load-following capabilities. The robustness of metallic fuel is illustrated by the following sample history of a typical driver fuel irradiated during the EBR-II inherent passive safety tests conducted in 1986:

40 start-ups and shutdowns
5 15% overpower transients
3 60% overpower transients
45 loss-of-flow (LOF) and loss-of-heat-sink tests including a LOF test from 100% power without scram.

Metallic fuel also has benign run beyond cladding breach (RBCB) performance characteristics. As shown in Figure B-6 for the oxide fuel (9% burnup) RBCB test, the initial

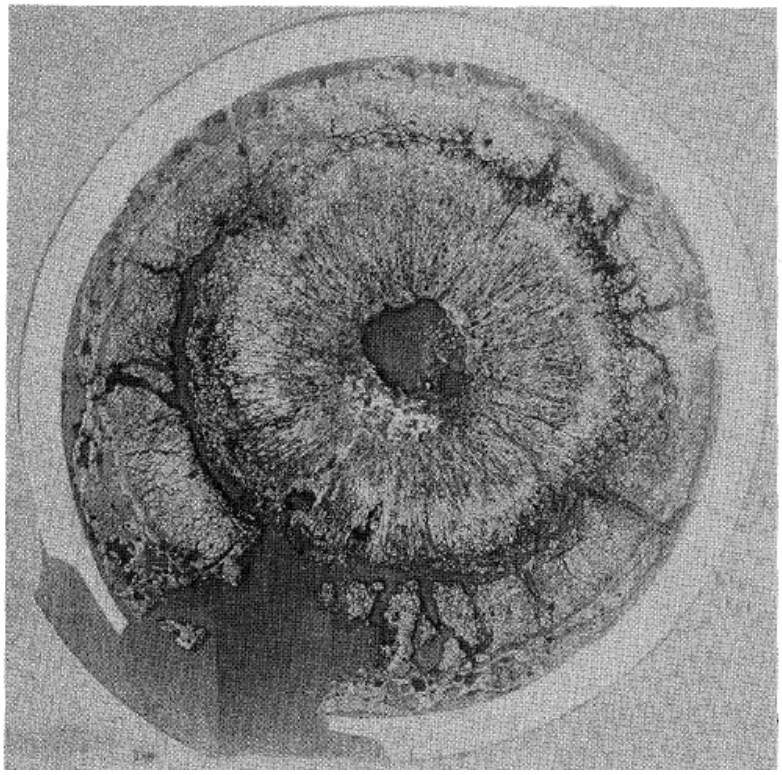

Figure B-6. Oxide Fuel (9% burnup) RBCB Test

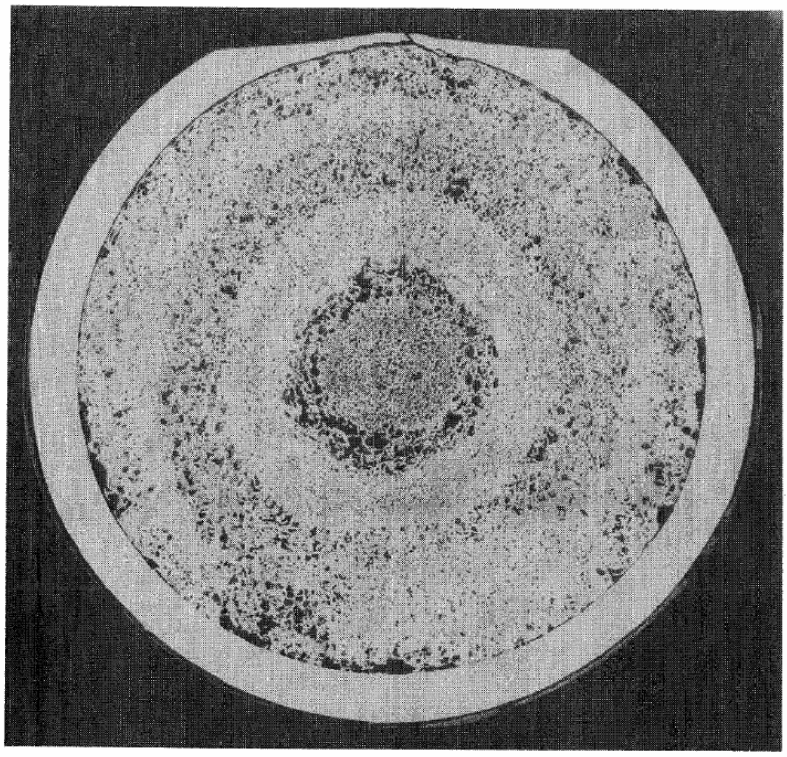

Figure B-7. Metallic Fuel (12% burnup) RBCB Test

breach site is widened due to fuel-cladding mechanical interaction caused by low density Na-fuel interaction product, $Na_3(PuU)O_4$, which results in a small amount of fuel loss to the coolant.

A RBCB test with metallic fuel (12% burnup) is illustrated in Figure B-7. Because metallic fuel is compatible with sodium, there is no reaction product and the fuel loss is practically zero. The post-irradiation examination shown in Figure B-7 is after operation in RBCB mode for 169 days and there is no indication of breach site enlargement. In another test, metallic fuel operated 223 days beyond cladding breach, including many start-up and shut-down transients, and the breach site remained small. Metallic fuel is expected to be very reliable. However, even if unforeseen fuel failure occurs, the failed fuel pins could be left in the core until the end of life without raising any safety concerns.

The eutectic formation temperature between the fuel and the cladding has been considered a critical parameter for the metallic fuel pin design. The onset of fuel-cladding eutectic formation starts at 700-725^{o}C range, depending on the fuel alloy and cladding types. However, at this onset temperature, not much interaction occurs. In fact, even at 100^{o}C above the eutectic temperature, the eutectic penetration into the cladding is minimal in one hour. Only at much higher temperatures, close to the fuel melting point itself, the eutectic penetration into cladding becomes rapid. Therefore, the eutectic formation is not a primary safety concern during transient overpower conditions as discussed in the next section. However, the eutectic temperature limits the coolant outlet temperature to 500-510^{o}C in order to provide adequate margins to onset of eutectic formation.

3. Inherent Passive Safety

Although the metallic fuel melting temperature is much lower than that of oxide fuel, it is also much more difficult to raise the fuel temperature because of the high thermal conductivity (~20 W/mK for metal compared to ~2 W/mK for oxide). As a result, operating margins in terms of power can, in fact, be greater for metal than for oxide cores.

Metallic fuel provides better or equal safety characteristics across the entire spectrum from normal behavior to postulated severe accidents. However, it is in the inherent passive safety characteristics under the generic anticipated transient without scram events, such as unprotected loss-of-flow (ULOF), unprotected loss-of-heat-sink (ULOHS), and unprotected transient overpower (UTOP), that the metallic fuel shows its greatest advantages over oxide fuel.

The inherent passive safety potential of the metallic fuel was demonstrated by two landmark tests conducted in EBR-II on April 3, 1986. These tests, ULOF and ULOHS, demonstrated that the unique combination of the high heat conductivity of metallic fuel and the thermal inertia of the large sodium pool can shut the reactor down during these potentially very severe accident situations, without depending on human intervention or the operation of active, engineered components. The coolant temperature responses during the ULOF test is presented in Figure B-8.

In an ULOF event, the coolant temperature increases as the flow is reduced rapidly. The increased coolant temperature results in the thermal expansion of core assemblies, which provides a negative reactivity feedback and starts a power rundown. During this initial period, it

is important to maintain a reasonable flow coastdown in order to avoid immediate sodium boiling.

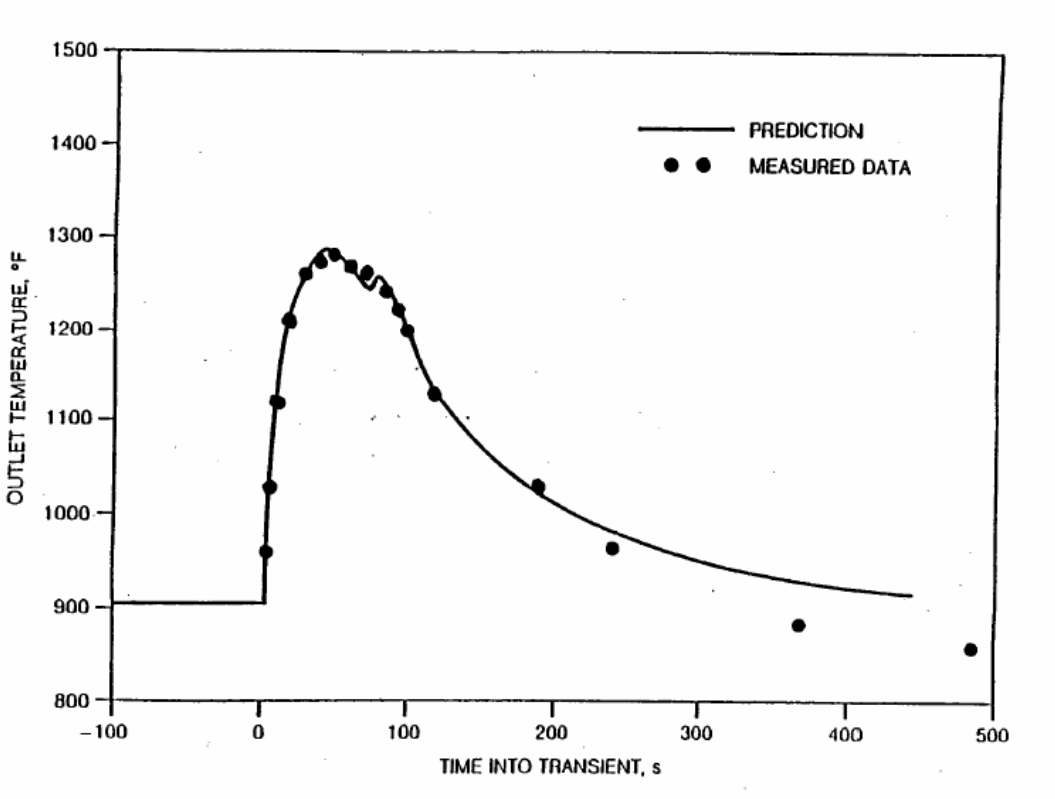

Figure B-8. Unprotected Loss-of-flow Test in EBR-II Demonstrated the Benign Behavior Predicted

The characteristics of the negative reactivity feedback caused by the increase in coolant temperature determine the reactor response. The most important factor differentiating the responses in metallic and oxide fuels is the difference in stored Doppler reactivity between the two fuel types. As the power is reduced, the stored Doppler reactivity comes back as a positive contribution, tending to cancel the negative feedback due to the thermal expansion of structures. The high thermal conductivity of metallic fuel and consequent low fuel operating temperature give a stored Doppler reactivity that is only a small fraction of overall negative reactivity feedback. As a result, the power is reduced rapidly. In contrast, oxide fuel has a much greater stored Doppler reactivity (primarily due to higher fuel temperatures rather than the difference in the Doppler coefficient itself), and the power does not decrease rapidly during the ULOF event. And when the power has been reduced to decay heat levels to counter the stored Doppler reactivity, the coolant temperature maintains a much higher value in an oxide core. This comparison between oxide and metal cores is illustrated schematically in Figure B-9.

The superior neutronics performance characteristics of metallic fuel allow core designs with minimum burnup reactivity swing even for small modular designs. This can be used not only in extending core life to 30 years but also in reducing the UTOP initiator caused by an unprotected control rod runout. Transient overpower tests on metallic and oxide fuels performed in Transient Reactor Test Facility (TREAT) have demonstrated a larger margin to cladding failure threshold

for the metallic fuel. As shown in Figure B-10, oxide fuel pins fail typically 2.5 –3 times nominal peak power (4-4.5 times in adiabatic conditions), whereas metallic fuel pins fail 4-4.5 times nominal peak power. Another significant finding from these TREAT tests is that fission gas driven axial expansion of fuel within the cladding before failure provides an intrinsic and favorable negative reactivity feedback in the metallic fuel that has no parallel in oxide. The metallic fuel prefailure axial extrusion as a function of burnup is illustrated in Figure B-11.

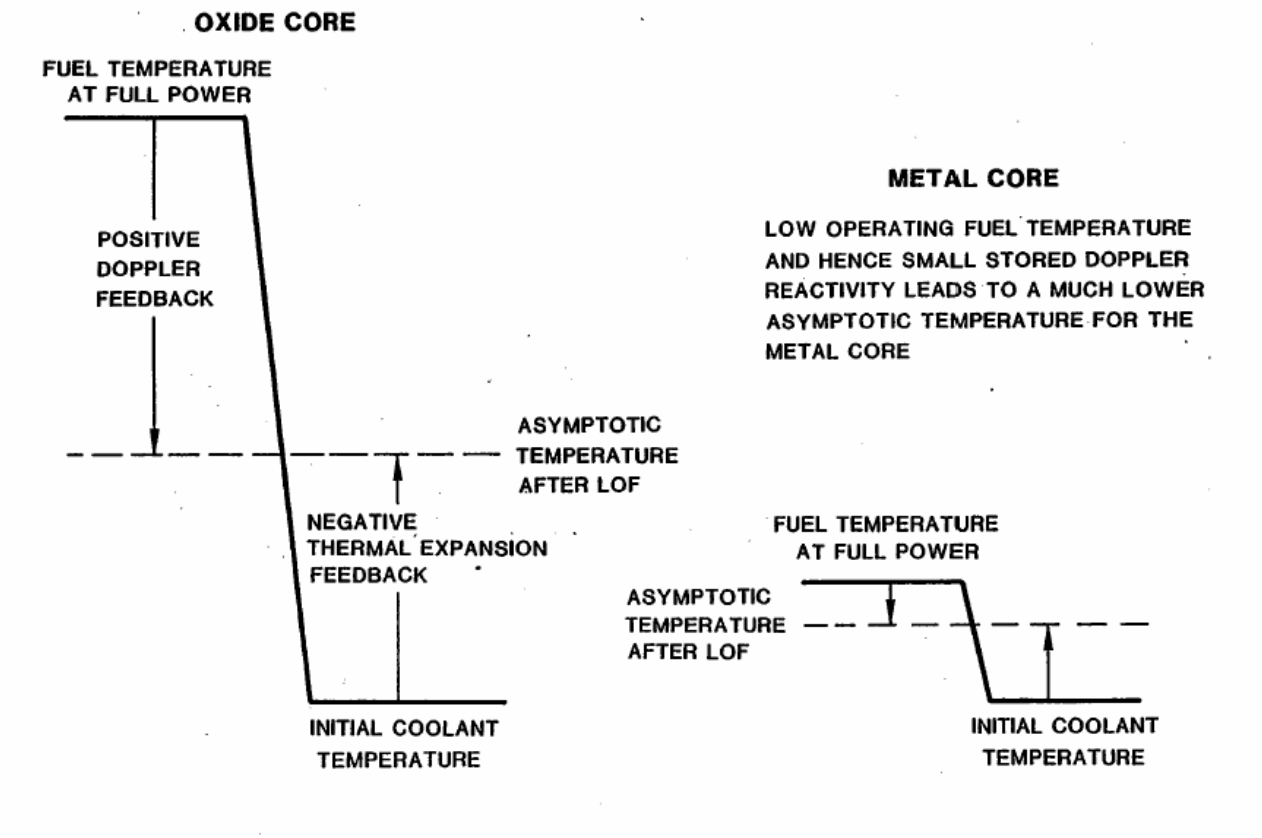

Figure B-9. Asymptotic Temperature Reached during LOFWS Event is Determined by Reactivity Balance: Comparison of Oxide and Metal Cores

4. Fuel Cycle Implications

Metallic fuel is easily fabricated using injection casting technique, requires no finishing, and allows a relaxed specification in dimensions and impurities that further simplifies the fabrication process. Furthermore, metallic fuel is compatible with pyroprocessing based on electrorefining. Although fuel cycle closure is not an immediate issue for the SMFR, the core at the end of life has to be processed for reuse and pyroprocessing could have a far reaching impact for fuel cycle closure in the long term.

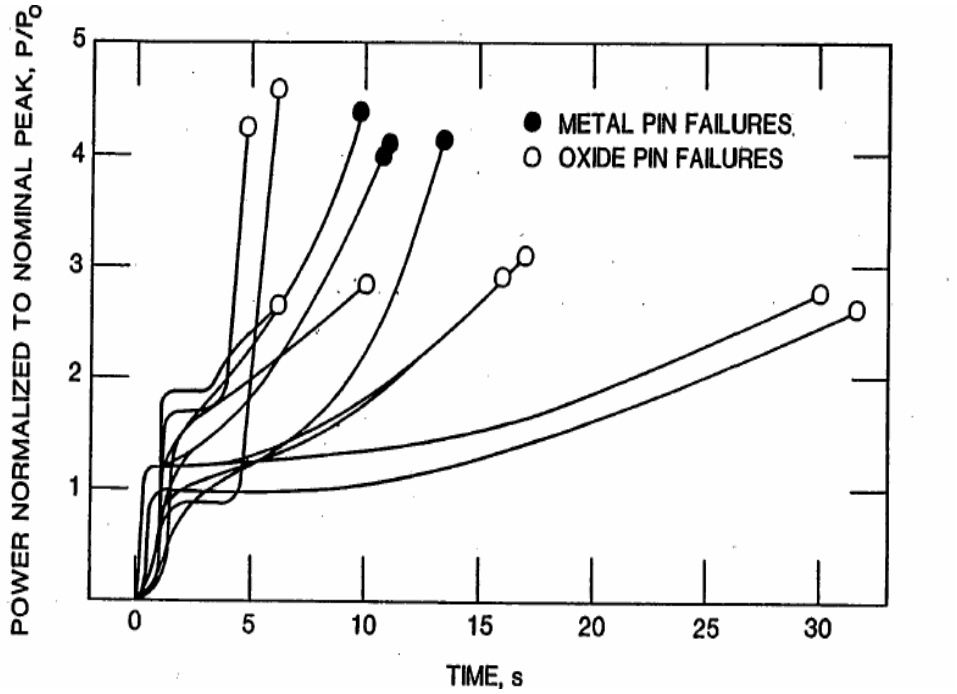

Figure B-10. Transient Overpower Failure Tests in TREAT Show Generally Greater Margins for Metallic Fuel

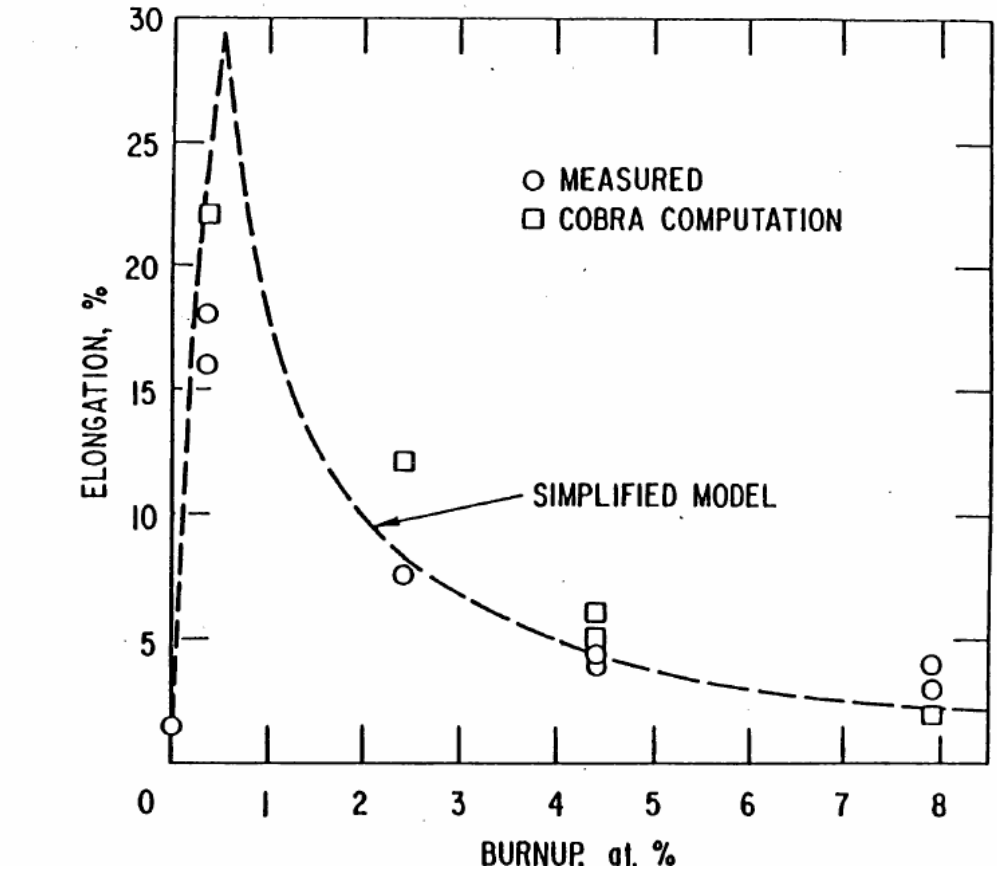

Figure B-11. Prefailure Axial Fuel Extrusion as a Function of Burnup for Metallic Fuel

APPENDIX C. SAFETY ANALYSES

This appendix presents preliminary analyses performed to assess the potential safety performance characteristics of the Small Modular Fast Reactor (SMFR) design. The limited scope of the analyses focuses on the ability of SMFR to provide inherent protection against damaging consequences in low probability accident sequences involving multiple equipment failures. This introductory section provides background on the safety analyses and a summary of analysis results.

1. Introduction and Summary

Analysis Background

One of the primary goals in the SMFR design has been to provide not only the customary safety margins in design basis events, but also to deliver superior safety performance in beyond design basis events involving multiple equipment failures or unplanned operator actions. These characteristics are desirable for all nuclear reactors, but especially in the case of SMFR, which is intended for remote sites and optimized for minimum attention in normal operation and maximum self-protection in upset conditions. Consequently, the preliminary analysis presented here examines the behavior of SMFR in response to an accident initiator that is normally considered to have a low occurrence frequency, but might have severe consequences, especially with failure of engineered safety systems.

The accident initiator examined here is the total loss of normal power to the reactor cooling system while the plant is operating at full rated power. This sequence may receive enhanced emphasis for remotely sited plants, where off-site power supplies may be less available or less reliable than for stations more closely connected to established power distribution grids. Within the plant, the effect of this initiator is the loss of normal operation of all reactor coolant pumps. According to design, the plant responds with a reactor scram, with activation of emergency power supplies (diesel generators and batteries), and with activation of the normal shutdown heat removal mode. The normal shutdown heat removal path is through the reactor coolant system and the power cycle (sodium-CO_2) heat exchanger, with auxiliary power supplied by the emergency power supplies. As a backup, a low-capacity emergency heat removal system is provided to remove heat directly from the reactor without the need for emergency power.

In the accident sequence analyzed here, the loss of power is accompanied by a complete failure of the emergency power supply system, resulting in a total loss of power to the reactor and intermediate coolant pumps. It is also assumed that the power generation plant immediate ceases operation, and provides no heat rejection capacity. The sole heat removal path following the loss of forced coolant flow is through the emergency heat removal system by natural circulation. This sequence was analyzed for the case with an immediate reactor scram, and for the case without reactor scram. For convenience, these cases will be called the protected loss-of-flow (PLOF) case and the unprotected loss-of-flow (ULOF), respectively. The PLOF and ULOF accident sequences both assume multiple equipment failures, failures of safety grade protection and cooling systems, and no operator actions. These sequences are an extreme test of the SMFR to provide inherent self-protection against the consequences of the most severe accident initiators.

Results Summary

The detailed analysis results for the PLOF and ULOF accident sequences are presented in Section 4. Although both sequences simulate accidents that for some reactor designs may cause damage to the fuel and possibly progress into severe accident conditions, in SMFR these events cause no damage. For both accident sequences in SMFR, reactor fuel, cladding, and coolant temperatures remain below safety limits.

In the PLOF sequence, the loss of forced coolant flow and normal heat removal is accompanied immediately by a reactor scram, which quickly brings the reactor power to decay heat levels. Early in the sequence, the emergency decay heat removal system does not have sufficient capacity to remove all the heat being produced, so system temperatures rise. But thanks to the large heat capacity of the sodium-cooled pool-type concept, the SMFR is able to absorb a significant amount of energy with only a slight temperature increase, and the good natural circulation capability of the SMFR promotes heat removal through the available emergency heat sink. After about 11 hours, the reactor decay heat falls to the capacity of the emergency heat removal system, and afterwards system temperatures decrease. The analysis predicts that the peak fuel cladding temperatures in the accident will be 40^{o}C lower than the normal operating temperature, so no fuel damage or cladding failures would occur.

In the ULOF accident, the reactor safety system fails to scram the reactor upon loss of forced coolant flow and normal heat removal, so the reactor remains at power, with only the emergency heat removal system available for heat rejection. In the first few minutes, the reactor temperatures rise as the coolant flow falls, and inherent reactivity feedbacks reduce the reactor power. During this time, peak cladding temperatures temporarily reach 735^{o}C for a short period, but the duration is not sufficient to cause cladding significant damage or failure. With a transition to natural circulation cooling, the reactor temperatures peak and then fall, but the reactor still produces heat at a rate higher than the capacity of the emergency heat removal system. This has the effect of slightly overheating the system, and causing a persistent negative reactivity that extinguishes fission power and maintains reactor heat production at decay heat.

After about 2 hours, the decay heat falls to the emergency heat rejection capacity, which has been enhanced by the elevated reactor temperatures. At this point, temperatures begin to fall, but this causes a positive reactivity that rekindles fission power. Subsequently, the inherent feedbacks control the reactor fission power to maintain equilibrium with the emergency decay heat removal capability, and system temperatures remain constant. In the long term, peak cladding temperatures remain stable at 538^{o}C, which is nearly identical to the normal operating temperature. Consequently, no fuel damage or cladding failures would occur.

The primary significance of the analysis results for the PLOF and ULOF accident sequences is that no fuel damage or cladding failures would occur, even when multiple safety systems are assumed to malfunction. The neutronic, thermal, and hydraulic performance characteristics of the SMFR design provide a defensive barrier to reactor damage for accident initiators that otherwise progress into severe accident conditions. Such superior safety characteristics are inherent to a metallic-fueled, sodium-cooled, pool-type reactor concept.

2. Analysis Scope

The analysis results reported here were selected on the basis that they show the safety margins and the inherent ability of a metallic-fueled, sodium-cooled, pool-type reactor system to provide inherent protection against severe, damaging consequences. The accident sequence analyzed here is near the end of the spectrum of the most pessimistic, challenging, and potentially damaging. The analysis results demonstrate the passive safety performance advantages. This performance is possible because of the favorable heat transfer and reactivity feedback characteristics of metallic fuel, and the natural circulation shutdown heat removal capability that is possible with low pressure sodium coolant in a pool configuration.

Accident Sequences

The basic accident sequence analyzed here is the loss of normal power to the reactor and intermediate coolant pumps, with failure of the emergency power supplies. The result is an immediate loss of forced flow in the primary and intermediate coolant circuits. The equipment that provides a programmed flow coast down of the reactor coolant pumps is assumed to operate. In addition, it is assumed that heat removal at the sodium-CO_2 heat exchanger ceases, so that the only heat removal path is through the emergency direct reactor auxiliary cooling system (DRACS).

The DRACS consists of a heat exchanger located in the cold pool region within the reactor vessel, an air dump heat exchanger located outside containment, and the connecting piping. The working fluid in the DRACS is NaK, and fluid flow is by natural circulation. Two independent DRACS units are provided for defense in depth. Each DRACS unit is designed to remove 0.5% of full power (625 kW) at normal operating conditions. The DRACS operates continuously, with heat losses limited in non-emergency operation. In all the accident sequences analyzed here, only one DRACS unit is assumed to operate.

The initial condition for the accident sequence is normal operation at full power and flow. With the loss of pumping power, flow in the primary circuit coasts down to natural circulation according to the programmed pump head decay. The energy for this flow coast down is provided by a safety grade energy storage device.

With the loss of power, forced flow in the intermediate coolant system is lost. Further, it is assumed that heat rejection through the sodium-CO_2 heat exchanger ceases. The intermediate heat transport system (IHTS) is alternately a heat sink or source in the accident sequence, depending on its temperature and the primary system temperature at the intermediate heat exchanger (IHX). During the transient, natural circulation flow in the IHTS may reverse, depending on transient temperature conditions.

Two variations of the loss-of-flow accident sequence have been analyzed. In the first, it is assumed that the reactor safety system acts as designed to insert control rods and reduce reactor power immediately to decay heat. This sequence is called the protected loss-of-flow (PLOF) accident. In the second analysis, it is assumed that the reactor safety system fails to insert the

scram control rods, and the loss of forced flow proceeds at full power. This sequence is called the unprotected loss-of-flow (ULOF).

In the PLOF sequence, the absence of normal shutdown heat removal through the reactor coolant system causes a slow system temperature rise following the reactor scram. This temperature increase occurs because the DRACS has insufficient heat removal capacity to overcome both the early decay heat production rate and the stored heat in the primary and intermediate systems. Eventually, the decay heat falls below the DRACS capacity, and system temperature declines.

In the ULOF sequence, the system temperature rises significantly with the flow coast down, but the core temperature rise introduces negative reactivity that acts to reduce the reactor power. The reactor, with its negative feedback characteristic, seeks equilibrium with the available heat sink by reducing fission power. But in the early stage of the sequence, the DRACS capacity is less than the heat production, and system temperatures rise. When the decay heat falls below the DRACS capacity, the temperature rise ceases, and the reactor temperatures begins to fall. Then, the inherent reactivity feedback acts to raise the reactor fission power so that the total power is in equilibrium with the DRACS, and the system temperature approaches an asymptotic value.

Reactor State

Safety analyses were performed for both the beginning-of-life (BOL) and end-of-life (EOL) reactor conditions described in Section IV. Only the BOL results are reported here because the EOL results are similar, even though the reactor radial power distribution changes with irradiation.

For the BOL safety analysis, it was assumed that sufficient irradiation had taken place to swell the fuel radially into contact with the cladding. Examination of EBR-II irradiated fuel has indicated that fuel-cladding contact will occur early in fuel life, depending on the initial geometry and local specific power. Fuel-cladding contact has the impact of lowering thermal resistance by eliminating the sodium-filled fuel-cladding gap.

For the PLOF analysis, the decay heat curve was taken as 120% of the ANSI 5.1 standard for U-235. For the ULOF analysis, the decay heat curve was combined with the computed fission power calculated using the reactivity feedbacks calculated in the reactor physics analysis of Section IV for the BOL core.

3. Analysis Methods and Input Data

This section provides descriptions of the safety analysis methods and input data used to determine the safety performance. The methods described here are programmed in the SAS4A/SASSYS-1 computer code [1], which was employed to produce all analysis results.

Reactor Thermal Hydraulics

The thermal/hydraulic performance of the reactor core is analyzed with a geometric model

consisting of a number of single-pin channels. In this multiple-channel whole-core model, each channel represents a single fuel pin and the associated coolant and structure. The single pin is assumed to characterize the average pin in a fuel subassembly, and subassemblies with similar reactor physics and thermal-hydraulics characteristics are grouped, so a number of channels are selected to represent all the pins in the reactor core.

The geometry assumed in the channel thermal-hydraulic model is shown in Figure C-1. Heat generated in the fuel is assumed to travel through the cylindrically-symmetric pin to the upward-flowing coolant. The structure field is used to represent part of the hexagonal duct and the wire wrap. One-dimensional, radial heat transfer calculations are performed at many axial locations

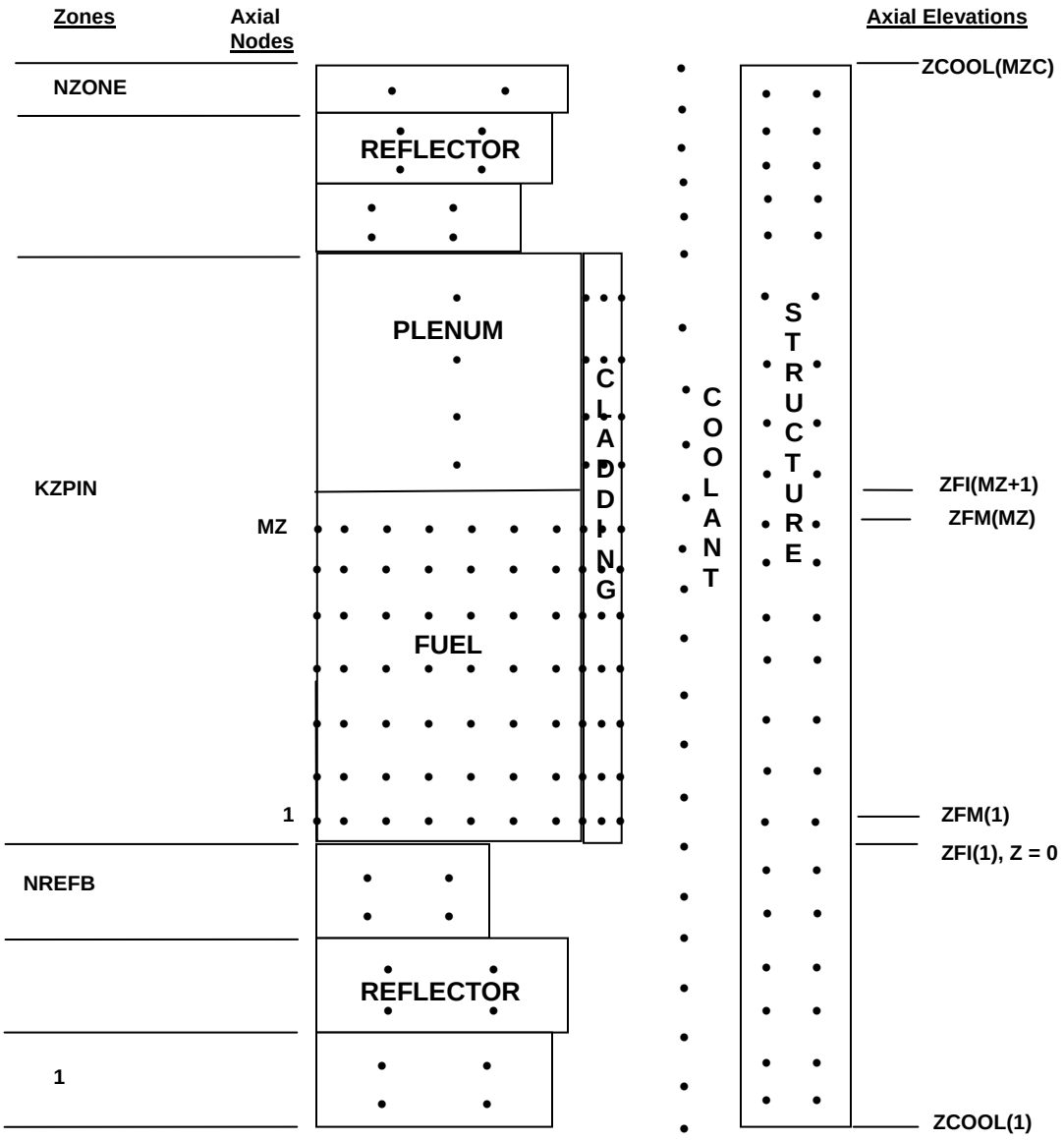

Figure C-1. Single-Pin Channel Model

to model heat transfer from the fuel through the cladding to the coolant, and from the coolant to the structure, the gas plenum, and the reflectors. One-dimensional (axial) coolant mass flow is modeled with a momentum equation solution for the axial pressure profile, and convective heat transfer conditions are assumed at the interfaces between the coolant and the cladding, the reflectors, and the structure. Temperatures are calculated at multiple radial nodes in the fuel, the cladding, the reflectors, and the structure. A single bulk temperature is calculated at each axial location. Axial heat conduction is neglected.

Thermal, transport, and physical properties data for the coolant were taken as the temperature-dependent liquid sodium properties available in SAS4A/SASSYS-1. Cladding properties were taken as the HT9 data presented in Ref. 2. Fuel properties were taken from the SSCOMP correlations in SAS4A/SASSYS-1 Version 3.0; these correlations are based on data generated in the Integral Fast Reactor (IFR) Program.

On the basis assumed for the reactor physics calculations reported in Section IV.C, the multiple-channel model depicted in Figure C-2 was selected for safety analysis calculations. This model utilizes the full heterogeneity of the reactor physics model, and assigns two channels to each fuel enrichment zone, for a total of six fuel channels. A seventh channel was used to represent all of the non-fuel subassemblies.

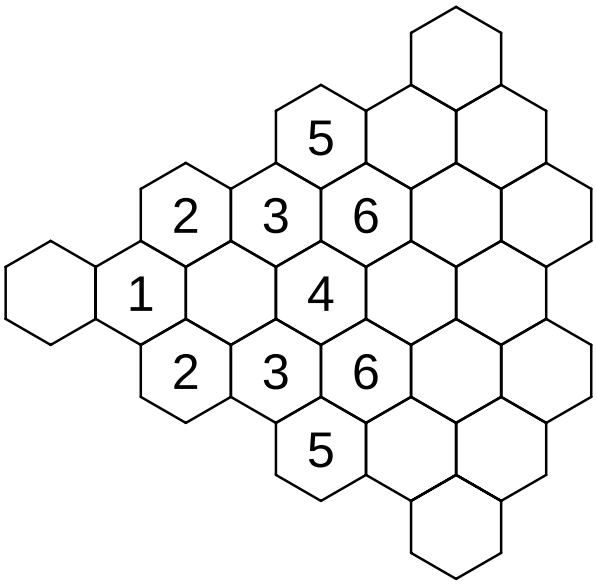

Figure C-2. Channel Assignment for Reactor Core Thermal-Hydraulic Model

Table C-1 presents geometric input data employed in the multiple-channel whole-core model. In this data, it has been assumed that the irradiated fuel has swollen into contact with the cladding.

Figure C-3 presents subassembly coolant flow rates determined in Section IV.C, and Fig. C-4 shows subassembly powers for the beginning-of-life (BOL) condition. Figures C-5, -6, and –7 present coolant outlet, peak cladding, and peak fuel temperatures calculated from these data.

Table C-1. Fuel Assembly, Pin, and Coolant Channel Model Data.

No. Pins per Assembly	127
No. Assemblies	
Channels 1, 2, 4, and 5	6
Channels 3 and 6	12
Fuel Height (mm)	1000
Gas Plenum Height (mm)	1500
Upper Reflector Height (mm)	500
Lower Reflector Height	750
Axial Node Height (mm)	
Core	50
Gas Plenum	250
Upper Reflector	100
Lower Reflector	150
Hydraulic Diameter (mm)	4.22
Coolant Flow Area (mm^2)	67.8
Outer Fuel Radius (mm)	8.25
Inner Cladding Radius (mm)	8.25
Outer Cladding Radius (mm)	8.75
Structure Thickness (mm)	3.0
Structure Perimeter (mm)	6.93
Reflector Thickness (mm)	1.0
Reflector Perimeter (mm)	55.0

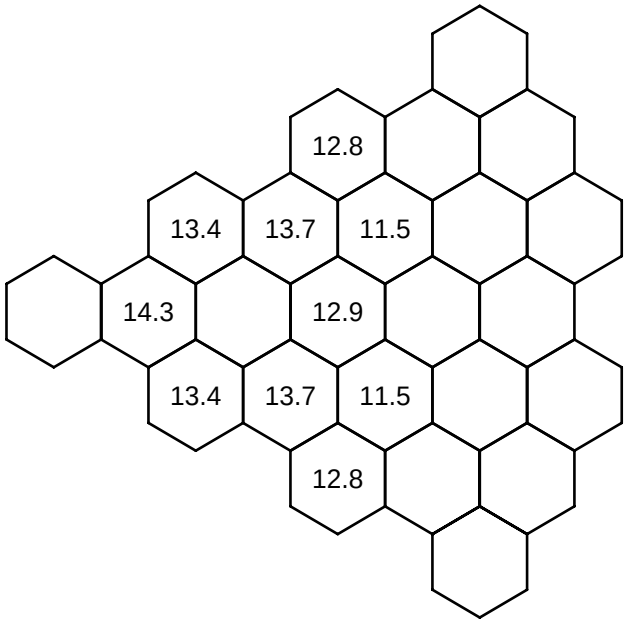

Figure C-3. Initial Subassembly Coolant Flow (kg/s)

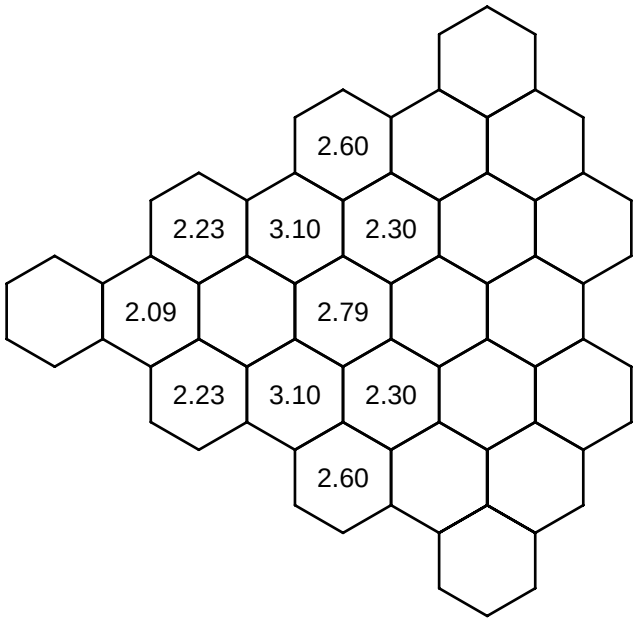

Figure C-4. BOL Initial Subassembly Power (MW)

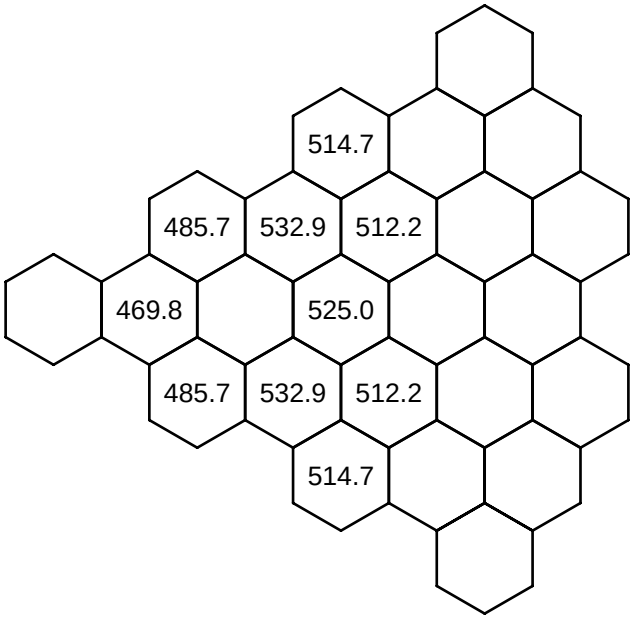

Figure C-5. BOL Initial Coolant Outlet Temperature (^{o}C)

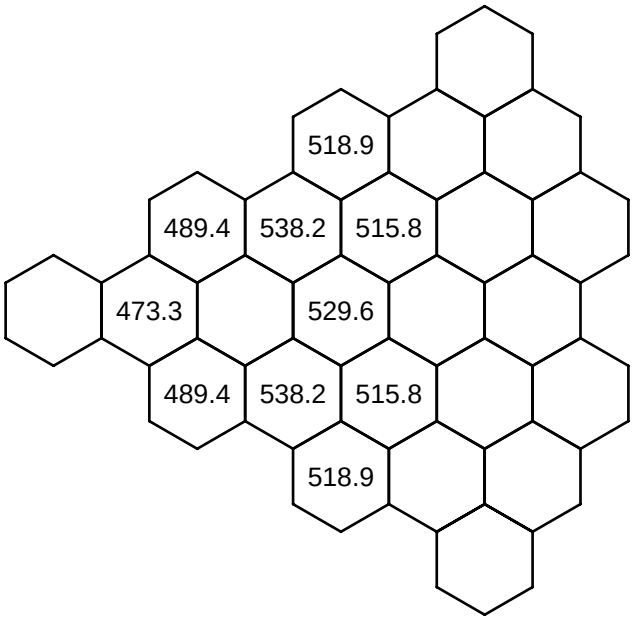

Figure C-6. BOL Initial Peak Cladding Temperature (^{o}C)

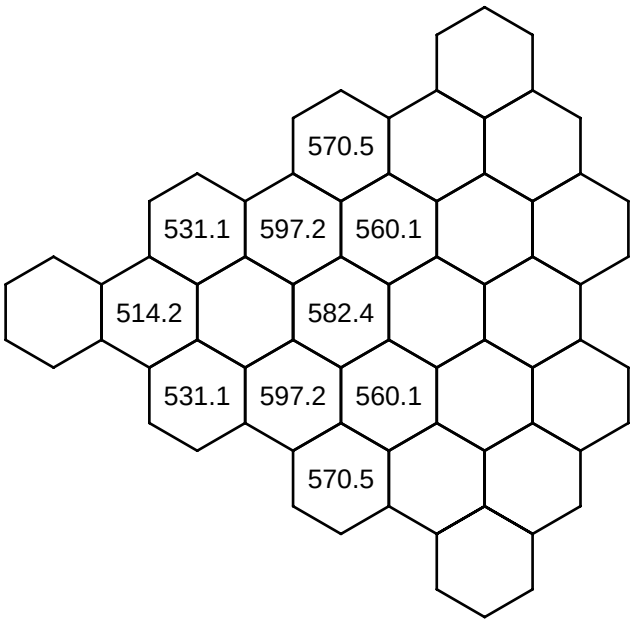

Figure C-7. BOL Initial Peak Fuel Temperature (^{o}C)

Figure C-8 shows subassembly powers for the end-of-life (EOL) condition. Figures C-9, -10, and –11 present coolant outlet, peak cladding, and peak fuel temperatures calculated from these data. These results show that for the calculated BOL and EOL power distributions and the flow orificing selected, the peak coolant temperatures in the BOL state are nearly the same as in the EOL state, although in a different position. This similarity, together with other performance characteristics, cause the accident analysis results for the BOL and EOL states to be very similar, because safety margins tend to be most closely associated with coolant temperatures.

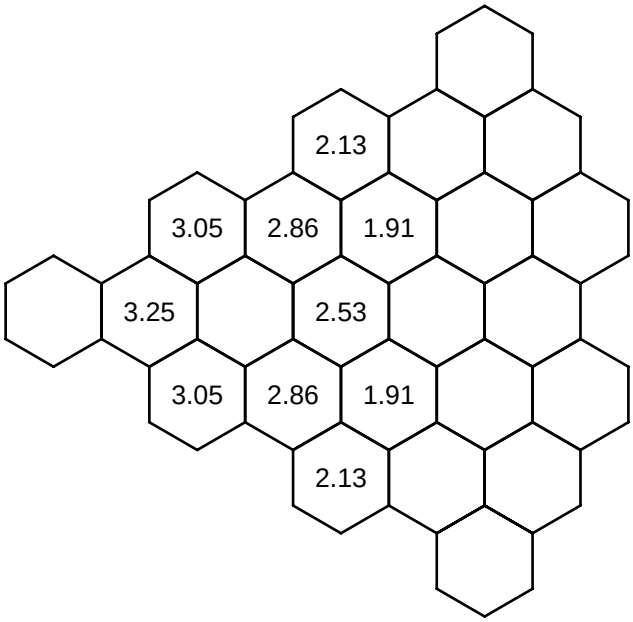

Figure C-8. EOL Initial Subassembly Power (MW)

Coolant Systems Thermal Hydraulics

The coolant systems thermal hydraulics model represents coolant flow and heat transfer in the primary and intermediate sodium systems, and in the emergency decay heat removal system, with a network of volumes and components connected by flow paths. The coolant systems model is shown in Figure C-12. Cold coolant flows from the inlet plenum through the core to the outlet plenum, and then to the shell side of the intermediate heat exchangers (IHXs). Cold primary coolant exits the IHXs and flows to the cold pool. The primary coolant electromagnetic (EM) pumps take suction from the cold pool and deliver the coolant back to the inlet plenum. Emergency decay heat removal is provided by the direct reactor auxiliary cooling system (DRACS), a natural circulation system that removes heat by means of a heat exchanger in the upper region of the primary circuit cold leg and rejects heat through an air dump heat exchanger outside the containment. The working fluid in the DRACS system is NaK.

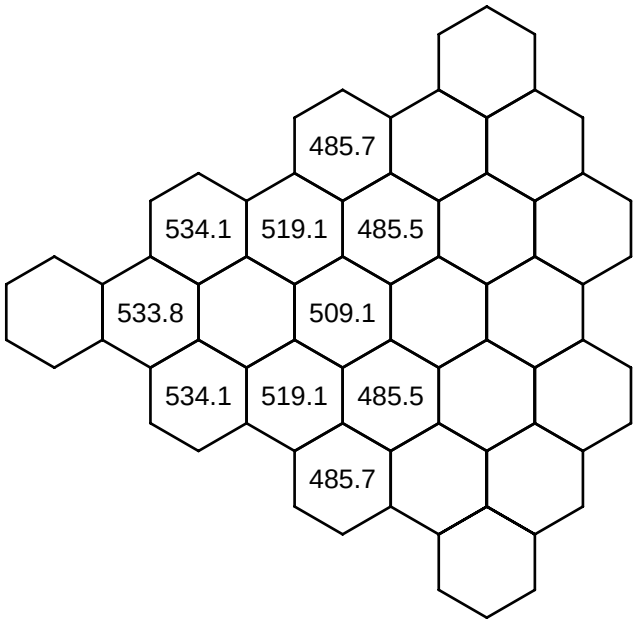

FigureC-9. EOL Initial Coolant Outlet Temperature (^{o}C)

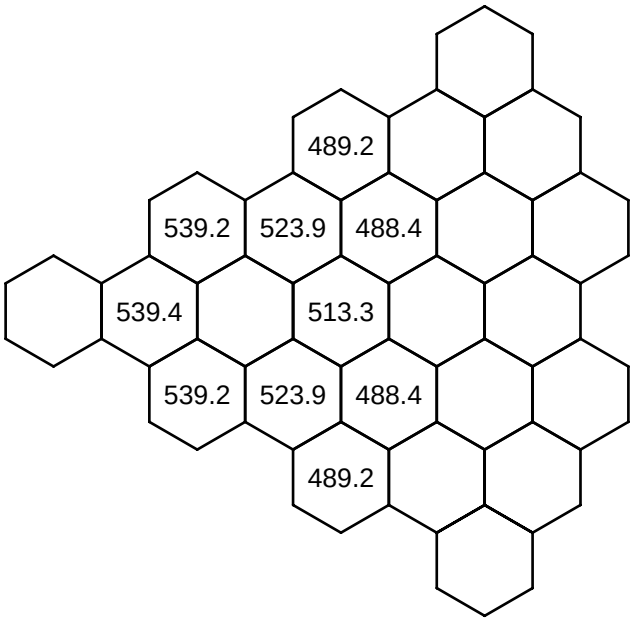

Figure C-10. EOL Initial Peak Cladding Temperature (^{o}C)

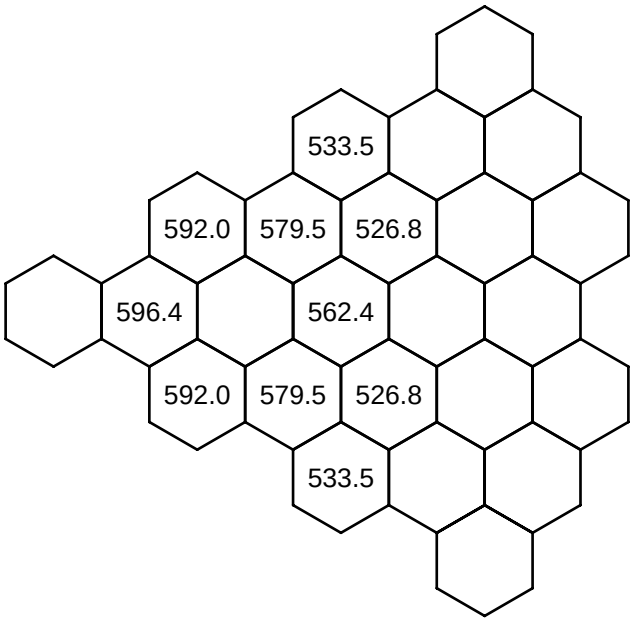

Figure C-11. EOL Initial Peak Fuel Temperature (^{o}C)

In the primary coolant circuit, volumes 1 and 2 represent the inlet and outlet plenums, and volumes 3 and 4 stand for regions of the primary circuit cold leg; the coolant in volume 4 is essentially stagnant. Volumes 5 and 6 simulate the gas expansion volumes in the intermediate loop and decay heat removal system, respectively. Design parameters assumed for the volumes in the model are shown in Table C-2. All of the volumes in the model are perfectly mixed (i.e. characterized by a single temperature) except for the upper region of the cold pool, which is treated by a stratification model for low flow conditions.

Volumes in the model are connected by one-dimensional flow segments, which are further subdivided into temperature elements for heat transfer calculations. Table C-3 shows the parameters assumed for the liquid segments. Flow segment 1 stands for the core channels, and flow segment 2 represents the shell side of the IHX. The SMFR has two IHXs, but only a single IHX is modeled, and it is assumed in this work that both primary circuits behave identically. Segment 4 represents the two primary coolant pumps and the discharge pipes connected to the inlet plenum. Segment 5 represents the primary coolant flow path through the decay heat removal heat exchanger, and segment 6 connects the upper region of the cold pool with the near stagnant lower region. Segment 7 represents the intermediate heat transfer loop, and includes the loop piping, the intermediate heat exchanger, and the intermediate coolant pump. Segment 8 represents natural circulation flow in the DRACS loop. In normal operation, heat addition takes place in segment 1, and heat is rejected in segments 3 and 5. Segment 2 is thermally connected through the IHX to the intermediate loop, and segment 5 is thermally connected to the DRACS loop through the DRACS heat exchanger.

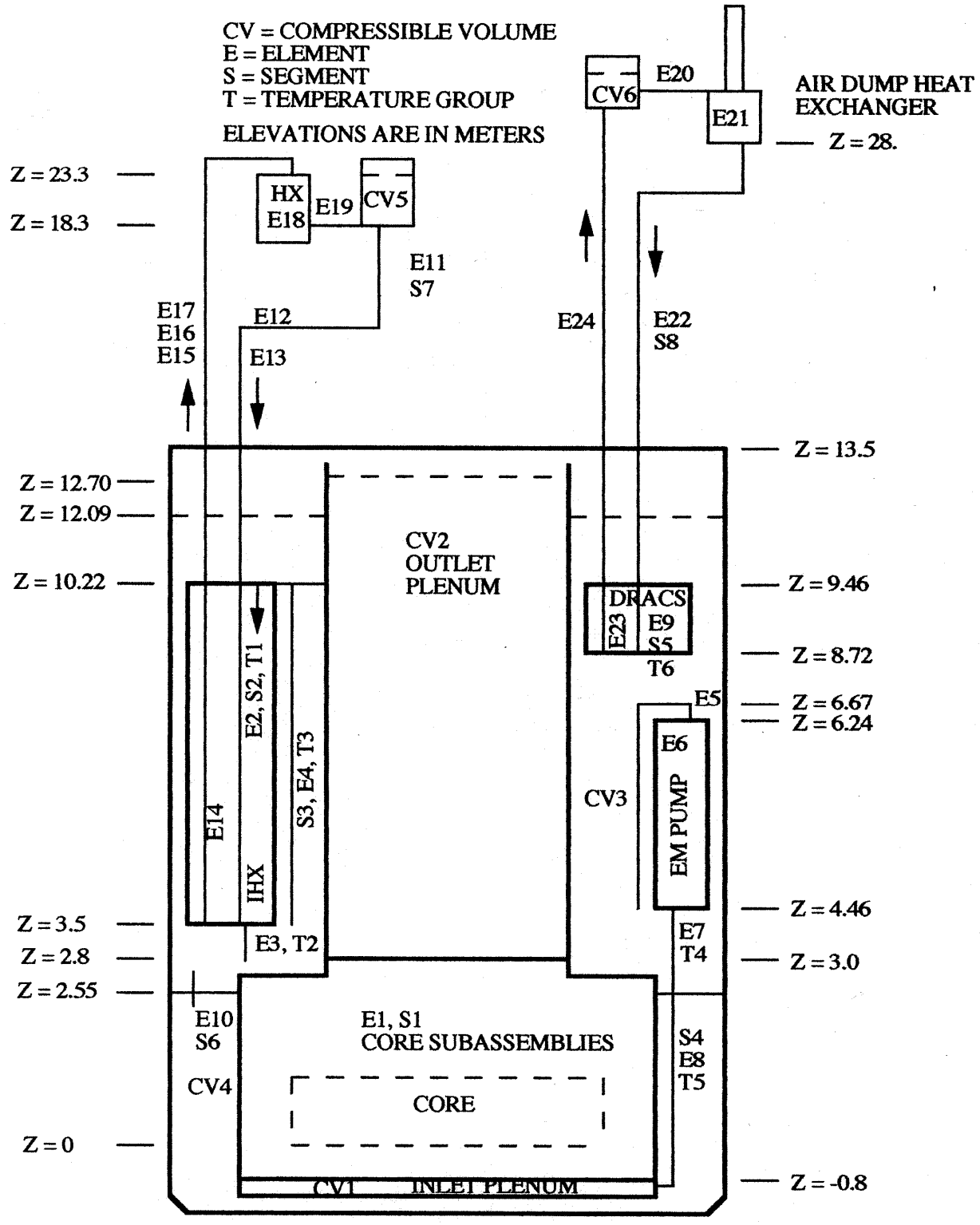

Figure C-12. Coolant Systems Thermal Hydraulics Model

Table C-2. Compressible Volumes Input Data.

Volume Number	1	2	3	4	5	6
Volume Description	Inlet Plenum	Outlet Plenum	Upper Cold Pool Region	Lower Cold Pool Region	Intermediate Loop Junction	DRACS Loop Junction
Total Volume (m^3)	1.53	31.35	65.7	14.07	3.0	2.0
Initial Gas Volume (m^3)	-	5.5	12.0	-	0.5	0.3
Reference Liquid Elevation (m)	-0.75	3.0	7.0	0.	18.3	27.0
Liquid/Gas Interface Area (m^2)	-	4.26	6.92	-	0.5	0.4
Wall Surface Area (m^2)	10.5	0.182	80.0	44.0	13.0	10.0
Wall Heat Capacity (MJ/K)	2.5	0.011	19.0	10.0	0.76	0.5

Table C-3. Liquid Segments Input Data.

Segment Number	Description	Compressible Volume In/Out	Inlet Elevation (m)	Liquid Element In/Out	Initial Flow (kg/s)
1	Reactor Sub-Assemblies	1/2	-0.75	1/1	633.2
2	IHX Shell Side	2/3	10.22	2/3	316.6
3	Intra-Volume Heat Transfer	3/3	3.4	4/4	0.0
4	Primary EM Pump	3/1	4.46	5/8	316.6
5	DHRX to Cold Pool	3/3	9.46	9/9	0.0
6	Cold Pool Transition	3/4	2.6	10/10	0.0
7	Intermediate Loop	5/5	18.2	11/19	316.6
8	DRACS Loop	6/6	28.0	20/24	0.0

In the model, liquid flow segments are divided into a number of elements for the purpose of heat transfer and pressure drop calculations. The liquid elements in the coolant systems model are described in Table C-4.

Table C-4. Liquid Elements Input Data.

Element Number	Description	Outlet Elevation (m)	Length (m)	Flow Area (m^2)	Hydraulic Diameter (m)
1	Reactor	*	*	*	*
2	IHX Shell	3.5	6.7	0.9	0.035
3	IHX Outlet	2.8	0.7	0.09	0.24
4	Cold Pool HT	4.7	1.3	0.0001	0.001
5	Pump Inlet	4.5	0.04	0.07	0.29
6	Primary Pump	4.5	2.7	0.03	0.08
7	Pump Outlet	2.5	2.0	0.07	0.24
8	Pump Discharge	-0.8	3.5	0.07	0.24
9	DRACS HX	8.7	0.7	0.15	0.04
10	CP Transition	2.5	0.1	0.05	0.24
11	IHTS Pipe	13.0	6.4	0.05	0.24
12	IHTS Pipe	13.0	4.3	0.05	0.24
13	IHTS Pipe	3.5	8.3	0.05	0.24
14	IHX Tube	10.2	6.7	0.3	0.01
15	IHTS Pipe	12.4	4.3	0.05	0.24
16	IHTS Pipe	12.4	5.2	0.05	0.24
17	IHTS Pipe	23.3	6.0	0.05	0.24
18	Na/CO_2 HX	18.3	4.0	1.8	0.005
19	IHTS Pump	18.3	1.0	0.05	0.24
20	DRACS Pipe	28.0	1.0	0.008	0.01
21	Air Dump HX	27.0	5.7	0.08	0.04
22	DRACS Pipe	8.7	18.0	0.008	0.1
23	Na/NaK HX	9.5	0.7	0.06	0.02
24	DRACS Pipe	26.9	18.0	0.008	0.1

* See core channel model in Table C-1.

Flows in the primary and intermediate circuits are driven by both forced circulation at the pumps and by buoyancy due to heat exchange, so transient natural circulation flows adjust to changing heat generation and transfer conditions. The natural circulation flow in the DRACS loop can change due to temperature changes in the DRACS heat exchanger and the air dump heat exchanger, and heat transfer at the air dump heat exchanger can be enhanced by opening air flow dampers (normally closed).

The SMFR design features an electromagnetic primary coolant pump with a power supply that can be programmed to provide an optimized flow coast down for normal pump trips and in the event of loss of power. For the analyses reported here, it is assumed that the power supply provides a pump head that initially falls rapidly to a fraction of full flow, and then falls more

gradually as stored energy (rotating mass or battery) is used. It is also assumed that the shape of the pump head decay history may be different for scrammed and unscrammed events, to reduce transient peak coolant temperatures and resulting damage to the system.

Reactor Kinetics and Reactivity Feedbacks

A point kinetics model is employed to calculate the reactor fission power response to the transient reactivity state in unscrammed sequences. At any time, the net reactivity is the sum of a number of individual reactivity feedbacks that are determined by the transient thermal, hydraulic, mechanical, and neutronic state of the reactor. The feedback reactivities considered are fuel Doppler, coolant density, fuel and cladding axial expansion, radial core expansion, and control rod driveline thermal expansion.

A decay heat model is integrated with the point kinetics model for the fission power to track shutdown events in sub-critical conditions.

The fuel Doppler feedback is calculated from the spatially dependent fuel temperature distribution and the input spatial distribution of the fuel Doppler reactivity coefficient. In each single-pin channel, the axial distribution of the radial pin-average fuel temperature is used to calculate the reactivity feedback.

The coolant density reactivity feedback is calculated from the spatially dependent coolant density distribution and the input distribution of the coolant density reactivity coefficient calculated from perturbation theory. The reactivity feedback data is entered as a coolant void worth (the negative of the coolant mass worth), and the coolant density feedback reactivity is calculated from the time-dependent axial density distribution in each single-pin channel.

Transient fuel and cladding temperatures are employed to predict fuel and cladding axial dimension changes, and in each single-pin channel, the reactivity feedbacks associated with fuel and cladding axial expansion are computed from first order perturbation theory.

A simple radial core expansion model accounts for core dilation due to thermal expansion of the hexcan load pads and thermal expansion of the core support grid plate. Reactivity feedback is then calculated from the computed core dimension change and an input linear reactivity coefficient based on stand-alone neutronics eigenvalue calculations.

For the control rod driveline feedback model, it is assumed that the control rod drivelines are washed by the outlet coolant from the core. Thermal expansion of the drives due to a rise in core outlet temperature will cause the control rods to be inserted further into the core, providing a negative reactivity component. On the other hand, if the control rod drives are supported on the vessel head, and if the core is supported by the vessel walls, then heating the vessel walls will lower the core, leading to a positive reactivity component. Both control drive expansion and vessel wall expansion are accounted for.

4. Analysis Results

This section presents detailed results from analysis of protected loss-of-flow (PLOF) and

unprotected loss-of-flow (ULOF) accidents. The analyses were performed with coupled heat transfer, thermal-hydraulics, and reactor kinetics models that have been validated during many applications to EBR-II and FFTF transient tests. Additionally, temperature criteria for assessments of cladding damage thresholds have been established by results from testing of metallic fuel in EBR-II and TREAT. Consequently, there is high confidence that the PLOF and ULOF accident analyses obtained here give a true characterization of the physical performance that could be obtained in the SMFR design.

Protected Loss-of-Flow (PLOF) Accident Sequence

Results from analysis of the PLOF accident sequence are shown in Figures C-13, -14, and –15. Figure C-13 shows the early history of the reactor power, the coolant flow through the highest temperature subassembly (Channel 3), and the DRACS heat removal rate. Recall that this transient is initiated by a complete loss of forced coolant flow in the primary and intermediate loops, save the primary pump head decay augmentation which drops rapidly in the first 50 seconds to less than 10% and disappears by 200 seconds. After this time, the flow is entirely by natural circulation. Almost immediately at initiation, the reactor control system scrams the reactor, giving the power reduction to decay heat shown in Figure C-13, and the dampers on the DRACS air dump heat exchanger open, permitting the DRACS to operate at its full capacity of 0.5% (One of two DRACS assumed to function). Not indicated in this figure is the loss of heat removal to the balance-of-plant, which is assumed to occur linearly in the first 2 seconds. The channel 3 flow results in the figure indicate the high rate of natural circulation coolant flow through the core. This is due to the relatively open lattice geometry, and the correspondingly low friction pressure drop along the pin length compared to other sodium-cooled reactor designs. The enhanced natural circulation coolant flow characteristic contributes significantly to relatively low transient coolant temperatures and relatively large coolant temperature safety margins.

Figure C-14 shows the long term histories for the reactor power, the coolant flow in channel 3, and the DRACS heat removal for the transient to about 17 hours. During this time, the only heat removal is through the DRACS, and all coolant flow is due only to natural circulation. As the system temperature rises, as shown in Figure C-15, the DRACS heat removal capability increases due to an increase in heat rejection at the air dump heat exchanger. The decay heat production declines throughout the transient, until it becomes equal to the DRACS heat removal. The system temperatures reach peak values about 11 hours after accident initiation, after which the temperatures decrease.

The transient peaks in the coolant flow indicated in Figure C-14 and in the cladding temperature in Figure C–15 are caused by the relatively coarse spatial mesh used in the analysis to represent stratification in the cold pool. As coolant mass and energy is redistributed by the stratification model over the coarse mesh, the impact on temperatures that drive the natural circulation is over-emphasized. In the plotted data, this introduces perturbations that are eventually damped by temperature and flow transients, and the overall solution returns to the correct long-term trend. These perturbations are not physical, and should be ignored in interpretation of the results.

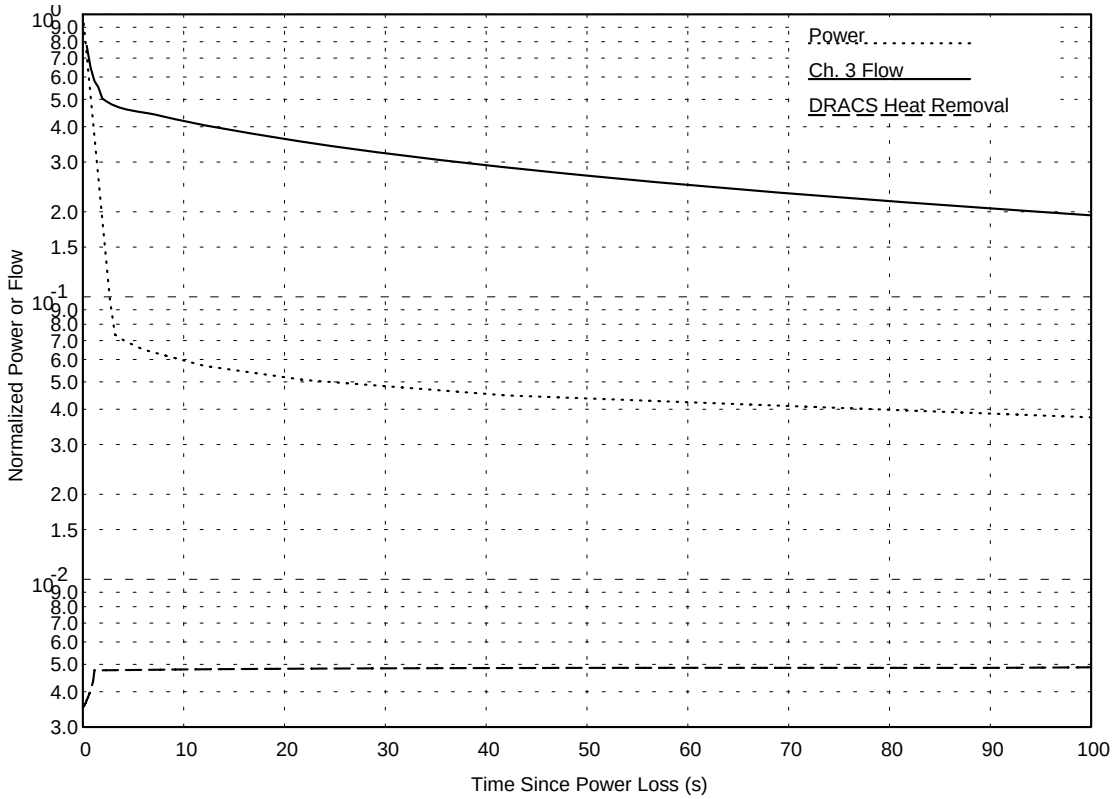

Figure C-13. PLOF Early Power and Flow History

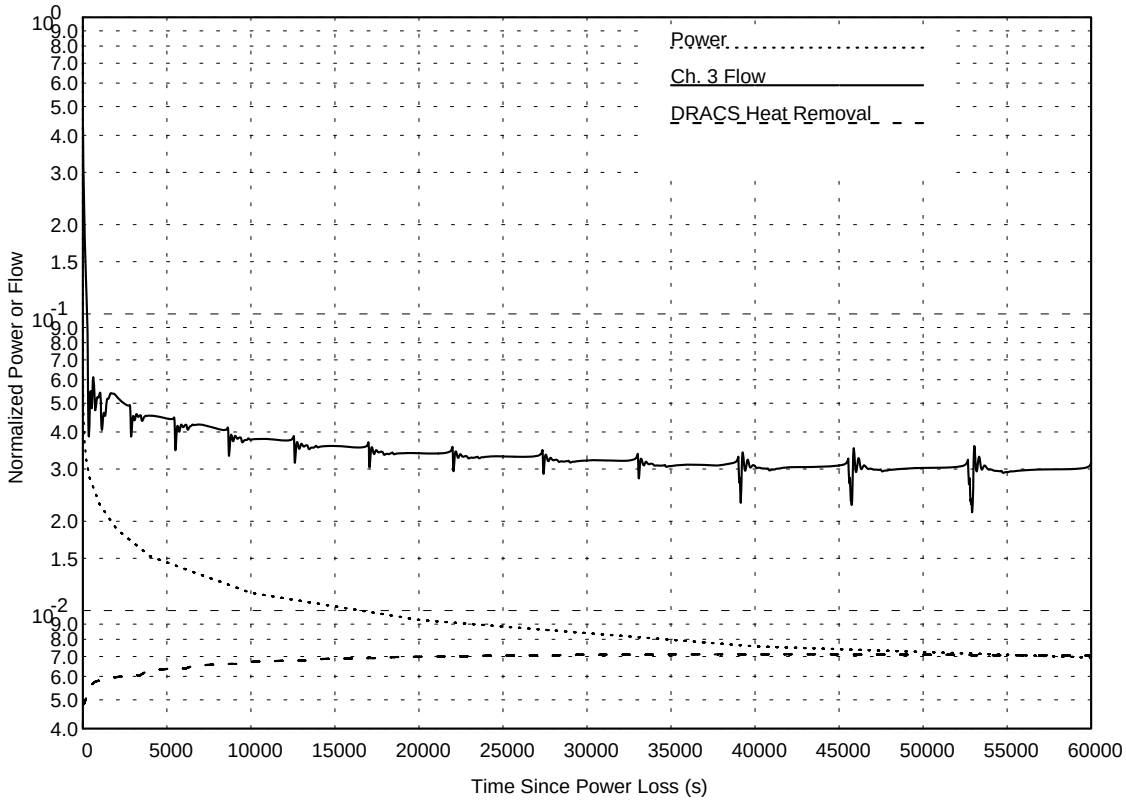

Figure C-14. PLOF Power and Flow History

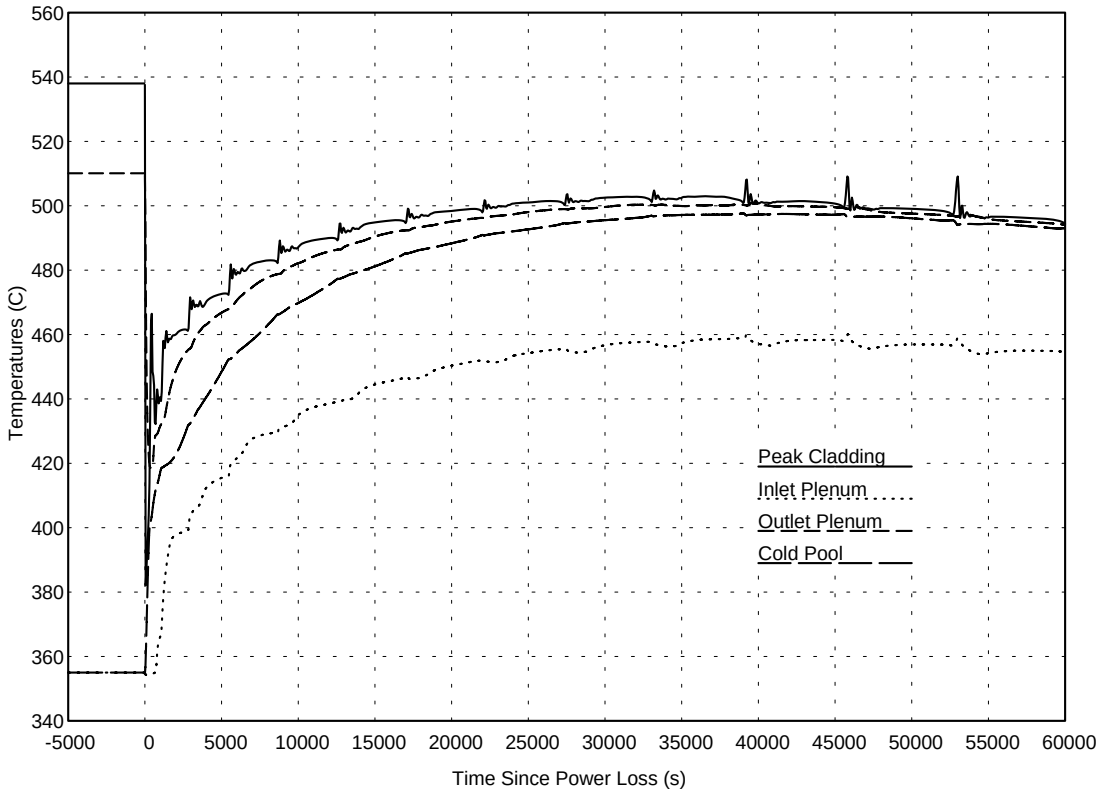

Figure C-15. PLOF Temperature History

The significance of the PLOF analysis results is emphasized in Figure C-15 which shows the initial peak cladding temperature (538.2^{o}C) in channel 3, compared to the transient peak cladding temperature, just above 500^{o}C at around 11 hours (40000 seconds). In the PLOF transient, the peak temperatures in the accident are lower than the normal operating temperatures. Stated in another way, the temperature safety margins in the accident are greater than the margins at normal operating conditions. This very significant result is obtained as a result of the enhanced natural circulation capability.

Unprotected Loss-of-Flow (ULOF) Accident Sequence

Results from the analysis of the ULOF accident sequence are shown in Figures C-16 through C-21. Figures C-16, -17, and –18 show plots for the first 500 seconds of transient time after accident initiation, following about 1000 seconds of calculation to establish a steady set of initial conditions. The ULOF transient is initiated by the same set of failures as for the PLOF accident (loss of forced flow and loss of normal heat rejection), but for the ULOF case, the reactor control system also fails to scram the reactor, so the accident proceeds from full power. All heat rejection is through the single DRACS loop, with a design heat rejection of 0.5% of full power at nominal conditions.

Figure C-16 shows the early histories for the total reactor power, the decay heat production, and the coolant flow in channel 3. The initial power-to-flow imbalance results in significant transient heating of the reactor, causing the reactivity feedbacks shown in Figure C-17, and the

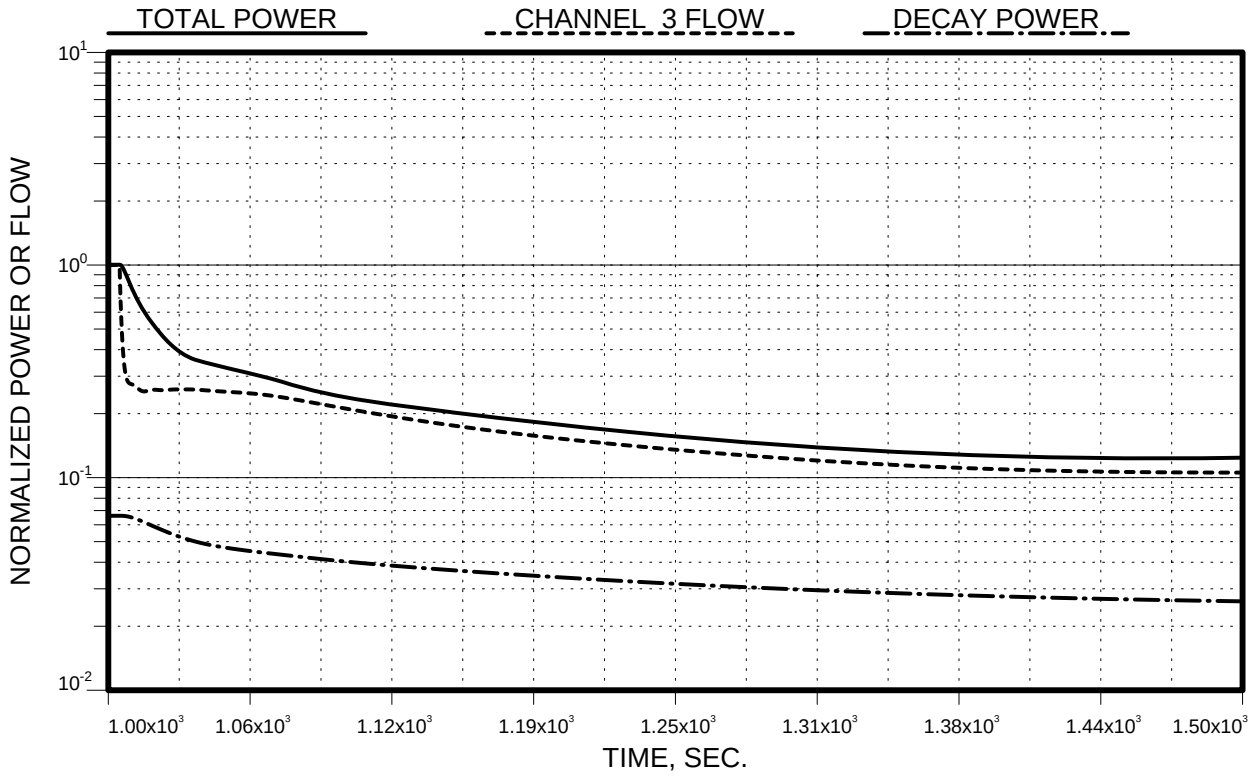

Figure C-16. ULOF Early Power and Flow History

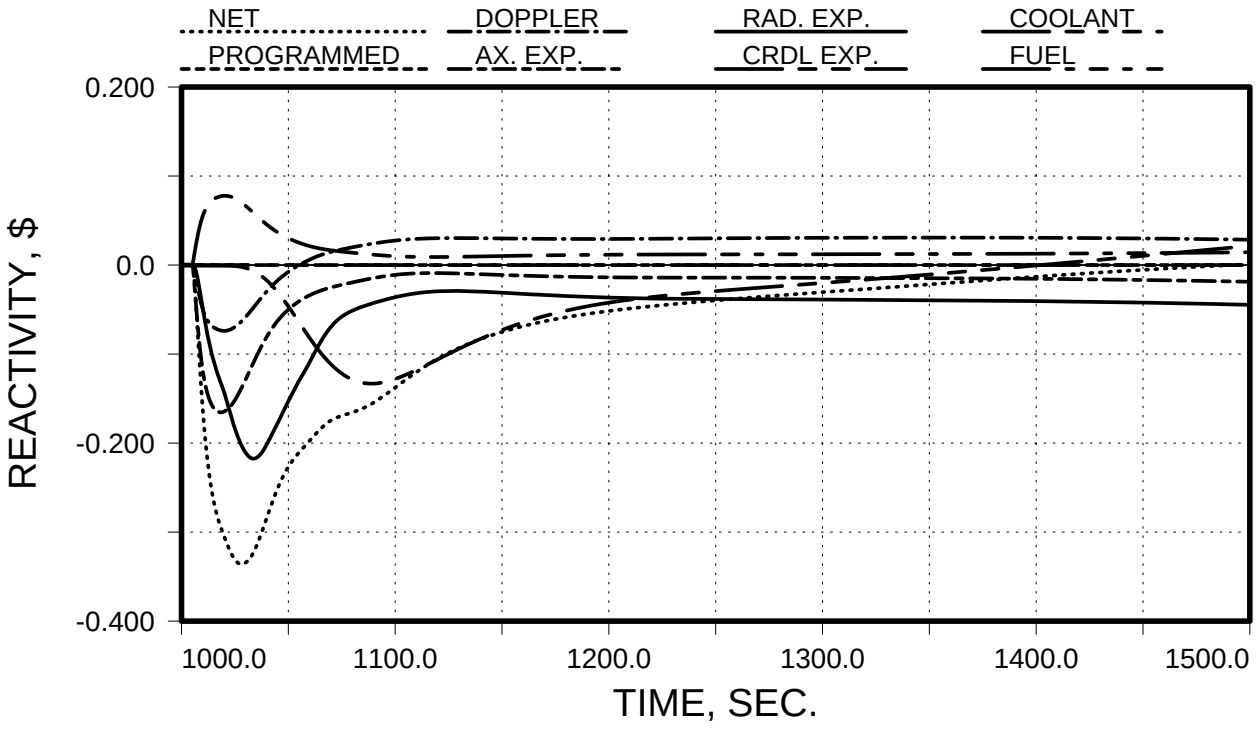

Figure C-17. ULOF Early Reactivity History

temperature transients shown in Figure C-18. The net negative reactivity effect causes the reactor fission power to decrease, until at about 30 seconds into the transient, the peak temperatures are obtained. The peak coolant temperature in channel 3 is approximately 735°C. After this time, the power continues to decrease and reactor temperatures fall to approach asymptotic values. The still negative net reactivity rises to zero at 500 seconds, indicating a progression toward equilibrium among the power, the net reactivity, and the temperatures. However, not shown in these graphs is the DRACS heat rejection, which is rising from its original value but not yet able to remove the power being produced.

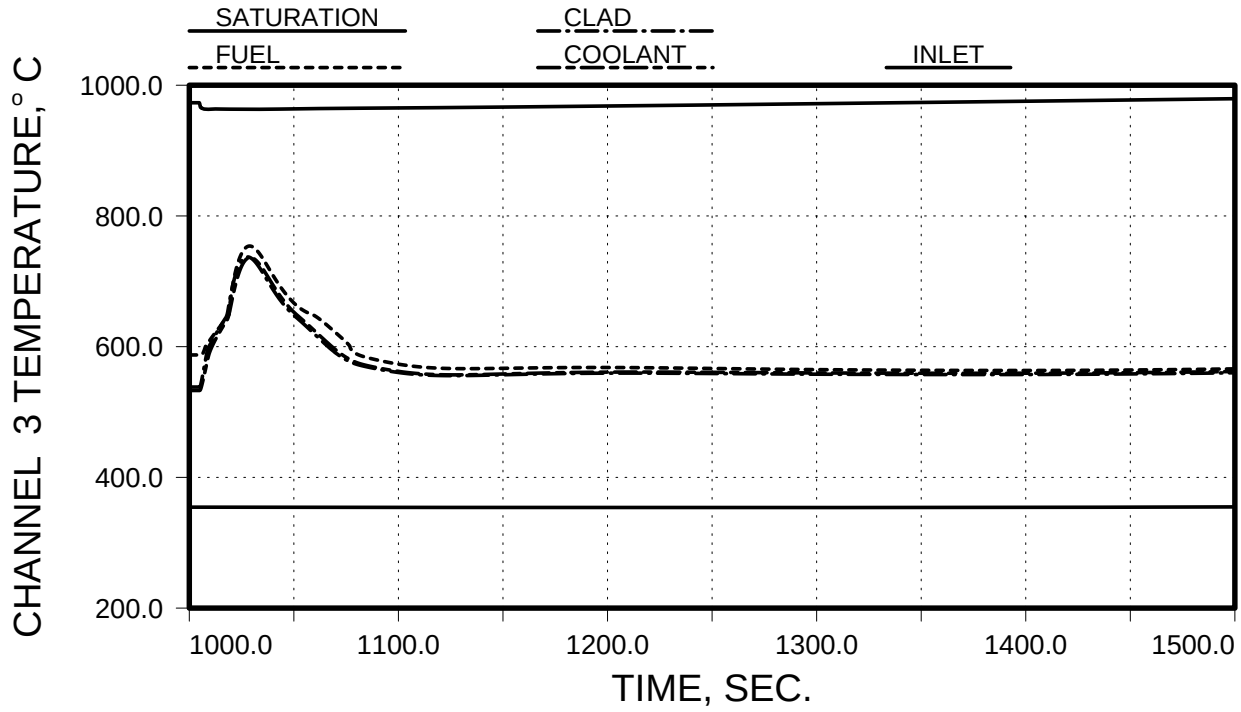

Figure C-18. ULOF Early Temperature History

Figures C-19, -20, and –21 show the long term transient results for the ULOF accident. As shown in Figure C-19, the fission power is extinguished as the total power becomes equal to decay heat production at about 2 hours into the accident. Figure C-20 shows that the net reactivity remains slightly negative at this and subsequent times. Along with the rising inlet temperature, shown for this period in Figure C-21, the negative reactivity indicates that the DRACS system heat removal capability is less than the decay heat production, and the system temperature is consequently increasing. With more time, the decay heat production falls, the continued cold pool heating increases the DRACS heat rejection, and eventually, at around five hours into the transient (~19000 seconds), the DRACS capacity exceeds the decay heat production. This causes a temporary positive net reactivity that rekindles the fission power, and increases the total power (sum of fission and decay heat) to equal the DRACS capacity. For all times following this event, the fission power increases as the decay heat production falls (See Figure C-19), and the total power remains in equilibrium with the DRACS capacity, at around

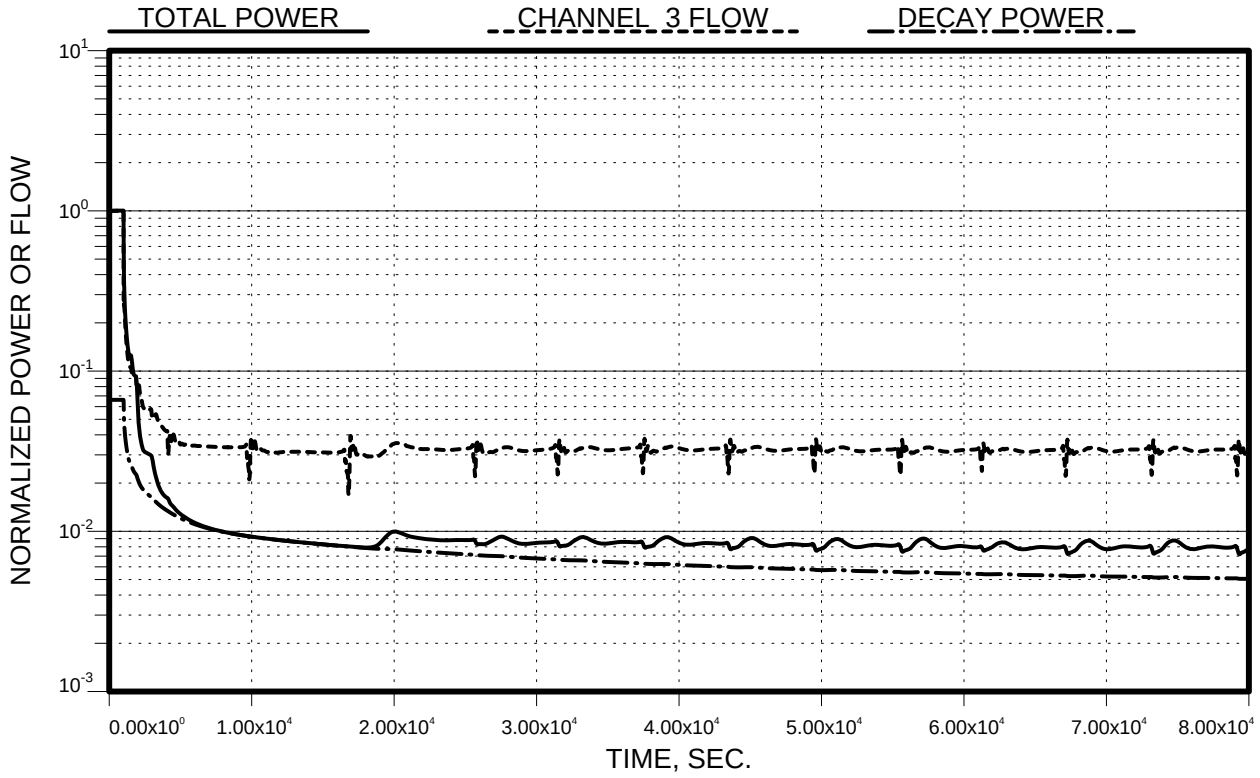

Figure C-19. ULOF Power and Flow History

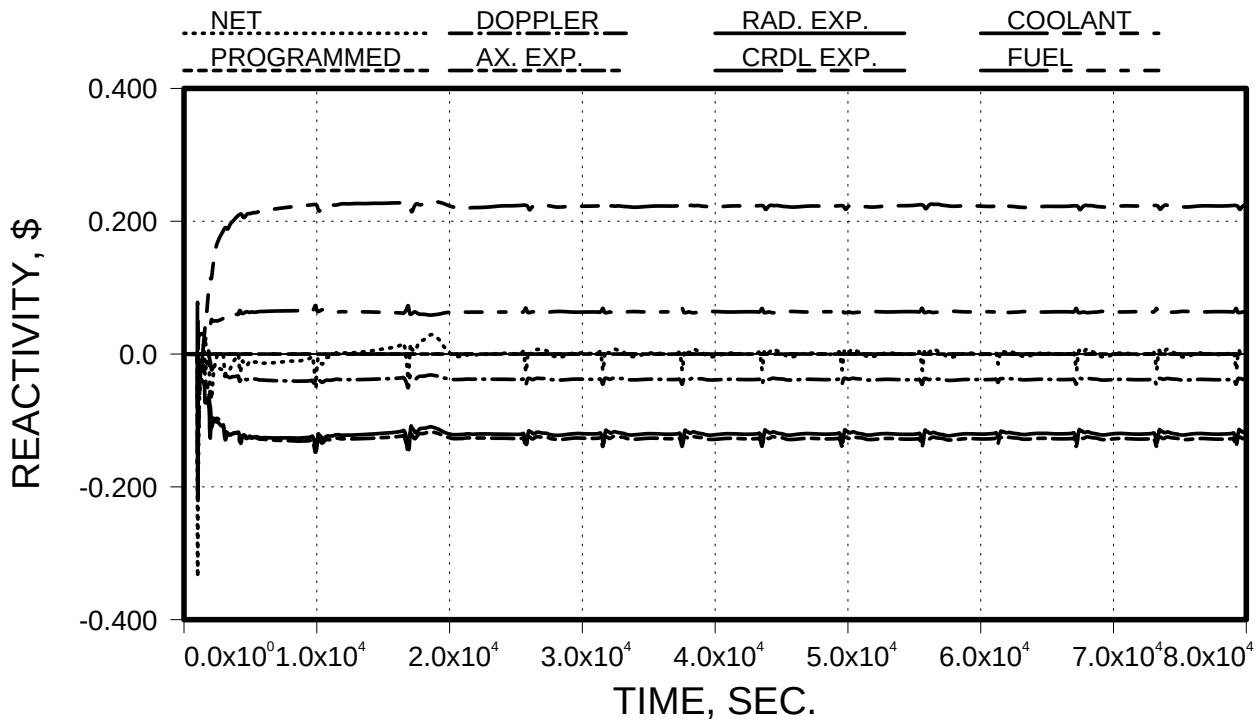

Figure C-20. ULOF Reactivity History

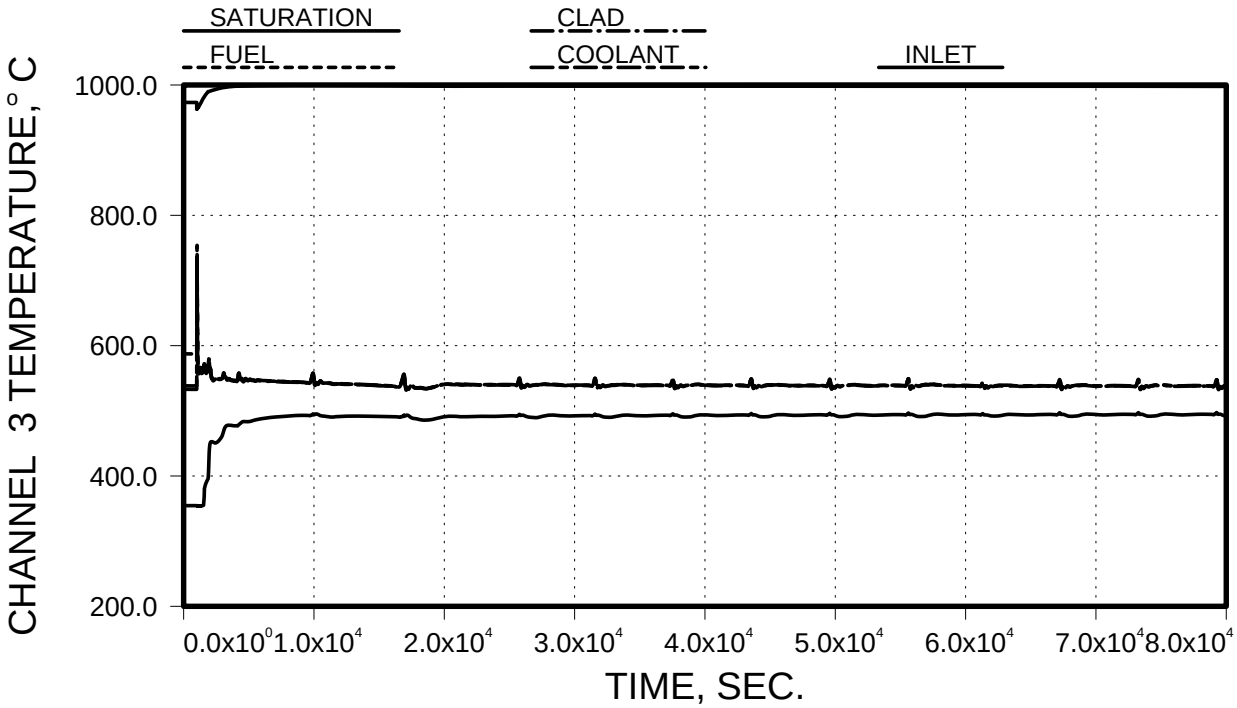

Figure C-21. ULOF Temperature History

0.8%. All system temperatures remain essentially constant after about 5 hours, denoting achievement of an equilibrium condition.

The intermittent, short term perturbations in the histories for the power, flow, reactivities, and temperatures in Figures C-19, -20, and –21 are caused by the coarse spatial mesh used in the cold pool stratification model, as described in the previous section. These perturbations are not physical, and should be ignored in interpretation of the results.

The significance of the ULOF accident analysis results is captured in Figure C-21. This figure shows that the eventual, long term peak cladding temperature (538^{o}C) in channel 3 is equal to the normal operating temperature. Although the peak cladding temperature rises to 735^{o}C early in the transient, this condition is insufficiently lasting to cause a concern about cladding damage leading to pin failure. The analysis indicates that the core would survive an unprotected loss-of-flow accident without pin failures or fuel damage, and that long term equilibrium peak cladding temperatures would remain near the normal operating condition. This very favorable result comes about because of 1) the high thermal conductivity of metallic fuel (low fuel operating temperature, low cold-to-hot reactivity invested at startup), 2) the capability of a sodium-cooled reactor in a pool-type primary system to remove decay heat in natural circulation, and 3) the efficient reactor physics performance permitting an open lattice that further enhances natural circulation capability by reducing the reactor coolant flow pressure drop.

References

1. J. E. Cahalan, A. M. Tentner, and E. E. Morris, "Advanced LMR Safety Analysis Capabilities in the SASSYS-1 and SAS4A Computer Codes," Proceedings of the International Topical Meeting on Advanced Reactors Safety, American Nuclear Society, Vol. 2, pp. 1038-1045, Pittsburgh, PA, April 17-21, 1994.

2. L. Leibowitz and R. A. Blomquist, "Thermal Conductivity and Thermal Expansion of Stainless Steels D9 and HT9," International Journal of Thermophysics, Vol. 9, No. 5, pp. 873-883, September, 1988.

APPENDIX D. THERMAL-HYDRAULIC ANALYSES

A set of computational fluid dynamics (CFD) analyses were performed to assess at steady-state flow patterns in the primary reactor system, sodium pool temperature distributions, and temperature distributions in the reactor vessel and the reactor vessel closure structures. For these analyses the CFD code STAR-CD was used.

The CFD model includes the reactor pumps, the lower and upper reactor plena, the reactor core, lower reflector, upper shield, radial reflector, and radial shielding, the core barrel, the redan, the intermediate heat exchangers (IHXs), the reactor vessel and the DRACS heat exchangers inside the sodium pool. The reactor pumps were modeled as momentum sources. The lower reflector, reactor core, upper plenum, the upper shield, and the IHXs were modeled as porous media. The heat generation in the core was modeled as a volumetric heat source, and the heat removal in the IHXs and the DRACS heat exchangers was modeled as volumetric heat sink.

In the porous media model of STAR-CD, the pressure drop along a length L is computed from

$$\Delta p = -KuL, \qquad (1)$$

where the resistance K is given as

$$K = \alpha|u| + \beta. \qquad (2)$$

The pressure drop in a channel can be computed from

$$\Delta p = \frac{1}{2}\rho u^2 \left(K_L + f\,\frac{L}{D_h} \right), \qquad (3)$$

where

K_L = loss coefficient,

f = friction coefficient,

and D_h = hydraulic diameter.

From equations (1) and (3)

$$K = \frac{1}{2}\rho u \left(\frac{K_L}{L} + \frac{f}{D_h} \right), \qquad (4)$$

and from equations (2) and (4)

$$\alpha = \frac{1}{2}\rho \left(\frac{K_L}{L} + \frac{f}{D_h} \right), \qquad (5)$$

and

$$\beta << \alpha\,|\,u\,|. \qquad (6)$$

Equations (5) and (6) are used to compute the constants α and β in the core and the IHX. The friction factor f in the core and the IHX is computed from

$$f = 0.316\,\mathrm{Re}^{-0.25}. \qquad (7)$$

In the IHX, there are18 plates having a loss coefficient of 3.8 each.

To develop a computational grid computer assisted design (CAD) surfaces were used to define the significant components of the primary system, while details of these components that are not significant for the purposes of this analysis were ignored. The reactor is represented as a set of cylindrical rings that includes a central control rod ring, three core-assembly rings (inner core, middle core, and outer core), a radial reflector ring, and a radial shield ring. The core-assembly rings are surrounded by coolant rings. The radii of the rings have been computed from the requirement to preserve the volume fraction of the coolant and solid materials (fuel and structural material) in each core region. This requirement also preserves the coolant flow area in each region.

To expedite parametric analyses, two computational models were developed. The first model includes all the components below the sodium free surface, and the second model all the components above the sodium free surface. The temperature distributions at the top boundary of the first model were used as boundary conditions in the bottom boundary of the second model. Both models are relatively coarse. The first model has about 120,000 computational cells, and the second about 55,000 cells. Because the auxiliary cooling systems have not been sized yet, in the first model, an adiabatic boundary condition was used on the outside surface of the reactor vessel and on the top of the sodium pool. Heat conduction between the hot and cold sodium pools through the thin redan wall was allowed. The boundary conditions of the second model will be discussed later.

Figure D-1 shows the computational grid in the fluid domain for one half (symmetry) of the first model. Figure D-2 shows the pump shells, the pipes from the pumps to the inlet plenum, the inlet plenum, the redan, and the lower part of the outer IHX shells. Figure D-3 shows the core coolant channels (cylindrical rings).

Figure D-4 shows the sodium flow in the hot pool. The main flow pattern is a strong upward flow towards the inlet of the IHXs with a weak recirculation zone above the cone of the redan. Figure D-5 shows the coolant velocities in the hot pool on a vertical plane perpendicular to the axis passing through the centers of the IHXs. There is no recirculation on this plane. Figure D-6 shows the sodium flow in the cold pool. The main flow is from the outlet of the IHXs to the inlet of the pumps, while there are some weak recirculation flows.

Figure D-7 shows the temperature distribution at the top of the redan cone. There is an azimuthal variation of about 11 °C. It should be noted that at this time neither the design of the inlet plenum nor the core inlet flow distribution has been optimized. Figures D-8 and D-9 show the temperature distribution in the hot pool. There is a central hot plume where the temperature is close to that of the core outlet, with a loss of about 4^{o}C from the core outlet (510^{o}C) to the top of the pool (Figure D-10). This central zone is surrounded by a colder zone which in the lower half of the pool reaches a minimum temperature of about 483^{o}C above the cone of the redan.

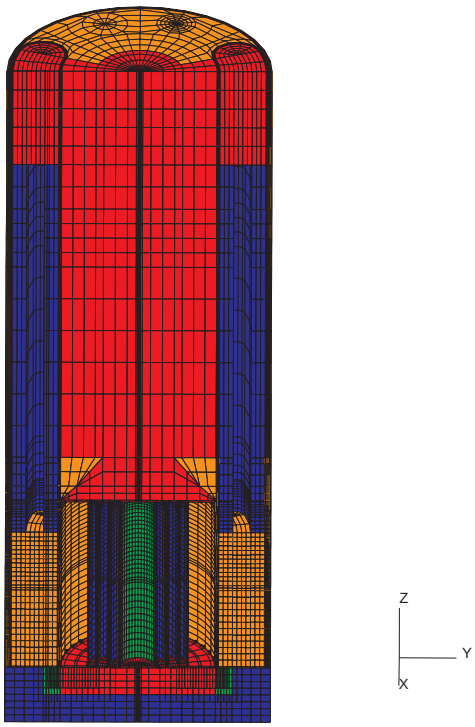

Figure D-1. Computational grid (first model)

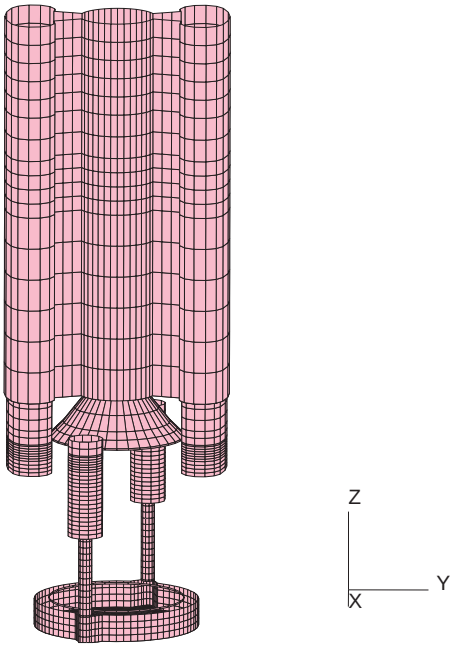

Figure D-2. Some primary system components

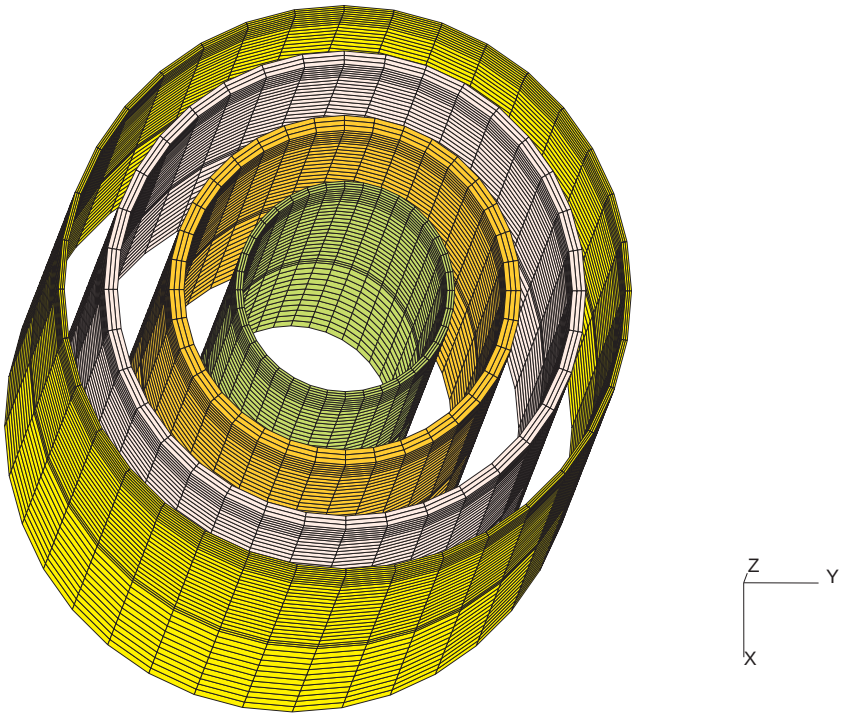

Figure D-3. Core coolant channels

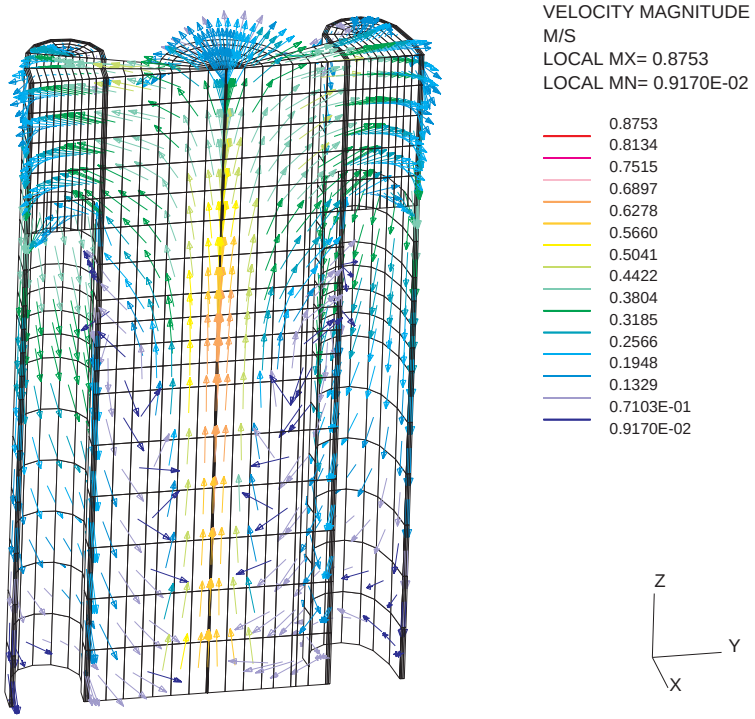

Figure D-4. Sodium velocity in the hot pool

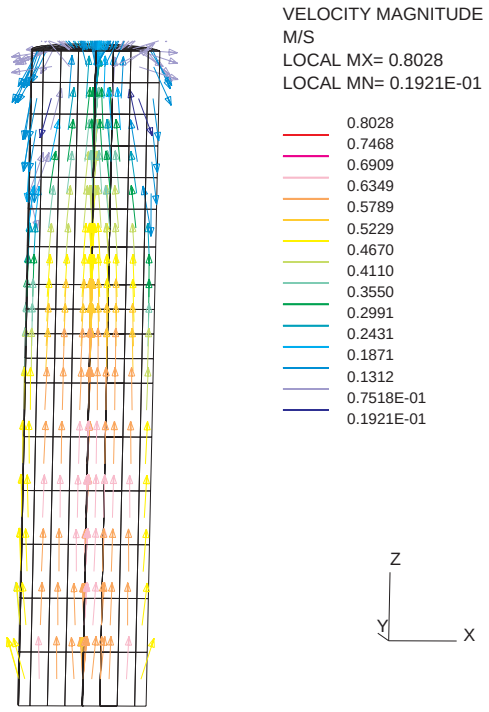

Figure D-5. Sodium velocity in the hot pool
(plane perpendicular to axis passing through the centers of the IHXs)

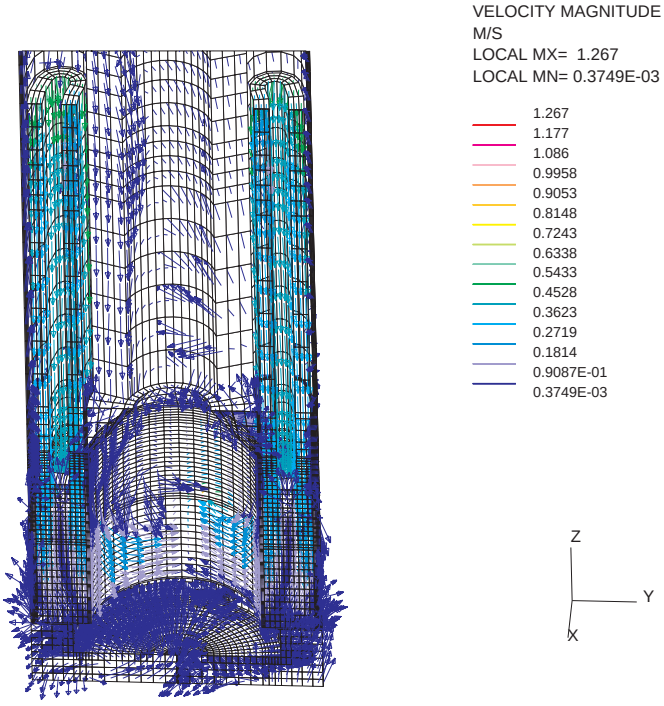

Figure D-6. Sodium velocities in the cold pool

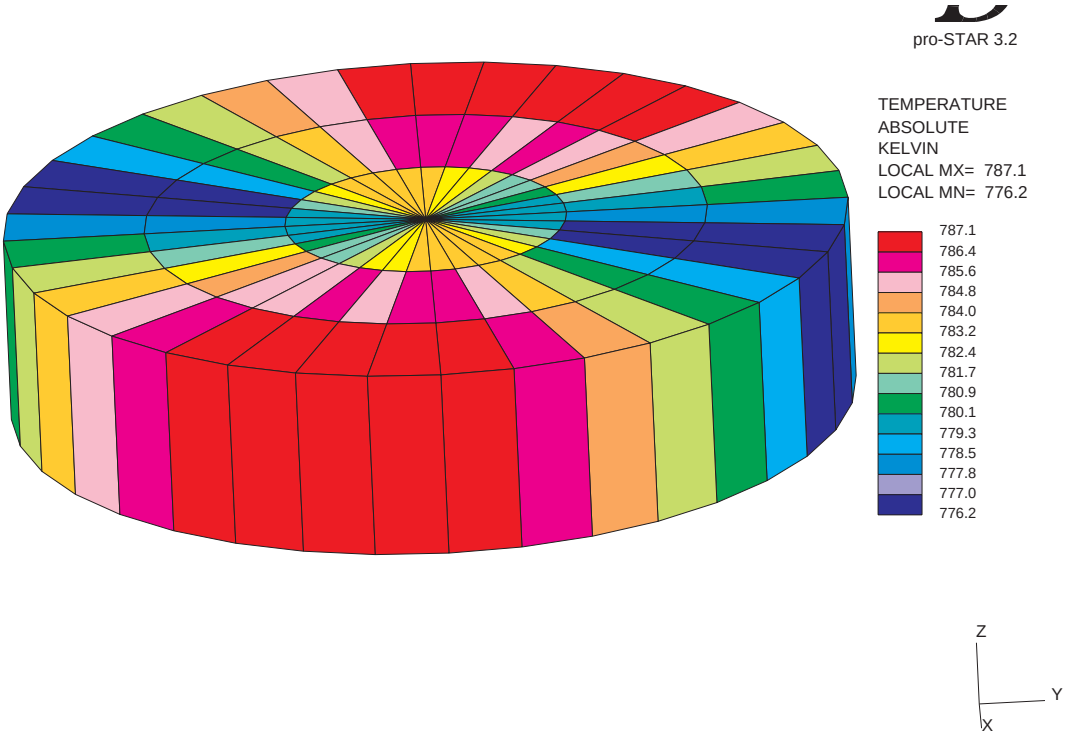

Figure D-7. Temperature distribution at the top of the redan core

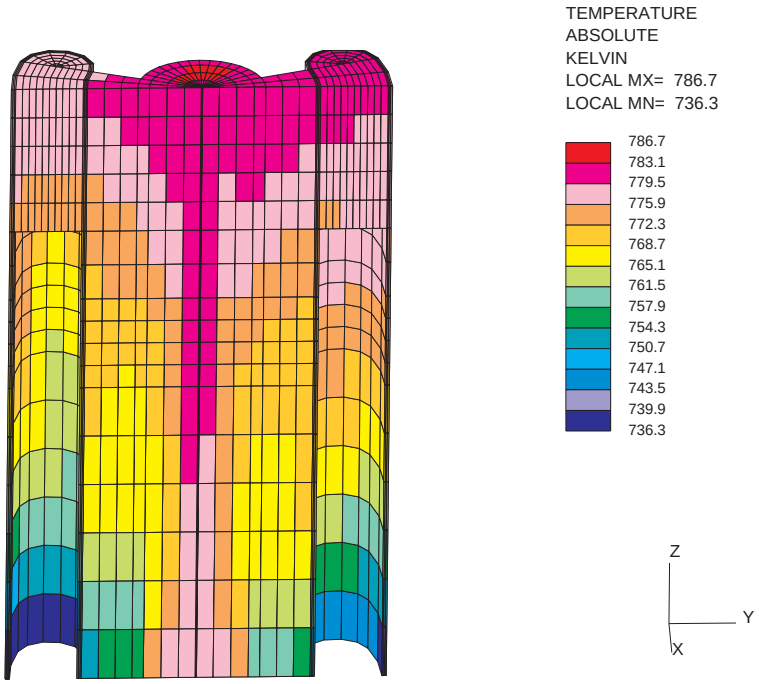

Figure D-8. Temperature distribution in the hot pool

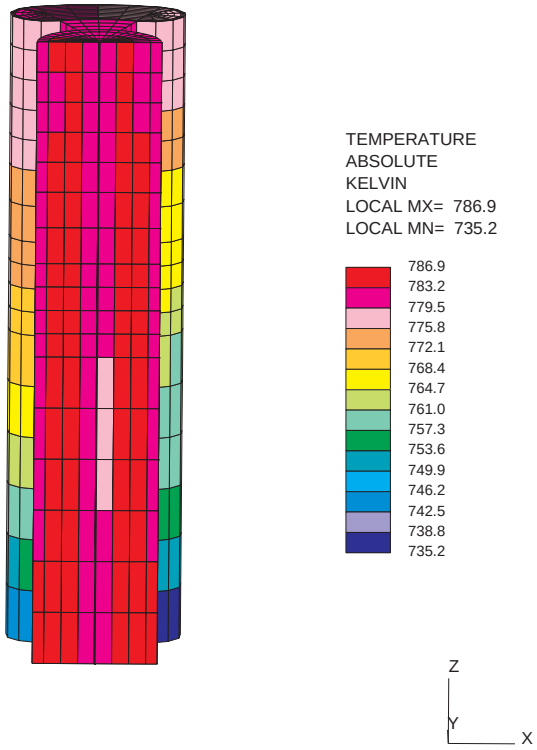

Figure D-9. Temperature distribution in the hot pool
(plane perpendicular to axis passing through the centers of the IHXs)

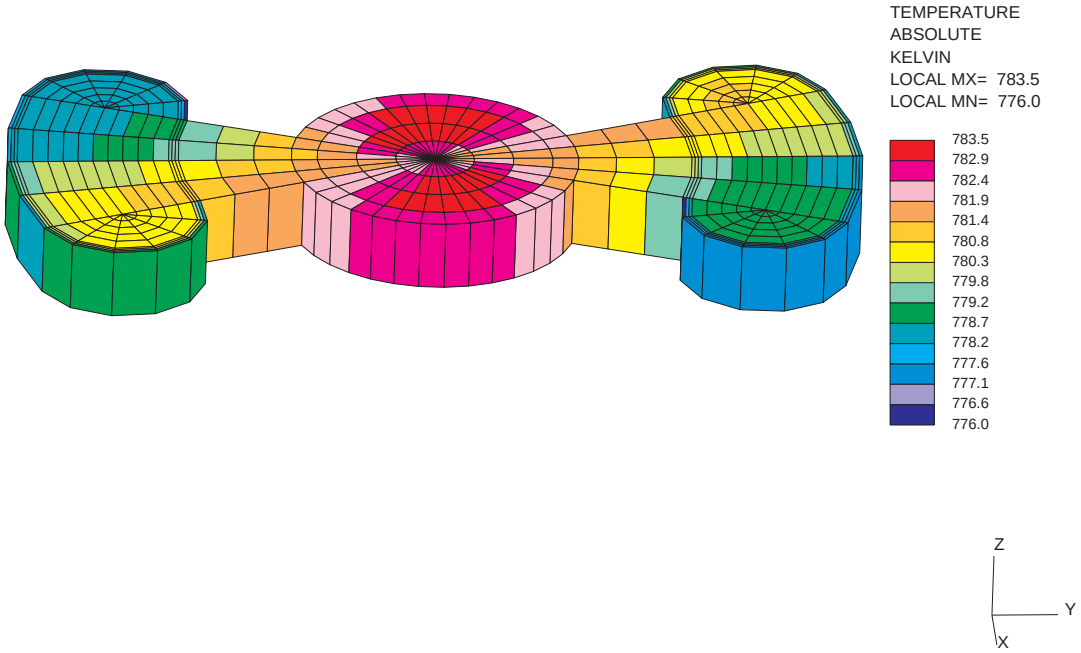

Figure D-10. Temperature distribution at the top of the hot pool

There are some small asymmetries in the temperature distribution of the hot pool. This model uses a relatively coarse representation of the lower plenum flow-distribution ring (Figure D-11) which does not provide a symmetric flow distribution (θ direction) in the core. There is a heat transfer through the thin redan structure from the hot pool to the cold pool, which reduces the sodium temperature at the inlet of the IHX by about 6^{o}C below the core outlet temperature (Figures D-12 and D-13). Figure D-12 also shows that the temperature at the inlet of the IHX is not uniform. In these simulations, the IHX inlet plenum was not modeled, and as Figure D-14 shows, this results in an inlet flow maldistribution.

Figures D-15 and D-16 show the temperature distribution in the cold pool. There is a maximum variation of about 130°C from the top of the pool to the bottom of the pool. Figure D-15 also shows the effect of the flow maldistribution in the IHX, which results in some cold spots (temperatures below 330^{o}C) in the cold pool, and Figure D-16 shows that the azimuthal temperature variation in the upper cold pool also affects the azimuthal temperature variation in the lower cold pool. It should also be noted that the simulation of the secondary side of the IHX as a uniform volumetric heat sink enhances the effect of the small flow maldistribution in the IHX.

Figure D-17 shows the temperature distribution in the reactor vessel. There is a significant azimuthal temperature variation in the upper section of the reactor vessel, which reaches a peak temperature of 471°C in the neighborhood of the IHXs (Figure D-18). There are also significant temperature variations in the redan, which may need to be considered in assessing its structural behavior

Figure D-19 shows the second model that simulates the components above the sodium free surface. It includes the argon cover gas above the sodium free surface, the redan, a set of 22 shield plates, a volume filled with steel balls, a glass wool insulation layer, a gap filled with argon, a top slab of concrete, the upper section of the reactor vessel, and a ring of argon gas around the upper section of the "steel ball" volume. A simulation was also performed with this argon ring been replaced with glass wool insulation (Figure D-20).

In this model, the following boundary conditions were used: (a) the temperature distribution at the free surface of the sodium; (b) the temperature distribution at the bottom boundary of the reactor vessel (upper section); (c) a constant temperature on the top of the concrete slab; and (d) an adiabatic boundary condition on all other external boundaries. An emissivity of 0.65 was used [1] for the sodium free surface, and an emissivity of 0.7 for all other radiating surfaces.

A simulation was first performed to assess the significance of the thermal insulation provided by the 22 shield plates to the concrete cover. In this simulation: the temperature of the sodium surface was set to 510°C; the temperature of the bottom boundary of the tank to 460°C; the temperature of the top surface of the concrete cover to 90°C; and the radiation between the plates was ignored. The latter maximizes the thermal resistance provided by the plates and the argon gas between them.

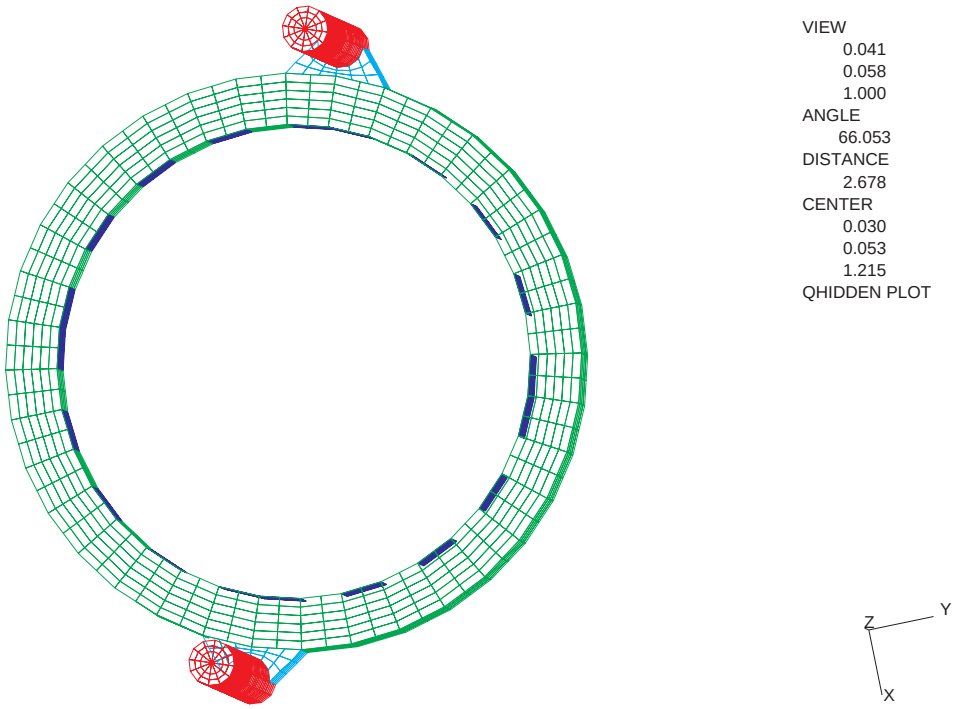

Figure D-11. Flow distribution ring at the inlet plenum
(flow is allowed only through the spaces between the blue walls of the distribution ring)

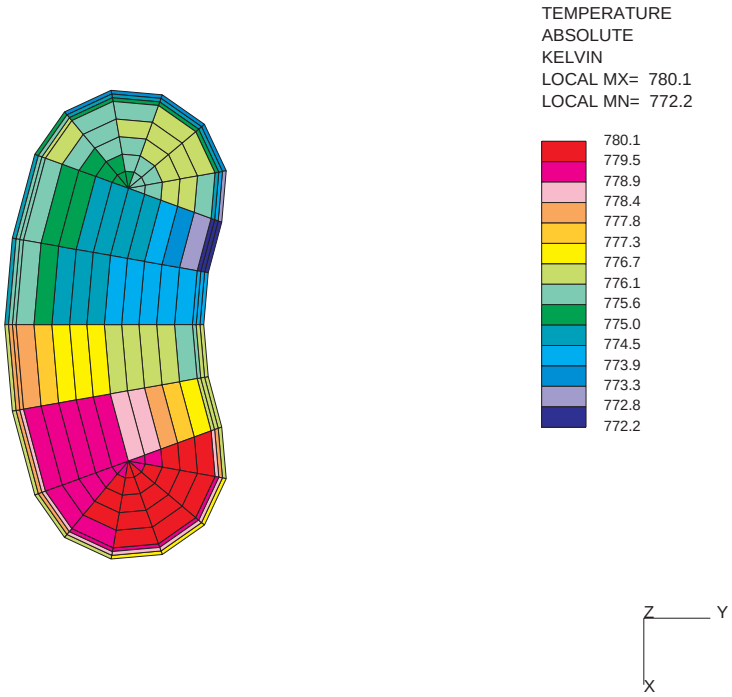

Figure D-12. Temperature distribution at the IHX inlet

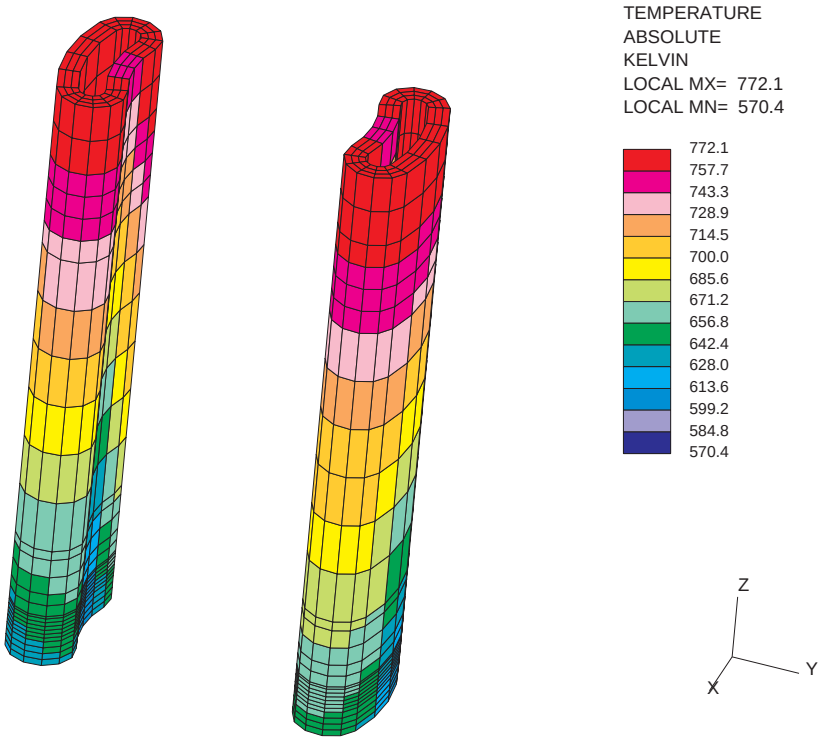

Figure D-13. Temperature distribution in the IHX

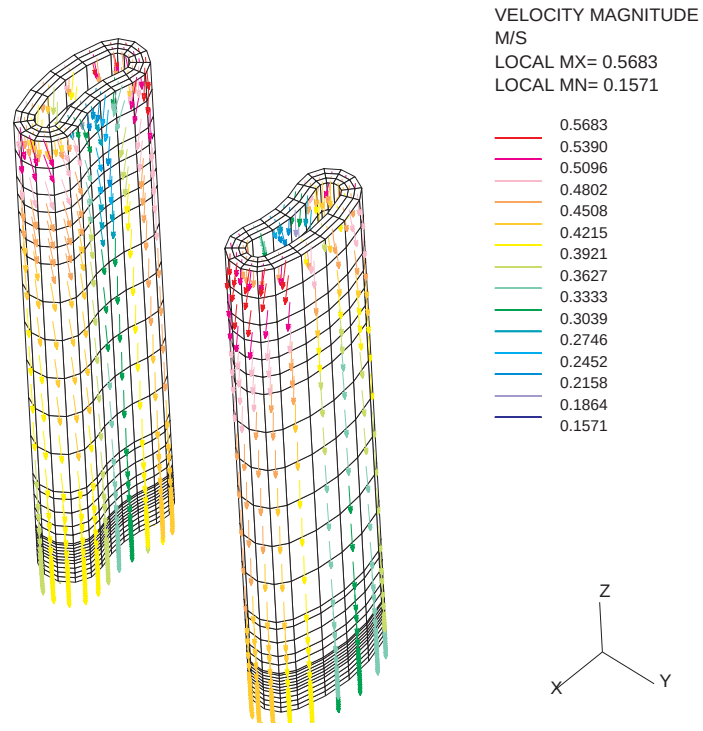

Figure D-14. Flow distribution in the IHX

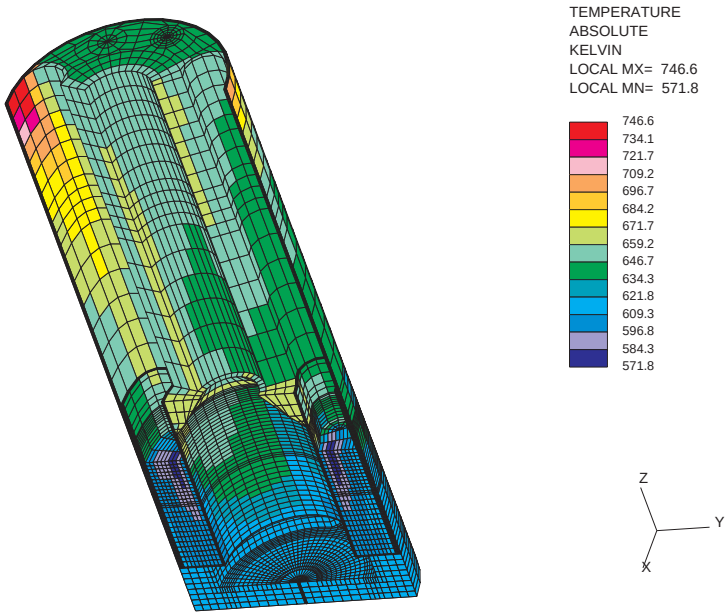

Figure D-15. Temperature distribution in the cold pool

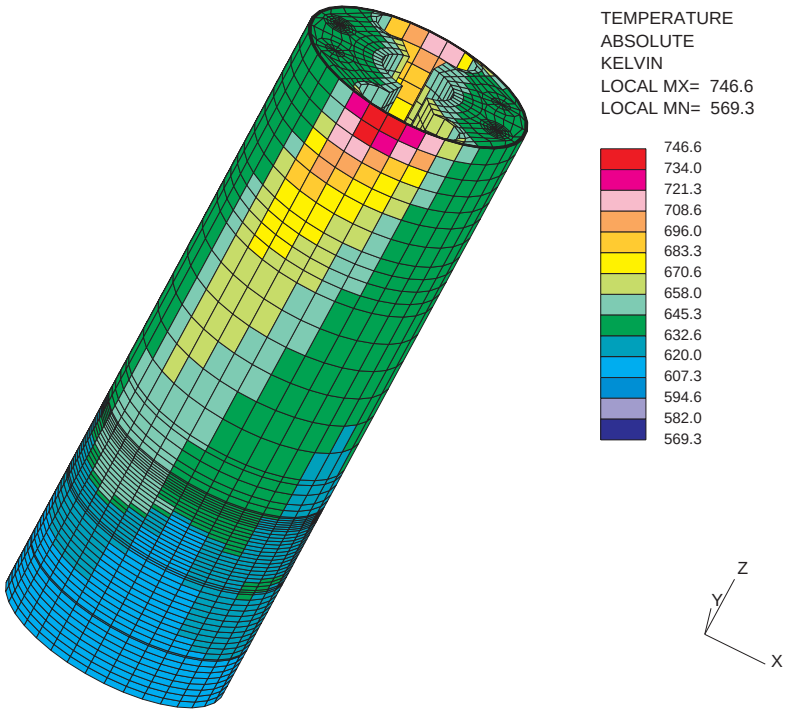

Figure D-16. Temperature distribution in the cold pool

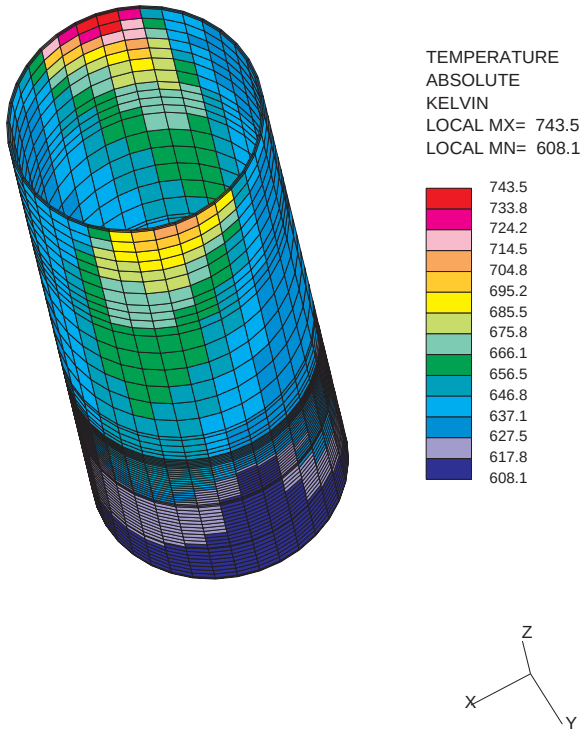

Figure D-17. Temperature distribution in the reactor vessel (below sodium free surface)

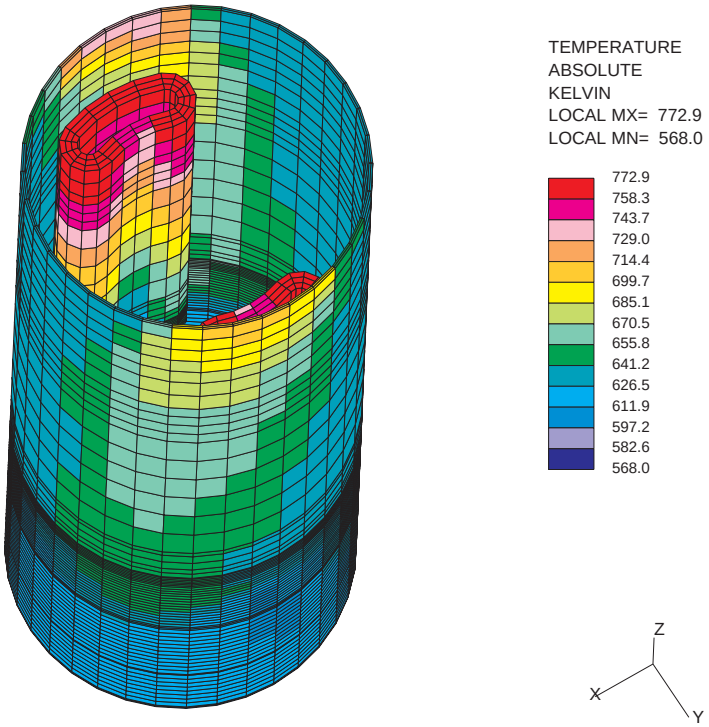

Figure D-18. Temperature distribution in the reactor vessel and the IHXs

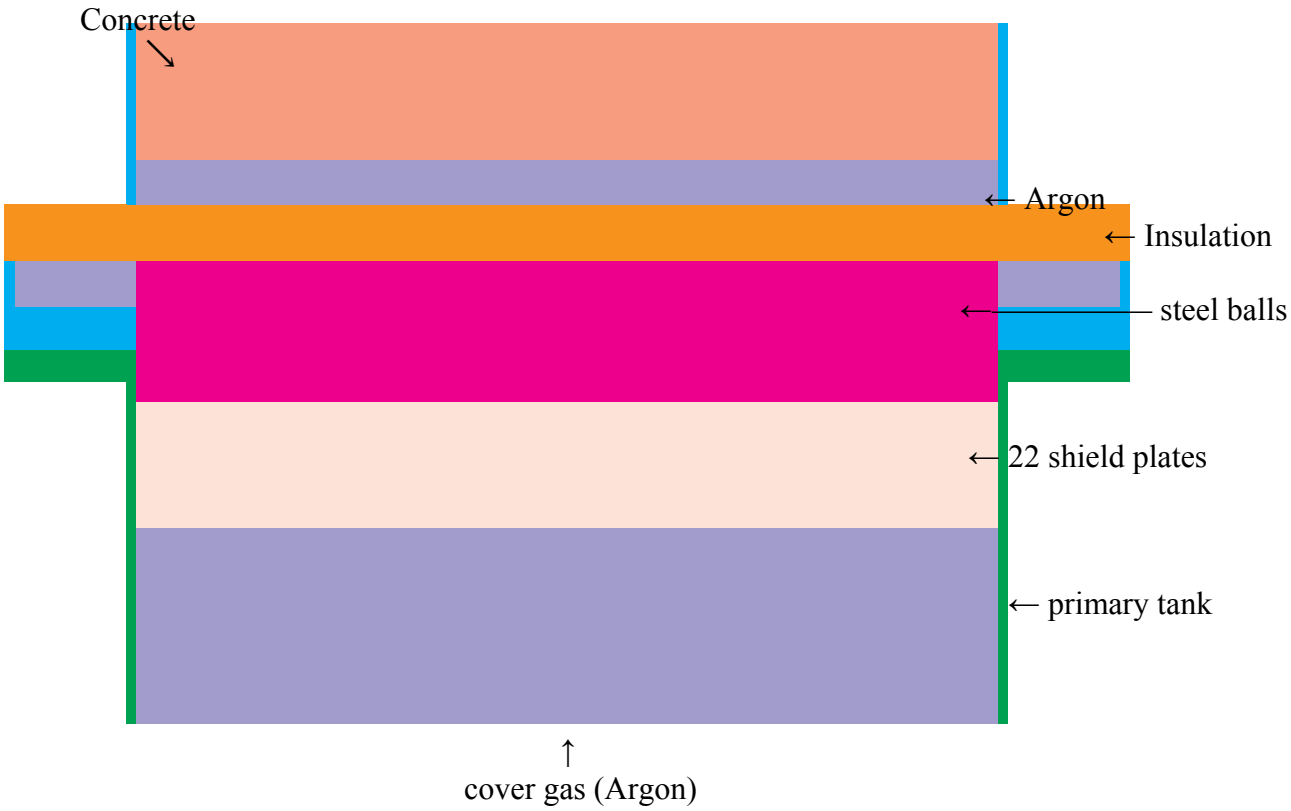

Figure D-19. Model of components above the sodium free surface

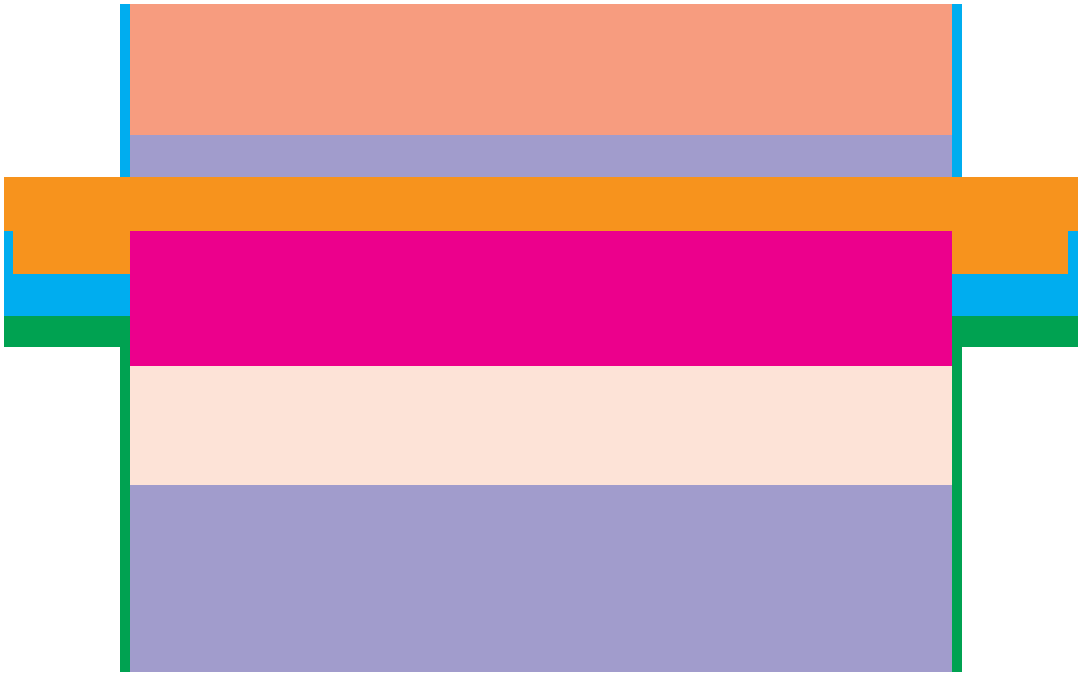

Figure D-20. Model geometry (argon ring replaced with insulation)

Figures D-21 to D-25 show the predicted temperature distributions for the whole model and for each of its components ("22 plates", "steel ball" volume, insulation, and concrete cover). The maximum temperature drop across the "22 plates" is 43°C. The maximum temperature drop across the "steel ball" volume is 12°C, that across the insulation is 283°C, and that across the concrete cover is 14°C. These results show that for the concrete cover most of the thermal protection is provided by the insulation (steel wool). Figure D-26 shows the temperature distribution in the upper section of the reactor vessel.

Subsequently a simulation was performed were: radiation between the 22 shield plates was accounted; the temperature distribution at the bottom boundary of the model (sodium surface and primary tank) was set equal to that predicted from the first model (Figure D-1); the argon ring around the "steel ball" volume was replaced by insulation (Figure D-20); and a temperature of 73°C was used at the top boundary of the concrete cover to assure that its inner surface does not exceed a temperature of about 90°C.

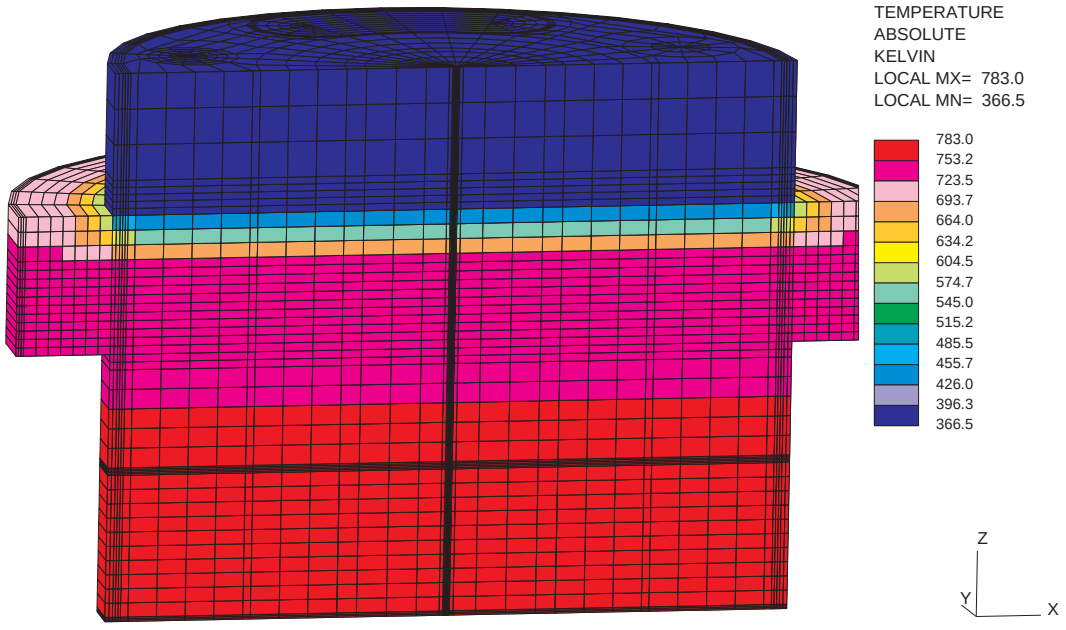

Figure D-21. Temperature distribution
(no radiation between shield plates)

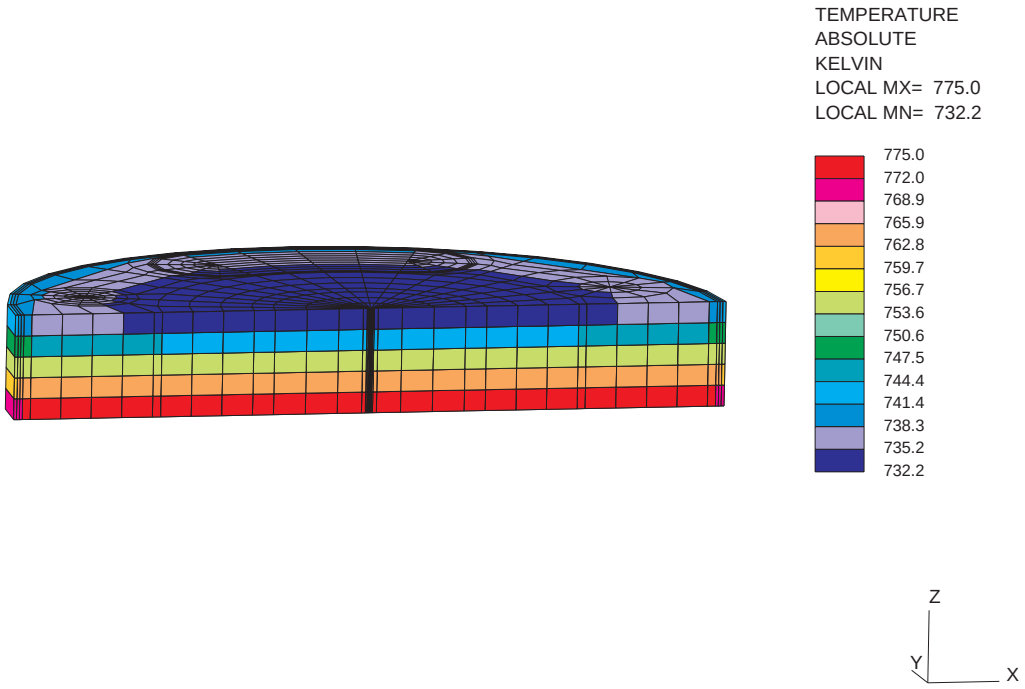

Figure D-22. Temperature distribution in shield plates
(no radiation between shield plates)

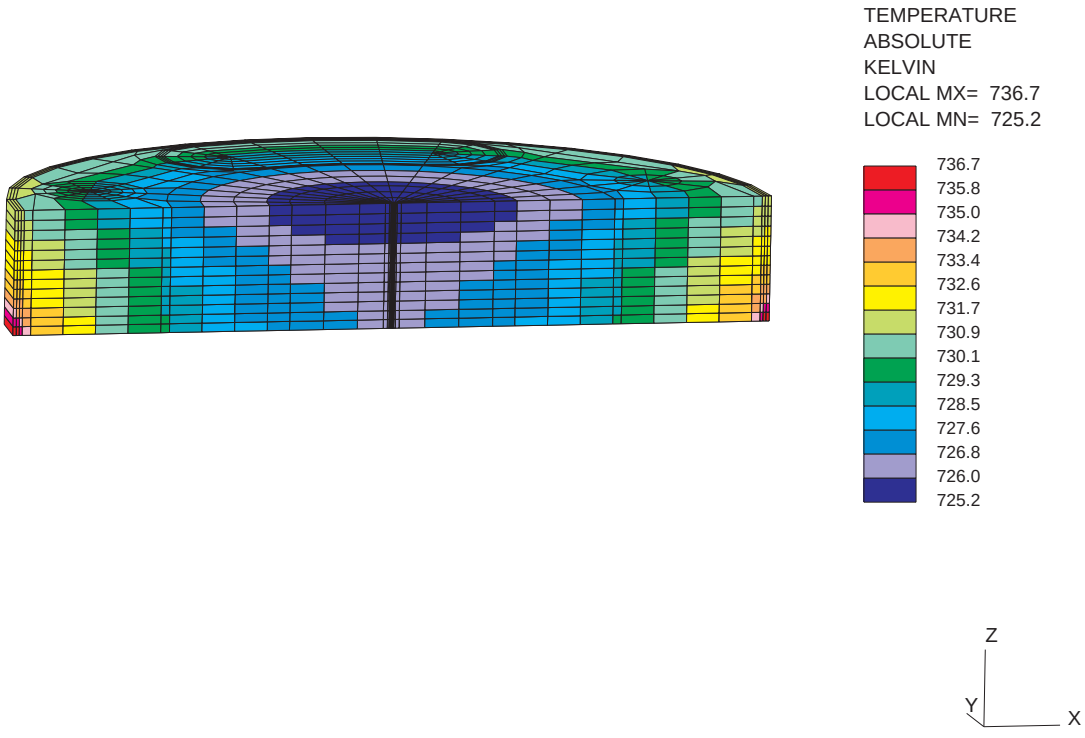

Figure D-23. Temperature distribution in "steel balls"
(no radiation between shield plates)

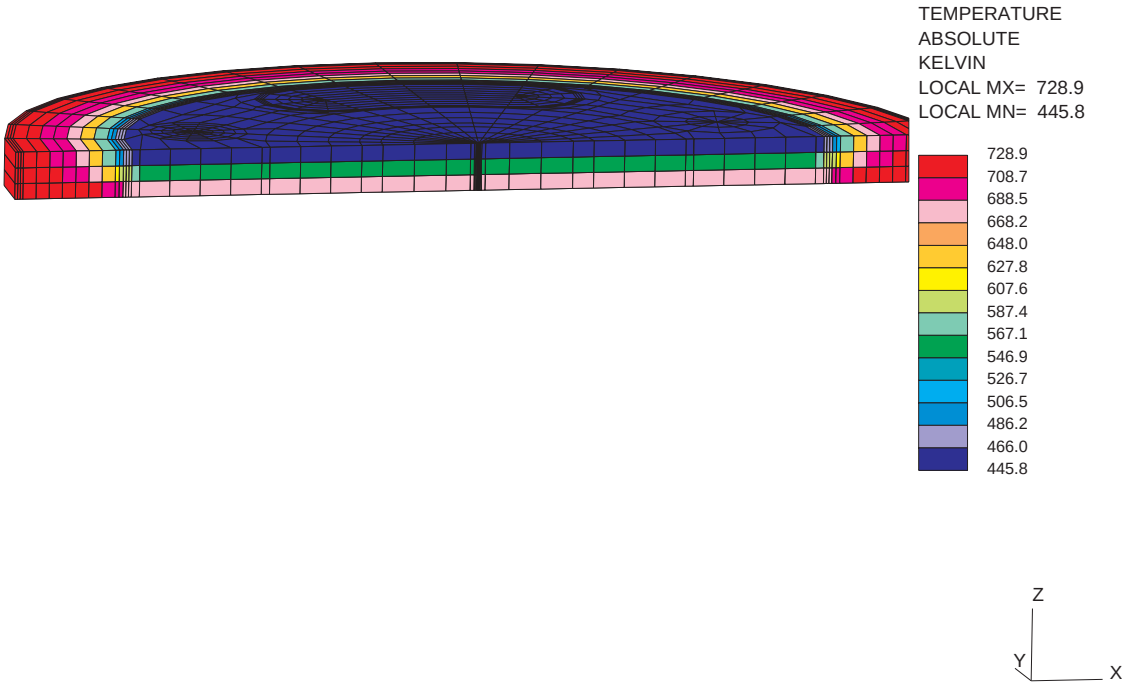

Figure D-24. Temperature distribution in insulation
(no radiation between shield plates)

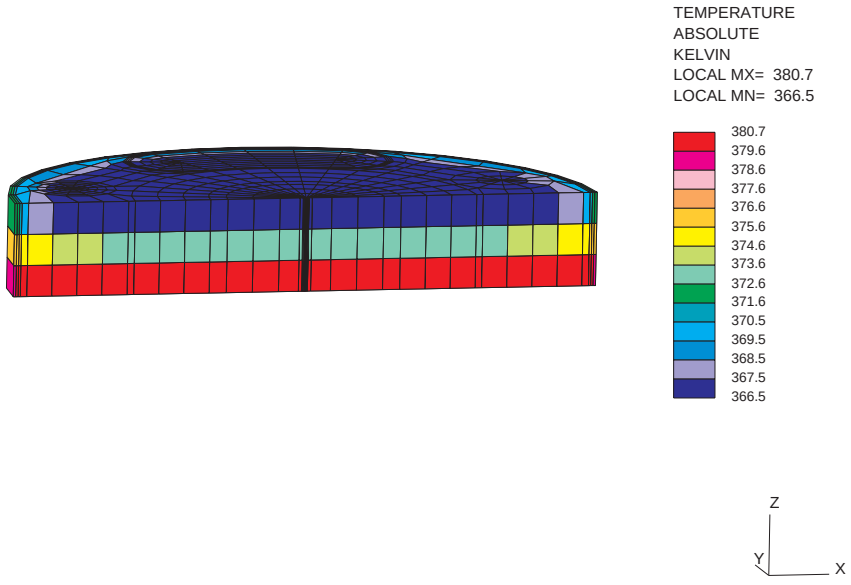

Figure D-25. Temperature distribution in concrete
(no radiation between shield plates)

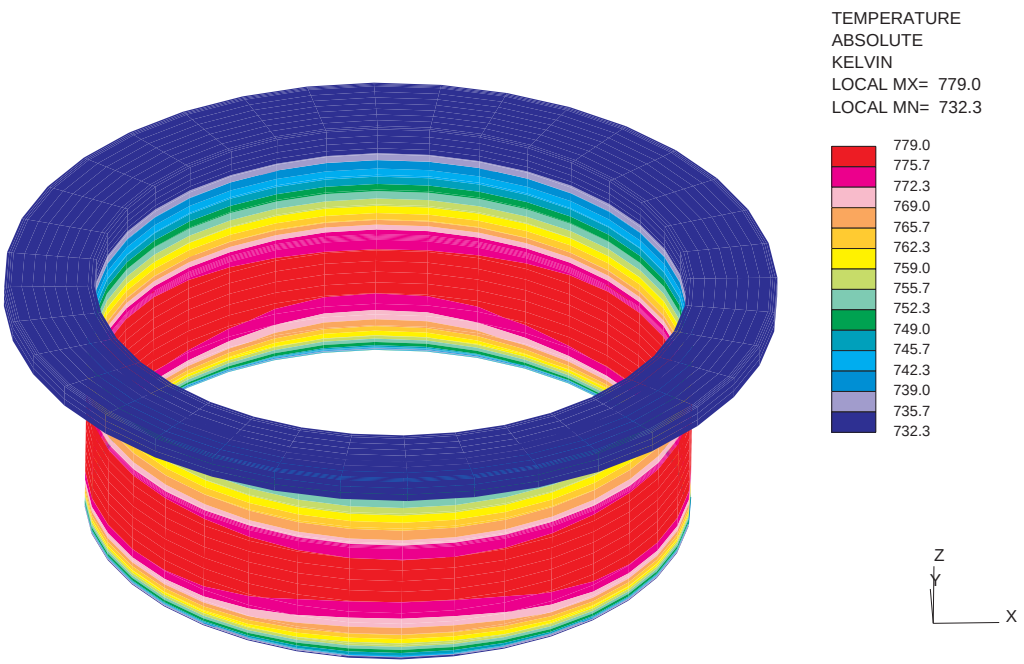

Figure D-26. Temperature distribution in the reactor vessel
(no radiation between shield plates)

Figure D-27 shows the temperature distribution for the whole model on a vertical plane passing through the symmetry axis of the IHXs. Figure D-28 shows in more detail the temperature distribution in the concrete cover on the same plane. The maximum temperature on the inner surface of the concrete cover is 93°C. Figure D-29 shows the temperature distribution in the upper section of the reactor vessel. There is a significant azimuthal temperature variation in the lower section of the reactor vessel that is a reflection of the azimuthal temperature variation in its section that is filled with sodium (hot regions next to the IHXs).

Parametric analyses show that the heating of the reactor vessel section above the sodium free surface is mainly due to conduction of heat from the lower section of the vessel that is filled with sodium. To keep the temperature of the concrete that supports the reactor vessel (Figure D-30) below 90°C, it is estimated that about 19 kW of heat need to be discharged to the shield cooling system.

References

1. A. Yamaguchi and Y. Tajima, "Numerical Investigation of Mass and Heat Transfer in Sodium Pool Combustion," Numerical Heat Transfer, Part A, 41:697-709, 2002

Figure D-27. Temperature distribution
(radiation between shield plates)

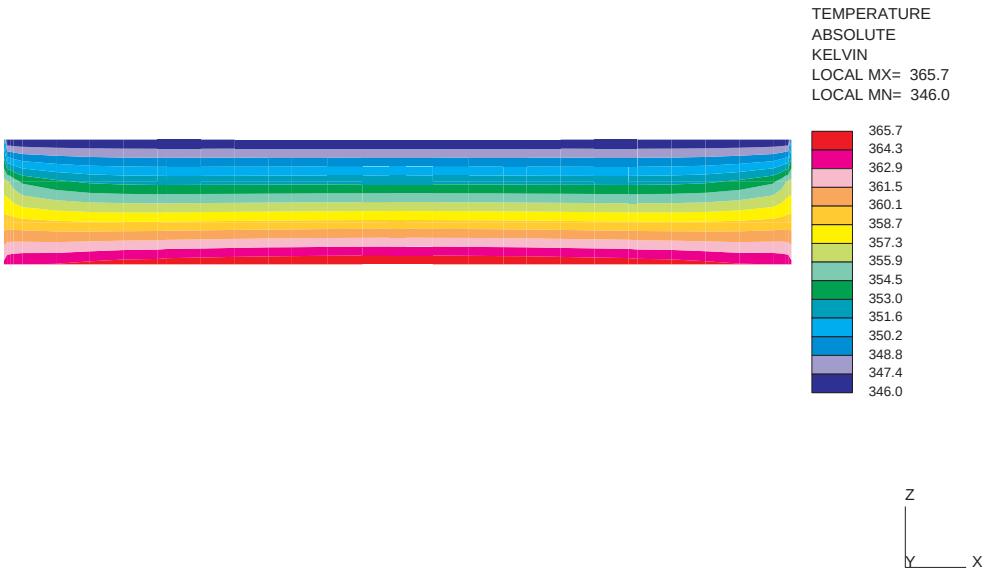

Figure D-28. Temperature distribution in concrete
(radiation between shield plates)

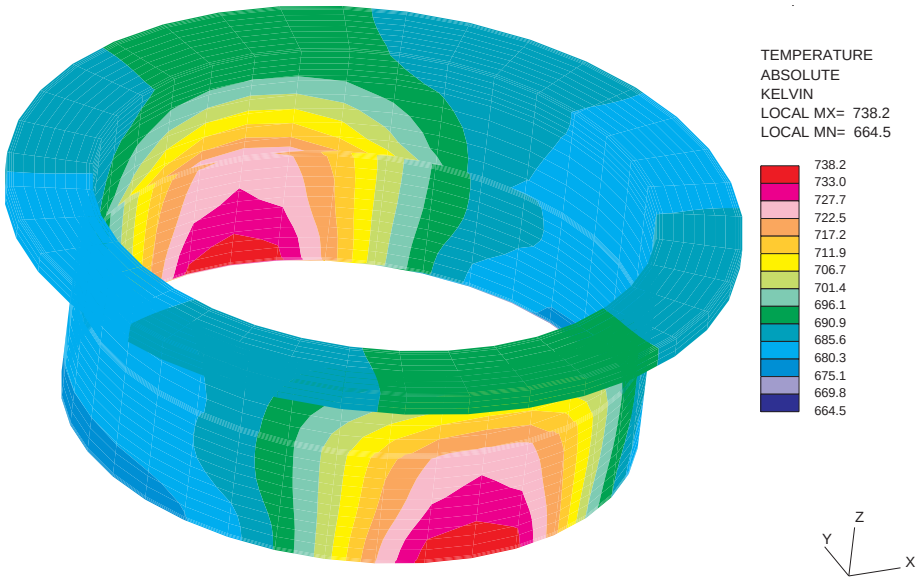

Figure D-29. Temperature distribution in the reactor vessel (radiation between shield plates)

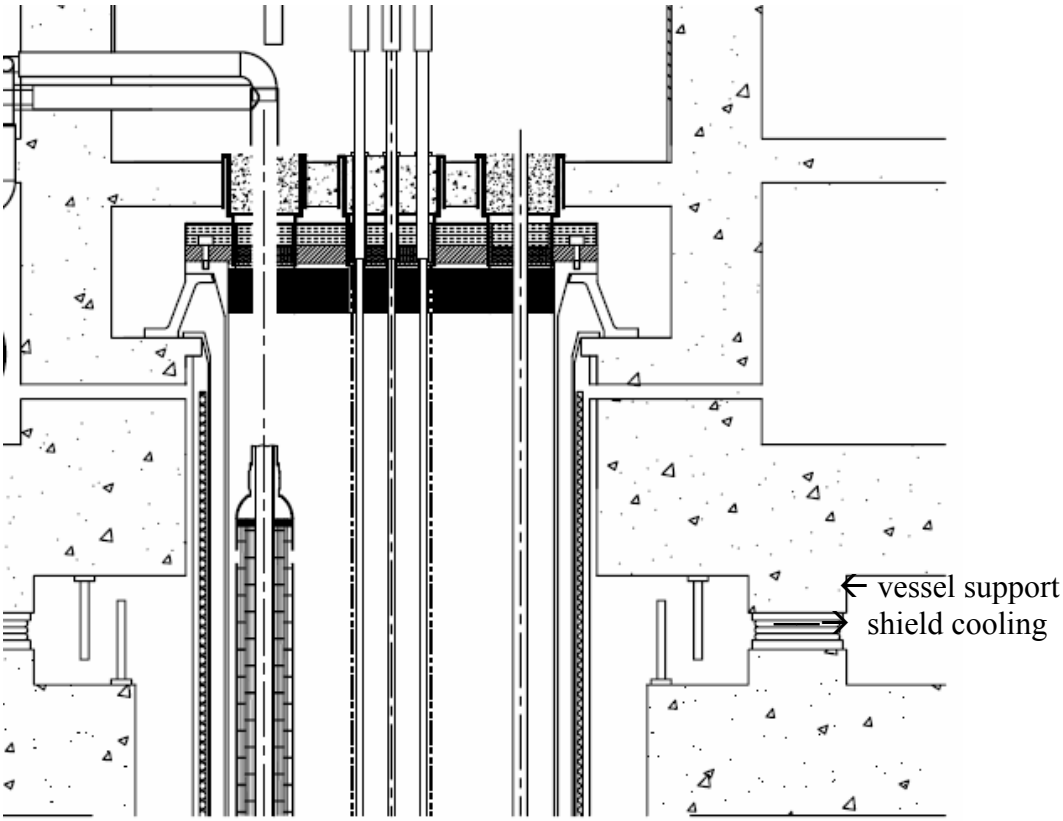

Figure D-30. Reactor vessel support

APPENDIX E. ADVANCED DESIGN CONCEPT

This Appendix describes examples of advanced design concept that can be achieved with further research and development. For example, the core outlet temperature can be increased from the reference design value of 510°C to 550°C, if additional R&D is carried out to successfully develop the qualifying irradiation database.

1. Advanced Loop Concept

The design described in this section has been developed by JNC as part of the Japanese fast reactor feasibility study over the past several years. (This study is one of the outcomes of collaborative study between JNC and JAPC in the accordance with "The Agreement about the Development of a Commercialized Fast Breeder Reactor Cycle System")

Fuel and Core Design

One of the core concepts which has been tried to obtain stable radial power distribution is the BREST-300 middle-size lead-cooled nitride-fueled core with the idea of a single Pu-enrichment and 3 radial regions of fuel with different diameter pins. [1,2] The local conversion ratio is uniform throughout the core due to a single Pu-enrichment arrangement. The radial power distribution is flattened by controlling the heavy metal fraction of each region. In addition, the specification of an adequate Pu-enrichment allows for maintaining criticality and the break-even conversion ratio without blanket fuel. The adequate Pu-enrichment is attained by balancing the U-238 capture and Pu-239 absorption reaction rates and ranges from 12 to 14wt% in Pu-enrichment and around 8wt% in fissile-enrichment. Since the local conversion ratio is near 1.0 throughout the core of single Pu-enrichment fuel, radial power distribution is stable during core operation.

This kind of core concept was applied to a design study on a middle-size sodium-cooled metal-fuel core [3], in consideration of the same feature of high heavy metal content as that found with the nitride-fuel core. Figures E-1 and E-2 represent the radial power profile during core operation period in the conventional two Pu-enrichment zoned (10.2 and 12.6wt%) core and a single Pu-enrichment (12.4wt%) core with two Zr-content zoned (16 and 10wt%) core, respectively. The power profile of the Pu-enrichment zoned core is not stable because local conversion ratios of inner and outer cores are different due to the difference of the Pu-enrichment. On the contrary, the power profile of the single Pu-enrichment core is much more stable than that of the conventional zoned core. Such a stable radial power profile rationalizes the enveloping core radial power and enables a high core outlet temperature of 550°C.

The rationale for the choice of power level, core life, fuel configuration, core outlet temperature, primary circuit pressure drop, and reactivity control system are described below:

Power Level: 50 MWe with around 120 MW thermal output is a primary choice solely for electricity generation for remote locations. Around 400 MW thermal output can be an alternative, because electricity generation ~120 MWe should reduce unit capital cost, or applying

partly for electricity (50MWe) and partly for hydrogen co-generation should become an attractive energy source.

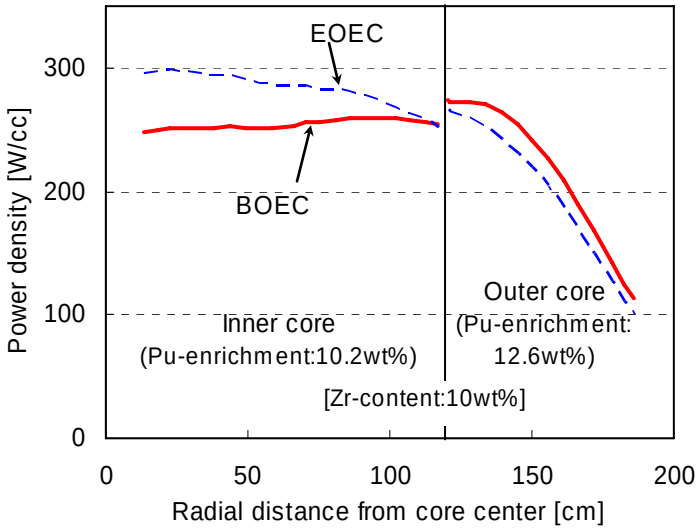

Figure E-1. Radial power profile of conventional two Pu-enrichment zoned metal-fuel core

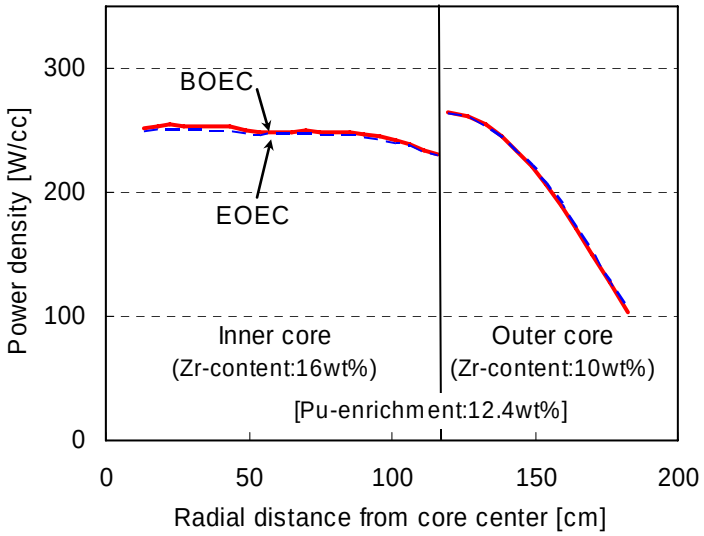

Figure E-2. Radial power profile of single Pu-enrichment with two Zr-content zoned core

Core Life: Long-life power source of a few decades is attractive for remote location users. 30-year lifetime can be a primary choice, although a shortened core lifetime with a mid-life refueling could be an alternative with increased life-cycle costs. Secondary recommended core

life is 60 years, coincident with the plant system lifetime of 60 years, which can eliminate core changeover altogether and the associated costs.

Fuel Configurations: 'Breed and burn' with metal fuel (U-Pu-Zr) fits for a small-scale long-life core, which necessitates a compact fissile fuel loading in high volume fraction configurations as much as possible (within material/thermal constraints). Recommended key design parameters are: large fuel pin diameter (15mm), narrow pin gap (1mm), graded smear density (around 75%T.D.), graded Zr concentration (around 10wt%), thin duct thickness (2mm) and gap (1mm). Current design parameters as starting points are listed in the parentheses above.

Core Outlet Temperature: Core outlet (primary circuit) sodium temperature should reach 550°C. This is mainly for the adaptation of, so-called, hybrid chemical hydrogen co-generation system. We choose the electricity and hydrogen co-generation multi-purpose system. Moreover, higher outlet temperature achieves high thermal efficiency (ex. supercritical CO_2 Brayton or water-steam Rankine cycle) for electricity generation.

Pressure Drop in a Primary Circuit: Long-term continuous operation for 20~60 years necessitates quite reliable coolant circulation system. Electromagnetic pumps without mechanical rotating shaft or blades are to be selected as reasonable devices. Designed discharge pressure of an electromagnetic pump is up to around 0.4~0.6 MPa, thus, a core pressure drop (including inner fuel bundle, orifice, and inlet/outlet losses) should be designed around 0.2 MPa or below.

Reactivity and Power Distribution Control System: The most reliable mechanism should be selected for the reactivity control and reactor shutdown system. A conventional control rod system using, for example, B_4C pellets, is recommended to be used for primary, secondary, and self-actuated shutdown systems. Reactivity control by vertically mobile reflector blocks may not suitable for long-term operational reliability, although stationary radial/axial reflectors are necessary. Roles of the primary control system are power distribution management and reactor shutdown. On the other hand, the secondary system is only for shutdown.

The core design parameters are listed in Table E-1, the assembly and pin design parameters in Table E-2, and the core performance characteristics in Table E-3. The core layout is depicted in Figure E-3.

Plant Design

A sketch of the reactor vessel is shown in Figure E-4. The basic features of the reactor vessel are simplification and minimized dimensions adopting no refueling system with the long life core. The upper structure of the reactor vessel is a dome type without rotating plug nor cooling system. The fuel subassemblies are directly supported by the primary vessel and the reactor vessel diameter is minimized by adopting the nozzled piping and elimination of the ordinary fuel relay point outside the core barrel. In the conventional loop type reactor, the sodium level is decided to keep the top of subassemblies under the sodium level during refueling operation. In this concept, the height of the reactor vessel is reduced because the sodium level is decided only considering normal operation.

Table E-1. Core Design Parameters

Thermal Power	120 MWth
Electric Power	50 MWe
Primary Coolant	Sodium
Core Inlet Temperature	395^{o}C
Core Outlet Temperature	550^{o}C
Secondary Coolant	Sodium
Ternary Coolant	Water/Steam
Core Lifetime	30 years (No refueling)
Number of Assemblies	
Driver Fuel	78
Primary Control	5
Secondary Control	2 (w/ SASS mechanism)
Reflector	42
Core Barrel, ID	231cm
Average Linear Power	12 kW/m
Average Coolant Velocity	1.4 m/sec
Pressure Drop Across Pin Bundle	0.026MPa

Table E-2. Assembly and Pin Design Parameters

Lattice Pitch	18.8 cm
Duct Outside Flat-to-Flat	18.7 cm
Interassembly Gap	0.1 cm
Duct Wall Thickness	0.2 cm
Number of Pins of Driver Fuel Assembly	127
Fuel Pin Diameter	1.50 cm
Pitch-to-Diameter Ratio	1.067
Cladding Thickness	0.78 mm
Fuel Material	U-Pu-TRU-Zr
Diametral Gap	0.15 cm
Bond Material	Na
Cladding/Duct Material	ODS / FMS
Active Core Length	101 cm
Upper Plenum	151.5 cm
Upper Shield	40 cm
Core Volume Fractions	
Fuel (of Non-Smeared)	0.41-0.50
Structure	0.19
Sodium (Coolant) / Sodium (Entire)	0.21 (0.40-0.31)
Reflector Volume Fractions	
Structure	0.7
Sodium	0.3

Table E-3 Core Performance Characteristics

Core Lifetime	30 years [60yrs achievable]
Capacity Factor	1.0
Fuel Loading	
U	14,837 kg
Np	11 kg
Pu	2,060 kg
Am	65 kg
Cm	22 kg
Total HM	16,993 kg
Specific Power	7.1 kW/kg
Power Density	46 kW/l
Average Discharge Burnup	77 MWD/kg
Peak Fast Fluence	5 x 10^{23} nvt
Enrichment Zoning: Inner/Intermediate/Outer	12.1/12.1/12.1Pu_wt%
Fissile Enrichment: Inner/Intermediate/Outer	7.4/7.4/7.4Pufissile_wt%
Conversion Ratio: Inner/Intermediate/Outer	1.10/1.09/1.04
k-effective	
BOL	1.000
7.5 yr	1.009
15.0 yr	1.011
22.5 yr	1.008
EOL	1.000

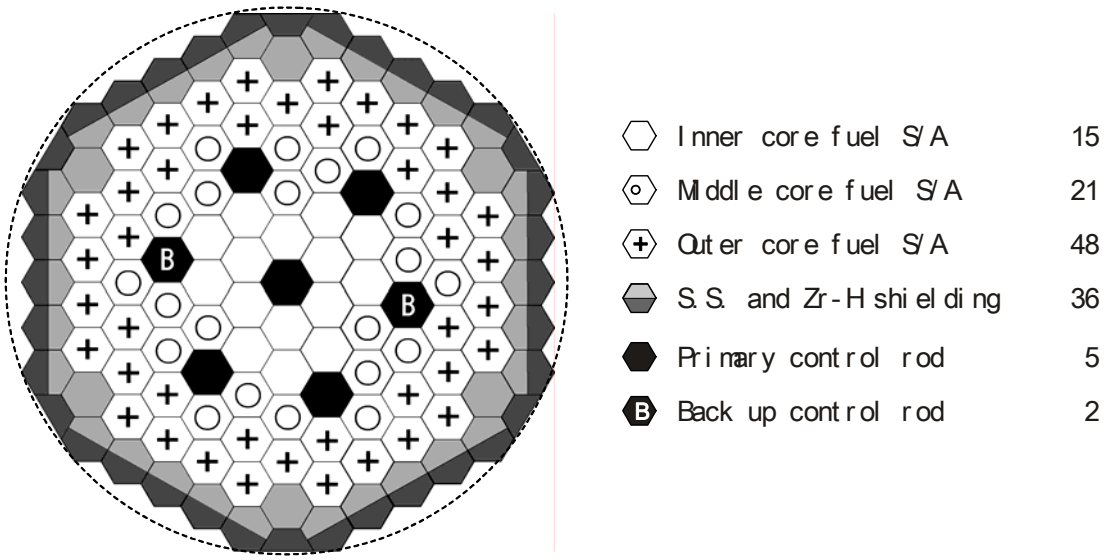

Figure E-3. Core Layout

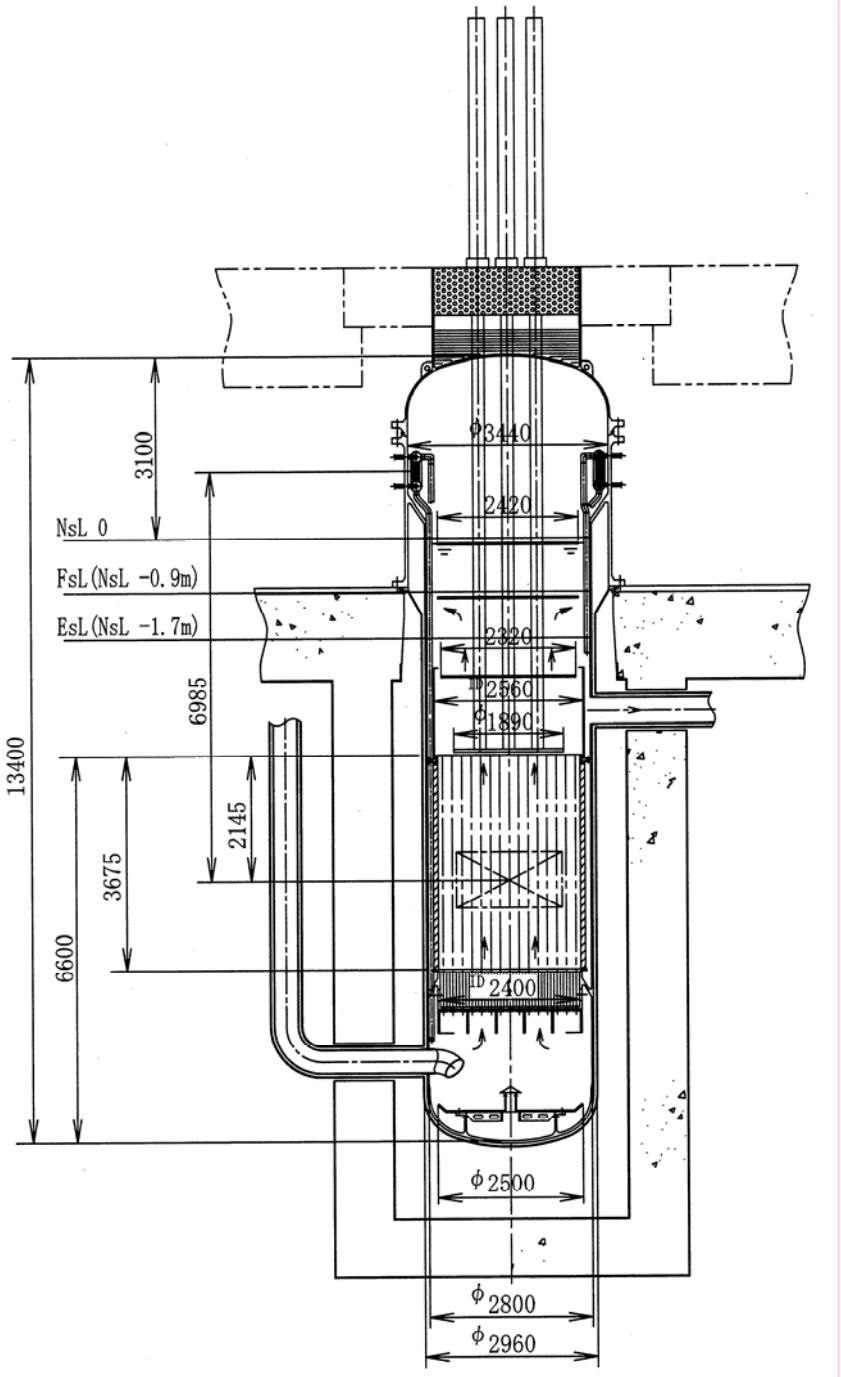

Figure E-4. Reactor Vessel

A schematic illustration of the main cooling system with heat balance is shown in Figure E-5. The main cooling system loop number is one adopting two independent electromagnetic pumps arranged in series. When one electromagnetic pump is tripped in an accident, the other pump can maintain the core flow to reach a safe reactor shutdown. The main pumps in the primary cooling system are arranged in the shell of the intermediate heat exchanger to simplify the primary cooling system. The major specifications and a sketch of the intermediate heat exchanger are shown in Table E-4 and Figure E-6.

The primary circuit material is 316FR stainless steal which is the same of that of the reactor vessel to eliminate dissimilar material welds in the primary system. The secondary cooling system loop number is also one and the steam generator is a helical coil type which has experience in Super Phenix and Monju. The steam generator tube material is 12Cr steel which has high heat conductivity to reduce heat exchange area. The major specifications and a sketch of the steam generator are shown in Table E-5 and Figure E-7. The main steam temperature is 495deg-C in 16.7MPa with the core outlet sodium temperature 550^{o}C. The steam cycle efficiency with this steam condition is estimated to be 42% using a conventional steam turbine.

Figure E-8 shows the plant bird's-eye view. The total steal mass of NSSS is 309 ton which is much less than that of the reference design. [4,5] There is a potential in the advanced concept to achieve a further economic goal.

Table E-4. Intermediate Heat Exchanger Dimensions and Conditions

Items	Value
Capacity	120MW
Tube Outer Diameter	25.4mm
Tube Thickness	1.1mm
Tube Length	2.82m
Tube Quantity	1742
Tube Arrangement	Triangle
Tube Pitch	32mm
Primary Sodium Temperature	550/395^{o}C
Secondary Sodium Temperature	335/520^{o}C
Heat Transfer Area	392m^{2}
Material	316FR

Table E-5 Steam Generator Dimensions and Conditions

Items	Value
Capacity	120MW
Tube Outer Diameter	31.8mm
Tube Thickness	3.3mm
Heat Transfer Area Height	4.92m
Tube Quantity	102
Tube Arrangement	Herical Coil
Tube Pitch	50/50mm
Sodium Temperature	520/335deg-C
Steam Water Temperature	497/233deg-C
Steam Pressure	17.1MPa
Heat Transfer Area	650m^{2}
Material	12Cr Steel

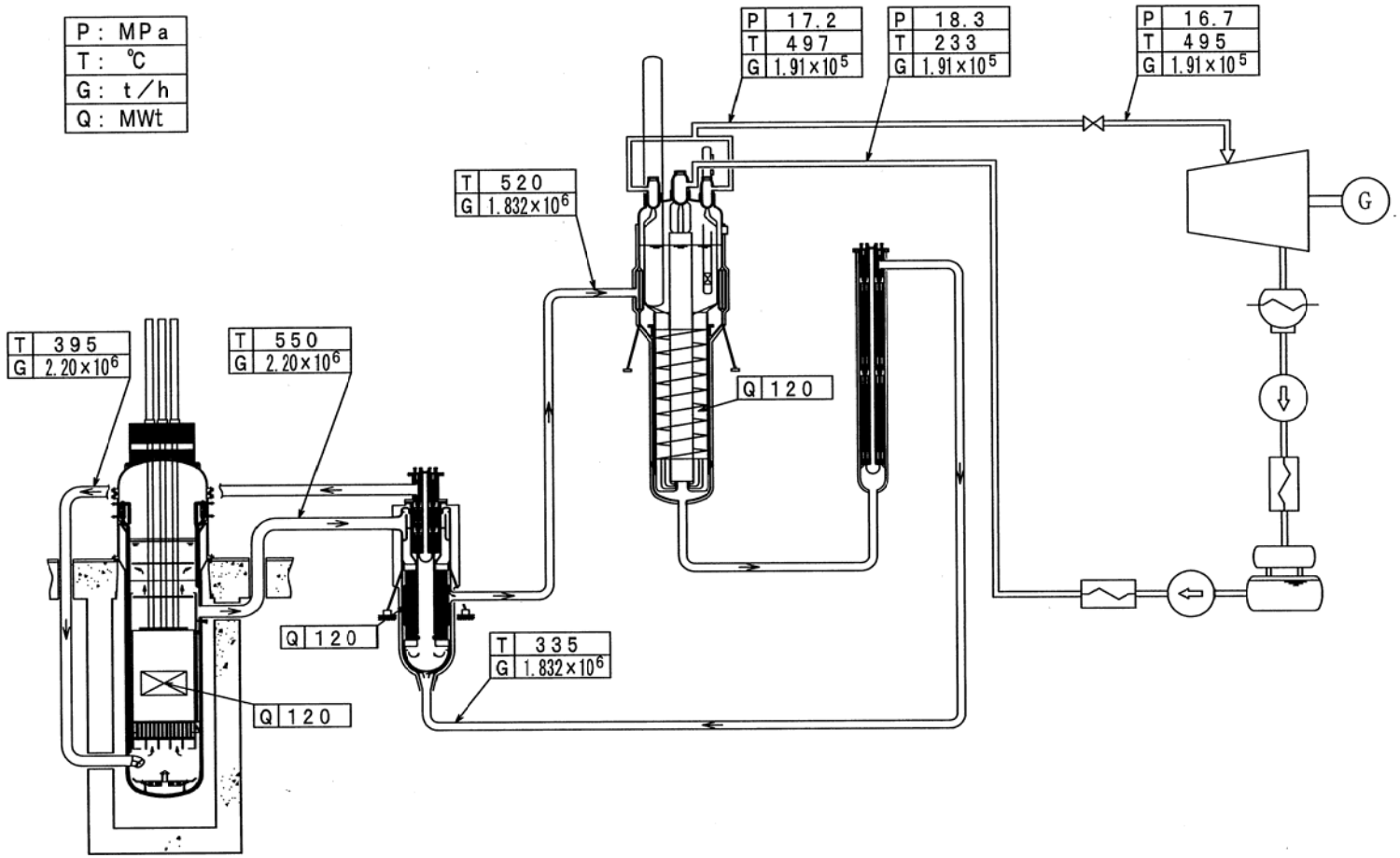

Figure E-5. Schematic Illustration of Main Cooling System

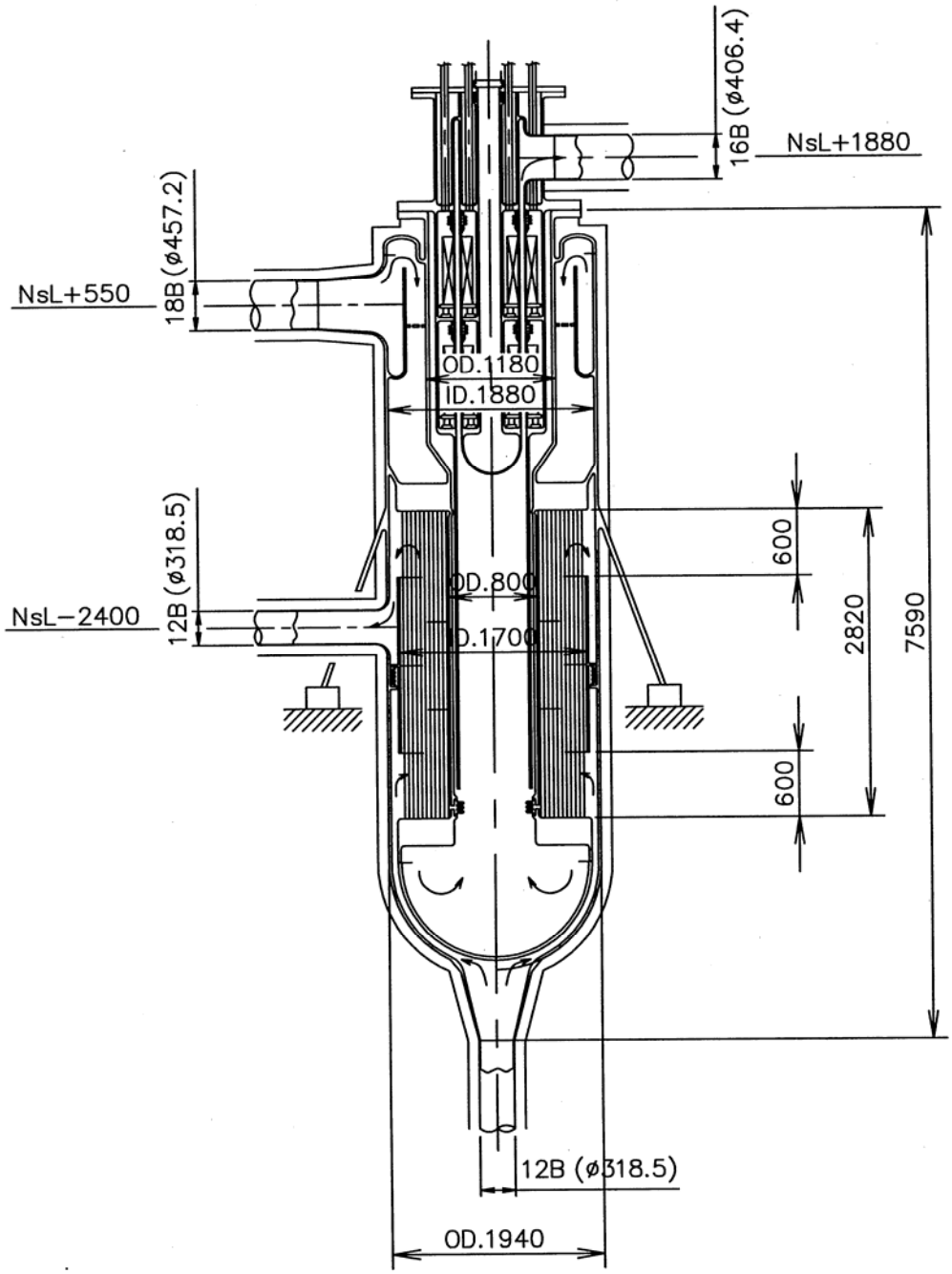

Figure E-6, Intermediate Heat Exchanger with Primary Pump

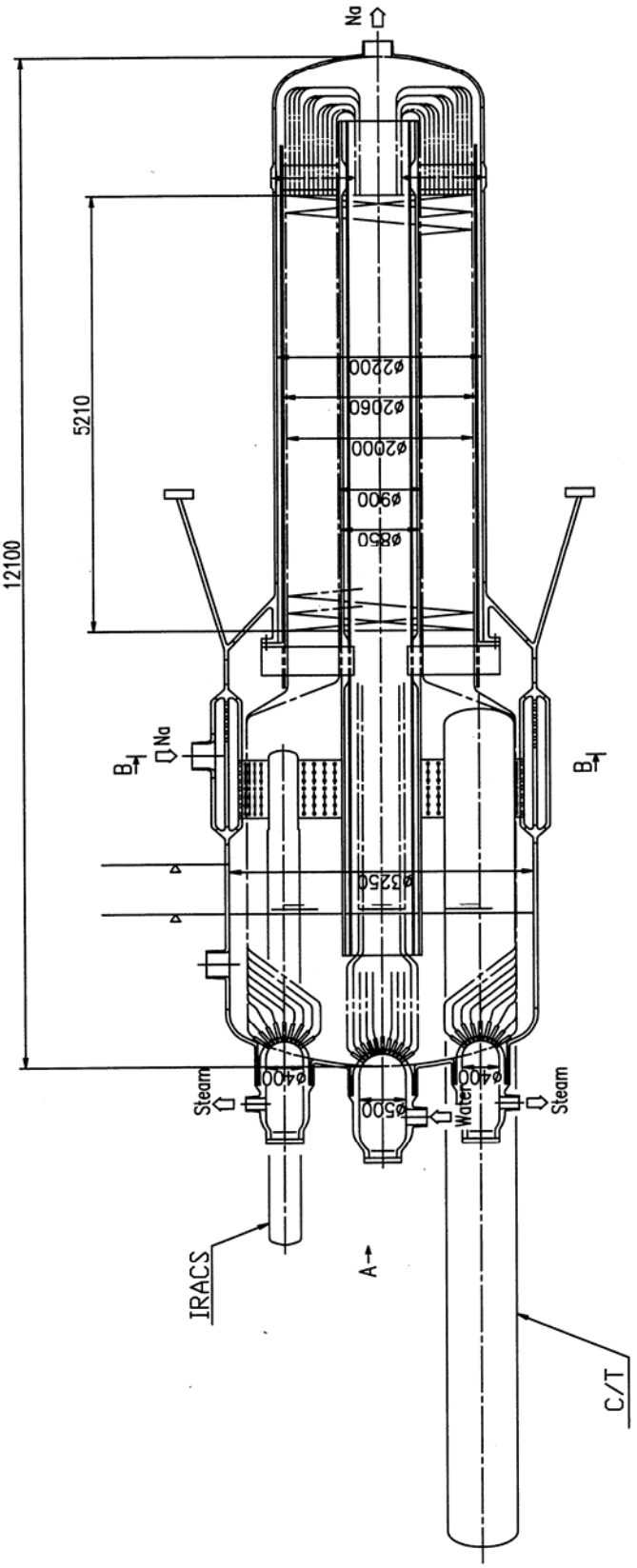

Figure E-7. Steam Generator

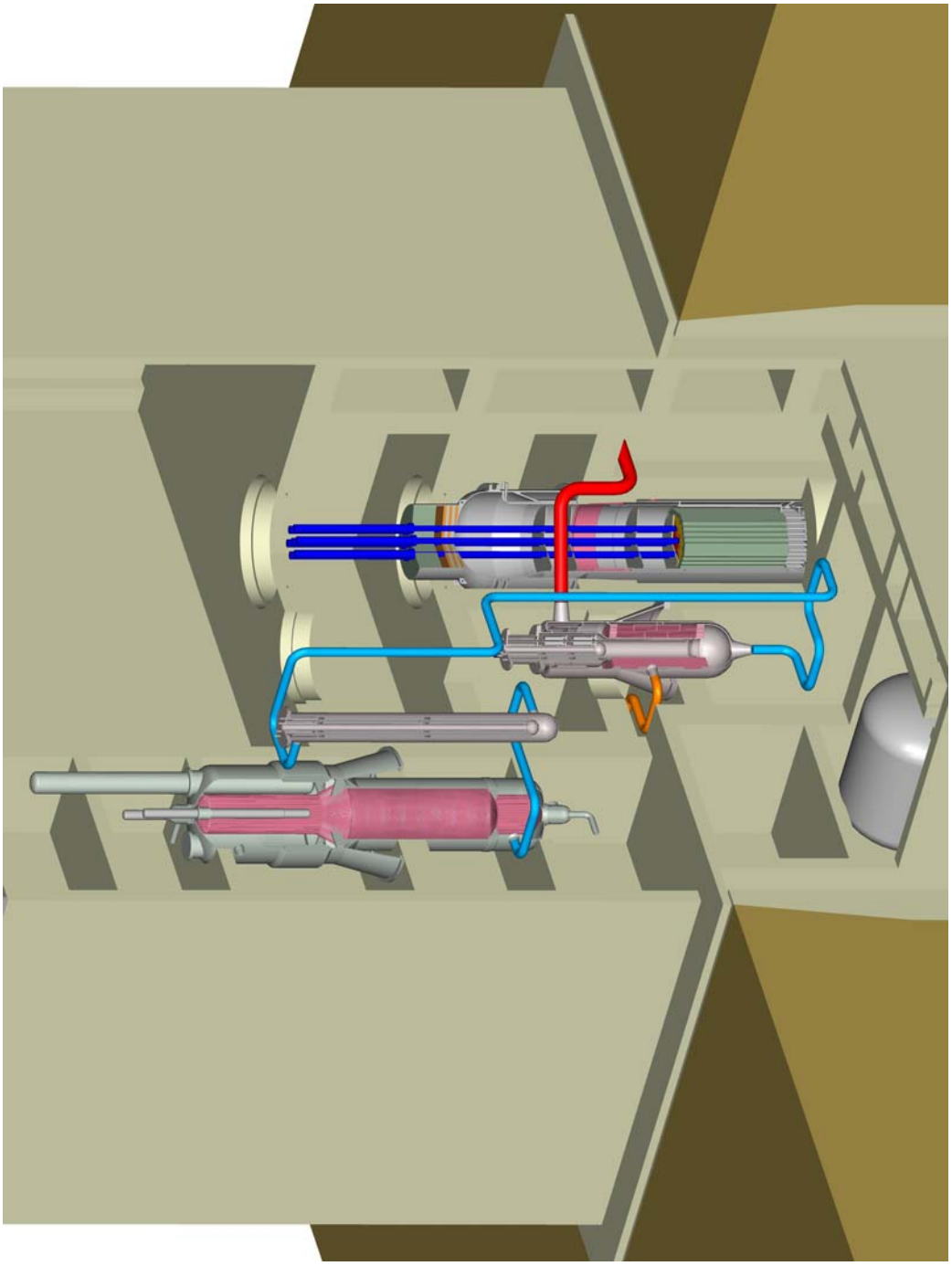

Figure E-8. Plant Bird's-eye View

2. Advanced Pool-Loop Concept

This section describes another example of an advanced design concept, developed by CEA, which incorporates innovative design options with further competitive potential in economy as well as in safety.

The loop design concept offers a potential for reactor bloc compactness. Moreover, suppression of the intermediate heat transport system (IHTS), for economic purpose in the future, seems more feasible starting from a loop-type than a pool-type reactor (non in-vessel sodium/CO_2 heat exchangers). On the other hand, the pool concept offers advantages in other safety fields: emergency shutdown heat removal (natural circulation), prevention of larger leakage of radioactive sodium, occupational exposure, etc. So, the present proposal is to attempt to combine the respective advantages of both reactor-types in a unique innovative hybrid concept, whereas the primary loop is kept for its economic potential in eliminating intermediate heat transport system.

The elimination of IHTS also enables a higher hot temperature to the secondary system, favorable both for the supercritical CO_2 Brayton cycle efficiency and for hydrogen production process. The IHTS and fuel handling system represent two major parts within the investment cost breakdown of a conventional sodium-cooled fast reactor. Use of a long-life metal fuel core, as in the reference SMFR option, can then contribute too from economic viewpoint. A simplified concept of fuel handling is then proposed, in addition to the long-term target of eliminating the IHTS. Consensus between proliferation resistance objective, feasible handling of faulted fuel assembly and economic concerns is sought.

Design directions

The innovative concept proposed has the following design directions:

- Aiming at keeping the advantages of the pool concept, the reactor-bloc is similar to that of a pool design except for the heat exchangers: the IHXs are replaced by the integrated HXs of the emergency heat system (DRACS). These HXs assure if needed the in-vessel primary circulation trough the redan, in case of loss of the primary circuit.
- The primary circuit has no direct connection with the core inlet, unlike a conventional loop concept. This innovative option prevents :
    - any gas passage through the core in case of tube rupture of the sodium/CO_2 HXs,
    - sodium voiding of the reactor vessel whatever the relative location of the primary circuit or of the pipe break.
- The primary circuit has a pump in addition to the in-vessel main primary pumps, in order to balance the primary pressure drops and thereby the sodium levels of the hot and cold plenums by a level control system ($V_{IP} = V_{EP} + PI.[\Delta L_C - \Delta L_M]$). In case of control

defect or pump coast-down or primary pipe loss, there is no safety impact thanks to a sodium flow induced passively through the DRACS heat exchangers or over the redan. This concept is the so-called "reactor with balanced sodium plenums" issued from the CEA studies in the past (ECRA design studies); design concept without external pump is an alternative but with a higher reactor vessel (non balanced sodium levels).

- The intermediate system is not totally suppressed as a first design step before a future RWIHTS (long-term solution), and this despite that the above concept is suitable for a RWIHTS and that the CO_2 is less reactive with sodium than a secondary water/steam coolant. So, an intermediate sodium zone, either stagnant or flowing, is kept in the ongoing design of primary Na/S-CO_2 heat exchanger as a medium-term solution.

Main features of the first design

Based on the design directions described above and complying with the SMFR objectives, a preliminary design called pool-loop (PL) system was developed with the following main features illustrated by Figures E-9 and -10:

- Only one loop for cost saving and easier design laying out;
- One hot leg at the top of core axis and two cold legs outside the internal skirt, so as to reduce the vessel diameter and to keep a radial symmetry;
- Level of legs insertion is fitted versus the sodium plenum level at cold shutdown state and cumulating a postulated vessel leakage (despite availability of the primary loop is not necessary in this faulted situation);
- The cold legs are equipped with EM pumps (half -flow);
- All these three pipes have jackets outside the reactor block, against primary sodium risks.
- The sodium/CO_2 heat exchanger incorporates an intermediate heat transport zone with secondary sodium, instead of a conventional intermediate loop (This design corresponds to a temporary approach, in anticipation of eliminating IHTS in the future). Two options are considered with quite same compactness :
    - HX concept with concentric tubes Na1/Na2/S-CO_2 , inner and outer tubes are separated by a wire; the secondary sodium is quite stagnant but with possible tube failure detection (option with better CO_2 heating);
    - HX component incorporating two separated heat exchangers (Na1/Na2 and Na2/CO_2); the secondary sodium can operate at natural circulation for shutdown conditions (option with easier ISIR but need for Na2 pump).
- Numerous EM pumps (6) in order to :
    - mitigate asymmetric loss of flow accidents (+ non-return valves);
    - reduce the vessel diameter;
    - suppress the connection pipes with the core inlet plenum which has a large diameter.
- The core support is a modular matting with redundant supporting structures, so that the need for ISI is limited regarding the safety function. At the bottom, a space for possible implementation of a core debris catcher with protective layer is planned.

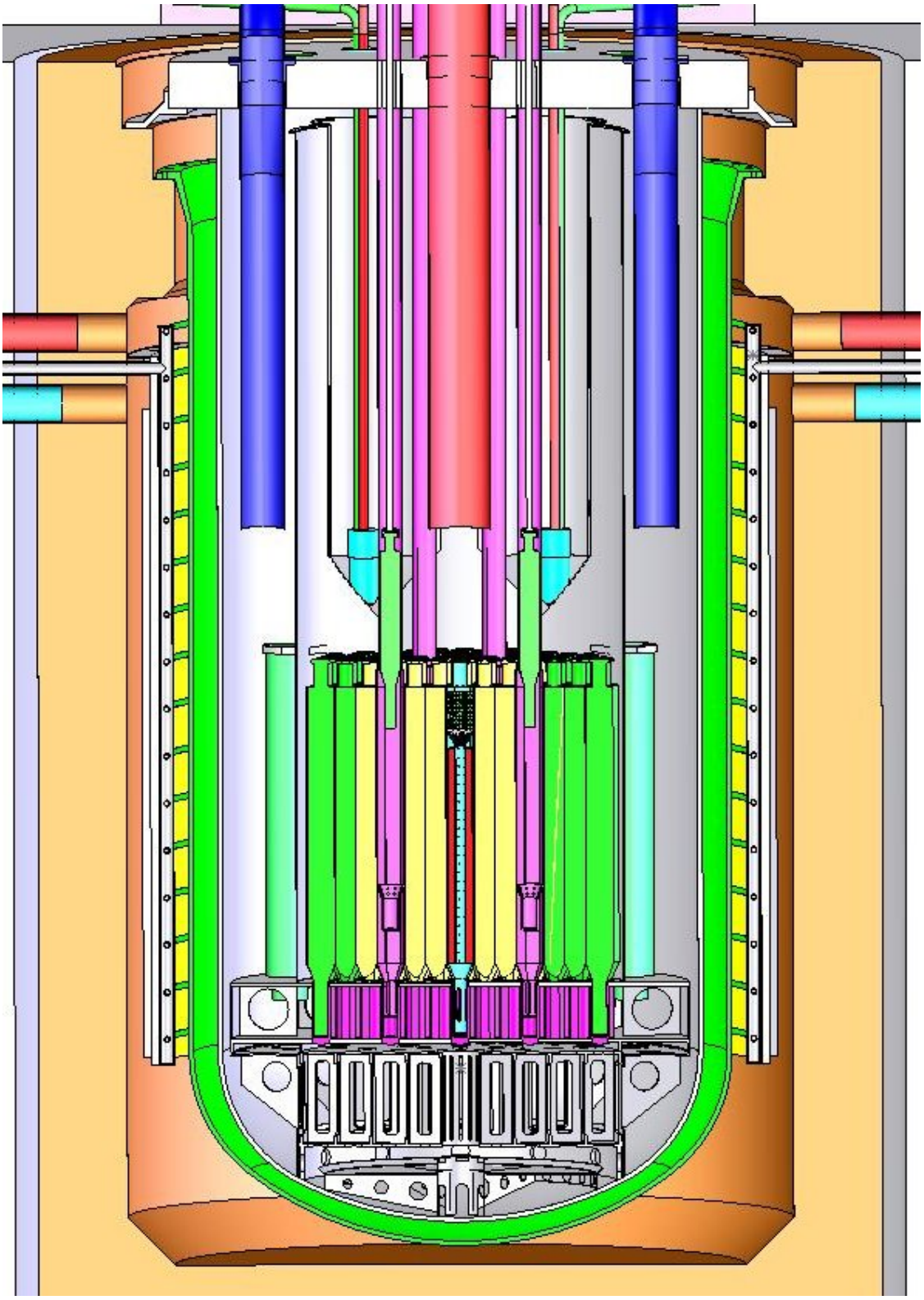

Figure E-9. Reactor Block of Pool-Loop Concept

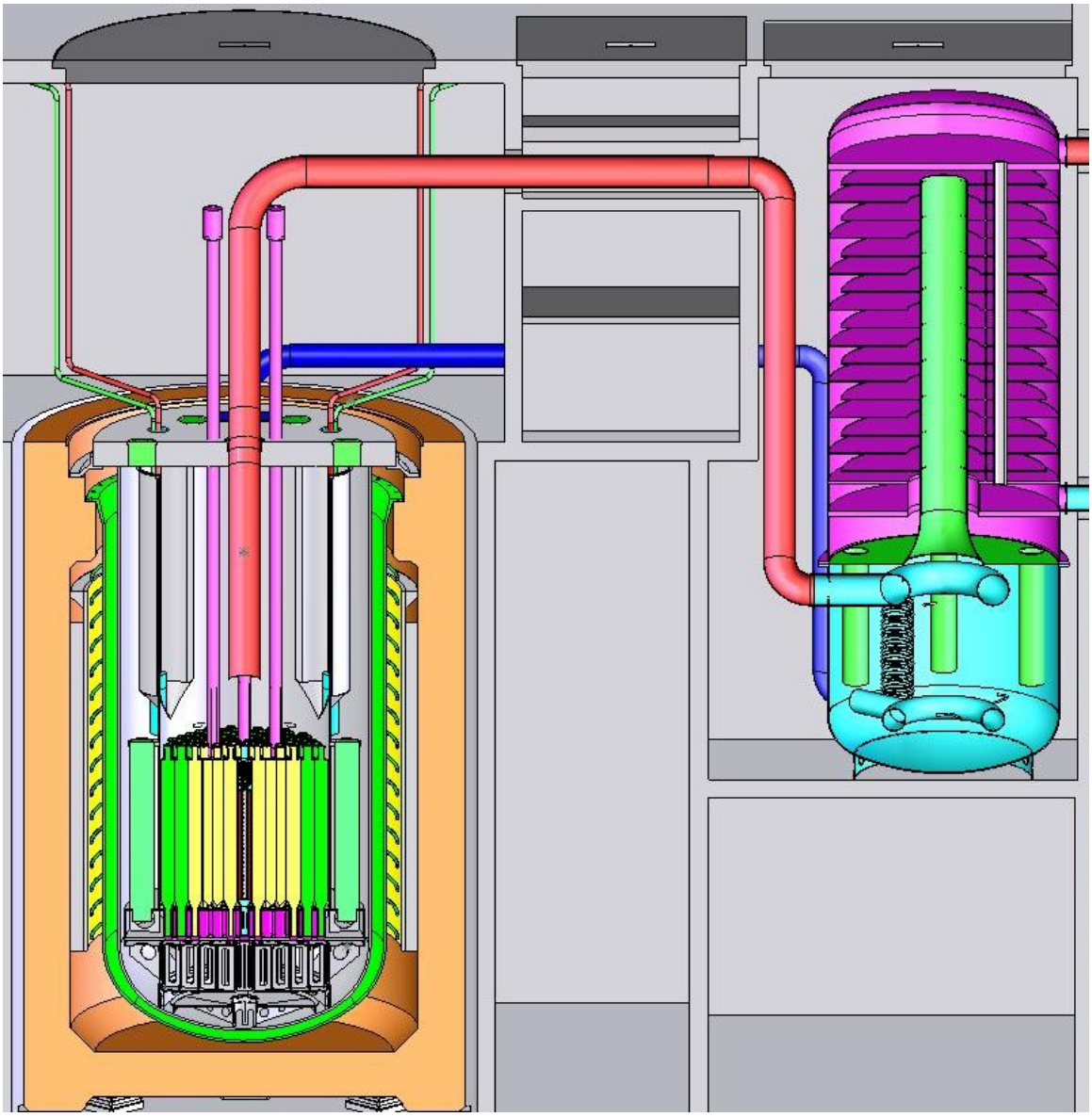

Figure E-10. Nuclear Plant Layout of Pool-Loop Concept

- The internal skirt (outside the core restraining barrel) is quite cylindrical to have a good 'cold/hot' sodium volumes ratio. It has four handle-shape passes through for in-vessel circulation, if need be, and lodging the integrated heat exchangers of the DRACS. The skirt is also equipped with collars for the EM pump axial bearing (+ electric connection).
- The core configuration is quite the same as for the reference SMFR but with a change concerning the control rods :
    - two diversified shutdown systems (2x3 rods) are located at the last but one ring (n-1) of the fissile zone. This is due to a need for larger space to implement the primary loop outlet (hot leg) at the central zone above the core.
    - The central position of the core has a multipurpose use:
        - Totally autonomous and passive shutdown system (fuse concept) without any driveline connection with the reactor roof;

        - Possible in-core instrumentation;
        - Intermediate core handling station. This feasible reactor configuration is very exceptional during the reactor life time and is a voluntary heavy operation contributing to proliferation resistance: implementation of this in-core device needs to remove the primary loop hot-leg and to replace it by a core handling plug at the reactor roof level.
- The reactor roof is a metallic component with limited number of penetrations (DRACS and primary pipes) and plugs for EM pump handling. The main vessel having a minimized H/D ratio is anchored to the roof. The vessel suspension part facing the cover argon plenum is protected against thermal gradients.

Shutdown Heat Removal Provisions

- The shutdown heat removal is normally assured by a part of the supercritical CO_2 BOP system. When this latter is unavailable, air cooling outside the skirt of the sodium/CO_2 heat exchanger, where the primary sodium is in the outer tubes space, is an additional means.
- The main shutdown heat removal system having a safety function is the redundant and diversified DRACS: 2 systems of 2 sodium loops (4x1MW) optimized for natural circulation mode from the integrated Na1/Na2 exchanger to the Na2/air exchanger. Among the diversification provisions, two operating modes (forced or natural) of the secondary sodium are possible.
- Although the previous means are sufficient to reach the reliability objective of the shutdown heat removal safety function, feasibility of implementation of a RVACS was demonstrated through the design. For that the first option of a guard vessel anchored to a modular concrete vault is replaced by a guard vessel hanging from the top of the reactor vault (option similar to the reference SMFR design). Then a passive RVACS with mixed cooling means is planned :
    - Option of "water spray" towards the guard-vessel outer face, passively acting during a high temperature phase of a transient (high heat removal capacity);
    - Option of "air chimney" for the remainder large phase of the transient (low heat removal capacity).

Range of Main Data of Preliminary Design

The design data of the innovative PL version of SMFR are summarized below:

- Reactor vessel: H= 8.0m, ID= 4.01m; Guard vessel: ID= 4.50m; Inter-vessel= 0.20m
- Inner shroud: OD= 2.73 m
- Bottom zone: diagrid: H= 0.6m, OD= 2.71m; matting: H= 0.6m; catcher zone H= 0.8m
- Pumps: Internal EMP: OD= 0.4m, H= 0.75m; external EMP: Q= 0.36 m3/s
- Primary pipes: hot-leg OD= 0.51m; cold-legs OD= 0.36m
- DRACS: integrated HX: shell OD= 0.25m, length= 1.0 m; HR= 1 MW/loop (630°C)
- RVACS: "H_2O spray"= 20 g/m^2.s; HR= 1.5MW; autonomy= 2h30; chimney: 2x 0.45m

- Na1/Na2/S-CO_2 heat exchanger (option: concentric-tubes):
  - number of tubes: 45650; length= 5.1m; thickness tubes in/out= 2mm/1mm.

The preliminary design proposed can offer a high level of safety through the choice of redundant and diversified means for each safety function. In addition, as a competitive indicator, the compactness of the reactor block (in term of volume) was compared with other projects or existing fast reactors. Figure E-11 shows that the PL version of SMFR, ranked among the loop-type reactors, is in a good range with respect to its small plant power (125 MWth).

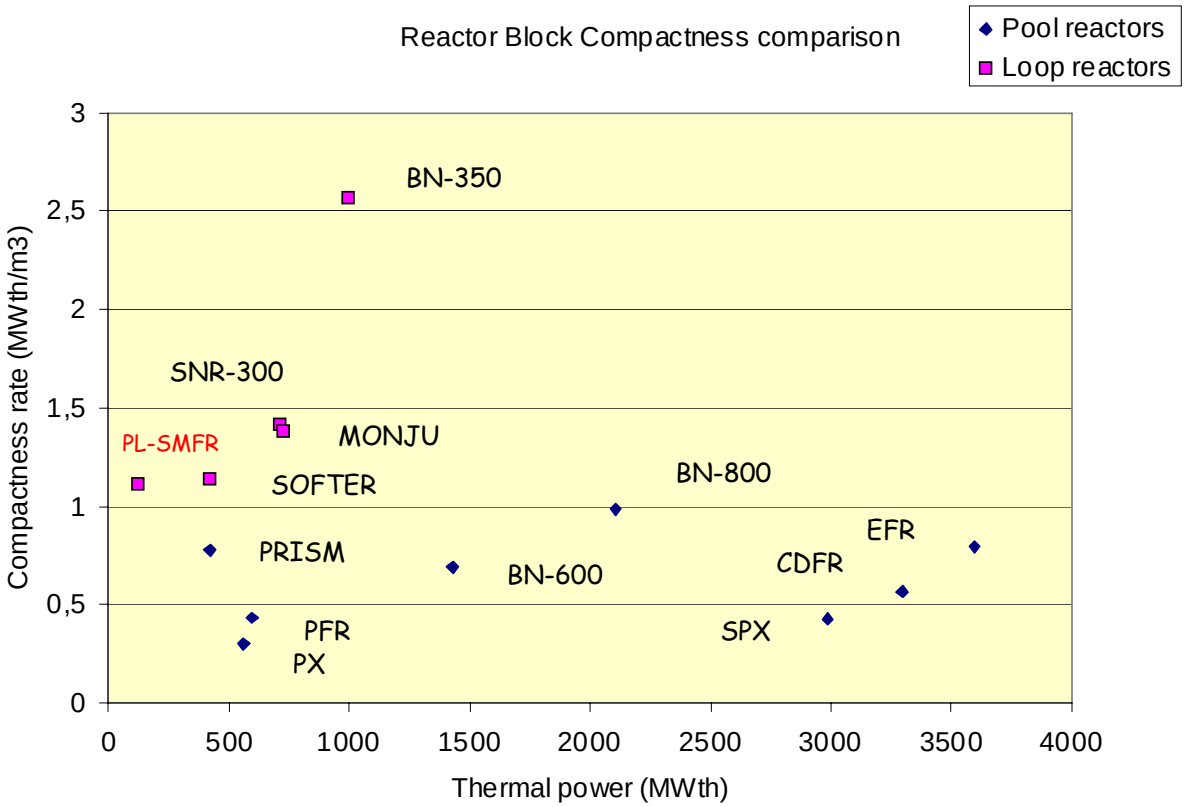

Figure E-11. Reactor Block Compactness Comparison

References

1. V. Orlov, et al., "Mono-nitride fuel and large-scale nuclear power industry," Proc. Tech. Con. Meet. Studies on Fuels with Low Fission Gas Release, RDIPE,1-4 Oct., IAEA-TECDOC-970, Moscow, Russia (1996).
2. V. Orlov, et al., "Physical characteristics of lead cooled fast reactor," Proc. Top. Meet. Advances in Reactor Physics, Vol.1, Knoxville, TN. (1994).
3. K. Sugino and T. Mizuno: "A New Concept of Sodium Cooled Metal Fuel Core for High Core Outlet Temperature," Proc. 2004 International Congress on Advances in Nuclear Power Plants (ICAPP '04), Pittsburgh, PA (2004).
4. Y. Chikazawa et al., "Conceptual Design of Small Sodium Cooled Reactors," JNC TY9400 2005-004, (2005), in Japanese.
5. Y. Chikazawa et al., " Feasibility Study of a Compact Loop Type Fast Reactor without Refueling for a Remote Place Power Source," GLOBAL 2005, Tsukuba, Japan, Oct. 2005, to be published.

APPENDIX F. SCALE-UP POTENTIAL

The 50 MWe size the SMFR was chosen for niche market applications, but the unit capital cost in terms of $/kWe is expected to be too high to be competitive in the conventional market. Whether the SMFR technology be applicable in the conventional market depends on its scale-up potential in order to reach a competitive unit capital cost.

Lessons learned from existing economic comparisons in the past (such as the comparison between a large monolithic EFR-type and a modular PRISM type plant) show that there are two viable approaches for reaching competitiveness with a given reactor type:

- Economies of scale with monolithic design leading to a large reactor power close to 1,500 MWe
- Modular design that takes advantage of factory construction, faster learning in multiple components, etc.

The SMFR technology appears to be more suitable to the latter approach, since the concept is already based on modular approach. It is conceivable that a 1,500 MWe plant made up of five or six SMFR-based modules would be economically attractive. Therefore, a scale-up potential of the SMFR design features to about 300 MWe will be evaluated in the next phase of the project.

This Appendix describes an example of such 300 MWe plant. The design described here is one of the outcomes of collaborative study between JNC and JAPC in accordance with "The Agreement about the Development of a Commercialized Fast Breeder Reactor Cycle System."

1. Fuel and Core Design

The basic core concept is the same as the core described in Appendix E, which is a single Pu-enrichment core.

Around 400-600 MW thermal output can be an alternative design for scale up potential of small-scale sodium-cooled fast reactor, to obtain scale-up economical benefits as a power reactor. In addition, we can rely on our experience of demonstration scale sodium cooled fast reactors in Japan, Europe and U.S.

A 1~2 years cycle time with batch refueling is applied for this design, which is commonly used in the existing thermal/fast spectrum reactors. This technique helps to reduce core reactivity change and power peaking factor from the viewpoints of neutronics design, to reduce required coolant mass flow for driver core region, and to decrease coolant and fuel temperatures.

The fuel and assembly configurations are enveloped to be within, or nearly within, the existing metal/MOX fuel designs and irradiation experiences. Recommended key design parameters are; fuel pin diameter (~6-8mm), pin gap (1-2mm), graded smear density and Zr content, duct thickness (5mm) and gap (4.2mm).

The primary core design parameters are presented in Table F-1, the assembly and pin design parameters in Table F-2, and the core performance characteristics in Table F-3. The core layout

is depicted in Figure F-1.

Table F-1. Core Design Parameters

Thermal Power	714 MWth
Electric Power	300 MWe
Primary Coolant	Sodium
Core Inlet Temperature	395°C
Core Outlet Temperature	550°C
Secondary Coolant	Sodium
Ternary Coolant	Water/Steam
Operating period / # of Batch	2 years / 4 batches
Number of Assemblies	
Driver Fuel	243
Primary Control	7
Secondary Control	3 (w/ SASS mechanism)
Reflector	126
Core Barrel, ID	336cm
Average Linear Power	13.5 kW/m
Pressure Drop Across Pin Bundle	0.14MPa

Table F-2. Assembly and Pin Design Parameters

Lattice Pitch	15.7 cm
Duct Outside Flat-to-Flat	15.3 cm
Interassembly Gap	0.42 cm
Duct Wall Thickness	0.5 cm
Number of Pins	217
Fuel Pin Diameter	0.85 cm
Pitch-to-Diameter Ratio	1.12
Cladding Thickness	0.50 mm
Fuel Material	U-Pu-TRU-Zr
Bond Material	Na
Cladding/Duct Material	ODS / FMS
Active Core Length	100 cm
Upper Plenum	175 cm
Core Volume Fractions	
Fuel (of Non-Smeared)	0.45
Structure	0.25
Sodium (Entire)	0.30
Reflector Volume Fractions	
Structure	0.7
Sodium	0.3

Table F-3. Core Performance Characteristics

Capacity Factor	1.0
Fissile Pu Loading of Initial Entire Core	2.3 ton
Power Density	131 kW/l
Average Discharge Burnup	80 MWD/kg
Peak Fast Fluence	5 x 10^{23} nvt
Enrichment Zoning: Inner/Outer	12.3/12.3 Pu_wt%
Fissile Enrichment: Inner/Outer	7.5/7.5 Pufissile_wt%
k-effective change during an operating period	0.46 %Δk/kk'

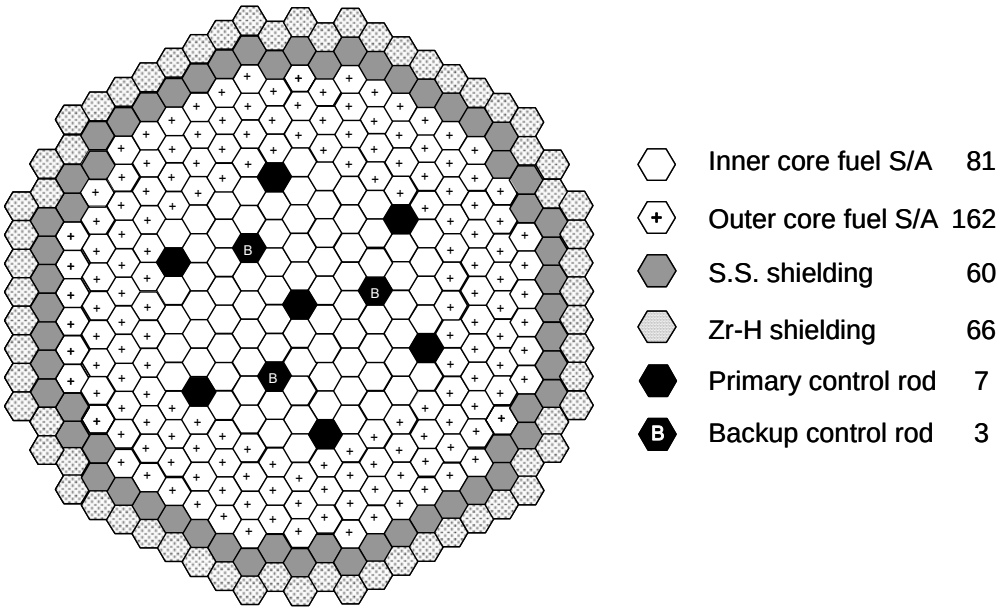

Figure F-1. Core Layout

2. Plant Design

In scale-up concepts, the demand for cost reduction is more severe because the electricity generation cost is more competitive in sites where such a large reactor is needed. In this concept, the core diameter is minimized to increase power density and a refueling interval of 2 years is needed. A sketch of the reactor vessel is shown in Figure F-2. The reactor vessel has a permanent fuel handling system. There is a rotating plug at the top of the reactor vessel and the upper internal structure (UIS) has a slit to reduce the diameter of the reactor vessel considering access of the fuel handling machine to every fuel assembly.

The space outside the core barrel is utilized for the fuel relay point, piping inlet and outlet without nozzles, the in-vessel storage (IVS) of the spent fuel assemblies, etc. The maximum

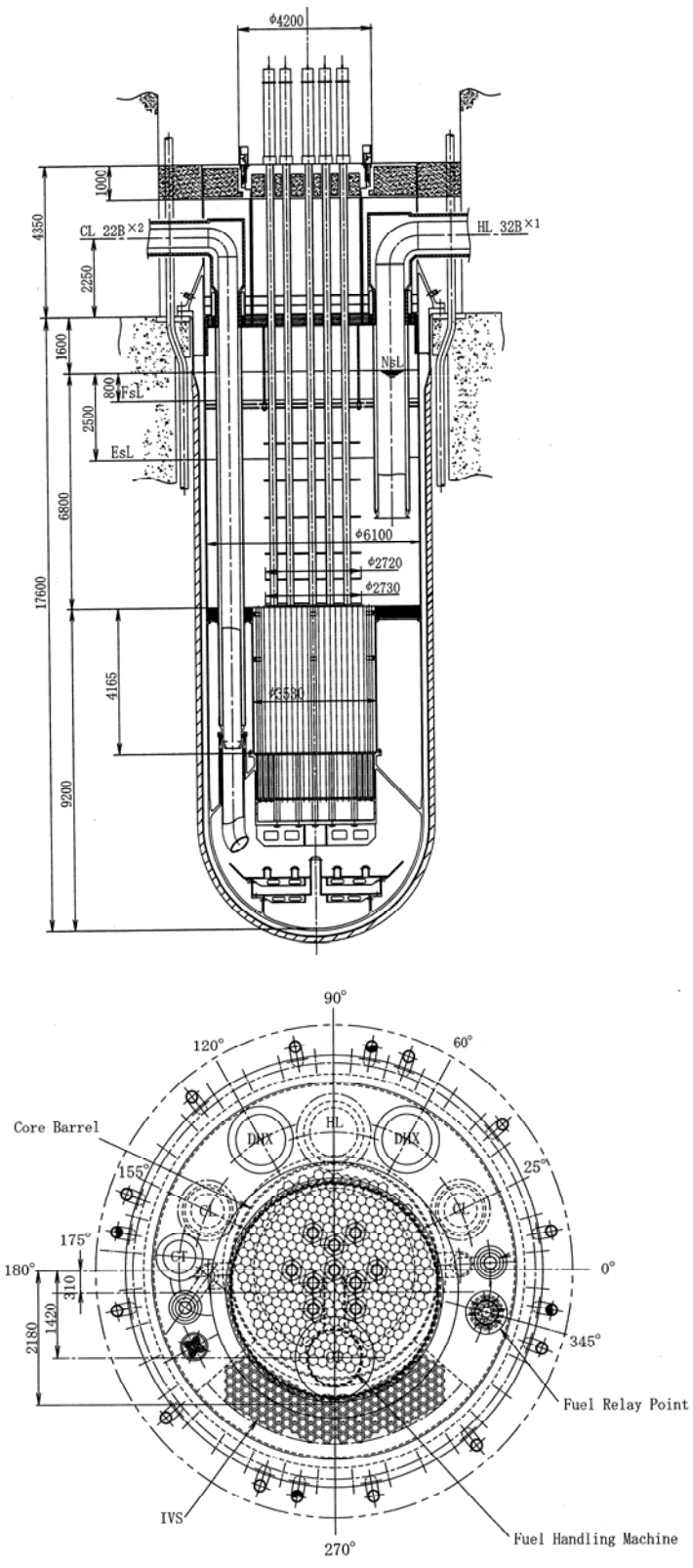

Figure F-2. Reactor Vessel

spent fuel decay heat which can treat outside the sodium is about 2 kW/assembly. A 4 years storage is needed to reduce the decay heat to such a level. In this concept, the minimum capacity for 4year storage is 122 (2 batches) and the IVS can store more than 140 assemblies. An ex-vessel storage facility is not need in this concept.

The schematic illustration of the main cooling system is shown in Figure F-3. The loop number is one adopting two independent electromagnetic pump arranged in series. The piping, the intermediate heat exchanger and the steam generator material is 12Cr steel with high thermal conductivity and low thermal expansion. The plant bird's eye view is shown in Figure F-4. The arrangement of the reactor components are simple adopting one loop system and the reactor building can be compact without any ex-vessel fuel storage system. [1]

References

1. Y. Chikazawa, et al., "Conceptual Design of Small Sodium Cooled Reactors," JNC TY-9400-2005-004 (2005), in Japanese.

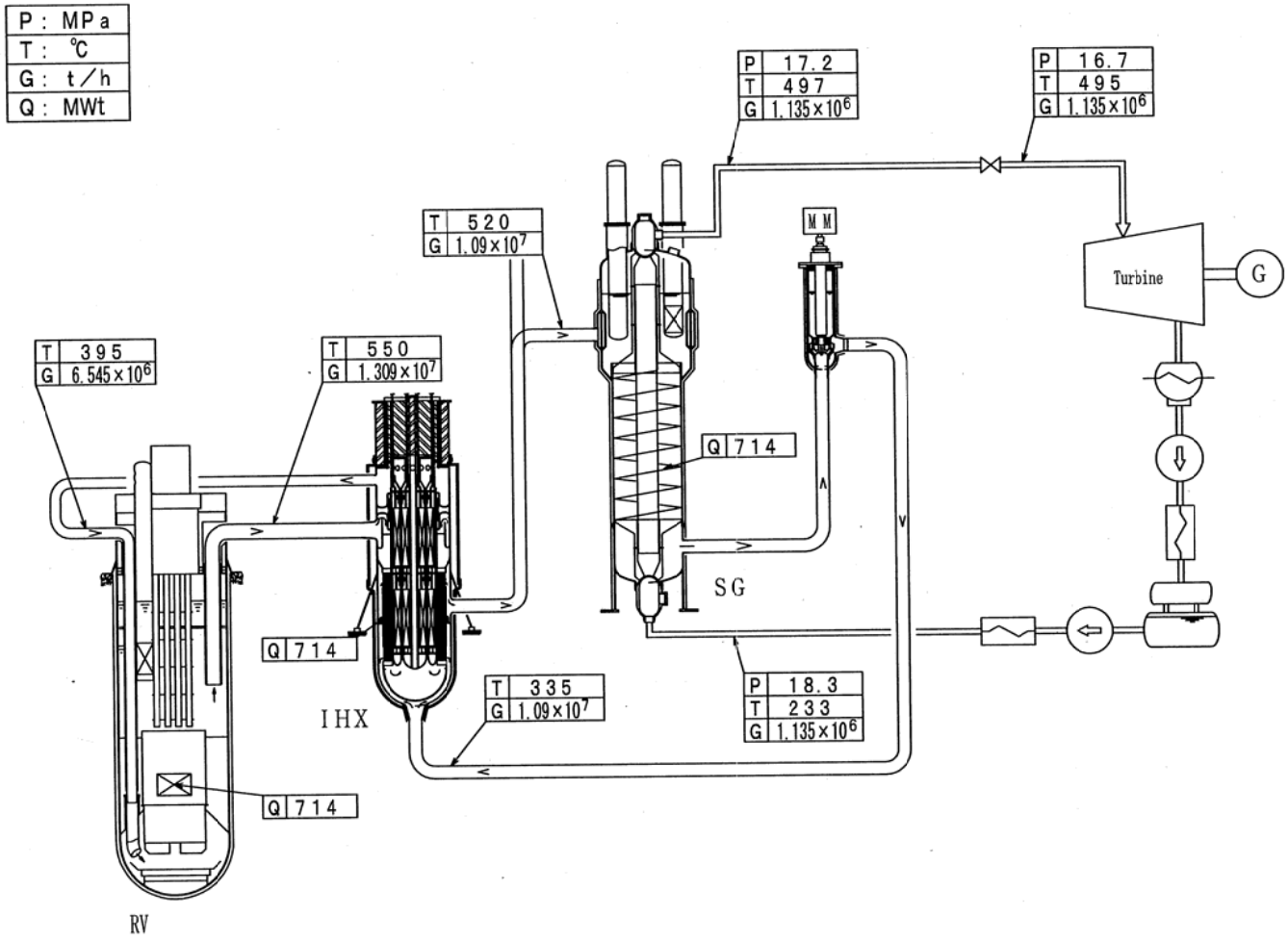

Figure F-3. Schematic Illustration of Main Cooling System with Heat Balance

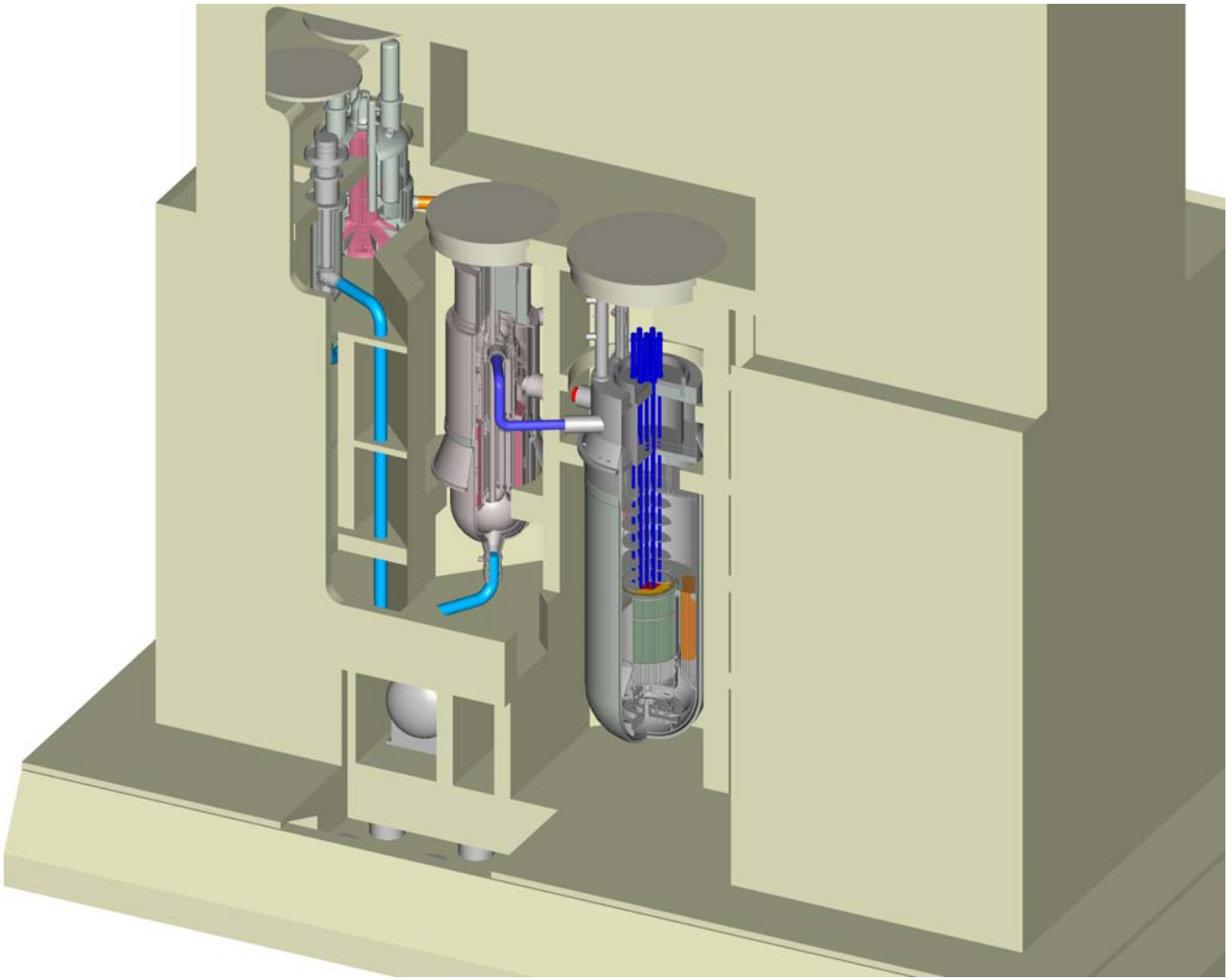

Figure F-4. Plant Bird's Eye View